

Ultrafast Electron Dynamics Following Ionization



Alexander I. Kuleff

Habilitationsschrift zum Thema

Ultrafast Electron Dynamics Following Ionization

**vorgelegt
der Fakultät für Chemie und Geowissenschaften
der Ruprecht-Karls-Universität Heidelberg**

**von Dr. Alexander I. Kuleff
aus Sofia (Bulgarien)**

April 2012

Copyright ©2012 by Alexander Kuleff

To Irina, Philip, and Anna

Contents

Acknowledgments	ix
Summary	xi
1 Introduction	1
2 Theoretical background	7
2.1 The hole density	7
2.2 Choice of cationic basis and initial state	9
2.3 Direct propagation	12
3 Basic mechanisms	15
4 Results	21
4.1 Electron dynamics of electronically stable ionic states	21
4.1.1 Chain-like molecules	21
4.1.2 Non-chain-like molecules	25
4.2 Electron dynamics of electronically decaying ionic states	27
4.3 Radiation generated by ultrafast electron dynamics	29
5 Conclusions and perspectives	33
Bibliography	37
6 Publications	43
6.1 Multielectron wave-packet propagation	44
6.2 ICD in real time and space	55
6.3 The role of nuclear dynamics	59
6.4 Charge migration in PENNA	68
6.5 The role of the donor site	73
6.6 Electron dynamics within single-determinant approaches	85
6.7 Impact of relaxation satellites	93
6.8 Charge migration in 4-methylphenol	100
6.9 Radiation generated by electron dynamics	105
6.10 Electron dynamics in porphyrins	109

6.11 Electron correlation in real time	116
6.12 Charge migration in oligopeptides	137
Appendix A Full list of publications	143

Acknowledgments

First and foremost, I would like to thank Lorenz Cederbaum, my advisor and, I dare to say, friend, who introduced me to the fascinating field of correlated electron dynamics and afterwards guided me through it with an invisible hand. His enthusiasm in doing science and his unlimited curiosity to understand the underlying physical mechanisms were an invaluable source of motivation and a great school for me. Thank you, Lenz!

Nearly all my knowledge in quantum-chemical many-body methods I owe to Jochen Schirmer, and I am very grateful to him for that. I have to acknowledge Jochen also for the countless political discussions I had with him during lunch breaks. Although our nearly orthogonal views on how society should be organized never got any closer, the discussions kept me updated about the sneaky ambitions of the American imperialism and, moreover, I really enjoyed them.

I got much help in writing and debugging my Lanczos propagation code from Hans-Dieter Meyer. I thank Dieter for always being available when I had questions and for being always very precise and constructive when answering them.

I would also like to thank the people with whom I closely collaborated on the subject of this Thesis — Jörg Breidbach, Siegfried Lünemann, and Andreas Dreuw. Jörg introduced me at the beginning to the computer codes he had written and has been always very responsive afterwards in helping me with the necessary modifications. Sigi performed many of the calculations gathered in this Thesis. His chemical knowledge and intuition were also very helpful in finding relevant and interesting systems to study. I had a very fruitful collaboration with Andreas in showing that even ‘big shots’ in the field could be wrong.

In my daily work, I was lucky to be surrounded by a friendly and cheerful group of fellows, creating a wonderful working atmosphere. First of all, these were my past and present office mates. Especially Spas, who was always helping me with the tangled chemical nomenclature and in whom I found a wonderful partner to discuss the intricacies of Bulgarian politics, and Philipp, who showed me that one can do wonderful science with superluminal speed. There were also numerous colleagues and friends who helped me in matters scientific and others and with whom I shared a lot of memorable moments. Etienne, Kirill, Markus, Ofir, Oriol, Shirin, Susana, Tony, Yassen, thank you all, guys!

I thank our secretary, Annette Braun, for always being ready to help me in administrative and personal matters.

Special thanks go to my parents, whose permanent support and encouragement were and are very precious to me.

Finally, I would like to thank my family for the patience and understanding that scientific work comes with a somewhat irregular working schedule, late hours, and often travel.

Summary

In recent years, the tremendous development of laser pump-probe experimental techniques made possible a direct observation in real time of different kinds of ultrafast processes with sub-femtosecond resolution. This opened the door for investigation of processes in the attosecond/femtosecond time scale that take place before the nuclear dynamics come into play. Thus, processes like the rearrangement of the electronic cloud following an ionization of a multielectron system can now be traced in time and space and analyzed. More than ten years ago it was shown that if an electron is removed rapidly from the system the electronic many-body effects *alone* can beget rich ultrafast electron dynamics. The positive charge created after the ionization can migrate throughout the system on a femtosecond time scale *solely* driven by the electron correlation and electron relaxation. If the energy of the excited state is sufficiently high the system can also undergo a non-radiative decay and eject a secondary electron. In order to describe correctly such kind of dynamical processes an *ab initio* method for multielectron wave-packet propagation was developed within this work. It gives the possibility to describe fully *ab initio* the dynamics of various de-excitation processes taking into account *all* electrons of the system and their correlation. The approach is equally suitable for tracing in real time and space the electron dynamics of both decaying and non-decaying electronic states. Employing this method, different fundamental physical phenomena triggered by ionization of a variety of systems were studied. We were able to trace in real time and space the evolution of the electronic cloud during the interatomic Coulombic decay process in NeAr following Ne2s ionization. Our results allowed for a detailed analysis of the relative contributions and time scales of the different decay channels open. It was shown that although typical for inner-valence ionized states, the charge-migration process can take place also after ionization out of the outer-valence shell. We found also that the charge migration depends strongly on the particular nuclear geometry suggesting that the nuclear dynamics that will enter the picture at later times will play an important role and can even trap the charge. Therefore, the charge migration can be regarded as the first step of an effective transfer of the charge from one moiety of the system to another. Moreover, we found out that the charge migration triggered by ionization generates a characteristic radiation. The emission is usually in the infra-red spectrum, reflecting the typical few-femtosecond charge oscillation time. We studied also the effect of the ultrafast ionization and found that in this case a much stronger ultra-violet emission is generated. This emission appears as an ultrafast response of the remaining electrons to the perturbation caused by the sudden ionization and as such is a universal phenomenon to be expected in every multielectron system.

Chapter 1

Introduction

According to one of the most fundamental laws of physics, many-electron systems, like atoms and molecules, with excess internal energy relax towards states of lower energy by rearranging their electronic and molecular structure. Studying the dynamics throughout such processes is the key to understand not only the internal structure but also the chemical reactivity of the systems under study. Although, the development of advanced beam and laser experimental techniques has produced a wealth of data, providing information on chemical reactivity and energy transfer processes at a molecular level, very often the interpretation of the experimental results cannot be done without a detailed dynamical calculations. In addition, many dynamical effects cannot be measured with the existing experimental techniques but are indispensable for understanding the structure and properties of matter. That is why, computing the time development of relaxation processes has concentrated a lot of efforts over the last several decades. Nevertheless, the availability of high-performance computers has only recently made it feasible to integrate the Schrödinger equation of experimentally interesting cases with the aim to understand their quantum evolution.

Much has been done in this respect in the field of molecular nuclear dynamics where various methods for propagation of the nuclear wave packet have been developed [1]. Based on the different time scales of the electron and nuclear motion¹, for treating nuclear dynamics problems, the total wave function of the system is usually represented as a product of the electronic wave function and the wave function describing the nuclei (Born-Oppenheimer approximation). In that way, the Schrödinger equation is decoupled into a static equation for the electronic part, and an equation of motion for the nuclear wave function, which then is an object of different propagation schemes. The Born-Oppenheimer approximation, however, is inapplicable when the spacing between the electronic levels becomes very small, and breaks down completely when a real crossing of levels, known as

¹Quantum mechanics connects the time scale of dynamics with the energy spacing between the stationary states determined by the corresponding potential. That is, in polyatomics the millielectronvolt-scale energy spacing of the vibrational levels implies that the molecular vibrations occur on a time scale of tens to hundreds of femtoseconds ($1 \text{ fs} = 10^{-15} \text{ s}$), while the spacing between the electronic levels in the atoms and molecules ranges from sub-eV to tens of keV determining the time scale of the electronic motion from tens of femtosecond to even below attosecond ($1 \text{ as} = 10^{-18} \text{ s}$).

conical intersection [2, 3], occurs. In these cases the nuclear and electronic motions are strongly coupled and one has to use non-adiabatic molecular dynamics approaches [2, 3]. The development in theoretical methods went hand in hand with the development of the pump-probe experimental techniques [4] permitting to follow in time the rearrangement of the molecular skeleton during a chemical reaction, thus giving birth to the research area known nowadays as femtochemistry [5].

An important aspect of the possibility to follow the motion of atoms in molecules and to make “molecular movies” is that knowing how the system evolves in time allows to design techniques to control this evolution and to steer the particular molecular process, e.g., to predetermine the outcome of a chemical reaction.

Various dynamical effects in a molecular system can take place, however, before the nuclear dynamics come into play. Such ultrafast processes are, for example, different intraatomic (intramolecular) decay processes, like the well known Auger decay of deep core levels, the recently reported charge-migration phenomenon [6, 7], or the attosecond response of the system to the removal of an electron [8, 9]. For the proper description of such processes one needs a dynamical treatment of the electronic wave function. In these cases, we may consider the nuclear frame as fixed, and solve a dynamical Schrödinger equation for the electronic part — *multielectron wave-packet dynamics*. Of course, the ultimate goal will be to treat dynamically on a full quantum mechanical level both the electronic and the nuclear wave functions, but this is currently beyond reach for realistic systems. We have to mention, however, that first steps in this direction were recently undertaken [10] (see also Ref. [11]).

The multielectron dynamical calculations become especially important in the light of the tremendous development in the last years of the time-resolved spectroscopic techniques and the availability of attosecond laser pulses (see, e.g., the review articles [12, 13]), which made possible the direct observation in real time of ultrafast processes with sub-femtosecond resolution [14–18]. With pulses as short as few tens of attoseconds available nowadays [19, 20], one is able to initiate and probe processes that take place before the nuclear dynamics come into play, i.e. to study electron dynamics on their natural time scale. In particular, the possibility to characterize electronic processes determined by electron correlations, i.e. caused by the interaction between electrons, is attracting a great interest (for a recent review see Ref. [21], P11 from the attached papers). To interpret properly the experimental results, one needs precise *ab initio* calculations which give the time-evolution of the electronic cloud taking into account various many-body effects, as electronic correlation and electronic relaxation.

Due to the complexity of problem and the enormous numerical obstacles it poses, not many theoretical methods for integrating the time-dependent Schrödinger equation for a many-electron system have been developed so far. The exact numerical solution is computationally extremely demanding and currently possible only for two-electron systems (see, e.g., Ref. [22]). The alternative multi-configurational time-dependent Hartree-Fock (MCTDHF) approach [23, 24] is computationally substantially cheaper and in principle can be applied to larger systems. However, the computational cost grows dramatically with the number of electrons, making the method prohibitively expensive for systems containing more than few electrons.

For treating electron dynamics of excited states, a promising time-dependent configuration-interaction (TD-CI) approach was also proposed [25–27]. Until now the method was applied mostly in its singles (TD-CIS) and singles and perturbative doubles (TD-CIS(D)) formulations and used to study the dynamics of laser-driven state-to-state transitions [26–28]. TD-CIS is relatively inexpensive computationally and can be applied to larger systems. In its CIS form, however, the approach does not give a quantitatively correct description of general valence excitations. This problem can, in principle, be overcome by including higher excitation classes¹. What is more important for the class of problems studied in the present work is the possibility to treat multistate dynamical processes. The molecular spectra often consist of a multitude of closely lying electronic states which can hardly be addressed individually by an ultrashort pulse. Such broad-band pulses can populate a large number of states creating a wave packet. Although the TD-CI approach can, in principle, be used to treat wave-packet dynamics, to the best of our knowledge this was not demonstrated until now.

Another popular approach to tackle time-dependent problems is the time-dependent density functional theory (TDDFT) [29]. However, the large variety of approximate exchange-correlation functionals proposed and the increasingly empirical way of their construction lend DFT methods not very high predictive power². Moreover, the most widely used TDDFT method, namely its linear-response formulation [31], accounts only for single excitations which is insufficient in many cases, like, for example, for treating electronic decay processes where the explicit inclusion of double excitations is essential.

In short, the available computational methods that can provide a quantitative description of electron dynamics processes are applicable only to small systems, or to special situations like pure state-to-state transition. On the other hand, the semi-empirical methods with which larger systems can be handled usually do not capture correctly the multielectron character of the dynamics.

One of the aims of the present work is to go beyond the few-electron systems and to develop an *ab initio* multielectron wave-packet propagation methodology allowing a correct description of the ultrafast electron dynamics triggered by ionization of a moderate-size molecular system. We have to mention that following the same ideas and techniques, a method allowing the description of electron dynamics initiated by excitation of a molecule was recently proposed [32]. Apart from the methodological development, the emphasis of the present work is put on studying the fundamental physical phenomena triggered by ionization. Depending on whether the initial cationic state created is below or above the double-ionization threshold, two distinct dynamical responses of the electronic cloud could be expected. Let us discuss briefly these two situations.

If the excess energy is insufficient for a second electron to be ejected, the system may

¹It has to be noted, however, that from the inclusion of the double excitations on, the method becomes size-inconsistent, making the quality of the description to decrease with the increase of the system size. The full-CI expansion, which is, of course, size-consistent, remedies this deficiency but is applicable only to few-electron systems due to the large computational costs.

²Although not of relevance to this work, we briefly mention that despite that TDDFT is traditionally assumed to be a formally exact theory, it was recently shown [30] that there is a serious flaw in the TDDFT founding theorems [29] and currently there is no rigorous proof that the TDDFT approach is in principle equivalent to solving the time-dependent Schrödinger equation.

react by rearranging its electronic cloud. As we are interested in the ultrashort time span immediately following the removal of an electron and before the nuclear motion starts to play a role, these dynamics will be solely driven by the electron correlation¹. Such kind of dynamical behavior was predicted more than 10 years ago [6] and was termed *charge migration* in order to distinguish it from the nuclear-dynamics-driven charge transfer process. The importance of the charge migration lies in the fact that although, as we will see, the charge migration typically represents an ultrafast charge oscillations from one side of the molecule to another, there are already strong indications [33–35] that the coupling to the nuclear motion can lead to a trapping of the charge and, thus, achieving irreversibility of the process. In other words, the process can be regarded as the first step of an effective transfer of the charge from one moiety of the system to another. The charge transfer itself is a fundamental process in nature and plays an essential role in many chemical and biological processes [36].

In real molecular systems, both mechanisms, the charge transfer and the charge migration, are hardly separable and individually observable, since, as we mentioned above, the electronic and nuclear motions are always coupled. With the help of attosecond laser pulses, though, it becomes possible to monitor the motion of the electrons separately from that of the nuclei. However, although the charge transfer and charge migration are to some extent similar, the important difference is the underlying concept. In the first, the charge transfer is triggered by the nuclear dynamics [36], while in the latter, the charge migration triggers some nuclear motion, as long as (at least within Born-Oppenheimer approximation) the electronic motion governs the effective potential seen by the nuclei. Therefore, the detailed knowledge of the ultrafast charge migration can provide hints how one can modulate this initial step and in that way steer the succeeding charge transfer process. This shows that apart from its fundamental importance, the study of the charge-migration phenomenon may have far reaching practical consequences.

Let us now examine the situation when the initially created ionic state is above the double-ionization threshold of the system itself or, if the system interacts with an environment, of the compound system-environment complex. In both cases an electronic decay may take place and a secondary electron may be ejected. There is an important difference between these decay processes though. In the first type the system gets rid of the excess energy by ejecting one of its electrons, or, in other words, autoionizes, while in the second type, the system transfers its excess energy to the environment which uses it to eject an electron. In the first category falls the mentioned above Auger decay which is usually triggered by a core-level ionization. In this process the initial vacancy is filled by a valence electron and another one is ejected into the continuum. Depending on the energy of the core hole and the strength of the electronic coupling, the Auger decay process transpires typically in the femtosecond, entering even the attosecond time regime. Therefore, in the vast majority of cases the time-evolution of an Auger decay can be calculated without taking into account the nuclear dynamics and thus, in principle, can be studied with the help of the methodology presented in this work.

¹Very often in the present text the term “electron correlation” will be used as a synonym for “electronic many-body effects”, i.e. it will designate both the electron correlation and the electron (or orbital) relaxation effects. When needed, an explicit distinction between these effects will be made.

The second category of electronic decay processes are those that take place via an ultrafast energy transfer from the initially ionized system to its environment. Contrary to core ionization, the ionization of inner-valence electrons of an isolated atom or a small molecule usually produces ions in excited states lying energetically below the double-ionization threshold. Therefore, the slow radiative decay, or processes involving nuclear dynamics in the case of a molecule, are the only possible de-excitation mechanisms. The situation is fundamentally different if the ions are embedded in an environment or have neighbors like in a cluster. Then, the possibility to distribute the positive charges between cluster subunits substantially lowers the double-ionization threshold of the cluster compared to that of the isolated subunit giving rise to an interatomic (intermolecular) decay mechanism, in which the excess energy of the ion with the inner-valence hole is utilized to ionize a neutral neighbor. This environment-mediated electronic decay process, named *interatomic (intermolecular) Coulombic decay (ICD)*, was predicted in the late 90's by Cederbaum and co-workers [37] and in the last 10 years found its full confirmation in a series of spectacular experiments. The theoretical [37–47] and experimental [48–54] work on ICD performed until now and the progress achieved established the generality of the phenomenon and opened new horizons for the ICD research. In particular, the high efficiency of the ICD compared to various photoinduced processes like photon emission, isomerization, and charge transfer, makes the ICD extremely attractive for quenching in a controllable fashion such fundamental processes in biophysically relevant systems. Furthermore, the ICD phenomenon produces low-energy electrons that have been proven to induce serious damages in DNA via dissociative electron attachment mechanism [55, 56].

The high efficiency of the ICD process often allows to compute its time-evolution without taking into account the nuclear dynamics. Indeed, the predicted ICD lifetimes vary between a few [42] and a few tens [39, 40] of femtoseconds which in many cases is orders of magnitude faster than the nuclear rearrangement that the primary ionization can induce. Therefore, we can trace in time and space such ICD relaxations and analyze them with the help of the methodology reported in this work.

The Thesis is organized as follows. In Chapter 2 a concise description of the methodology used and developed is given. In Chapter 3 the different mechanisms underlying the ultrafast dynamics following ionization are analyzed. The main results obtained are summarized in Chapter 4. For more details the reader is referred to the attached papers. We discuss the implications of the results obtained and give some perspectives for the directions the future studies should go in Chapter 5.

Chapter 2

Theoretical background

2.1 The hole density

A possible way to trace and analyze the electron dynamics following ionization of a molecular system is to compute the evolution of the positive charge left after the removal of the electron. This can be done by evaluating the density of the initially created hole, or the hole density, which is given by [6]

$$Q(\vec{r}, t) := \langle \Psi_0 | \hat{\rho}(\vec{r}, t) | \Psi_0 \rangle - \langle \Phi_i | \hat{\rho}(\vec{r}, t) | \Phi_i \rangle = \rho_0(\vec{r}) - \rho_i(\vec{r}, t). \quad (2.1)$$

In the above definition $|\Psi_0\rangle$ is the ground state of the neutral molecule, $\hat{\rho}$ is the local density operator, and $|\Phi_i\rangle$ is the initially prepared cationic state. The first term in Eq. (2.1), ρ_0 , is the time-independent ground-state density of the neutral system and the second one, ρ_i , is time-dependent, since $|\Phi_i\rangle$ is not an eigenstate of the cation. In the Heisenberg picture, the time-dependent part reads (atomic units, $e = m_e = \hbar = 1$, will be used throughout the text unless otherwise specified):

$$\rho_i(\vec{r}, t) = \langle \Phi_i | e^{i\hat{H}t} \hat{\rho}(\vec{r}) e^{-i\hat{H}t} | \Phi_i \rangle, \quad (2.2)$$

where \hat{H} is the cationic Hamiltonian. Using resolution of identity within a complete set of cationic eigenstates $\{|I\rangle\}$ and inserting it in Eq. (2.2), one gets

$$\begin{aligned} \rho_i(\vec{r}, t) &= \sum_{I,J} \langle \Phi_i | I \rangle \langle I | e^{i\hat{H}t} \hat{\rho}(\vec{r}) e^{-i\hat{H}t} | J \rangle \langle J | \Phi_i \rangle \\ &= \sum_{I,J} x_I^* \rho_{IJ}(\vec{r}) x_J e^{-i(E_J - E_I)t}, \end{aligned} \quad (2.3)$$

where E_I is the ionization energy corresponding to the state $|I\rangle$, $x_I = \langle \Phi_i | I \rangle$ is the transition amplitude with respect to the initial cationic state $|\Phi_i\rangle$, and $\rho_{IJ} = \langle I | \hat{\rho}(\vec{r}, 0) | J \rangle$ is the charge density matrix between the states $|I\rangle$ and $|J\rangle$. Without loss of generality, one can assume the quantities x_I and ρ_{IJ} to be real, bringing the expression for $\rho_i(\vec{r}, t)$ in the following form

$$\rho_i(\vec{r}, t) = \sum_{I,J} x_I \rho_{IJ}(\vec{r}) x_J \cos((E_J - E_I)t). \quad (2.4)$$

To evaluate the hole density we can use the second-quantization representation of the density operator within a one-particle basis (orbitals)

$$\hat{\rho}(\vec{r}) = \sum_{p,q} \varphi_p^*(\vec{r}) \varphi_q(\vec{r}) \hat{a}_p^\dagger \hat{a}_q, \quad (2.5)$$

with \hat{a}_p^\dagger and \hat{a}_p being the corresponding creation and annihilation operators, respectively. The operators \hat{a}_p^\dagger creates an electron in orbital φ_p and the operator \hat{a}_p destroys an electron in orbital φ_p . Within this representation the hole density, Eq. (2.1), takes the following form [7]

$$Q(\vec{r}, t) = \sum_{p,q} \varphi_p^*(\vec{r}) \varphi_q(\vec{r}) N_{pq}(t), \quad (2.6)$$

where the matrix $\mathbf{N}(t)$, referred to as hole-density matrix, is given by

$$N_{pq}(t) = \langle \Psi_0 | \hat{a}_p^\dagger \hat{a}_q | \Psi_0 \rangle - \langle \Phi_i | \hat{a}_p^\dagger \hat{a}_q | \Phi_i \rangle + \sum_{I,J} x_I \langle I | \hat{a}_p^\dagger \hat{a}_q | J \rangle x_J [1 - \cos((E_I - E_J)t)]. \quad (2.7)$$

Diagonalizing the hole-density matrix $\mathbf{N}(t)$ at each time point t leads to

$$Q(\vec{r}, t) = \sum_p |\tilde{\varphi}_p(\vec{r}, t)|^2 \tilde{n}_p(t), \quad (2.8)$$

where $\tilde{\varphi}_p(\vec{r}, t)$ are called *natural charge orbitals*, and $\tilde{n}_p(t)$ are their *hole-occupation numbers*. The hole-occupation number, $\tilde{n}_p(t)$, contains the information what part of the initially created hole charge is in the natural charge orbital $\tilde{\varphi}_p(\vec{r}, t)$ at time t . At each instant of time the natural charge orbitals are different linear combinations of the initial orbital basis $\{\varphi_p(\vec{r})\}$.

From the definition of the hole density, Eq. (2.1), it is clear that $Q(\vec{r}, t)$ is normalized at all times, namely

$$\int d\vec{r} Q(\vec{r}, t) = 1,$$

which leads to the following relation for the hole-occupation numbers:

$$\sum_p \tilde{n}_p(t) = 1.$$

The hole-occupation numbers, together with the natural charge orbitals, are central quantities in the analysis and interpretation of the multielectron dynamics taking place after the removal of an electron.

The description of the electron dynamics following ionization via the above defined hole density implies that the process of ionization and the rearrangement of the electronic cloud during this process are not taken into account. In other words, we suppose that the ionized electron is removed from the system on a much shorter time scale than that of the triggered electron dynamics and, therefore, the initially created ionic state can be described by a separable manyelectron wave function neglecting the interaction between the ionized

electron and the remaining ionic core. This is the so-called sudden approximation (see, e.g., Refs. [57, 58]). Such a situation can be realized when the ionization is performed, for example, by a high-energy photon (well above the corresponding ionization threshold) such that the removed electron has a high kinetic energy and thus leaves rapidly the interaction volume. In the weak-field regime, the pulse length will not play a role in the preparation of the state, as long as the intensity is weak enough such that the probability for multiphoton absorption is low. In the strong-field regime, in which multiphoton processes can take place, in addition to the photon energy the pulse length becomes important. To minimize the probability of multiphoton absorption, the pulse should be extremely short, e.g., with a sub-femtosecond duration. In both cases, however, in order to observe field-free charge dynamics, it is preferable that the ionizing pulse is as short as possible.

2.2 Choice of cationic basis and initial state

If as a one-particle basis $\varphi_p(\vec{r})$ we use natural orbitals that diagonalize the density matrix [59, 60], the first term in Eq. (2.7) will be simply $n_p\delta_{pq}$, with n_p being the occupation number of orbital $\varphi_p(\vec{r})$. One would get the same result if $\varphi_p(\vec{r})$ are Hartree-Fock (HF) orbitals and one assumes a weakly correlated ground state, i.e., $|\Psi_0\rangle \approx |\Phi_0\rangle$, where with $|\Phi_0\rangle$ we denote the uncorrelated HF ground state. For the ease of presentation and for keeping the discussion as transparent as possible, we will assume that the system is ionized out of a weakly correlated ground state. We note, however, that the methodology presented is not restricted to such cases. In what follows we will also exclusively use HF orbital basis, since it provides the most natural one-particle picture of ionization¹.

Equation (2.7) is further simplified if we suppose that the initial cationic state is created via a removal of an electron from a single orbital, i.e. $|\Phi_i\rangle = \hat{a}_i|\Phi_0\rangle$. This particular choice of initial state will reduce the second term in Eq. (2.7) to $n_p\delta_{pq} - \delta_{pi}\delta_{qi}$, bringing the hole-density matrix to the following simpler form

$$N_{pq}(t) = \delta_{pi}\delta_{qi} + \sum_{I,J} x_I \langle I | \hat{a}_p^\dagger \hat{a}_q | J \rangle x_J [1 - \cos((E_I - E_J)t)]. \quad (2.9)$$

The initial state can, of course, be constructed such that it corresponds to a removal of an electron from a linear combination of HF orbitals. This allows one to reproduce the hole density of practically every particular initial vacancy. In this case the first term in Eq. (2.9) will be $\sum_r w_r \delta_{pr} \delta_{qr}$ with w_r being the weight with which each orbital contributes to the initial hole density and satisfying the normalization condition $\sum_r w_r = 1$. However, to avoid investigating many linear combinations of HF orbitals of interest in what follows we will assume that the initial hole is created by removal of an electron from a specific HF orbital. In this way we can unambiguously identify the basic mechanisms leading to charge migration (see Chapter 3). Since the time-dependent Schrödinger equation which governs the electron dynamics is a linear equation, these mechanisms are also operative when other choices of initial states are used.

¹Within the Hartree-Fock theory the many-body corrections to the ionization energies begin to contribute at a higher order of perturbation theory than with other choices of approximations [59].

As we mentioned in the preceding Section, in our approach we suppose that the ionization is performed on an ultrashort time scale. Irrespective of the particular way of ionization, in the sudden ionization limit the remaining electrons will not have time to relax and therefore one may assume that the electron is removed from a single molecular orbital, being a result of an independent-particle model. Since, as we noted, the Hartree-Fock approximation provides the best independent-particle theory to describe the ionization, we may assume that the initial hole created upon sudden ionization is described favorably by a HF-orbital. We have to note that the time needed for the other electrons to respond to a sudden creation of a hole is about 50 asec [8] (see also Ref. [61]). It was shown [8] that this time is universal, i.e. it does not depend on the particular system, and as such appears as the time scale of the electron correlation. Thus, in practice, sudden ionization is equivalent to ionization performed faster than the electron correlation. Although so short laser pulses are still not available (as we mentioned above the shortest pulse reported in the literature is ~ 80 asec [20]), we believe that in the not-so-distant future one will be able to approach this limit experimentally.

Let us now discuss the question about the choice of cationic states $|I\rangle$ needed for constructing the hole-density matrix. Since the exact cationic states and energies are not at our disposal, appropriate approximations for these quantities have to be used.

The simplest approximation for obtaining the hole density is to use the Hartree-Fock method. For the ground state of the system one can use the single-determinant HF ground state $|\Phi_0\rangle$, while for the cationic states the one-hole (1h) configurations with respect to $|\Phi_0\rangle$. In this case, the cationic states are constructed by removing an electron from an occupied orbital, i.e. $|I\rangle = \hat{a}_k|\Phi_0\rangle$. The ionization energies of these states are simply the HF orbital energies ε_k (Koopmans' theorem [59]). Therefore, the hole-density matrix will get the form

$$N_{pq}(t) = \delta_{pi}\delta_{qi} + x_px_q[1 - \cos((\varepsilon_p - \varepsilon_q)t)]n_pn_q. \quad (2.10)$$

We see that because of the factor n_pn_q , only occupied orbitals participate in possible charge dynamics. However, the hole density will be time-dependent only if the involved orbitals have non-vanishing transition amplitudes x_p between the initially prepared cationic state and the cationic basis used. Within the Hartree-Fock approach and Koopmans' approximation the transition amplitudes reduce to Kronecker delta symbols ($x_p = \langle\Phi_i|I\rangle = \langle\Phi_0|\hat{a}_i^\dagger\hat{a}_p|\Phi_0\rangle = \delta_{ip}$) and, therefore, the time-dependent term in Eq. (2.10) vanishes. As the combined Hartree-Fock and Koopmans' approximation defines the situation in which the electron correlation and electron relaxation effects are exactly absent (independent-particle model) [59], this result leads to the important statement that *in the absence of electron correlation and relaxation the hole charge will stay in the orbital in which it is originally created and no charge migration will take place* [6]. In other words, the charge-migration phenomenon that we will discuss in the following Chapters is *solely* due to the many-body effects, namely the electron correlation and electron relaxation.

Of course, one could use other single-determinant approaches, for instance, solving the HF equations for the cationic system and using the cationic orbitals as approximations for the states $|I\rangle$. In this case, $x_p \neq \delta_{ip}$ and the hole density will evolve in time. However, in practice, this approach is limited to cases in which the initial cationic state is prepared

by a removal of the electron from the highest occupied molecular orbital (HOMO), as it is usually very difficult to converge the HF equations to a desired excited cationic state (having a hole in a desired molecular orbital of the neutral system). More importantly, such an approach takes into account only the orbital relaxation and still considers the electrons as uncorrelated. In the vast majority of cases, including only the orbital relaxation effects will be insufficient to describe the electron dynamics following ionization of a many-electron system (for an illustrative example, see Ref. [62], which is P6 from the attached papers).

In this respect, it is tempting to turn towards density functional theory (DFT), since in many applications DFT yields reasonably accurate results at moderate computational cost, and, at least in theory, fully accounts for the electron correlation and relaxation. Indeed, such an approach was recently proposed [63, 64] in which the cationic states $|I\rangle$ were approximated by Kohn-Sham (KS) orbitals [65] resulting from solving the cationic KS-DFT equations [66]. However, in a detailed numerical analysis [62] we showed that the conventional KS-DFT methods are inherently inapt to describe correctly the electron dynamics following ionization due to the well-known self-interaction error [67]. The incomplete cancellation of the self-interaction in the conventional exchange-correlation functionals leads to an unphysical delocalization of the orbital of the unpaired electron [68] and thus to spurious charge oscillations between different moieties of the ionic system even when these moieties practically do not interact [62]. We would like to note that although various schemes for construction of self-interaction-free functionals exist in the literature (see, e.g., Refs. [69–71]), single-determinant approaches based on DFT appear to be not adequate for describing electron dynamics following ionization owing to the unclear physical meaning of the KS orbitals. The correct time-propagation of the hole density implies the use of exact (or reasonable approximation of) cationic electronic states as a basis rather than cationic or neutral SCF orbitals.

We should add to the above analysis another serious drawback of all single-determinant methods. These approaches are by definition unable to describe an important class of ionic states, namely the so-called satellites or shake-up states (see Chapter 3 below), which further reduces their applicability. We may conclude that for a meaningful investigation of electron dynamics following ionization, the inclusion of many-body effects is indispensable and, therefore, one has to go beyond the single-determinant approximation for the ionic states $|I\rangle$ needed for constructing the hole-charge density.

One possibility to include many-body effects in the construction of cationic states $|I\rangle$ is to expand the wave function in electronic configurations as it is traditionally done in the configuration-interaction (CI) formalism [59]. Using the HF based configurations, the CI expansion of the cationic state reads

$$|I\rangle = \sum_j c_j^{(I)} \hat{a}_j |\Phi_0\rangle + \sum_{a,k<l} c_{akl}^{(I)} \hat{a}_a^\dagger \hat{a}_k \hat{a}_l |\Phi_0\rangle + \dots, \quad (2.11)$$

where $c^{(I)}$'s are the expansion coefficients. In Eq. (2.11), as well as throughout the text, the indices a, b, \dots refer to unoccupied (virtual) orbitals (or particles), whereas the indices i, j, \dots indicate occupied orbitals (or holes)¹. Accordingly, the terms $\hat{a}_j |\Phi_0\rangle$ are

¹We will reserve p, q, \dots for general indices.

the one-hole configurations mentioned above, since one electron has been removed from the corresponding occupied orbital, the terms $\hat{a}_a^\dagger \hat{a}_k \hat{a}_l |\Phi_0\rangle$ are referred to as two-hole-one-particle (2h1p) configurations, indicating that in addition to the removal of one electron another one is excited to a virtual orbital, and so forth.

Since the states $|I\rangle$ are eigenstates of the cationic Schrödinger equation they can be chosen orthonormal, $\langle I|J\rangle = \delta_{IJ}$. In practice, the states $|I\rangle$, as well as the corresponding ionization energies E_I , are obtained by diagonalizing the cationic Hamiltonian matrix. Using the orthonormality condition and the standard second-quantization formalism of the creation and annihilation operators, the term $\langle I|\hat{a}_p^\dagger \hat{a}_q|J\rangle$ of Eq. (2.9) can easily be evaluated. For every pair of $|I\rangle$ and $|J\rangle$ it represents a matrix whose elements are functions of the expansion coefficients $c^{(I)}$ and $c^{(J)}$. The explicit form of this matrix can be found in Refs. [7, 72].

The CI method is only one of the approaches that can be used for obtaining the cationic eigenstates. In fact, it is not a very practical one since, as a rule, the CI calculations are very demanding, due to the extended configuration space involved, and the lack of size-consistency represents an additional obstacle for obtaining meaningful results in applications to large systems consisting of well separated moieties. The CI form of the cationic states, Eq. (2.11), is, however, very transparent and helpful for analysis, as we will see in Chapter 3.

A very suitable alternative are the one-particle many-body Green's function methods. The Green's function (GF) methods possess numerous computational and interpretative advantages in calculating ionization energetics, and reduce the problem to the diagonalization of an effective, relatively compact Hermitian matrix [73–75]. An important advantage of the GF-based methods, compared to the wave-function-based ones (like CI), is that they allow one to compute the entire spectrum of ionic states of the system in a single run. A computationally very successful approach to obtain the Green's function is the *algebraic diagrammatic construction* (ADC(n)) scheme which represents infinite partial summations being exact up to n -th order of perturbation theory [73, 74]. A point to stress in this connection is that the perturbative character of the method applies only to the ground state of the system and *not* to the final states which are treated non-perturbatively [76]. The ADC method leads to cationic states in the form (2.11), except that the 1h, 2h1p, etc. configurations are with respect to the *exact* ground state $|\Psi_0\rangle$, rather than with respect to the uncorrelated HF determinant $|\Phi_0\rangle$.

However, despite of their compactness, the resulting ADC matrices, depending on the size of the system, the orbital basis set and the approximation scheme used, can become extremely large. This reduces the applicability of the approach to relatively small systems, or to moderate basis sets. An alternative approach allowing treatment of larger systems is presented in the next Section.

2.3 Direct propagation

Until now we have assumed that one can diagonalize the cationic Hamiltonian matrix and using the eigenstates $|I\rangle$ and eigenenergies E_I to compute the hole density via Eqs. (2.6)–

(2.8). However, as we mentioned above, depending on the size of the system and the one-particle basis set used the size of the Hamiltonian secular matrix can become extremely large making the full-diagonalization approach prohibitively expensive. A way to overcome this problem is to use the parallel filter diagonalization method [77], which give access to the eigenvectors and the eigenenergies located in a specific spectral range. Those states can be further used in the construction of the hole density. This approach supposes, however, some preliminary knowledge of the structure of the spectrum and of the specific spectral range of interest which is not always possible, especially for larger and more complicated systems. A much more suitable alternative is to use a direct-propagation technique, a method known as multielectron wave-packet propagation [78], P1 in the attached papers. Let us see how this can be achieved.

Suppose that we have at our disposal cationic states $|\tilde{\Psi}_M\rangle$ that form a complete basis but are not eigenstates of the cationic Hamiltonian. In this case, the time-dependent part of the hole density, Eq. (2.2), can be rewritten as

$$\begin{aligned}\rho_i(\vec{r}, t) &= \sum_{M,N} \langle \Phi_i | e^{i\hat{H}t} | \tilde{\Psi}_M \rangle \langle \tilde{\Psi}_M | \hat{\rho}(\vec{r}, 0) | \tilde{\Psi}_N \rangle \langle \tilde{\Psi}_N | e^{-i\hat{H}t} | \Phi_i \rangle \\ &= \sum_{M,N} \langle \Phi_i(t) | \tilde{\Psi}_M \rangle \rho_{MN} \langle \tilde{\Psi}_N | \Phi_i(t) \rangle,\end{aligned}\quad (2.12)$$

where ρ_{MN} is the matrix representation of the density operator in the cationic basis, and $|\Phi_i(t)\rangle = e^{-i\hat{H}t}|\Phi_i\rangle$ is the propagating multielectron wave packet.

Again, using the standard representation of the density operator in one-particle basis $\{\varphi_p(\vec{r})\}$ and occupation numbers $\{n_p\}$, the hole-charge density $Q(\vec{r}, t)$ can be brought to the form of Eq. (2.6) with the hole-density matrix being

$$N_{pq}(t) = \delta_{pq}n_p - \sum_{M,N} \langle \Phi_i(t) | \tilde{\Psi}_M \rangle \rho_{MN}^{pq} \langle \tilde{\Psi}_N | \Phi_i(t) \rangle,\quad (2.13)$$

where ρ_{MN}^{pq} stands for

$$\rho_{MN}^{pq} = \langle \tilde{\Psi}_M | \hat{a}_p^\dagger \hat{a}_q | \tilde{\Psi}_N \rangle.\quad (2.14)$$

The diagonalization of this matrix at each time point will again lead to the desired form of the hole-charge density, Eq. (2.8), expressed through time-dependent natural charge orbitals $\tilde{\varphi}_p(\vec{r}, t)$ and hole-occupation numbers $\tilde{n}_p(t)$.

A particularly suitable approach, giving a direct access to the quantities needed for the practical realization of the above sketched scheme for constructing the hole density, is the so-called non-Dyson ADC method [79] for computing the one-particle Green's function. This method, in which, contrary to the original ADC mentioned in the previous Section, the Dyson equation needs not to be solved, leads to a substantial reduction of the secular-matrix dimension opposed by a small additional expense in computing some higher order contributions to the secular-matrix elements. The scheme uses the so-called *intermediate state representation* (ISR) [76, 80] of the secular matrix, yielding the construction of a complete basis through successive Gram-Schmidt orthogonalization of different classes of correlated excitations.

Two important features of this approach should be pointed out. First, contrary to the Dyson schemes, in which the configuration space comprises of both $(N - 1)$ - and $(N + 1)$ -electron configurations, in the non-Dyson ADC method one has a complete decoupling of the ionization and affinity blocks yielding, among others, a substantial reduction of the problem dimension. Second, and more importantly, the non-Dyson scheme is realized within a complete multielectron basis (the ISR basis) which makes it possible to calculate different physical properties [81], because we can represent their operators in the ISR basis. The latter gives the possibility to compute ρ^{pq} , Eq. (2.14), needed to construct the hole-density matrix, Eq. (2.13). Therefore, the complete set of ISR states is used as the cationic basis $|\tilde{\Psi}_M\rangle$ introduced above.

The fact that the Hamiltonian matrix constructed via the non-Dyson ADC method contains information only about the $(N - 1)$ -particle space allows to use it for propagating the initial cationic state. This can be done, for example, through the short-iterative Lanczos time-propagation technique [82–84]. The idea behind the Lanczos algorithm is that the large Hamiltonian matrix can be reduced through its projection on the so-called Krylov space and the succeeding propagation can be performed within this much smaller Krylov subspace. In other words, the Lanczos algorithm replaces the expensive full (or partial) diagonalization of the large ADC matrix, and the consecutive time propagation of the eigenvalues, by a repetitive diagonalization of much smaller tridiagonal matrices.

Details of the multielectron wave-packet propagation technique and working formulas can be found in Ref. [78], P1 of the attached papers.

Chapter 3

Basic mechanisms

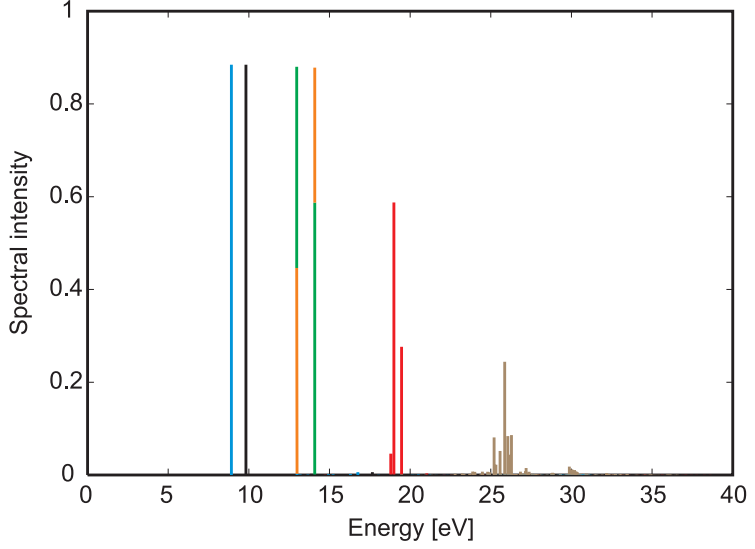
The general case of electron dynamics solely driven by the electron correlation is difficult to understand due to the many effects that can contribute. This makes sometimes the numerical calculation based on the above described methodology difficult to analyze. For that reason, it is useful to examine cases in which the dynamics are governed by a single mechanism. It appeared that there is an intimate relationship between the ionization spectrum of the system and electron dynamics that can be expected after removing of an electron from a particular orbital [7]. That is why it is illuminative to take a closer look at a typical ionization spectrum.

A typical ionization spectrum of a molecule computed at fixed nuclear geometry is given in Fig. 3.1. It consists of vertical lines, where each line represents a cationic eigenstate $|I\rangle$, see Eq. (2.11), positioned at the corresponding ionization energy E_I . The intensity, or the height, of each line is given by the transition amplitude, $x_I = \langle I|\hat{a}_i|\Psi_0\rangle$, a quantity closely related to the partial-channel ionization cross section [85]. Within the assumption of weakly correlated ground state, i.e. $|\Psi_0\rangle \approx |\Phi_0\rangle$, it is clear that only the 1h configurations ($\hat{a}_k|\Phi_0\rangle$) will contribute to the transition amplitude x_I .

Without correlation effects in the ion, i.e. within an independent particle model, the spectrum will consist of a finite series of lines, one for every occupied in the ground state orbital φ_i , with intensities equal to 1, and positioned at the corresponding orbital energies ε_i (Koopmans' theorem). If correlation effects are weak — and this is typically the case in the outer-valence shells of the system — the ionization spectrum will consist of *main lines* which have large overlap with the 1h configurations (see the 4 lowest in energy lines in Fig. 3.1). In this case the molecular orbital picture is still valid.

If the correlation effects are stronger, beside the main line *satellite lines* may appear (see the group of lines depicted in red in Fig. 3.1) representing excitations on top of the ionization. The intensities of the satellite lines are weaker than those of the main lines since they correspond to cationic states that are dominated by 2h1p configurations and have only small or moderate overlap with the 1h configurations. Two types of satellites can be distinguished [85]: *relaxation satellites* where at least one of the two holes in the 2h1p configuration is identical to the 1h orbital of the main line, and *correlation satellites* where both holes differ from the 1h orbital of the main line. For completeness, we mention here

Figure 3.1: Typical ionization spectrum of a molecule. Each vertical line is related to a cationic eigenstate and is located at the corresponding ionization energy. The height of the lines, or the spectral intensity, is given by the square of the transition amplitude. The different colors in the lines correspond to the contributions of different 1h configurations, describing an electron missing from a particular orbital.



that there is a third type of satellites, the *ground-state-correlation satellites*, stemming from the correlation effects present in the ground state of the neutral, but we will not discuss them further in this work because if the ground-state correlation effects are not strong such kind of states will be very weakly populated by the ionization process.

In the inner valence, where the correlation effects are strong, the distinction between the main lines and the satellites ceases to exist and the spectrum becomes a quasi-continuum of lines with small to moderate intensities. This phenomenon is known as breakdown of the molecular orbital picture of ionization [85].

Depending on the structure of the ionic states involved, three basic mechanisms of charge migration have been identified [7]: the hole-mixing case, the dominant-satellite case, and the breakdown-of-the-molecular-orbital-picture case. In what follows we will briefly describe them and discuss also a new one which was identified and studied within the present work.

(i) **Hole-mixing case.** For simplicity, we will consider the two-hole mixing, i.e. the situation when two lines in the spectrum correspond to ionic states which are linear combinations of two 1h configurations. In Fig. 3.1 these are the third and the fourth line where the contributions of the different 1h configurations are shown with different colors — orange for say a hole in orbital φ_i , and green for hole in φ_j . These two states can be written as

$$\begin{aligned} |I\rangle &= c_1 \hat{a}_i |\Phi_0\rangle + c_2 \hat{a}_j |\Phi_0\rangle, \\ |J\rangle &= c_2 \hat{a}_i |\Phi_0\rangle - c_1 \hat{a}_j |\Phi_0\rangle, \end{aligned}$$

where, due to the orthonormality of the states, the two coefficients c_1 and c_2 satisfy the equation $c_1^2 + c_2^2 = 1$. In this idealized case, if we create the initial hole in one of the orbitals, say φ_i , it can be shown easily [7] that the hole-occupation numbers will take the following form:

$$\tilde{n}_{i/j}(t) = \frac{1}{2} \pm \frac{1}{2} \sqrt{1 - 4(c_1 c_2)^2 \sin^2(\omega_{IJ} t)}, \quad (3.1)$$

where ω_{IJ} is the difference between the energies of the two lines in the spectrum, i.e., $\omega_{IJ} = (E_I - E_J)$. As can be seen, in this case the hole will oscillate between the two natural charge orbitals $\tilde{\varphi}_i(\vec{r}, t)$ and $\tilde{\varphi}_j(\vec{r}, t)$ with a frequency ω_{IJ} . It has to be mentioned again that the hole-occupation numbers give the occupation of the natural charge orbitals which at each time point are different linear combinations of the HF orbitals φ_i and φ_j . The time-evolution of the hole-occupation numbers for this case is shown in Fig. 3.2 where the contributions of the HF orbitals to the natural charge orbitals are color encoded. We see that at each odd quarter cycle an avoided crossing of the hole occupations $\tilde{n}_i(t)$ and $\tilde{n}_j(t)$ appear and the two natural charge orbitals interchange their character. Therefore, the charge dynamics represent oscillation between the two HF orbitals φ_i and φ_j involved in the hole mixing. If these two orbitals are localized on two different sites of the system, the hole-mixing mechanism will lead to an oscillation of the initially created positive charge between these two sites.

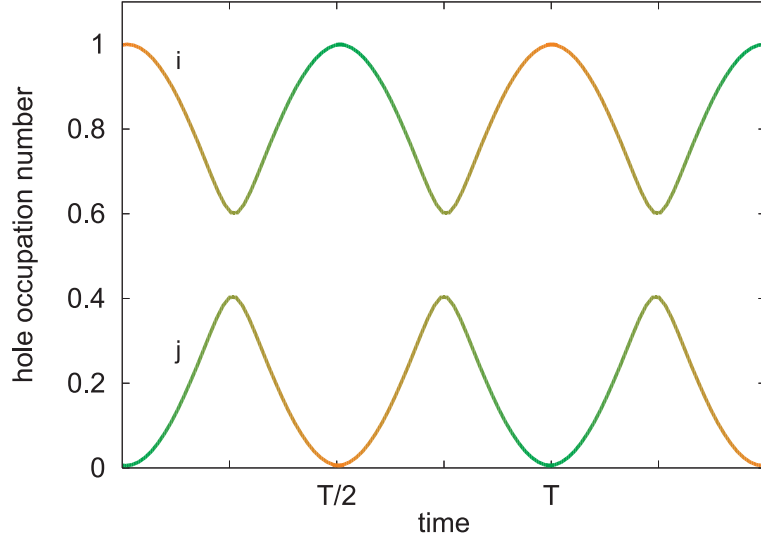


Figure 3.2: Time-evolution of the hole-occupation numbers in the case of two-hole mixing. The contributions of the two Hartree-Fock orbitals (φ_i and φ_j) to the natural charge orbitals ($\tilde{\varphi}_i$ and $\tilde{\varphi}_j$) are color encoded. As seen, at each odd quarter period an avoided crossing takes place and the character of the two natural charge orbitals is swapped. Within the first half period the initially ionized orbital (φ_i) “loses” its hole charge, which is transferred to the other orbital involved in the hole mixing (φ_j).

(ii) **Dominant-satellite case.** Let us consider the situation when we have two ionic states, a main state and a satellite, both having overlap with the original 1h configuration. In CI language these states can be written as

$$|I_m\rangle = c_1 \hat{a}_i |\Phi_0\rangle + c_2 \hat{a}_a^\dagger \hat{a}_k \hat{a}_l |\Phi_0\rangle, \quad (3.2a)$$

$$|I_s\rangle = c_2 \hat{a}_i |\Phi_0\rangle - c_1 \hat{a}_a^\dagger \hat{a}_k \hat{a}_l |\Phi_0\rangle, \quad (3.2b)$$

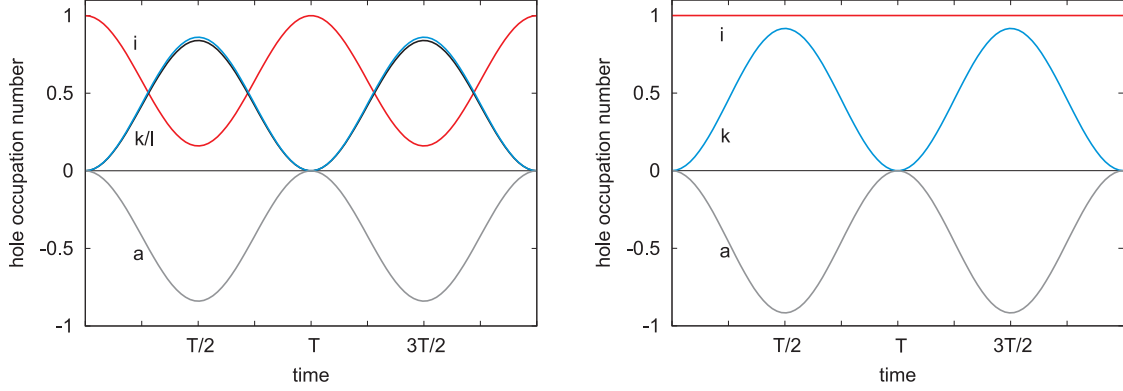


Figure 3.3: Time-evolution of the hole-occupation numbers in the case of dominant correlation satellite (left graph) and dominant relaxation satellite (right graph). In both cases the coefficients c_1 and c_2 are chosen to be $\sqrt{0.7}$ and $\sqrt{0.3}$, respectively. For convenience, in the dominant correlation satellite case the $\tilde{n}_k(t)$ and $\tilde{n}_l(t)$ curves are artificially made to differ slightly from each other.

where again the two coefficients c_1 and c_2 satisfy the equation $c_1^2 + c_2^2 = 1$.

As was mentioned above, two situations can be distinguished. When all involved occupied orbitals φ_i , φ_k , and φ_l are different, i.e. the case of a correlation satellite, and when one of the holes in the 2h1p configuration is identical to the that of the 1h configuration ($k = i$ or $l = i$), i.e. the case of a relaxation satellite. In the correlation-satellite case, one gets the following expressions for the hole-occupation numbers [7]:

$$\tilde{n}_i(t) = 1 - 2(c_1 c_2)^2 (1 - \cos \omega t), \quad (3.3a)$$

$$\tilde{n}_k(t) = \tilde{n}_l(t) = -\tilde{n}_a(t) = 2(c_1 c_2)^2 (1 - \cos \omega t), \quad (3.3b)$$

where $\omega = E_{I_m} - E_{I_s}$ and the initial ionization is performed from orbital φ_i . As seen, the dynamics are again oscillatory with a period determined by the energy differences between the states $|I_m\rangle$ and $|I_s\rangle$. The hole initially localized on orbital φ_i will migrate to the orbital φ_k (or φ_l) accompanied by an excitation from orbital φ_l (or φ_k) to the virtual orbital φ_a . The time-evolution of the hole-occupation numbers in this case is shown in the left panel of Fig. 3.3. One can imagine several different situations in which, depending on the spatial localizations of the four orbitals involved, the net positive charge can migrate between different sites of the system.

In the case of a relaxation satellite, for example when $l = i$ in Eqs. (3.2), one observes different dynamics [86], see P7 from the attached papers. The hole-occupation numbers in this case will be [86]

$$\tilde{n}_i(t) = 1, \quad (3.4a)$$

$$\tilde{n}_k(t) = -\tilde{n}_a(t) = 2c_1 c_2 \sin^2(\omega t/2). \quad (3.4b)$$

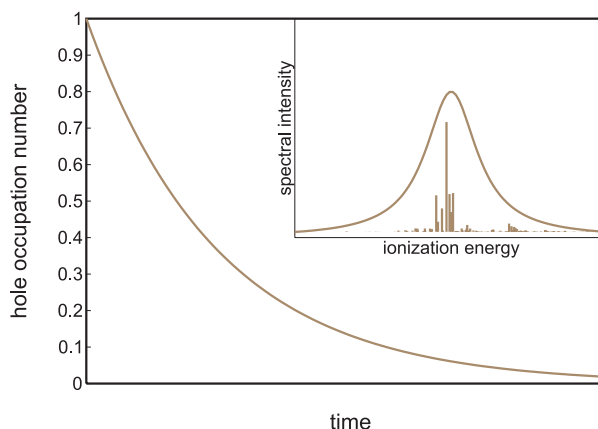


Figure 3.4: Time-evolution of the hole-occupation number of the initially ionized orbital in the case of a breakdown of the molecular orbital picture. For a continuous Lorentzian line shape in the ionization spectrum, the hole occupation of the initially ionized orbital will decay exponentially.

The hole initially localized on orbital φ_i will stay put, while an excitation-deexcitation alternations between orbitals φ_k and φ_a will take place with an oscillation period determined by the energy difference between the main state and the relaxation satellite. The time-evolution of the hole-occupation numbers in this case is shown in right panel Fig. 3.3.

Although the relaxation satellite does not affect the dynamics of the initial hole charge itself (the initial hole remains stationary), depending on the spatial distribution of the orbitals involved the dominant relaxation satellite mechanism can still lead to a charge migration via hole screening. If the electron is ejected from a localized orbital i and the unoccupied orbital a is localized in the same region of space then promoting an electron to the orbital a will cancel out in physical space the initially created hole in orbital i , i.e. the initial hole will be “screened” by the excitation $k \rightarrow a$. Thus, in the idealized case when the orbitals i and a are localized on one site of the system, while the orbital k is localized on a different site, the dominant relaxation satellite mechanism will lead to oscillations in the real space of the total hole charge between these two parts of the system.

(iii) **Breakdown of the molecular orbital picture case.** In the inner-valence region of the spectrum, where the quasi-continuum of lines appears, one can distinguish two general cases depending on whether the states are below or above the double ionization threshold of the system. Supposing that the quasi-continuum of states has a Lorentzian shape, in both cases the initially ionized orbital will “lose” its positive charge exponentially with time. This behavior is depicted in Fig. 3.4. If the states are below the double-ionization threshold, the charge will be typically shared among many other orbitals and at the end of the process will be spread more-or-less uniformly over the whole cation. If the states are above the double ionization threshold, i.e. an electronic decay channel is open, this mechanism will describe the process of emission of a secondary electron. In this case an electron from a higher orbital will fill the initial hole and a secondary electron will be

ejected from another orbital into the continuum.

Finally, we would like to stress again that if the removal of the electron from a particular orbital populates only a single state, like the pure 1h states show in blue and black in Fig. 3.1 (the first two lowest in energy states), the charge will stay put where it is originally created and no electron dynamics can be expected. Such a situation is usually realized after ionization out of the outermost shells of a molecule. However, as we will see in the next chapter, there are systems in which the electron correlation is strong enough already in the outermost shell leading to rich dynamical effects.

Chapter 4

Results

In what follows we briefly present the most important results obtained. For details and further discussion the reader is referred to the attached papers.

4.1 Electron dynamics of electronically stable ionic states

4.1.1 Chain-like molecules

In the course of our study we have analyzed the electron dynamics triggered by ionization in a large variety of small to medium size molecules. We found that the charge-migration phenomenon usually takes place after ionization in the inner-valence shell where the electron correlation effects are typically much stronger than in the outer-valence. In many of the studied cases the positive charge initially localized on one end of the molecule can migrate to the other in only few femtoseconds jumping over entire chemical groups. An example of such a charge-migration behavior taking place after inner-valence ionization of the oligopeptide $\text{CH}_3\text{-NH-Gly-Gly}$ is shown in Fig. 4.1 [87] (see P12 from the attached papers). The figure depicts snapshots of the evolution during the first 6 fs of the hole density $Q(\vec{r}, t)$, see Eq. (2.1), following sudden ionization out of the orbital $28a'$. We see that starting from the methylamine site the charge almost completely migrates to the other side of the molecule in about 6 fs. The process then continues in a reverse order bringing the charge back to the methylamine site. However, these oscillations are not purely repetitive and exhibit a beating pattern due to the large number of ionic states involved. It is worth noting that the center of charge migrates more than 8 Å during the first 6 fs of the process.

The mechanism underlying this particular charge-migration process is a 4-hole mixing (see Chapter 3) since the ionization out of orbital $28a'$ populates coherently mainly four ionic states being themselves a linear combination of four different 1h configurations. Although it may appear from Fig. 4.1 that the positive charge flows along the molecular backbone, this is just a result of the spatial localization of the four orbitals involved in this particular case. Being a many-body phenomenon, the charge-migration process actually proceeds such that the hole charge which disappears from its initial position appears on its final one without showing up in between. The charge movement is actually mediated

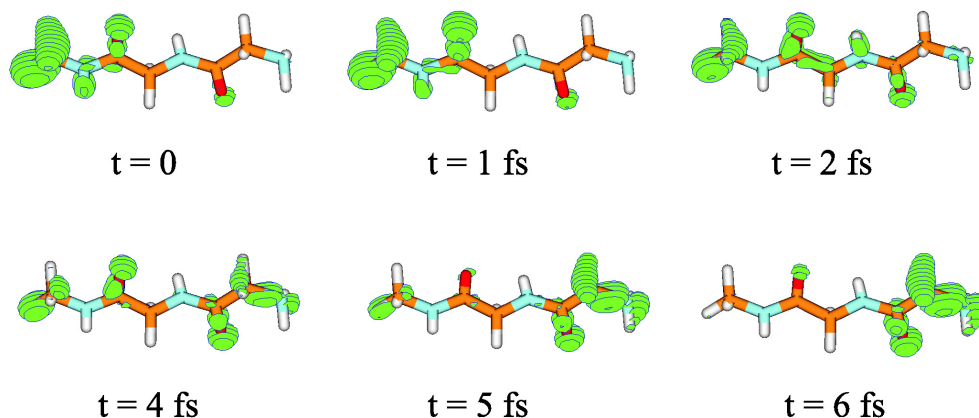


Figure 4.1: Snapshots of the evolution of the hole density $Q(\vec{r}, t)$ after ionization out of orbital $28a'$ of the C_s symmetric conformer of $\text{CH}_3\text{-NH-Gly-Gly}$ for the first 6 fs.

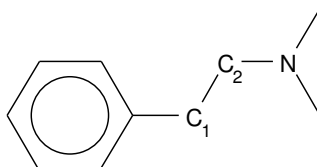
by the large number of $2h1p$ configurations to which the $1h$ configurations participating in the hole mixing are coupled.

An important question is whether the symmetry of the molecule plays a role in the charge-migration process. We have compared the charge-migration dynamics trigger by ionization of the same orbital in symmetric and non-symmetric conformers of the same molecule and found that in all studied cases a stronger migration of the charge takes place in the case of the symmetric system — larger amount of the charge migrates and/or it travels over longer distances. A possible explanation of this observation is that in the symmetric molecules the $2h1p$ configurations are more extended in space and, therefore, two remote orbitals can indirectly couple to each other via their direct interaction to these excitations. However, a more thorough study on the role of the symmetry on the charge migration is needed.

As we mentioned, the charge-migration process is usually triggered by an inner-valence ionization. We found, however, systems in which already in the outer-valence the electron correlation effects are strong enough such that they can beget a migration of the hole charge. The existence of such systems is very important from an experimental point of view, because they allow for a much better control. Indeed, a short pulse that is able to remove an electron from an inner-valence orbital and therefore to coherently populate the corresponding number of ionic states, will have enough energy to populate all the states lying lower in energy. Thus, in reality, the pulse will create an initial state being some linear combination of the $1h$ configurations corresponding to ionization out of the molecular orbitals contributing to all ionic states that are energetically accessible. The dynamical evolution of such an initial state will be, therefore, a superposition of the dynamics that one would expect if we were able to address each individual orbital separately, weighted by the corresponding probabilities. In the vast majority of cases, the states lying below the group of strongly coupled ionic states responsible for the charge migration will be $1h$ states, i.e. no electron dynamics can be triggered by their population. Nevertheless, their

contribution will somewhat blur the charge-migration signal making the whole dynamics much more difficult to analyze. That is why, from a practical point of view, it is desirable to perform experiments on systems in which the charge-migration process is triggered by an outer-valence ionization, for example by removing an electron from the HOMO.

An important example of such a system is the molecule 2-Phenylethyl-*N,N*-dimethylamine (PENNA), where a 3-hole mixing appears in the first 3 ionic states. Our study on this system (see the sketch) was motivated by the exciting experiments carried by Weinkauff, Schlag, and co-workers [88, 89], showing that after a local ionization of the chromophore site of PENNA molecule a bond breaking of the bridge between the chromophore and the amine sites occurs (C_1 - C_2 bond in the sketch) accompanied by a transfer of the positive charge to N-terminal fragment. The time of this process was reported to be 80 ± 28 fs [88].



In order to see how the positive charge created on the benzene ring evolves in time, we calculated the hole density $Q(\vec{r}, t)$ following the removal of an electron from the HOMO. In Fig. 4.2 the quantity $Q(z, t)$ is plotted, which is obtained from $Q(\vec{r}, t)$ after integration over the two remaining perpendicular axes. The axis z is chosen to pass through the longest spatial extension of the molecule and is denoted as “molecular axis”. The relative positions of the atoms along this axis are indicated. Figure 4.2a shows the evolution of the hole density calculated using the equilibrium geometry of the neutral molecule. At time 0 the charge is localized on the benzene ring and only after 4 fs a fraction of it has already migrated to the nitrogen (the hump on the right-hand side of the surface). Afterwards the charge returns mainly to its initial position and the whole process starts again.

First principles molecular dynamics simulations of the cationic ground state at DFT (BP86/SV(P)) level starting with the equilibrium geometry of the neutral indicate a stretching of the C_1 - C_2 bond of 0.05 \AA within the first 5 fs. This is the bond which was observed to break in the experiments of Weinkauff *et al.* [88, 89]. To gain an idea about the impact of this stretching on the charge migration, we calculated the hole density and traced the hole migration at several different geometries along the dissociation path. It was observed that more and more charge migrates to the N-terminal as the C_1 - C_2 bond elongates. This is clearly seen from Fig.4.2b where the hole density for a geometry in which the C_1 - C_2 bond is elongated by 0.2 \AA is displayed. One clearly sees that in this case almost the entire charge is transferred from the chromophore to the N-terminal, and this again within 4 fs.

Our conclusion is that in this case one observes a strong interplay between the purely electronic charge-migration process and the nuclear dynamics. The localized initial ionization of the chromophore triggers an ultrafast charge migration and some part of the positive charge starts to bounce between the chromophore and the N-terminal. As time

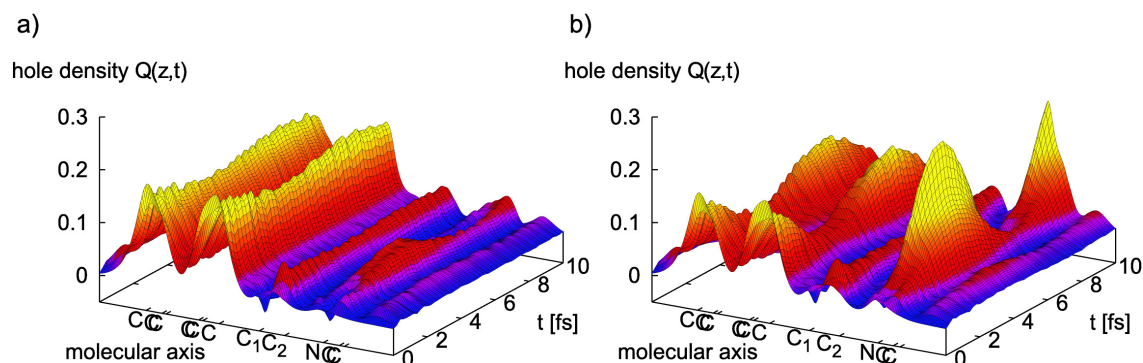


Figure 4.2: Time-evolution of the hole density $Q(z,t)$ of PENNA plotted against the longest spatial extension of the molecule z , termed “molecular axis”, after outer-valence ionization. $Q(z,t)$ is obtained by integrating the total charge over the coordinates perpendicular to the z axis. (a) at the ground-state geometry of the neutral. (b) at the geometry in which the C_1 - C_2 bond elongated by 0.2 \AA .

proceeds, the nuclear dynamics enter the picture and with the elongation of the C_1 - C_2 bond more and more charge oscillates between the two sites. These oscillations are not perfect, due to dissipation caused by the participation of many electronic states and nuclear dynamics, and when the bond breaks the charge is trapped at the energetically more favorable N-terminal fragment, i.e. the molecule dissociates into $C_6H_5CH_2$ radical and $H_2CN(CH_3)_2$ cation.

The results for the dynamics triggered by outer-valence ionization of PENNA molecule were collected and published in *Chemical Physics Letters*, Ref. [35], see P4 from the attached papers.

In a separated study we investigated the dependence of the charge-migration phenomenon on the donor site. For this purpose we compared the electron dynamics triggered by outer-valence ionization of PENNA with its Butadiene (MePeNNA) and Ethylene (BUNNA) derivatives. The molecules have different chromophore-donor sites, but nearly identical amine-acceptor sites (see Fig. 4.3).

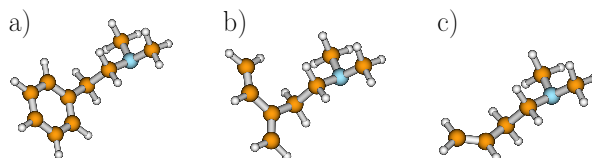


Figure 4.3: Ground-state structures of the molecules (a) PENNA, (b) MePeNNA, and (c) BUNNA.

The results showed that the charge-migration process depends strongly on the particular donor site, varying from ultrafast migration of the entire charge from the donor

to the acceptor site (4 fs for MePeNNA) to no migration at all (for BUNNA). The influence of the geometrical structure of the molecule on the charge migration was also investigated showing that energetically closely lying conformers may exhibit dramatically different charge-migration behavior. The results of this study were published in *Journal of Chemical Physics*, Ref. [34], see P5 from the attached papers.

The analysis of the charge-migration process in different conformers was a continuation of our previous study published in *Chemical Physics*, Ref. [33] (P3 from the attached papers). In this work we investigated the importance of the momentary nuclear geometry by tracing the charge migration following ionization out of three different orbitals of three different glycine conformers. The results showed that in all three cases the migration is very much conformer dependent, and can vary from an ultrafast migration of the hole charge (few femtoseconds) to a very slow migration (hundreds of femtoseconds), or even to no migration at all. Such dissimilarities in the electron dynamics following ionization are surprisingly strong in view of the fact that the studied glycine conformers differ mainly in the mutual orientation of the hydrogen atoms.

All results on the dependence of the charge migration on the particular nuclear geometry clearly show that the nuclear dynamics that will enter the picture at later times will play an important role, since the movement of the nuclei can trap the charge and block the migration process. If the charge is blocked at the remote end of the molecule, the entire process will represent a charge transfer on a very short time scale.

4.1.2 Non-chain-like molecules

In cases discussed above, the molecules possessed a chain-like structure and it was observed that the created positive charge can jump over one or even few C-C or C-N bonds. In this respect it is important to know whether the charge-migration phenomenon is inherent only to chain-like molecules. In order to study this issue we investigated the electron dynamics triggered by inner-valence ionization of the molecule 4-methylphenol, $(\text{CH}_3)\text{C}_6\text{H}_4(\text{OH})$, and showed that the ‘bridge’ between the two sites involved in the migration process does not need to possess a chain-like structure. We found that after a localized inner-valence ionization on the methyl group the hole charge jumps over the whole aromatic ring to the hydroxyl group in less than 2 fs (see Fig. 4.4).

Note also that in the course of its migration from the CH_3 to the OH group and back the charge does not flow throughout the molecule (the charge density on the benzene ring stays small), but rather jumps from side to side without showing up in between. As we commented above, this behavior is a typical signature of the many-body character of the charge-migration process.

The results of this study were published in *Journal of Physical Chemistry A*, Ref. [90], see P8 from the attached papers.

Another example of a non-chain-like molecule that we studied is the organic unsaturated nitroso compound 2-Nitroso[1,3]oxazolo[5,4-d][1,3]oxazole. It is known that this system possesses low-lying relaxation satellites [91] and we wanted to study the influence of such states on the electron dynamics (see Chapter 3). Our results showed that the initially created hole charge remains stationary but on top of it the system reacts by an

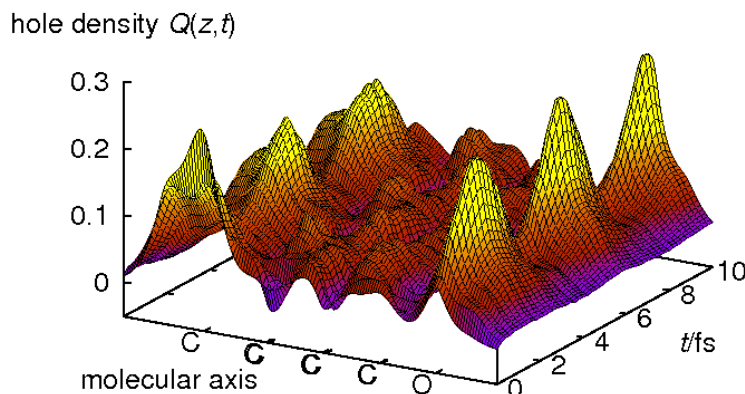


Figure 4.4: Time-evolution of the hole density $Q(z, t)$ along the longest spatial extension of the molecules 4-methylphenol following inner-valence ionization. Nearly the whole charge, initially located at the CH₃ group, migrates back and forth between the CH₃ and OH groups with a period of less than 4 fs. Note that the charge jumps over the whole aromatic ring.

ultrafast $\pi - \pi^*$ excitation followed by a cyclic excitation-deexcitation process leading to a redistribution of the charge. The $\pi - \pi^*$ excitation following the removal of the HOMO electron takes place on a sub-femtosecond time scale and the period of the excitation-deexcitation alternations is about 1.4 fs. In real space the processes of excitation and de-excitation represent ultrafast delocalization and localization of the charge. The results of this study were published in *Journal of Chemical Physics*, Ref. [86], see P7 from the attached papers.

Very recently, we studied also the electron dynamics following outer-valence ionization of the free-base porphyrin (H2-P) and Mg(II) porphyrin (Mg-P). Porphyrins play an important role in a large variety of biological and chemical processes. They are one of the key structures in photosynthesis, oxygen transport, or charge transfer, to name only a few. Of particular importance are the cation radicals of porphyrin-type molecules, known to be involved, for example, in the chemistry of the photosynthetic reaction center. In order to study the reactivity of the cationic porphyrin radicals, it is crucial to know how does the positive charge created upon ionization distribute throughout the molecular backbone.

Our results showed that due to the very strong correlation effects in these systems, giving rise to pronounced shake-down (correlation) satellites, the removal of an electron from an outer-valence orbital of H2-P and Mg-P leads to an ultrafast reorganization of the electronic cloud. After being initially localized on the B and D pyrrole rings, the hole charge created upon ionization spreads throughout the molecule in only few femtoseconds (see Fig. 4.5 where the example of H2-P is given). In both systems the electron dynamics triggered by the ionization represent alternating ultrafast delocalizations and localizations of the charge. The paper summarizing these results is currently in press in *Chemical Physics*, Ref. [92], see P10 from the attached papers.

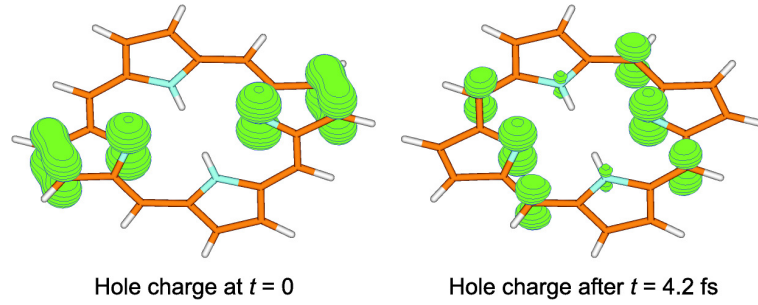


Figure 4.5: Snapshots of the evolution of the hole density $Q(\vec{r}, t)$ at times $t = 0$ and 4.2 fs after ionization of the HOMO-2 of the free-base porphyrin molecule.

4.2 Electron dynamics of electronically decaying ionic states

Employing the methodology developed we were able to trace in real time and space the evolution of the electronic cloud during the interatomic Coulombic decay process in NeAr following Ne2s ionization. As we mentioned in the Introduction, this fundamental decay process involves an ultrafast energy transfer between, in general, the ionized system and its environment. In the studied case of NeAr the ICD process proceeds as follows (see Fig. 4.6): A 2p electron from the neon atom fills the initial 2s vacancy, the gained energy is transferred to the neighboring argon atom who uses it to emit one of its 3p electrons.

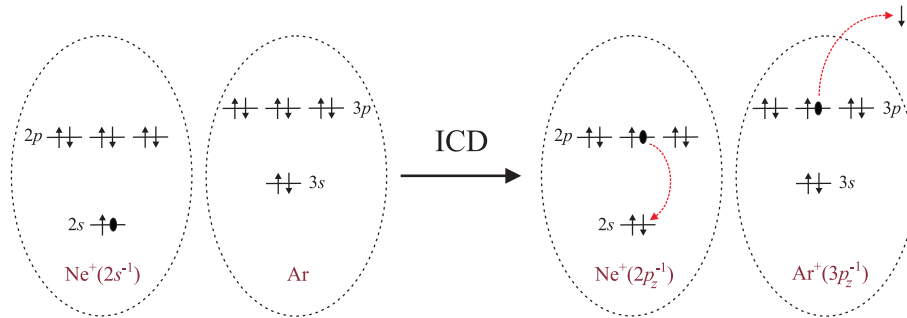


Figure 4.6: Schematic representation of the ICD process in NeAr following Ne2s ionization.

The major difficulty in applying the methodology presented in Chapter 2 for such cases is that the wave function of the decaying (continuum) electron is not square-integrable and, hence, very hard to be properly represented within \mathcal{L}^2 basis set. To overcome this difficulty we developed a scheme for constructing special Gaussian basis sets that can give a reasonable description of the scattering wave at least in some volume around the origin. The scheme is a combination of the recipe for constructing continuum-like Gaussian basis sets proposed by Kaufmann, Baumeister, and Jungen [93], and a specially designed distributed Gaussian basis. The approach of Kaufmann, Baumeister, and Jungen is based on

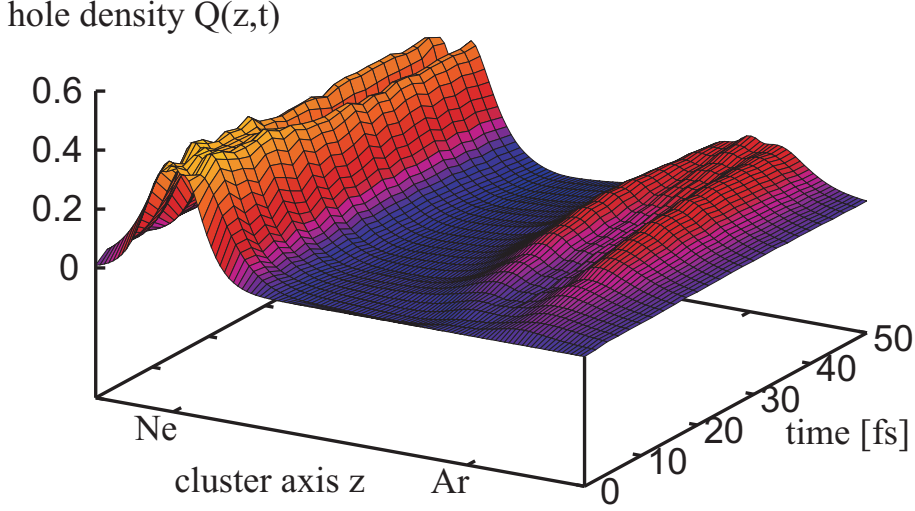


Figure 4.7: Hole density $Q(z,t)$ plotted against the Ne-Ar axis z as a function of time after Ne $2s$ ionization of NeAr. The initial hole density changes its character from an one- to a two-ridge surface, corresponding to the filling of the Ne $2s$ -hole predominantly by a Ne $2p_z$ -electron. In the same time a Ar $3p_z$ -hole is created (right-hand side of the plot), which also has mainly p_z -character up to about 40 fs. One clearly sees that the dominant ICD-channel is $\text{Ne}^+(2s^{-1})\text{Ar} \rightarrow \text{Ne}^+(2p_z^{-1})\text{Ar}^+(3p_z^{-1}) + e_{ICD}^-$.

the generation of optimized sequences of Gaussian exponents by maximizing the overlap with a series of Laguerre-Slater functions, where the latter are characterized by a constant exponent and variable principle and orbital quantum numbers. The complementary distributed functions are obtained by optimizing their positions and exponents such that they reproduce the radial part of the corresponding Coulomb wave in some volume around the system.

The energetics of the ICD process in NeAr show that the secondary emitted ICD-electron has an energy of about 9 eV. Thus, the exponents and the positions of the additional basis-set functions were optimized such that they reproduce up to 15 Å from the cluster the radial part of a Coulomb s -wave of that energy seeing two positive charges in the center. It is clear that when the ICD electron reaches the spatial end of the basis set it can be reflected back and interfere with the ionic core. For the present parameters such unphysical interference appears after about 60 fs. That is why, the size of the space covered by the basis set is of crucial importance for the proper description of decaying states. In the case of NeAr this time span is sufficient to fully trace the ICD process.

We were able not only to follow the development of the process but also to analyze the relative contributions of the different decay channels open. In Fig. 4.7 the hole density $Q(z,t)$ obtained by integrating $Q(\vec{r},t)$ over the coordinates perpendicular to the Ne-Ar axis (z axis) is plotted. As seen, the initial hole density (left-hand side of the surface in Fig. 4.7) changes with time its character from a one- to a two-ridge surface, corresponding

to the filling of the initial Ne2s-vacancy predominantly by a Ne2p_z-electron. The second hole opened on Ar (right-hand side of the surface) displays predominantly p_z-character up to about 40 fs. The channel ending with Ar⁺(3p_{x,y}⁻¹), seen as a tiny, steadily increasing ridge situated between the two wide humps on the right-hand side of the surface, becomes important after that time indicating a slower decay channel. Our calculations show, therefore, that the fastest decay channel is when 2p_z electron fills the 2s vacancy in neon and a 3p_z electron is ejected from the argon. This process takes about 35 fs. The channels involving Ne2p_{x,y} and Ar3p_{x,y} electrons become important after about 40 fs.

Possessing the multielectron wave packet enables also to analyze the contributions of other types of decay processes involving electron transfer from the argon atom. Our analysis showed that the decay probability of this pathway is negligible being several orders of magnitude smaller than that of the ICD process. The results of this study were published in *Physical Review Letters*, Ref. [61], see P2 from the attached papers.

4.3 Radiation generated by ultrafast electron dynamics

In all studied cases the charge migration represents a charge oscillating throughout the molecule. This means that before the nuclear dynamics start to perturb the charge-migration process, the molecule itself can be seen as an oscillating dipole. It is well known that the oscillating dipole emits radiation. The natural questions, therefore, are what kind of radiation is emitted and how strong it is?

We found that indeed the charge migration triggered by ionization generates a characteristic radiation. The emission is usually in the infra-red (IR) spectrum, reflecting the typical few-femtosecond oscillation time, and, according to our calculations, it is strong enough in order to be measured.

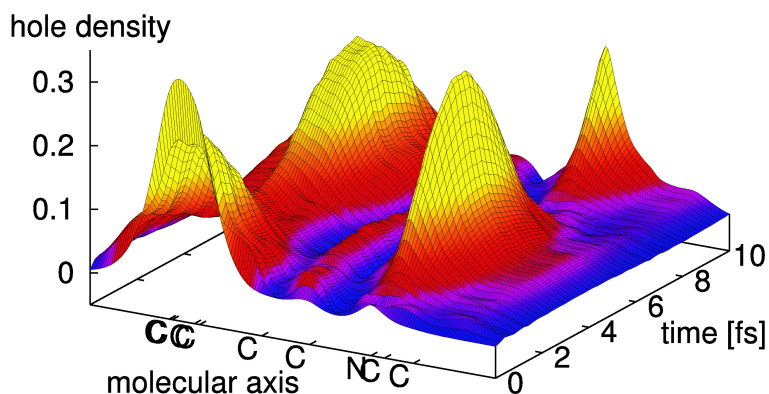


Figure 4.8: Hole density along the molecular axis of the molecule MePeNNA as a function of time after a localized ionization of the chromophore. The molecular axis is chosen to pass through the longest spatial extension of the molecule.

To exemplify this we performed calculations on the MePeNNA molecule in which ionization out of the HOMO (localized on the chromophore) triggers a strong charge

migration [34] (see also Sec. 4.1). The hole density of the molecule MePeNNA after creating the initial hole on the chromophore is shown in Fig. 4.8. It is clearly seen that immediately after the ionization, the hole starts to oscillate between the “left” and the “right” moiety of the system with a period of about 7.5 fs. These oscillations will be gradually distorted by the coupling to the nuclear degrees of freedom. The slower nuclear dynamics will eventually trap the charge on one of the two sites. However, the nuclear dynamics time scale is such that the hole will have time to perform a few, nearly perfect oscillations before the nuclear motion will distort the picture. Thus, within the first few periods this charge-migration process will represent an oscillating dipole.

The total power of the radiation emitted by a moving charge as a function of time can be calculated via the well-known Larmor formula (see, e.g., Ref. [94]), which in atomic units reads

$$P(t) = \frac{2}{3c^3} |\ddot{\vec{D}}(t)|^2, \quad (4.1)$$

where $\ddot{\vec{D}}(t)$ is the second time-derivative of the dipole moment

$$\vec{D}(t) = \langle \Psi(t) | \hat{D} | \Psi(t) \rangle, \quad (4.2)$$

and c is the speed of light. The spectrum of the emitted radiation can be obtained by substituting in Eq. (4.1) $\ddot{\vec{D}}(t)$ by its Fourier transform.

Therefore, in order to compute the radiation generated by the charge-migration phenomenon one has to be able to compute the time-dependent dipole moment of the system studied. For that purpose, the dipole operator has to be represented in the same many-body basis as the original cationic Hamiltonian and then compute its expectation value within the propagating multielectron wave packet. Within the non-Dyson ADC scheme employed by us, this can be done relatively straightforward, as far as the non-Dyson ADC scheme is realized within a formally complete basis (the ISR basis mentioned in Sec. 2.3) which makes it possible to represent any operator in this basis.

The emission spectrum generated by the charge migration triggered by ionization out of the HOMO of MePeNNA is shown by the red curve in the inset of Fig. 4.9 (see also Fig. 2 of Publication P9). We would like to note that we assumed that the ionization is performed by a laser pulse with about 1 fs duration that is able to coherently populate only the first two cationic states of the system. The spectrum in this case will consist of a single peak centered around 0.55 eV corresponding to the charge-oscillation period of about 7.5 fs.

In the same work we studied also the intriguing situation when the initial ionic wave packet is prepared by an extremely fast ionization (sudden ionization limit). We found that in this case a much stronger ultra-violet (UV) emission is generated. Moreover, the faster the ionization is performed the broader is the emission spectrum due to the larger number of coupled ionic states that can be populated. The emission spectrum after sudden ionization of the HOMO is shown by the black curve in Fig. 4.9. Our analysis shows that this emission appears as an ultrafast response of the remaining electrons to the perturbation caused by the extremely rapid ionization and as such is a universal phenomenon to be expected in every multielectron system.

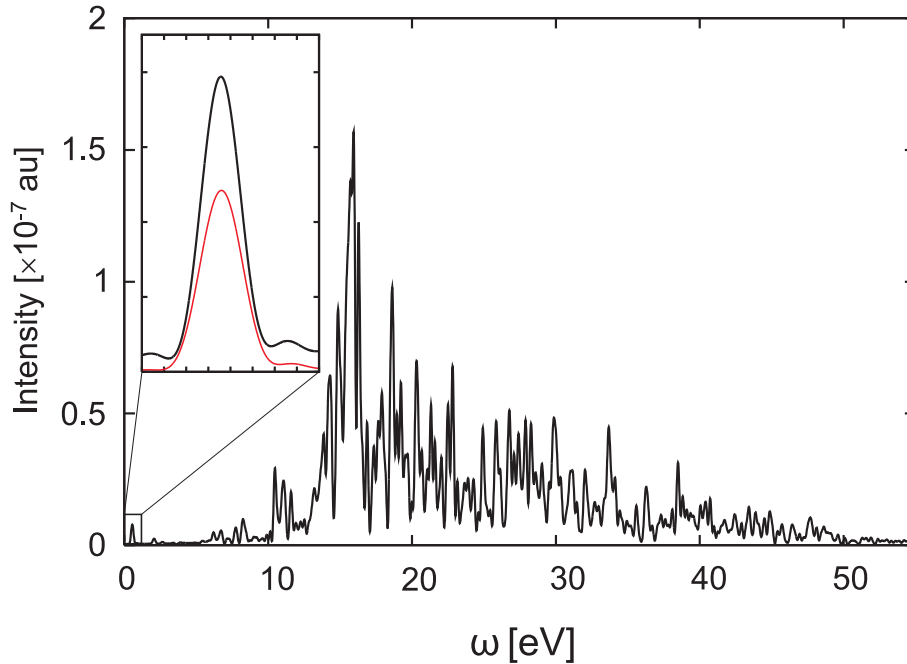


Figure 4.9: Emission spectrum generated by a sudden removal of an electron from the HOMO of the molecule MePeNNA. The inset shows a comparison of the emission spectrum generated by the charge migration triggered by the an ultrafast ionization (red curve) and a sudden ionization limit (black curve).

The results of our study on the emission generated by ultrafast electron dynamics were published in *Physical Review Letters*, Ref. [9], see P9 from the attached papers.

Here we would like to touch upon the possibility to measure the emission from the electron dynamics triggered by ionization. Let us discuss first the emission generated by the charge-migration process. In the example of MePeNNA shown above, the total energy emitted during a 10 fs radiation from a single molecule will be $\sim 2.3 \times 10^{-9}$ eV. For a density of $\sim 10^{18}$ molecules/cm³, a typical density used in high-harmonic-generation gas chambers [95], and interaction volume of $\sim 10^{-7}$ cm³ [95], the charge migration will generate ~ 115 IR photons¹. Such an emission is detectable with the present-day instruments. Moreover, not long ago, the IR emission caused by the charge-separation step of the phototransduction process of bacteriorhodopsin has been successfully measured [96, 97]. We would like to note that since the charge migration generates a characteristic radiation, the experimental observation of such an emission will be a direct proof of existence of the charge-migration phenomenon.

As we saw in the case of MePeNNA, and confirmed also by our other unpublished calculations, the UV emission generated by the response of the electronic cloud to an

¹Assuming an ionization cross-section of 10 Mb and an ionizing pulse with duration of 1 fs and intensity of 10^{14} W/cm² which will ionize about half of the molecules in the interaction volume.

extremely rapid ionization is orders of magnitude stronger than that generated by the charge-migration process. Therefore, the experimental observation of this emission should not be a problem. More challenging would be the ultrafast preparation of the initial state. As discussed in Sec. 2.2 the sudden ionization limit can be approached, for example, by an attosecond laser pulse. Alternatively, ultrafast ionization can be achieved by a bombardment with highly charged relativistic ions. Annihilation of an electron by a positron is also sudden and, in principle, can be used. The effective cross-section of this mechanism is inversely proportional to the velocity of the scattering positron and becomes appreciable only for thermal and sub-thermal energy positrons, which strongly reduces the control over the precise moment of ionization. Consequently, pump-probe measurements will be difficult to perform, but the appearance of IR and UV radiation will be a clear signal of the phenomena.

Chapter 5

Conclusions and perspectives

Within the present work a new *ab initio* method for multielectron wave-packet propagation alongside with the necessary computer codes have been developed. The method gives the possibility to describe fully *ab initio* the dynamics of various de-excitation processes taking into account *all* electrons of the system and their correlation. The approach is equally suitable for tracing in real time and space the electron dynamics of both decaying and non-decaying ionized systems. Employing this method, different fundamental physical phenomena triggered by ionization of a variety of systems have been studied. We were able to trace in real time and space the evolution of the electronic cloud during the interatomic Coulombic decay process in NeAr following Ne2s ionization. Our results allowed for a detailed analysis of the relative contributions and time scales of the different decay channels open. In the case when the initial ionic state is non-decaying, an ultrafast rearrangement of the charge density, or a charge migration, may take place. The created hole charge can migrate from one moiety of the system to another on a time scale of just few femtoseconds. It was shown that although typical for inner-valence ionized states the charge migration can occur also after ionization out of the outer-valence shell. Moreover, we found out that the charge migration triggered by ionization generates a characteristic radiation. The emission is usually in the infra-red spectrum, reflecting the typical few-femtosecond charge oscillation time. We studied also the effect of the ultrafast ionization and found that in this case a much stronger ultra-violet emission is generated. This emission appears as an ultrafast response of the remaining electrons to the perturbation caused by the sudden ionization and as such is a universal phenomenon to be expected in every multielectron system.

We found also that the charge migration depends strongly on the particular nuclear geometry, suggesting that the nuclear dynamics that will enter the picture at later times will play an important role and can even trap the charge. Therefore, the charge migration can be regarded as the first step of an effective transfer of the charge from one moiety of the system to another.

There are many scenarios what the impact of nuclear motion could be. Particularly attractive is the following conceivable situation. The hole is initially created at one end of the molecule and then migrates very fast, before the nuclei move, to another remote

site where the bonding is weak. In the presence of the hole this weak bond will start to break. Due to its fast migration, the hole may still escape and oscillate back to the initial site. The oscillations may proceed for some time and become slower until the bond eventually breaks. Dissociation of the molecule is a clear possibility to dispose of the excess electronic energy. This could explain the experimental observations of Weinkauff, Schlag and co-workers [98–101] (see also the case of PENNA molecule discussed above and Refs. [35, 88, 89]), in which, after a localized ionization on a specific site of a peptide chain, a bond breaking on a remote site of the chain occurs. If bond breaking does not occur, we may ask whether the nuclei will relax and stabilize the charge. This is likely to occur in large molecules, but only after a much longer time than the hole-migration times discussed in this work. In small, free molecules the initially pure electronic oscillations will gradually go over into combined electronic-nuclear oscillations which may last for very long times. In the presence of a solvent, we may expect even for small molecules a similar situation as for large ones: the nuclei relax and stabilize and trap the charge. The time scale of this stabilization can be very long and will strongly depend on the solvent. For instance, in a polar solvent, the solvent molecules will reorient themselves to stabilize the charge. We anticipate that because of the ultrafast charge migration which takes place before the nuclei relax, many interesting scenarios are possible at later times due to the nuclear motion and the environment.

Whatever the succeeding electron-nuclear dynamics are, it is clear that the initial pure electronic step of charge migration or charge redistribution will have a strong influence on the processes that may take place at later times. Therefore, it is extremely important to study the question of how one can manipulate or control this initial step, for example by appropriately chosen laser pulses. Knowing how to control the charge-migration process in molecular systems through the pulse parameters may give a tool to control and predetermine chemical reaction pathways. One may draw an analogy between this possibility and the quantum-control techniques to guide chemical reaction processes developed in femtochemistry. The difference is, however, at what stage the steering manipulation is applied. In femtochemistry, by specially designed femtosecond laser pulses one is able to influence directly the movement of the nuclei and in such a way to guide the evolution of the system in a desired direction by choosing a particular reaction pathway. Here, by influencing the electron dynamics by an ultrashort (attosecond) laser pulse, one might be able to preselect and put the system on the particular reaction pathway on a very early stage of its quantum evolution.

This enormous potential for practical applications of the charge-migration phenomenon rapidly attracts interest in the scientific community. Stimulated by our findings, several experimental groups [102–104] are currently intensively working on preparing measurements to study the process of charge migration using novel attosecond-pulse techniques and different pump-probe schemes. The importance of the charge-migration step was recently recognized by the leading British funding agency for natural sciences, EPSRC, that funded a 6 years project for the experimental study of this phenomenon [105]. Another large-scale proposal for exploration of the new high-intensity light sources, in which the study of the charge-migration phenomenon constitutes an important part, is currently under consideration in the US Department of energy [106].

Therefore, theoretical investigation of the charge-migration phenomenon in the presence of external fields is an important direction for the future studies to go. We would like to note that the formal inclusion of the pulse within the methodology developed and presented in this Thesis is possible. Within the dipole approximation the operator describing the coupling to the electric field is a one-particle operator which can be represented within the many-electron basis of our cationic Hamiltonian (the ISR basis).

Naturally, it will be also interesting to study the electron dynamics of decaying ionic states in the presence of an external field. Studying the influence of the external field on an electronic decay process will give the important information how through the pulse parameters one can modulate the decay process and predetermine, for example, the scattering direction.

At the end we would like to briefly discuss another direction for further studies. We saw that any many-electron system will react upon ultrafast ionization by attosecond reorganization of the electronic cloud generating a UV radiation. Moreover, the faster the ionization is performed the broader is the emission spectrum due to the larger number of coupled ionic states populated. In this respect, it has to be studied how one can preselect certain frequencies by a simultaneous irradiation of the molecule with an additional pulse that can quench some modes and enhance others by stimulated emission. In other words, this additional pulse will play the role of a filter to the generated UV emission. The same idea can be applied in the case when the primary ionization pulse triggers a charge-migration process which we have shown generates typically an IR emission. In the presence of a properly chosen additional IR pulse the charge-migration process can be quenched or enhanced and from there the emission spectrum can be modulated.

Bibliography

- [1] G. D. Billing and K. V. Mikkelsen, *Advanced Molecular Dynamics and Chemical Kinetics* (Wiley, New York, 1997).
- [2] *Conical Intersections*, Adv. Series in Phys. Chem. Vol. 15, edited by W. Domcke, D. Yarkony, and H. Köppel (World Scientific, NJ, Singapore, 2004).
- [3] G. A. Worth and L. S. Cederbaum, *Annu. Rev. Phys. Chem.* **55** (2004) 127.
- [4] *An Introduction to Laser Spectroscopy*, edited by D. A. Andrews and A. A. Demidov (Kluwer Academic/Plenum Publishers, New York, 2002).
- [5] A. H. Zewail, *Femtochemistry*, Vol. I and II (World Scientific, Singapore, 1994).
- [6] L. S. Cederbaum and J. Zobeley, *Chem. Phys. Lett.* **307**, 205 (1999).
- [7] J. Breidbach and L. S. Cederbaum, *J. Chem. Phys.* **118**, 3983 (2003).
- [8] J. Breidbach and L. S. Cederbaum, *Phys. Rev. Lett.* **94**, 033901 (2005).
- * [9] A. I. Kuleff and L. S. Cederbaum, *Phys. Rev. Lett.* **106**, 053001 (2011).
- [10] L. S. Cederbaum, *J. Chem. Phys.* **128**, 124101 (2008).
- [11] J. Miller, *Physics Today* **61**(5), 15 (2008).
- [12] F. Krausz and M. Ivanov, *Rev. Mod. Phys.* **81**, 163 (2009).
- [13] M. Nisoli and G. Sansone, *Prog. Quantum Electron.* **33**, 17 (2009).
- [14] M. Drescher, M. Hentschel, R. Kienberger, M. Uiberacker, V. Yakovlev, A. Scrinzi, Th. Westerwalbesloh, U. Kleineberg, U. Heinzmann, and F. Krausz, *Nature* **419**, 803 (2002).
- [15] H. Niikura, D. M. Villeneuve, and P. B. Corkum, *Phys. Rev. Lett.* **94**, 083003 (2005).
- [16] O. Smirnova, Y. Mairesse, S. Patchkovskii, N. Dudovich, D. Villeneuve, P. Corkum, and M. Yu. Ivanov, *Nature* **460**, 972 (2009).
- [17] O. Smirnova, S. Patchkovskii, Y. Mairesse, N. Dudovich, and M. Yu. Ivanov, *Proc. Natl. Acad. Sci. USA* **106**, 16556 (2009).

- [18] E. Goulielmakis, Z.-H. Loh, A. Wirth, R. Santra, N. Rohringer, V. S. Yakovlev, S. Zherebtsov, T. Pfeifer, A. M. Azzeer, M. F. Kling, S. R. Leone, and F. Krausz, *Nature* **466**, 739 (2010).
- [19] G. Sansone, E. Benedetti, F. Calegari, C. Vozzi, L. Avaldi, R. Flammini, L. Poletto, P. Villoresi, C. Altucci, R. Velotta, S. Stagira, S. De Silvestri, and M. Nisoli, *Science* **314**, 443 (2006).
- [20] E. Goulielmakis, M. Schultze, M. Hofstetter, V. S. Yakovlev, J. Gagnon, M. Uiberacker, A. L. Aquila, E. M. Gullikson, D. T. Attwood, R. Kienberger, F. Krausz, and U. Kleineberg, *Science* **320**, 1614 (2008).
- * [21] G. Sansone, T. Pfeifer, K. Simeonidis, and A. I. Kuleff, *ChemPhysChem*, **13**, 661 (2012).
- [22] M. Awasthi, Y. V. Vanne, and A. Saenz, *J. Phys. B* **38**, 3973 (2005).
- [23] M. Nest, T. Klamroth, and P. Saalfrank, *J. Chem. Phys.* **122**, 124102 (2005).
- [24] O. Koch, W. Kreuzer, and A. Scrinzi, *Appl. Math. Comput.* **173**, 960 (2006).
- [25] T. Klamroth, *Phys. Rev. B* **68**, 245421 (2003).
- [26] P. Krause, T. Klamroth, and P. Saalfrank, *J. Chem. Phys.* **123**, 074105 (2005).
- [27] S. Klinkusch, T. Klamroth, and P. Saalfrank, *Phys. Chem. Chem. Phys.* **11**, 3875 (2009).
- [28] P. Krause, T. Klamroth, and P. Saalfrank, *J. Chem. Phys.* **127**, 034107 (2007).
- [29] E. Runge and E. K. U. Gross, *Phys. Rev. Lett.* **52**, 997 (1984).
- [30] J. Schirmer and A. Dreuw, *Phys. Rev. A* **75**, 022513 (2007).
- [31] E. K. U. Gross and W. Kohn, *Phys. Rev. Lett.* **55**, 2850 (1985).
- [32] A. D. Dutoi, L. S. Cederbaum, M. Wormit, J. H. Starcke, and A. Dreuw, *J. Chem. Phys.* **132**, 144302 (2010).
- * [33] A. I. Kuleff and L. S. Cederbaum, *Chem. Phys.* **338**, 320 (2007).
- * [34] S. Lünemann, A. I. Kuleff, and L. S. Cederbaum, *J. Chem. Phys.* **129**, 104305 (2008).
- * [35] S. Lünemann, A. I. Kuleff, and L. S. Cederbaum, *Chem. Phys. Lett.* **450**, 232 (2008).
- [36] V. May and O. Kühn, *Charge and Energy Transfer Dynamics in Molecular Systems* (Wiley-VCH, Weinheim, 2004).
- [37] L. S. Cederbaum, J. Zobeley, and F. Tarantelli, *Phys. Rev. Lett.* **79**, 4778 (1997).

- [38] J. Zobeley, L. S. Cederbaum, and F. Tarantelli, *J. Chem. Phys.* **108**, 9737 (1998).
- [39] R. Santra and L. S. Cederbaum, *Phys. Rep.* **386**, 1 (2002).
- [40] S. Scheit, V. Averbukh, H.-D. Meyer, N. Moiseyev, R. Santra, T. Sommerfeld, J. Zobeley, and L. S. Cederbaum, *J. Chem. Phys.* **121**, 8393 (2004).
- [41] V. Averbukh, I. B. Müller, and L.S. Cederbaum, *Phys. Rev. Lett.* **93**, 263002 (2004).
- [42] V. Averbukh and L. S. Cederbaum, *Phys. Rev. Lett.* **96**, 053401 (2006).
- [43] A. I. Kuleff, K. Gokhberg, S. Kopelke, and L. S. Cederbaum, *Phys. Rev. Lett.* **105**, 043004 (2010).
- [44] N. Sisourat, N. V. Kryzhevoi, P. Kolorenč, S. Scheit, T. Jahnke, and L. S. Cederbaum, *Nature Physics* **6**, 508 (2010).
- [45] S. D. Stoychev, A. I. Kuleff, and L. S. Cederbaum, *J. Am. Chem. Soc.* **133**, 6817 (2011).
- [46] N. V. Kryzhevoi and L. S. Cederbaum, *Angew. Chem. Int. Ed.* **50**, 1306 (2011).
- [47] Ph. V. Demekhin, S. D. Stoychev, A. I. Kuleff, and L. S. Cederbaum, *Phys. Rev. Lett.* **107**, 273002 (2011).
- [48] S. Marburger, O. Kugeler, U. Hergenhahn, and T. Möller, *Phys. Rev. Lett.* **90**, 203401 (2003).
- [49] T. Jahnke, A. Czasch, M. S. Schöffler, S. Schössler, A. Knapp, M. Kász, J. Titze, C. Wimmer, K. Kreidi, R. E. Grisenti, A. Staudte, O. Jagutzki, U. Hergenhahn, H. Schmidt-Böcking, and R. Dörner, *Phys. Rev. Lett.* **93**, 163401 (2004).
- [50] G. Öhrwall, M. Tchapygine, M. Lundwall, R. Feifel, H. Bergersen, T. Rander, A. Lindblad, J. Schulz, S. Peredkov, S. Barth, S. Marburger, U. Hergenhahn, S. Svensson, and O. Björneholm, *Phys. Rev. Lett.* **93**, 173401 (2004).
- [51] Y. Morishita, X.-J. Liu, N. Saito, T. Lischke, M. Kato, G. Prümper, M. Oura, H. Yamaoka, Y. Tamenori, I. H. Suzuki, and K. Ueda, *Phys. Rev. Lett.* **96**, 243402 (2006).
- [52] T. Jahnke, H. Sann, T. Havermeier, K. Kreidi, C. Stuck, M. Meckel, M. Schöffler, N. Neumann, R. Wallauer, S. Voss, A. Czasch, O. Jagutzki, A. Malakzadeh, F. Afaneh, Th. Weber, H. Schmidt-Böcking, and R. Dörner, *Nature Phys.* **6**, 139 (2010).
- [53] M. Mucke, M. Braune, S. Barth, M. Förstel, T. Lischke, V. Ulrich, T. Arion, U. Becker, A. Bradshaw, and U. Hergenhahn, *Nature Phys.* **6**, 143 (2010).
- [54] T. Ouchi, K. Sakai, H. Fukuzawa, X.-J. Liu, I. Higuchi, Y. Tamenori, K. Nagaya, H. Iwayama, M. Yao, D. Zhang, D. Ding, A. I. Kuleff, S. D. Stoychev, Ph. V. Demekhin, N. Saito, and K. Ueda, *Phys. Rev. Lett.* **107**, 053401 (2011).

- [55] B. Boudaïffa, P. Cloutier, D. Hunting, M. A. Huels, and L. Sanche, *Science* **287**, 1658 (2000).
- [56] F. Martin, P. D. Burrow, Z. Cai, P. Cloutier, D. Hunting, and L. Sanche, *Phys. Rev. Lett.* **93** 068101 (2004).
- [57] B. T. Pickup, *Chem. Phys.* **19**, 193 (1977).
- [58] H. W. Meldner and J. D. Perez, *Phys. Rev. A* **4**, 1388 (1971).
- [59] A. Szabo and N. S. Ostlund, *Modern Quantum Chemistry* (McGraw-Hill, New York, 1989).
- [60] P.-O. Löwdin, *Phys. Rev.* **97**, 1474 (1955).
- * [61] A. I. Kuleff and L. S. Cederbaum, *Phys. Rev. Lett.* **98**, 083201 (2007).
- * [62] A. I. Kuleff and A. Dreuw, *J. Chem. Phys.* **130**, 034102 (2009).
- [63] F. Remacle and R. D. Levine, *Proc. Natl. Acad. Sci. U.S.A.* **103**, 6793 (2006).
- [64] F. Remacle and R. D. Levine, *J. Chem. Phys.* **125**, 133321 (2006).
- [65] R. G. Parr and W. Yang, *Density-Functional Theory of Atoms and Molecules* (Oxford University Press, Oxford, 1994).
- [66] W. Kohn and L. J. Sham, *Phys. Rev.* **140**, A1133 (1965).
- [67] J. P. Perdew and A. Zunger, *Phys. Rev. B* **23**, 5048 (1981).
- [68] Y. A. Mantz, F. L. Gervasio, T. Laino, and M. Parrinello, *J. Phys. Chem. A* **111**, 105 (2007).
- [69] A. J. Cohen, P. Mori-Sánchez, and W. Yang, *J. Chem. Phys.* **126**, 191109 (2007).
- [70] J. Tao, J. P. Perdew, V. N. Staroverov, and G. E. Scuseria, *Phys. Rev. Lett.* **91**, 146401 (2003).
- [71] V. N. Staroverov, G. E. Scuseria, J. Tao, and J. P. Perdew, *J. Chem. Phys.* **119**, 12129 (2003).
- [72] J. Breidbach and L. S. Cederbaum, *J. Chem. Phys.* **126**, 34101 (2007).
- [73] J. Schirmer, L. S. Cederbaum, and O. Walter, *Phys. Rev. A* **28**, 1237 (1983).
- [74] L. S. Cederbaum, in *Encyclopedia of Computational Chemistry*, edited by P. von Ragué Schleyer *et al.* (Wiley, Chichester, 1998), p. 1202.
- [75] Y. Öhrn and G. Born, *Adv. Quant. Chem.* **13**, 1 (1981).
- [76] J. Schirmer, *Phys. Rev. A* **43**, 4647 (1991).

- [77] R. Santra, J. Breidbach, J. Zobeley, and L. S. Cederbaum, *J. Chem. Phys.* **112**, 9243 (2000).
- * [78] A. I. Kuleff, J. Breidbach, and L. S. Cederbaum, *J. Chem. Phys.* **123**, 044111 (2005).
- [79] J. Schirmer, A. B. Trofimov, and G. Stelter, *J. Chem. Phys.* **109**, 4734 (1998).
- [80] F. Mertins and J. Schirmer, *Phys. Rev. A* **53**, 2140 (1996).
- [81] J. Schirmer and A. B. Trofimov, *J. Chem. Phys.* **120**, 11449 (2004).
- [82] C. J. Lanczos, *J. Res. Natl Bur. Stand.* **45**, 255 (1950).
- [83] T. J. Park and J. C. Light, *J. Chem. Phys.* **85**, 5870 (1986).
- [84] C. Leforestier, R. H. Bisseling, C. Cerjan, M. D. Feit, R. Friesner, A. Guldborg, A. Hammerich, G. Jolicard, W. Karrlein, H.-D. Meyer, N. Lipkin, O. Roncero, and R. Kosloff, *J. Comp. Phys.* **94**, 59 (1991).
- [85] L. S. Cederbaum, W. Domcke, J. Schirmer, and W. von Niessen, *Adv. Chem. Phys.* **65**, 115 (1986).
- * [86] S. Lünemann, A. I. Kuleff, and L. S. Cederbaum, *J. Chem. Phys.* **130**, 154305 (2009).
- * [87] A. I. Kuleff, S. Lünemann, and L. S. Cederbaum, *Chem. Phys.* (in press) DOI:10.1016/j.chemphys.2012.02.019.
- [88] R. Weinkauff, L. Lehr, and A. Metsala, *J. Phys. Chem. A* **107** (2003) 2787.
- [89] L. Lehr, T. Horneff, R. Weinkauff, and E. W. Schlag, *J. Phys. Chem. A* **109**, 8074 (2005).
- * [90] A. I. Kuleff, S. Lünemann, and L. S. Cederbaum, *J. Phys. Chem. A* **114**, 8676 (2010).
- [91] W. Wardermann and W. von Niessen, *Chem. Phys.* **159**, 11 (1992).
- * [92] A. I. Kuleff, S. Lünemann, and L. S. Cederbaum, *Chem. Phys.* (in press) DOI:10.1016/j.chemphys.2011.10.015.
- [93] K. Kaufmann, W. Baumeister, and M. Jungen, *J. Phys. B* **22**, 2223 (1989).
- [94] J. D. Jackson, *Classical Electrodynamics*, 3rd ed., (Wiley, New York, 1999).
- [95] B. Shan, A. Cavalieri, and Z. Chang, *Appl. Phys. B* **74**, S23 (2002).
- [96] G. I. Groma, A. Colonna, J.-C. Lambry, J. W. Petrich, G. Várlo, M. Joffre, M. H. Vos, and J.-L. Martin, *Proc. Natl. Acad. Sci. U.S.A.* **101**, 7971 (2004).

- [97] G. I. Groma, J. Hebling, I. Z. Kozma, G. Várló, J. Hauer, J. Kuhl, and E. Riedle, Proc. Natl. Acad. Sci. U.S.A. **105**, 6888 (2008).
- [98] R. Weinkauff, P. Aicher, G. Wesley, J. Grotemeyer, and E. W. Schlag, J. Phys. Chem. **98**, 8381 (1994).
- [99] R. Weinkauff, P. Schanen, A. Metsala, E. W. Schlag, M. Bürgle, and H. Kassler, J. Phys. Chem. **100**, 18567 (1996).
- [100] R. Weinkauff, E. W. Schlag, T. J. Martinez, and R. D. Levine, J. Phys. Chem. A **101**, 7702 (1997).
- [101] E. W. Schalg, S.-Y. Sheu, D.-Y. Yang, H. L. Selzle, and S. H. Lin, Angew. Chem. Int. Ed. **46**, 3196 (2007).
- [102] J. Marangos (Imperial College London), private communication.
- [103] G. Sansone (Politecnico di Milano), private communication.
- [104] H. J. Wörner (ETH Zürich), private communication.
- [105] J. Marangos *et al.*, *Attosecond Electron Dynamics in Molecular and Condensed Phase Systems*, Project funded by EPSRC, UK,
<http://gow.epsrc.ac.uk/NGBOViewGrant.aspx?GrantRef=EP/I032517/1>
- [106] R. Falcone *et al.*, Lawrence Berkeley National Laboratory, *Science with new x-ray lasers*, Project proposal submitted to the DOE, USA.

References denoted by * are publications included in the present Habilitation thesis.

Chapter 6

Publications

P1. A. I. Kuleff, J. Breidbach, and L. S. Cederbaum, *Multielectron wave-packet propagation: General theory and application*, J. Chem. Phys. **123**, 044111 (2005).

P2. A. I. Kuleff and L. S. Cederbaum, *Tracing ultrafast interatomic electronic decay processes in real time and space*, Phys. Rev. Lett. **98**, 083201 (2007).

P3. A. I. Kuleff and L. S. Cederbaum, *Charge migration in different conformers of glycine: The role of nuclear geometry*, Chem. Phys. **338**, 320 (2007).

P4. S. Lünemann, A. I. Kuleff, and L. S. Cederbaum, *Ultrafast charge migration in 2-Phenylethyl-N,N-dimethylamine*, Chem. Phys. Lett. **450**, 232 (2008).

P5. S. Lünemann, A. I. Kuleff, and L. S. Cederbaum, *Charge migration following ionization in systems with chromophore-donor and amine-acceptor sites*, J. Chem. Phys. **129**, 104305 (2008).

P6. A. I. Kuleff and A. Dreuw, *Theoretical description of charge migration with a single Slater-determinant and beyond*, J. Chem. Phys. **130**, 034102 (2009).

P7. S. Lünemann, A. I. Kuleff, and L. S. Cederbaum, *Ultrafast electron dynamics following outer-valence ionization: The impact of low-lying relaxation satellite states*, J. Chem. Phys. **130**, 154305 (2009).

P8. A. I. Kuleff, S. Lünemann, and L. S. Cederbaum, *Ultrafast charge migration following valence ionization of 4-methylphenol: jumping over the aromatic ring*, J. Phys. Chem. A **114**, 8676 (2010).

P9. A. I. Kuleff and L. S. Cederbaum, *Radiation generated by the ultrafast migration of a positive charge following the ionization of a molecular System*, Phys. Rev. Lett. **106**, 053001 (2011).

P10. A. I. Kuleff, S. Lünemann, and L. S. Cederbaum, *Ultrafast reorganization of the hole charge created upon outer-valence ionization of porphyrins*, Chem. Phys. (in press).

P11. G. Sansone, T. Pfeifer, K. Simeonidis, and A. I. Kuleff, *Electron correlation in real time*, ChemPhysChem **13**, 661 (2012).

P12. A. I. Kuleff, S. Lünemann, and L. S. Cederbaum, *Electron-correlation-driven charge migration in oligopeptides*, Chem. Phys. (in press).

[HTML ABSTRACT + LINKS](#)

THE JOURNAL OF CHEMICAL PHYSICS 123, 044111 (2005)

Multielectron wave-packet propagation: General theory and application

Alexander I. Kuleff,^{a)} Jörg Breidbach,^{b)} and Lorenz S. Cederbaum^{c)}
*Theoretische Chemie, Physikalisch-Chemisches Institut (PCI), Universität Heidelberg,
Im Neuenheimer Feld 229, 69120 Heidelberg, Germany*

(Received 20 April 2005; accepted 26 May 2005; published online 3 August 2005)

An *ab initio* method for multielectron wave-packet propagation in relatively large systems is presented. It allows the description of ultrafast electron dynamics processes before the coupling with the nuclear motion becomes important. The method is applied to the amino acid glycine for the investigation of the migration of hole charge following the ionization of the system. Two different mechanisms of ultrafast charge migration are identified and discussed. It is shown that the electron correlation can be the driving force for the charge-transfer dynamics in glycine. © 2005 American Institute of Physics. [DOI: 10.1063/1.1961341]

I. INTRODUCTION

Computing the time development of quantum systems has concentrated many efforts in the last decades. However, due to the complexity of the problem and the formidable numerical obstacles it poses, the real-time evolution induced by microscopic Hamiltonians has been restricted to a few discrete quantum levels. But the availability of high-performance computers has now made it feasible to integrate the Schrödinger equation of experimentally interesting cases with a view to understanding their evolution. Much has been done in this respect in the field of molecular nuclear dynamics, where various methods for propagation of the wave packet (a representation of the quantum-mechanical probability distribution of the system at a given time) have been developed.¹ For treating nuclear dynamics problems, the total wave function of the system is usually represented as a product of the electronic wave function and the wave function describing the nuclei (Born-Oppenheimer approximation). In that way, the Schrödinger equation is decoupled into a static equation for the electronic part, and an equation of motion for the nuclear wave function, which then is an object of different propagation schemes. The Born-Oppenheimer approximation, however, is inapplicable when the spacing between the electronic levels becomes very small and breaks down completely when a real crossing of levels, known as conical intersection,^{2,3} occurs. In these cases the nuclear and electronic motions are coupled and one has to use nonadiabatic molecular-dynamics approaches.^{2,3}

However, various dynamical effects in a molecular system can take place before the nuclear dynamics comes into play. Such ultrafast processes are, for example, different intra-atomic (intramolecular) decay processes, such as the well-known Auger decay of deep core levels or the recently reported charge-migration mechanism^{4,5} and attosecond response of the system to the removal of an electron.⁶ For the

proper description of such processes one needs a dynamical treatment of the electronic wave function. In these cases, we may consider the nuclear frame as fixed, and solve a dynamical Schrödinger equation for the electronic part—a *multielectron wave-packet dynamics*. Of course, the ultimate goal will be to treat dynamically both electronic and nuclear wave functions, but this is currently beyond reach for realistic systems.

The multielectron dynamical calculations become especially important in the light of the tremendous development in the last years of laser pump-probe experimental techniques, which made possible a direct observation in real time of ultrafast processes with subfemtosecond resolution.^{7,8} To interpret the experimental results properly, one needs precise *ab initio* calculations which give the time evolution of the electronic cloud, taking into account various effects, such as electronic correlation and electronic relaxation. Different theoretical approaches for the propagation of electronic wave packets have been developed to treat the dynamics of Rydberg electrons (see, e.g., Ref. 9 and references therein). However, most of these approaches are limited to the full dynamical description of one or at most two electrons⁹ and are insufficient when correlation of more than two electrons has to be taken into account.

In the present work we propose an *ab initio* method for a direct propagation of the multielectronic wave packet after ionization of a molecular system. It should be stressed, however, that the proposed approach is general and is not restricted to treatment of ionization problems. The method needs a matrix representation of the Hamiltonian of the problem at hand, and since every operative Hamiltonian can be cast into a matrix representation in some efficient multielectron basis, the application of the approach is general.

For calculating the energetics of the ionized system we use Green's function formalism, in particular, the *algebraic diagrammatic construction* (ADC) scheme^{10,11} which defines a compact Hamiltonian matrix, but we stress that any method which gives a compact Hamiltonian matrix can be used as well. One can gain insight into the electronic processes following the ionization by describing the time evolution of the charge density of the system. This can be done within the

^{a)}On leave from the Institute for Nuclear Research and Nuclear Energy, BAS, 72, Tzarigradsko Chaussee Blvd., 1784 Sofia, Bulgaria. Electronic mail: alexander.kuleff@pci.uni-heidelberg.de

^{b)}Electronic mail: joerg.breidbach@tc.pci.uni-heidelberg.de

^{c)}Electronic mail: h35@ix.urz.uni-heidelberg.de

recently proposed *ab initio* method of *charge-migration analysis* (CMA).^{5,12}

The propagation of the eigenstate of the underlying Hamiltonian itself is performed through the short iterative Lanczos time propagation technique.^{13,14} Using this algorithm one actually replaces the full (or partial) diagonalization of the large Hamiltonian matrix (in our case the ADC matrix), and the consecutive time propagation of the eigenvalues, with a repetitive diagonalization of much smaller tridiagonal matrices. In such a way, the whole scheme becomes applicable to relatively large molecules, e.g., oligopeptides, which are practically inaccessible within approaches demanding a full diagonalization of the secular matrix. An additional important advantage of the direct propagation is the possibility to include an external pulse and in that way to achieve a realistic time-resolved description of the ionization or other processes.

The paper is organized as follows. In Sec. II the theoretical ground of the method is presented. Emphasis is put on the Lanczos propagation algorithm, while the ADC and CMA methods are only briefly reviewed. Section III is devoted to the application of the proposed approach to the molecule of glycine. The multielectron dynamics following a sudden ionization out of two different orbitals of glycine is traced in time and space and analyzed. It is shown that an effective, ultrafast (few femtoseconds) migration of the hole charge within the molecule occurs. In Sec. IV we summarize the results and conclude.

II. THEORY

A. Direct propagation

It is known that the time-dependent Schrödinger equation has a formal solution:

$$|\Psi(t)\rangle = \hat{U}(t,0)|\Psi(0)\rangle = T \exp\left(-\frac{i}{\hbar} \int_0^t \hat{H}(t') dt'\right) |\Psi(0)\rangle, \quad (1)$$

where $T \exp$ is the so-called chronological exponent which represents the evolution operator $\hat{U}(t,0)$. If we assume a time-independent Hamiltonian, the evolution operator, describing the evolution of the system from time t to time $t + \Delta t$, is then given by

$$\hat{U}(\Delta t) \equiv \hat{U}(t + \Delta t, t) = \exp\left(-\frac{i}{\hbar} \hat{H} \Delta t\right). \quad (2)$$

The latter is also approximately true for a time-dependent Hamiltonian if for a sufficiently small time increment Δt the variation of the Hamiltonian is negligible. In that way, we can represent the evolution operator as a product of such operators, propagating the wave function from t to $t + \Delta t$, for which Eq. (2) is valid. In other words, we can break up a time interval into many small intervals with duration Δt and thus represent the evolution of the wave function as successive small steps. In the present work a time-independent Hamiltonian is assumed and hence we have no physical restrictions on the size of Δt .

It is obvious that if $|\Psi(0)\rangle$ is an eigenfunction of \hat{H} one gets

$$|\Psi(t)\rangle = e^{-(i/\hbar)E_0 t} |\Psi(0)\rangle, \quad (3)$$

where E_0 is the eigenvalue of \hat{H} corresponding to the eigenvector $|\Psi(0)\rangle$. In that way, if we know the eigenvalues and eigenvectors of the Hamiltonian, i.e., we have diagonalized the Hamiltonian matrix, the time propagation is straightforward. Unfortunately, the full diagonalization can be performed with reasonable expense only for relatively small systems or on a low level of approximation. Since the processes we want to treat result mainly from electronic correlation, the level of approximation should be as high as possible, which leads to large secular matrices even for small systems. It should be mentioned that if some knowledge for the system and the electronic process under study is available, one may encounter situations where not all the eigenstates are needed, i.e., a partial diagonalization can be sufficient. Nevertheless, even in such cases the determination of the usually many eigenstates needed is very costly for multi-electron systems. The main idea of this work is to propose a scheme which provides the possibility of treating realistic multielectron systems by circumventing the diagonalization of large matrices.

B. Lanczos propagation schemes

The Lanczos algorithm¹³ was originally proposed as a reduction technique for linear operators, yielding matrices in a Hessenberg form. It was also proven to be very efficient as a time propagation scheme for the nonrelativistic Schrödinger equation¹⁵ and is widely used in treating nuclear-dynamics problems.^{14,16,17} Here, we would like to utilize it for studying the dynamics of correlated electrons.

The Lanczos algorithm leads to the following polynomial expansion of the exponential in the evolution operator:

$$\hat{U}(\Delta t) \approx \sum_{j=1}^K c_j P_j(-i\hbar^{-1} \hat{H} \Delta t), \quad (4)$$

where $P_j(-i\hbar^{-1} \hat{H} \Delta t)$ is a polynomial of degree j , and c_j are the expansion coefficients. This expansion is constructed through a three-term recurrence relation within the so-called Krylov subspace with dimension K , spanned by the vectors $\mathbf{q}_n = \mathbf{H}^n \Psi(0)$, $n=0, \dots, K-1$, \mathbf{H} and $\Psi(0)$ being the matrix representations of \hat{H} and $|\Psi(0)\rangle$, respectively, in some suitable basis. Moreover, the recurrence relation generates a tridiagonal matrix representation of the Hamiltonian in the Krylov subspace.

The Lanczos construction is initialized by a normalized start vector $\Psi(0)$:

$$\mathbf{q}_0 = \Psi(0). \quad (5)$$

By the Gram-Schmidt procedure a vector \mathbf{q}_1 orthogonal to \mathbf{q}_0 can be found:

$$\tilde{\mathbf{q}}_1 = \mathbf{H}\mathbf{q}_0 - (\mathbf{q}_0^\dagger \mathbf{H}\mathbf{q}_0)\mathbf{q}_0 \text{ and } \mathbf{q}_1 = \frac{\tilde{\mathbf{q}}_1}{\|\tilde{\mathbf{q}}_1\|}, \quad (6)$$

where $\|\tilde{\mathbf{q}}_1\| = \sqrt{\tilde{\mathbf{q}}_1^\dagger \tilde{\mathbf{q}}_1}$ is the norm of the vector $\tilde{\mathbf{q}}_1$. Obviously, it is assumed that \mathbf{q}_0 is not an eigenvector of \mathbf{H} , otherwise the algorithm terminates. Defining

$$\alpha_0 = \mathbf{q}_0^\dagger \mathbf{H}\mathbf{q}_0 \text{ and } \beta_1 = \|\tilde{\mathbf{q}}_1\|, \quad (7)$$

we have

$$\mathbf{H}\mathbf{q}_0 = \alpha_0\mathbf{q}_0 + \beta_1\mathbf{q}_1. \quad (8)$$

This gives the first column/row of the tridiagonal subspace representation of \mathbf{H} . The general recursion is given by

$$\mathbf{H}\mathbf{q}_j = \alpha_j\mathbf{q}_j + \beta_j\mathbf{q}_{j-1} + \beta_{j+1}\mathbf{q}_{j+1}, \quad (9)$$

with

$$\alpha_j = \mathbf{q}_j^\dagger \mathbf{H}\mathbf{q}_j, \quad (10)$$

$$\tilde{\mathbf{q}}_{j+1} = \mathbf{H}\mathbf{q}_j - \alpha_j\mathbf{q}_j - \beta_j\mathbf{q}_{j-1}, \quad (11)$$

$$\beta_{j+1} = \|\tilde{\mathbf{q}}_{j+1}\|, \quad (12)$$

$$\mathbf{q}_{j+1} = \frac{\tilde{\mathbf{q}}_{j+1}}{\beta_{j+1}}. \quad (13)$$

After K steps an orthonormal basis $\{\mathbf{q}_j\}$ of the K -dimensional Krylov subspace is obtained, and the representation of the Hamiltonian projected on this subspace has the following tridiagonal form:

$$\mathbf{H}_K = (\mathbf{q}_0 \cdots \mathbf{q}_{K-1})^\dagger \mathbf{H} (\mathbf{q}_0 \cdots \mathbf{q}_{K-1}) = \begin{pmatrix} \alpha_0 & \beta_1 & 0 & \cdots & 0 \\ \beta_1 & \ddots & \ddots & \ddots & \vdots \\ 0 & \ddots & \ddots & \ddots & 0 \\ \vdots & \ddots & \ddots & \ddots & \beta_{K-1} \\ 0 & \cdots & 0 & \beta_{K-1} & \alpha_{K-1} \end{pmatrix}. \quad (14)$$

Then, the unitary propagation operator $\hat{U}(\Delta t)$ can be approximated by its representation in the Krylov subspace:

$$\mathbf{U}_K(\Delta t) = e^{-(i\hbar)\mathbf{H}_K\Delta t}, \quad (15)$$

and the propagated vector by

$$\Psi(\Delta t) \approx \mathbf{U}_K(\Delta t)\Psi(0). \quad (16)$$

The propagation of the initial wave function is hence performed in the projected subspace by the tridiagonal Hamiltonian \mathbf{H}_K , which is easy to diagonalize, and thus for $\mathbf{U}_K(\Delta t)$ one gets

$$\mathbf{U}_K(\Delta t) = \mathbf{Z}^\dagger e^{-(i\hbar)\mathbf{D}_K\Delta t} \mathbf{Z}, \quad (17)$$

where \mathbf{Z} is the eigenvector matrix of \mathbf{H}_K , and \mathbf{D}_K is its diagonal matrix of eigenvalues. For the propagated wave function we can then write

$$\Psi(\Delta t) = e^{-(i\hbar)\mathbf{H}_K\Delta t}\Psi(0) = \sum_{k=0}^{K-1} a_k \mathbf{q}_k, \quad (18)$$

where

$$a_k = \sum_{j=0}^{K-1} Z_{kj} e^{-(i\hbar)\lambda_j\Delta t} (Z^{-1})_{j0}, \quad (19)$$

or since the eigenvector matrix \mathbf{Z} is unitary

$$a_k = \sum_{j=0}^{K-1} Z_{kj} e^{-(i\hbar)\lambda_j\Delta t} Z_{0j}. \quad (20)$$

In Eqs. (19) and (20) the λ_j denote the eigenvalues of the matrix \mathbf{H}_K , i.e., the diagonal elements of \mathbf{D}_K .

The propagated wave function, Eq. (18), is then used as initial vector, Eq. (5), for the next iteration.

One has a very convenient estimate of the error, i.e., the difference between the propagated and exact wave functions, when using the Lanczos integrator. This error is proportional to the magnitude of the first vector, \mathbf{q}_K , lying outside of the Krylov space used,¹⁴ namely,

$$\|\Psi_{\text{exact}}(\Delta t) - \Psi_{\text{Lanczos}}(\Delta t)\| \approx \frac{\beta_1 \cdots \beta_K}{K!} (\Delta t)^K. \quad (21)$$

This quantity can be used to adjust either the time-step size Δt or the order K . In our calculations we propagate with a fixed time-step, and Eq. (21) is used as a criterion for the convergence of the recurrence (9)–(13) and the determination of the dimension of the Krylov space K .

Several features of the Lanczos algorithm should be pointed out. First, as it is seen from Eqs. (8)–(11), when computing the tridiagonal matrix \mathbf{H}_K , the full Hamiltonian matrix \mathbf{H} is needed only for a simple matrix vector product and remains unchanged during the whole procedure. Second, the method is computationally cheap, at each time-step memory has to be allocated only for three vectors: \mathbf{q}_{j-1} , \mathbf{q}_j , and \mathbf{q}_{j+1} , and hence allows treatment of relatively large systems, described by large Hamiltonian matrices, for which the full diagonalization is either very expensive or even impossible. And, last but not least, the method is unitary and conserves the norm and the energy.

For completeness we will conclude this section with a brief review of the more general complex Lanczos, or Lanczos-Arnoldi, algorithm,^{18,19} allowing propagation with non-Hermitian Hamiltonians. In this case, the recursion for building the reduced Hamiltonian matrix \mathbf{H}_K is the following:

$$\text{for } i = 0, \dots, j: \begin{cases} \tilde{\mathbf{q}}_{j+1}^{(0)} = \mathbf{H}\mathbf{q}_j \\ \tilde{\mathbf{q}}_{j+1}^{(i+1)} = \tilde{\mathbf{q}}_{j+1}^{(i)} - \beta_{ij}\mathbf{q}_i, & \text{where } \beta_{ij} = \mathbf{q}_i^\dagger \tilde{\mathbf{q}}_{j+1}^{(i)} \\ \mathbf{q}_{j+1} = \tilde{\mathbf{q}}_{j+1}^{(j+1)} / \beta_{j+1,j}, & \text{where } \beta_{j+1,j} = \|\tilde{\mathbf{q}}_{j+1}^{(j+1)}\|. \end{cases} \quad (22)$$

In that way, starting with a normalized state \mathbf{q}_0 , one constructs an orthonormal basis $\mathbf{q}_0, \dots, \mathbf{q}_{K-1}$, in which the reduced Hamiltonian \mathbf{H}_K is a complex upper Hessenberg matrix:

$$(\mathbf{H}_K)_{ij} = \mathbf{q}_i^\dagger \mathbf{H}\mathbf{q}_j = \begin{cases} \beta_{ij}, & i \leq j+1 \\ 0, & i > j+1 \end{cases} \text{ for } i, j = 0, \dots, K-1. \quad (23)$$

The propagated vector is constructed in the same way as in

the Hermitian case, i.e., from the eigenvalues and eigenvectors of the matrix (23) through Eqs. (18) and (19).

It is easy to check if the Hamiltonian is Hermitian, the matrix $\{q_i^\dagger \mathbf{H} q_j\}$ becomes symmetric, and thus tridiagonal. In that sense, the Hermitian Lanczos is just a special case of the more general Lanczos-Arnoldi algorithm. The complex version of the scheme is obviously more time consuming, since in addition to the diagonalization of the reduced Hamiltonian, in this case an upper Hessenberg matrix, one needs to perform an inversion of its eigenvector matrix [see Eq. (19)], which is now not unitary. Nevertheless, for non-Hermitian cases the Lanczos-Arnoldi algorithm appears to be very efficient.¹⁷ It can be used, for example, when a complex-absorbing potential²⁰ is added to the Hamiltonian, which then becomes complex symmetric. The use of a complex-absorbing potential can be of practical value when dealing with electronic decay processes,²¹ since it has the purpose of absorbing the emitted particle, making in that way its wave function square-integrable and hence treatable within the standard quantum chemistry techniques.²²

C. Non-Dyson ADC

Green's function-based approaches possess numerous computational and interpretative advantages in calculating ionization energetics and reduce the problem to the diagonalization of an effective, relatively compact Hermitian matrix.^{23–25} Despite their compactness, these matrices, depending on the size of the system, the orbital basis set and the approximation scheme used, can become extremely large. Thus, in order to circumvent the expensive diagonalization of the secular matrix, we can use the approach described above to directly propagate the initial ionic state in the basis in which the secular matrix is represented. This can be done within the non-Dyson version of ADC.¹¹ This scheme uses the so-called *intermediate state representation* (ISR)^{26,27} of the secular matrix, yielding the construction of a complete basis through successive Gram-Schmidt orthogonalization of different classes of correlated excitations.

In what follows we briefly review the non-Dyson ADC scheme and discuss some of its main advantages for treating ionization problems, referring the reader to Refs. 11 and 27 for details. In connection with charge migration, Ref. 12 is also useful.

Let us consider an N -electron system with ground-state $|\Psi_0^N\rangle$ and energy E_0^N . In energy representation the one-particle Green's function reads²⁸

$$G_{pq}(\omega) = \langle \Psi_0^N | \hat{a}_p(\omega - \hat{H} + E_0^N + i\eta)^{-1} \hat{a}_q^\dagger | \Psi_0^N \rangle + \langle \Psi_0^N | \hat{a}_q^\dagger(\omega + \hat{H} - E_0^N - i\eta)^{-1} \hat{a}_p | \Psi_0^N \rangle, \quad (24)$$

where \hat{a}_p^\dagger and \hat{a}_p denote creation and annihilation operators, respectively, \hat{H} is the Hamiltonian of the system, and η is a positive infinitesimal required to define the Fourier transformation between time and energy representations. The first term in Eq. (24) contains the physical information on the $(N+1)$ -particle system, and the second term on the $(N-1)$ -particle one. Since in the non-Dyson ADC the affinity and ionization parts are completely decoupled,¹¹ and in the

present study we are interested only in ionization, we mean in what follows by Green's function only the second term in Eq. (24).

In the ADC approach the Green's function has the following nondiagonal representation:

$$\mathbf{G}(\omega) = \mathbf{f}^\dagger(\omega \mathbf{1} - \mathbf{K} - \mathbf{C})^{-1} \mathbf{f}. \quad (25)$$

The latter is obtained through the representation of Green's function in the complete set of so-called intermediate states,^{26,27} $|\tilde{\Psi}_J^{N-1}\rangle$, where J runs over the excitation classes— one-hole ($1h$), two-hole-one-particle ($2h-1p$), etc. The ISR of the secular matrix is then given by

$$(\mathbf{K} + \mathbf{C})_{IJ} = \langle \tilde{\Psi}_I^{N-1} | E_0^N - \hat{H} | \tilde{\Psi}_J^{N-1} \rangle, \quad (26)$$

and the so-called effective transition moments are defined as

$$f_{Iq} = \langle \tilde{\Psi}_I^{N-1} | \hat{a}_q | \Psi_0^N \rangle. \quad (27)$$

In the ADC procedure $\mathbf{K} + \mathbf{C}$ and \mathbf{f} are constructed through the perturbation theory of the ground-state $|\Psi_0^N\rangle$.

For a given ISR, the ionization energies ω are given by the poles of Eq. (25), i.e., can be obtained by solving the secular equation

$$(\mathbf{K} + \mathbf{C})\mathbf{Y} = \mathbf{Y}\mathbf{\Omega}, \quad \mathbf{Y}^\dagger \mathbf{Y} = \mathbf{1}, \quad (28)$$

where $\mathbf{\Omega}$ is the eigenvalue matrix and \mathbf{Y} denotes the matrix of eigenvectors.

Two important features of this approach should be pointed out. First, contrary to the Dyson-type approximation schemes, where the configuration space comprises both $(N-1)$ - and $(N+1)$ -electron configurations, in the non-Dyson ADC one has a complete decoupling of the affinity and ionization blocks, yielding a substantial reduction of the problem dimension. Second, the scheme is realized within a complete basis—the ISR basis—which makes it possible to calculate different physical properties,²⁹ since we can represent their operators in the ISR basis. These two advantages of the approach give the possibility to use direct propagation techniques and in that way to avoid solving the secular problem (28). This enlarges the practical applicability of the scheme to larger molecules.

D. Charge-migration analysis

The CMA method was recently proposed for the investigation of the ultrafast dynamics of a hole, or a positive charge, created in a molecular system.^{5,12} It was shown^{4,5,12,30} that an efficient charge transfer, solely driven by electron correlation, is possible, and the created hole can migrate through the system. The process takes place in the femtosecond time scale and is referred to as *charge migration*, in order to distinguish it from the conventional charge transfer, where the nuclear dynamics plays the essential role and thus, in general, is much slower. Here we will give a brief description of the CMA method and how it can be used for analysis of the multielectron dynamics after a sudden ionization of a molecular system.

Suppose we have created a hole in a system, say through a sudden ionization. The density of the initially created hole, or the hole density, then is given by

$$Q(\vec{r}, t) := \langle \Psi_0 | \hat{\rho}(\vec{r}, t) | \Psi_0 \rangle - \langle \Phi_i | \hat{\rho}(\vec{r}, t) | \Phi_i \rangle = \rho_0(\vec{r}) - \rho_i(\vec{r}, t), \quad (29)$$

where $|\Psi_0\rangle$ is the ground state of the neutral molecule, $\hat{\rho}$ is the local density operator, and $|\Phi_i\rangle$ is the generated initial cationic state. For simplicity we have dropped the superscripts N and $N-1$ from Ψ_0 and Φ_i , respectively, used in the preceding subsection. The first term in Eq. (29) is the time-independent ground-state density of the neutral system, ρ_0 , and the second one, ρ_i , is time-dependent, since $|\Phi_i\rangle$ is not an eigenstate of the cation. In the Heisenberg picture, the time-dependent part reads

$$\rho_i(\vec{r}, t) = \langle \Phi_i | e^{i\hat{H}t} \hat{\rho}(\vec{r}, 0) e^{-i\hat{H}t} | \Phi_i \rangle. \quad (30)$$

Using resolution of identity within the complete set of ISR basis $\{|\tilde{\Psi}_M\rangle\}$ and inserting it in Eq. (30), one gets

$$\begin{aligned} \rho_i(\vec{r}, t) &= \sum_{M,N} \langle \Phi_i | e^{i\hat{H}t} |\tilde{\Psi}_M\rangle \langle \tilde{\Psi}_M | \hat{\rho}(\vec{r}, 0) | \tilde{\Psi}_N \rangle \langle \tilde{\Psi}_N | e^{-i\hat{H}t} | \Phi_i \rangle \\ &= \sum_{M,N} \langle \Phi_i(t) | \tilde{\Psi}_M \rangle \rho_{MN} \langle \tilde{\Psi}_N | \Phi_i(t) \rangle, \end{aligned} \quad (31)$$

where ρ_{MN} is the matrix representation of the density operator in the ISR basis and $|\Phi_i(t)\rangle = e^{-i(\hat{H})t} |\Phi_i\rangle$ is the direct propagation of $|\Phi_i\rangle$. The latter propagation can be performed since we can use the ISR representation of the state $|\Phi_i\rangle = \sum_L \langle \tilde{\Psi}_L | \Phi_i \rangle |\tilde{\Psi}_L\rangle$. If $|\Phi_i\rangle$ results from a sudden removal of an electron out of orbital i , its ISR representation is given by the h/h part of the matrix \mathbf{f} , Eq. (27).

Using standard representation of the density operator in a one-particle basis $\{\varphi_p(\vec{r})\}$ and occupation numbers $\{n_p\}$, Eq. (29) can be rewritten in the following form:

$$Q(\vec{r}, t) = \sum_{pq} \varphi_p^*(\vec{r}) \varphi_q(\vec{r}) N_{pq}(t), \quad (32)$$

where the matrix $\mathbf{N}(t) = \{N_{pq}(t)\}$ with elements

$$N_{pq}(t) = \delta_{pq} n_p - \sum_{M,N} \langle \Phi_i(t) | \tilde{\Psi}_M \rangle \rho_{MN} \langle \tilde{\Psi}_N | \Phi_i(t) \rangle \quad (33)$$

is referred to as the hole density matrix. Diagonalization of the matrix $\mathbf{N}(t)$ for fixed time points t leads to the following expression for the *hole density*:

$$Q(\vec{r}, t) = \sum_q |\tilde{\varphi}_p(\vec{r}, t)|^2 \tilde{n}_p(t), \quad (34)$$

where $\tilde{\varphi}_p(\vec{r}, t)$ are called *natural charge orbitals*, and $\tilde{n}_p(t)$ are their *hole occupation numbers*. The hole occupation number $\tilde{n}_p(t)$ contains the information about which part of the created hole charge is in the natural charge orbital $\tilde{\varphi}_p(\vec{r}, t)$ at time t . Because of the conservation of hole charge, one finds that $\sum_p \tilde{n}_p(t) = 1$ at any time. The hole occupation numbers, together with the hole density, are central quantities in the observation and interpretation of the multielectron dynamics taking place after the removal of an electron.

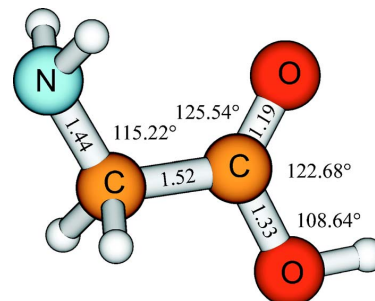


FIG. 1. (Color online.) Molecular geometry of glycine determined by geometry optimization on the Hartree-Fock level. Bond lengths are given in angstroms.

III. ILLUSTRATIVE EXAMPLE: CHARGE MIGRATION IN GLYCINE

Glycine ($\text{H}_2\text{NCH}_2\text{COOH}$) is the simplest of the 20 natural amino acids and often serves as a model system for investigating more complex compounds such as peptides or proteins. Additional motivation for the choice of the system to study was the series of measurements by Weinkauff *et al.*,³¹⁻³⁴ in which, after a localized ionization on a specific site of a peptide chain, a bond breaking on a remote site of the chain occurs. The authors proposed that a fast electronic-transfer mechanism is responsible for transporting the positive charge to the latter site of the molecule. The effect was observed in several different peptide chains such as Ala-Ala-Tyr and Gly-Gly-Trp, the initial ionization being localized on the aromatic site of tyrosine (Tyr) or tryptophan (Trp).

Our calculations consist of the following steps. First, the ground-state geometry of the neutral glycine was optimized in the Hartree-Fock level using the standard *ab initio* program package GAMESS-UK,³⁵ with the DZP basis set.³⁶ This basis set is also used in all the remaining calculations. The molecule is of plane geometry, except for the hydrogen atoms of the NH_2 and CH_2 groups, which lie in such a way that the whole molecule has a mirror symmetry (see Fig. 1). Accordingly, the system belongs to the C_s symmetry group with irreducible representations a' and a'' , and has the following electronic configuration:

$$\begin{aligned} &(\text{core})(6a')^2(7a')^2(8a')^2(9a')^2(10a')^2(11a')^2(12a')^2 \\ &\times (1a'')^2(2a'')^2(13a')^2(14a')^2(3a'')^2(4a'')^2(15a')^2(16a')^2. \end{aligned}$$

The next step is the calculation of the one-particle Green's function using the non-Dyson ADC(3) approximation scheme (here "3" means that the approach is correct up to third order of perturbation theory), briefly sketched in Sec. II C. The thus obtained ADC matrix contains the physical information on the system after ionization. Since the effects we want to study take place in an ultrashort time scale, a fixed geometry of the ionized molecule was used.

The third step is the direct propagation of the multielectron wave packet of the ionized system. As described in Sec. II B, this is done by propagating the initial cationic state through the Lanczos algorithm using the ADC matrix.

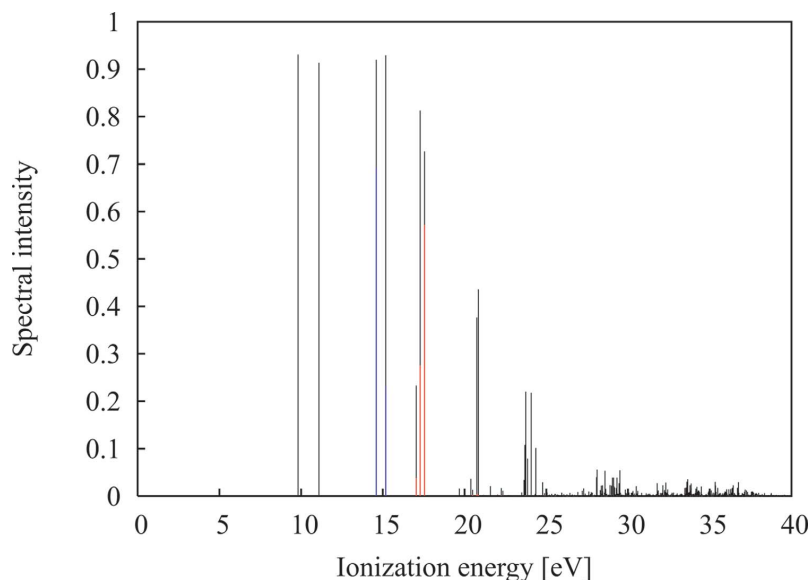


FIG. 2. (Color) Ionization spectrum of glycine belonging to the irreducible representation a' . The lines corresponding to the ionization out of the investigated orbitals $11a'$ and $14a'$ are given in red and blue, respectively. Each vertical line shown is related to a final cationic state and is located at the corresponding ionization energy. The outer valence lines appearing at the low energies in the spectrum are dominated by a single (the two leftmost lines) or by two or more $1h$ configurations (e.g., the two lines around 15 eV). At somewhat higher energies, weak satellite lines appear, since the $1h$ configuration is spread over several lines, due to the interaction with $2h-1p$ configurations (e.g., the lines around 20 eV). At higher energies, in the inner valence regime, this spreading is severe and a breakdown of the molecular-orbital picture occurs, resulting in a quasicontinuum of lines.

The last step is the application of the charge-migration analysis (Sec. II D). The latter consists, in particular, of building the matrix $\mathbf{N}(t)$ through Eq. (33), the subsequent diagonalization of which yields the natural charge orbitals $\tilde{\varphi}_p(\vec{r}, t)$ and hole occupation numbers $\tilde{n}_p(t)$ [see Eq. (34)]. With the aid of these quantities we can now trace in time and space the response of the electronic cloud of the system to the sudden removal of one of its electrons.

The direct propagation is performed using a fixed time step of 0.05 fs. The error of the propagation, given by Eq. (21), is set to be less than 10^{-6} . The choice of these parameters leads to dimensions of the Krylov space $K=18$ for irrep a' , and $K=17$ for irrep a'' . The dimensions of the ADC matrix for irreps a' and a'' are 9648 and 8367, respectively, in the DZP basis set. One could be tempted to draw the wrong conclusion that the larger the size of the matrix, the larger the size of the projected Krylov space needed in a propagation step. In fact, there is no correlation between these dimensions.³⁷ Typically, the size of the Krylov subspace is of the order of 10–30 (depending on the time step and error threshold chosen) *regardless* of the size of the Hamiltonian matrix. The advantage of the direct propagation is clearly seen. Instead of full diagonalization of a matrix with dimension of 10 000 or even much larger, one performs a repetitive diagonalization for each time point of a tridiagonal matrix with dimension around 20. However, for long-time propagation this procedure may become as time consuming as the full diagonalization, but from a certain size of the Hamiltonian matrix, when the diagonalization is impossible, propagation probably provides the only alternative.

The ionization out of the inner and outer valence shell of glycine reveals a whole zoo of interesting phenomena,³⁸ out of which we discuss here only two examples, namely, what happens after ionization out of orbital $11a'$ and of orbital $14a'$. The examples show two different mechanisms of charge migration. The first one is a combination of the so-

called *dominant-satellite* and *hole-mixing* mechanisms,⁵ and the second one is a pure hole-mixing case.

The ionization spectrum of the valence shell of glycine belonging to the a' irrep is shown in Fig. 2. The contributions to the lines corresponding to orbitals $11a'$ and $14a'$ are shown in red and blue, respectively. Each line represents an eigenstate of the cation, the position being given by the energy of the corresponding eigenstate, i.e., the ionization energy, and the height, representing the spectral intensity (related to the ionization cross section), given by the square of the transition amplitudes. In the non-Dyson ADC scheme the latter can be obtained through the effective transition moments, Eq. (27).

For a proper understanding of the investigated processes, a closer look at the ionization spectrum is illuminating. An exact cationic state $|I\rangle$ can be expanded in a series of electronic configurations, as is traditionally done in the configuration-interaction (CI) calculations³⁹

$$|I\rangle = \sum_j c_j^{(I)} \hat{a}_j |\Phi_0\rangle + \sum_{a,k < l} c_{akl}^{(I)} \hat{a}_a^\dagger \hat{a}_k \hat{a}_l |\Phi_0\rangle + \dots, \quad (35)$$

where $|\Phi_0\rangle$ is some approximation to the ground state of the neutral molecule, say Hartree-Fock, $c^{(I)}$'s are the expansion coefficients, and \hat{a}_p^\dagger and \hat{a}_q are creation and annihilation operators, respectively. In Eq. (35) we have used the following habitual convention: indices i, j, k, \dots denote occupied orbitals, or holes, whereas a, b, c, \dots refer to unoccupied (virtual) orbitals, or particles. Thus, the term $\hat{a}_a^\dagger \hat{a}_k \hat{a}_l |\Phi_0\rangle$, or the $2h-1p$ term, means that an electron from orbital φ_l has been removed, accompanied by an excitation of another electron from orbital φ_k to the unoccupied orbital φ_a . The $2h-1p$ and higher terms represent actually the electronic correlation. Without correlation effects, the spectrum in Fig. 2 will be a series of lines, one for each occupied orbital φ_i , with intensity equal to 1. If correlation effects are weak, which is typically the case when the outer valence shell is ionized, the

044111-7 Multielectron wave-packet propagation

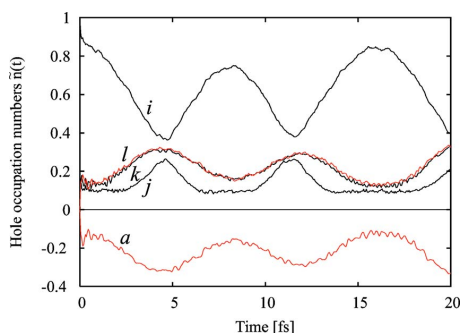


FIG. 3. (Color online.) Time-dependent hole occupation numbers of glycine after ionization out of orbital $11a'$. The orbitals belonging to irrep a'' are plotted in black and those belonging to a' in red. The initially ionized orbital, marked by i , loses its hole charge to the orbitals $4a''$ and $16a'$, marked by l and k , respectively, while the first unoccupied orbital $5a''$, marked by a , is filled by a fraction of an electron. In addition, avoided crossings between the natural charge orbitals i and j occur at around 4.7 fs and again around 11.2 fs. After an avoided crossing the characters of the natural charge orbitals i and j change from $11a'$ to $12a'$ and vice versa.

spectrum is dominated by *main lines* which have large overlaps with the $1h$ excitations. These are, for example, the two leftmost lines in Fig. 2. At higher energies, or deeper in the valence shell, where the correlation effects become more important, weaker lines beside the main lines appear, the so-called *satellite* lines. The satellites are dominated by $2h-1p$ excitations. Going deeper in the valence electronic shells, the correlation effects become stronger and the distinction between main lines and satellites ceases to exist. This phenomenon, called breakdown of the molecular-orbital picture,⁴⁰ is clearly seen in Fig. 2 after about 25 eV.

A closer examination of the ionization spectrum of glycine shows that the ionization out of the orbital $11a'$ gives contribution mainly to three cationic states, located at 17.55, 17.29, and 17.04 eV, respectively. The rest of the spectral intensities of these states are mainly due to the ionization out of the orbital $12a'$. Thus, the state at 17.55 eV with a spectral intensity of 0.73 is a superposition of the $1h$ configuration with a hole on $11a'$, having a weight of 0.57, and another $1h$ configuration, with a hole on $12a'$, having a much smaller weight (0.15). Contrary to that, the state at 17.29 eV with a spectral intensity of 0.81 is constructed dominantly from the $1h$ configuration with a hole on $12a'$ (weight of 0.53) and from the $1h$ configuration with a hole on $11a'$ having a moderate contribution (weight of 0.28). This situation represents a classical example of hole mixing (see Ref. 5). In addition to that, a correlation satellite appears at 17.04 eV with an intensity of 0.23. This satellite state has overlaps with both $1h$ configurations—0.04 with the hole on $11a'$ and 0.19 with the hole on $12a'$.

Let us first see what happens after the ionization out of orbital $11a'$. The hole occupation numbers of the natural charge orbital relevant to the process are depicted in Fig. 3. The initially ionized orbital $11a'$, having a hole occupation equal to 1 at time 0, loses its hole charge to the orbitals $4a''$ and $16a'$, marked by l and k in Fig. 3, respectively. At the same time, the virtual orbital $5a''$, marked by a starts to be

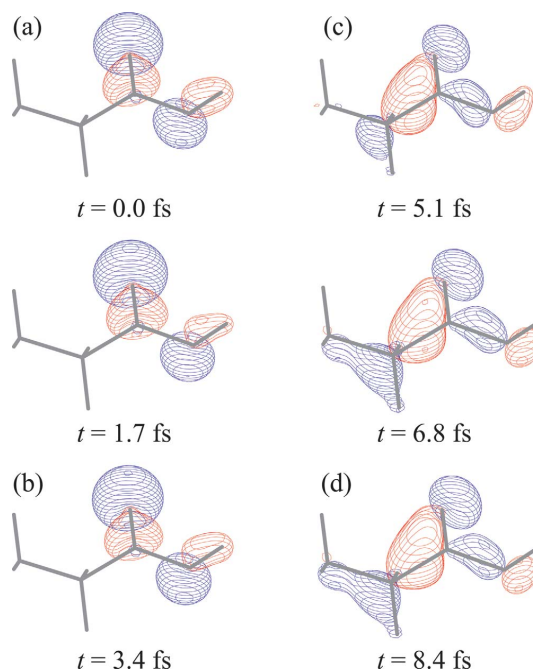
J. Chem. Phys. **123**, 044111 (2005)

FIG. 4. (Color) Migration of hole charge in glycine after ionization out of orbital $11a'$. The molecule is oriented such that the NH_2 group points left and the OH group right. (a) At $t=0$ the natural charge orbital is identical to orbital $11a'$, which is localized mainly on the CO and OH groups. (b)–(c) A substantial part of the charge migrates to the C–C bond. (d) At $t=8.4$ fs the natural charge orbital is essentially $12a'$ spread over almost the whole molecule, but having maximal density on the C– CH_2 and CH_2 – NH_2 groups.

filled by an electron (“negative” hole). Some part of the initial hole charge is transferred also to the orbital $12a'$ (marked by j on the figure). Thus, after around 4.7 fs more than 60% of the initial charge has been redistributed between the orbitals $4a''$, $16a'$, and $12a'$, accompanied by an excitation of more than 0.3 of an electron to the initially unoccupied orbital $5a''$. After that time an avoided crossing between natural charge orbitals $11a'$ and $12a'$ occurs, and the two orbitals are swapped—the orbital $11a'$ continues to lose its charge, and $12a'$ continues to be filled. This process lasts up to around 8.3 fs when more than 75% of the initial hole charge has flown to the orbital $12a'$, while the initially ionized orbital $11a'$ has lost more than 90% of its charge. At about 16 fs the two natural charge orbitals i and j have again interchanged their roles (after an avoided crossing at around 11.2 fs) and the hole charge has migrated back to the initially ionized orbital $11a'$. Thus, after about 16 fs nearly 85% of the charge is again on orbital $11a'$. After that time the whole process is repeated. Here, we want point out that the extremely fast response at the beginning of the process, on an attosecond time scale, is universal for multielectron systems, as has been discussed elsewhere.⁶

In order to see how the charge transfer takes place in the coordinate space, we can examine the evolution of the natural charge orbitals. In Fig. 4 is depicted the time evolution of the natural charge orbital $\varphi_i(\vec{r}, t)$ with hole occupation num-

044111-8 Kuleff, Breidbach, and Cederbaum

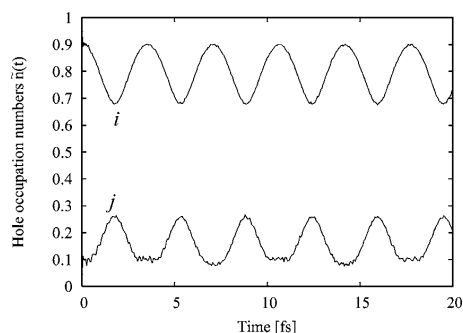
J. Chem. Phys. **123**, 044111 (2005)

FIG. 5. Time-dependent hole occupation numbers of glycine after ionization out of orbital $14a'$. Only the occupation numbers of the two natural charge orbitals involved in the process are depicted. The hole charge, initially localized on orbital $14a'$, oscillates between the orbitals $14a'$ and $13a'$. Note that each time when a minimum of curve i faces a maximum of curve j we have avoided crossings, and the nature of the natural charge orbitals is swapped from that of the orbital $14a'$ to that of the orbital $13a'$ and vice versa.

ber $\bar{n}_i(t)$ corresponding to curve i in Fig. 3. Only the first half of the charge oscillation is traced, i.e., up to $t=8.4$ fs. We can see that at $t=0$, when the natural charge orbital is identical to orbital $11a'$, the charge is localized mainly on the right-hand side of the molecule, namely, on CO and OH groups [Fig. 4(a)]. At $t=5.1$ fs a substantial part of the charge has already migrated to the C-CH₂ bond at the middle of the molecule [see Fig. 4(c)], and at $t=8.4$ fs a part of the charge is also transferred on CH₂-NH₂ bond further on the left. At this time, the natural charge orbital overlaps by more than 91% with the molecular orbital $12a'$. As we saw already from Fig. 3, after that time the process continues in reverse order until the charge migrates back to its initial position. However, after, say, 10 fs the nuclear dynamics could also start to play a role, which will additionally perturb the picture. The movement of the nuclei could even block the reverse process and force the charge to remain on orbital $12a'$.

Let us now consider the ionization out of orbital $14a'$. The corresponding lines in the spectrum are marked in blue in Fig. 2. In this case, the main state at 14.60 eV in the spectrum is found to be a mixture of the dominating $(14a')^{-1} 1h$ configuration with the $1h$ configuration of $(13a')^{-1}$. This means that this eigenstate of the ion [see Eq. (35)] is mainly given by the two $1h$ configurations corresponding to creating a hole in orbital $13a'$ and in orbital $14a'$, while all other configurations have very small weight. The hole occupation numbers of the natural charge orbitals involved in this hole mixing are given in Fig. 5. At time $t=0$ the natural charge orbital, marked by i , with hole occupation equal to 1 is identical to orbital $14a'$. As time proceeds, the charge flows to the natural charge orbital j , and at $t\approx 2.2$ fs an avoided crossing occurs. Now i becomes mainly orbital $13a'$, and j mainly orbital $14a'$. Thus, at $t\approx 3.5$ fs the two orbitals are swapped and more than 90% of the charge has migrated to orbital $13a'$. The full cycle of oscillation lasts 7 fs, with a second avoided crossing at around 5 fs. After that time the whole process starts again. However, as was mentioned

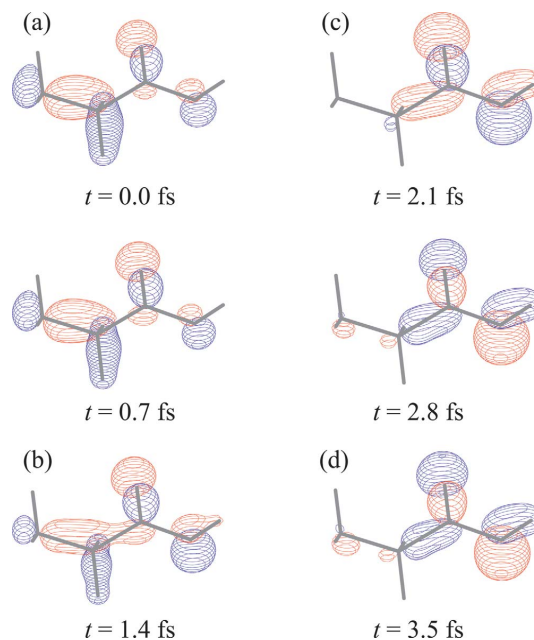


FIG. 6. (Color) Migration of hole charge in glycine after ionization out of orbital $14a'$. The molecule is oriented in the same way as in Fig. 4. (a) At $t=0$ the natural charge orbital is identical to orbital $14a'$, and the charge is mainly located on the left-hand side moiety of the molecule. (b)–(c) The charge migrates to the right-hand side moiety of the molecule. (d) At $t=3.5$ fs the natural charge orbital is essentially $13a'$, located almost entirely on the right-hand side of the molecule.

above, the coupling with the nuclear motion could block the back oscillation and thus trap the charge in orbital $13a'$.

In Fig. 6 we present the evolution of the natural charge orbital corresponding to the hole occupation shown by curve i in Fig. 5. At time $t=0$, the hole is on orbital $14a'$, which is spread over the entire molecule, but has its most significant part located on the N-terminal moiety. We can see that after 3.5 fs more than 90% of the hole is transferred to orbital $13a'$, which is localized mainly on the COOH moiety of the molecule. After that time, the process again continues in reverse order up to $t\approx 7$ fs when the charge has returned back to its initial position. Obviously, we encounter here a very efficient and ultrafast mechanism of charge transfer from essentially one part of the molecule to another part.

To illustrate this charge-migration mechanism in space and time, the hole density $Q(x,t)$ is calculated [see Eqs. (29) and (34)]. The axis x was chosen to lie in the symmetry plane of the molecule and to pass through its longest spatial extension. It is called molecular axis in the following. The values of $Q(x,t)$ were obtained by integrating $Q(\vec{r},t)$ over the remaining y and z components perpendicular to x . The hole density, obtained in that way, is shown in Fig. 7. For convenience, the positions of the atoms along the molecular axis are indicated. The hole density $Q(x,t)$ shows bold maxima at times $t=0$, $t\approx 3.5$, $t\approx 7$, and $t=10$ fs. These maxima are situated on different sides of the molecule. For more clarity, in Fig. 8 we show cuts through the three-dimensional (3D) pre-

044111-9 Multielectron wave-packet propagation

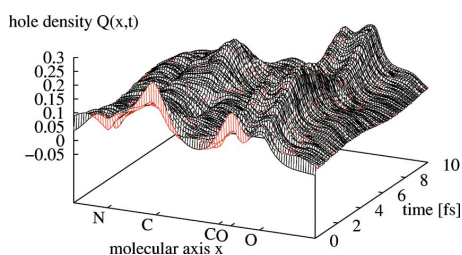
J. Chem. Phys. **123**, 044111 (2005)

FIG. 7. (Color online.) Hole density $Q(x,t)$ plotted against the molecular axis x as a function of time after ionization out of orbital $14a'$ of glycine. $Q(x,t)$ is obtained through integration of the total charge over the coordinates perpendicular to the molecular axis. An ultrafast charge migration over the C–C bond of glycine can be seen.

sentation at different times up to 3 fs. We see that at $t=0$ the main part of the hole charge is localized around the α -C atom (on the left-hand side of Fig. 8) and some smaller part around the carboxyl group. After 3 fs the charge around the α -carbon is transferred to the OH group (on the right-hand side of Fig. 8). At all times the hole occupation in the region of the C–C bond remains very small, the hole charge leaps over the C–C bond in its migration from one side of the molecule to the other.

IV. CONCLUSION

In this work an *ab initio* method for multielectron wave-packet propagation is proposed and applied to the molecule glycine to investigate the response of the electronic cloud to a sudden removal of one of its electrons. For this purpose all remaining 29 valence electrons of glycine were treated on equal footing during the time propagation of the electronic wave packet. The space of the ionic states is obtained through the non-Dyson ADC(3) scheme. The propagation itself is performed through the Lanczos algorithm, which replaces the expensive diagonalization of the secular matrix, by a repetitive diagonalization of much smaller tridiagonal matrices. The latter matrices are representations of the secular matrix in the Krylov space.

An estimate of the performance of the direct propagation can be obtained by comparing how the CPU time scales with

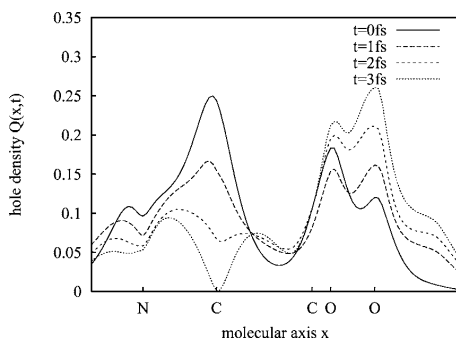


FIG. 8. The cuts through the hole density $Q(x,t)$ shown in Fig. 7 at times 0, 1, 2, and 3 fs. The hole charge migrates from the α -carbon (left-hand side) to the OH group (right-hand side). Note that at all times the hole density remains very small in the vicinity of the C–C bond.

the dimension N of the Hamiltonian matrix in the cases of full diagonalization and of direct propagation. We remark that the direct propagation has distinct advantages concerning the storage needed, but this issue is not discussed here further. For full diagonalization the computer time is proportional to N^3 , while for the Lanczos integrator it is $\sim N^2 K n_{\text{iter}}$, where K is the dimension of the Krylov space and n_{iter} is the number of iterations. As mentioned above, in the calculations presented in this work the dimension of the ADC matrix is a little less than 10^4 and the Krylov space is found to be ≈ 20 for the propagation time step (0.05 fs) and error threshold (10^{-6}) chosen. Thus, for propagation up to 20 fs, which means 400 iterations, the gain in CPU time of the direct propagation compared to the full diagonalization is a factor of 1.3. Once n_{iter} becomes of the order of N/K , the Lanczos procedure becomes as time consuming as the full diagonalization. It is clear that for Hamiltonian matrices with dimensions of the order of 10^5 – 10^6 , which is typically the case for Hamiltonians describing “small” biophysically interesting molecules even if moderate-size basis set are used, and for the same values of K and n_{iter} , the direct propagation is 10–100 times less time consuming. Nevertheless, this comparison is meaningful only if the diagonalization (full or partial) is possible at all. From a certain size of the Hamiltonian matrix the direct propagation is the only alternative.

The results obtained for the ultrafast electronic dynamics after ionization out of orbitals $11a'$ and $14a'$ of glycine show several interesting features. In both cases, a charge migration through the molecule takes place within a few femtoseconds. After the ionization out of orbital $11a'$, the hole charge, localized on a specific site of the molecule at $t=0$, spreads over almost the whole molecule for about 8 fs. Contrary to that, the investigated electronic dynamics after ionization out of orbital $14a'$ shows fast (~ 3 fs) localization of the charge on a specific site of glycine. However, the latter process can be regarded as a migration of the charge from one end of the molecule to the other, since at the beginning most of the charge is situated on the opposite moiety of the molecule than at the end of the process. It should be noted that during this process the hole density in the vicinity of the C–C bond remains very small at all times (see Figs. 7 and 8). Thus, the hole charge in a way “jumps” from one side of the molecule to the other. In both investigated examples, the electron correlation leads to an oscillation of the charge within the molecule. Nevertheless, the coupling with the nuclear motion at later times could lead to trapping of the charge and thus achieve irreversibility of the process. It should be mentioned, however, that the nuclear dynamics is not the only way to achieve irreversibility. When many ionic states participate in the process, which is typically the case in the inner-valence region, the back oscillation can also be blocked (see, e.g., the example in Ref. 12).

We found that an efficient ultrafast charge migration solely driven by electron correlation can occur in the molecule glycine. These results could inspire further investigation on possible charge migration in larger molecules such as small peptide chains. In this respect, it will be of high interest to compare our results with time-resolved experiments with time resolution on a subfemtosecond scale.

044111-10 Kuleff, Breidbach, and Cederbaum

J. Chem. Phys. **123**, 044111 (2005)

In conclusion, we would like to point out that the approach proposed in this work opens the door to the analysis of multielectron dynamical processes in larger, biophysically relevant systems.

ACKNOWLEDGMENTS

The authors wish to thank Jochen Schirmer for suggesting the use of the non-Dyson version of the ADC method in the direct propagation and charge-migration analysis. We thank Hans-Dieter Meyer for many helpful discussions on the Lanczos algorithm and for his help in developing the propagation code. One of us (A.I.K.) thanks the Alexander von Humboldt Foundation for his fellowship. Financial support by the DFG is gratefully acknowledged.

- ¹G. D. Billing and K. V. Mikkelsen, *Advanced Molecular Dynamics and Chemical Kinetics* (Wiley, New York, 1997).
- ²*Conical Intersections*, Advanced Series in Physical Chemistry Vol. 15, edited by W. Domcke, D. Yarkony, and H. Köppel (World Scientific, Singapore, 2004).
- ³G. A. Worth and L. S. Cederbaum, *Annu. Rev. Phys. Chem.* **55**, 127 (2004).
- ⁴L. S. Cederbaum and J. Zobeley, *Chem. Phys. Lett.* **307**, 205 (1999).
- ⁵J. Breidbach and L. S. Cederbaum, *J. Chem. Phys.* **118**, 3983 (2003).
- ⁶J. Breidbach and L. S. Cederbaum, *Phys. Rev. Lett.* **94**, 033901 (2005).
- ⁷M. Drescher, R. Kienberger, M. Uiberacker *et al.*, *Nature (London)* **419**, 803 (2002).
- ⁸H. Niikura, D. M. Villeneuve, and P. B. Corkum, *Phys. Rev. Lett.* **94**, 083003 (2005).
- ⁹F. Robicheaux and R. C. Forrey, *J. Phys. B* **38**, S363 (2005).
- ¹⁰J. Schirmer, L. S. Cederbaum, and O. Walter, *Phys. Rev. A* **28**, 1237 (1983).
- ¹¹J. Schirmer, A. B. Trofimov, and G. Staler, *J. Chem. Phys.* **109**, 4734 (1998).
- ¹²H. Hennig, J. Breidbach, and L. S. Cederbaum, *J. Chem. Phys.* **122**, 134104 (2005).
- ¹³C. J. Lanczos, *J. Res. Natl. Bur. Stand.* **45**, 255 (1950).
- ¹⁴T. J. Park and J. C. Light, *J. Chem. Phys.* **85**, 5870 (1986).
- ¹⁵C. Leforestier, R. H. Bisseling, C. Cerjan *et al.*, *J. Comput. Phys.* **94**, 59 (1991).
- ¹⁶G. Jolicard and E. Austin, *J. Chem. Phys.* **95**, 5056 (1991).
- ¹⁷M. H. Beck, A. Jänckle, J. A. Worth, and H.-D. Meyer, *Phys. Rep.* **324**, 1 (2001).
- ¹⁸W. E. Arnoldi, *Q. Appl. Math.* **9**, 17 (1951).
- ¹⁹R. A. Friesner, L. S. Tuckerman, B. C. Dornblaser, and T. V. Russo, *J. Sci. Comput.* **4**, 327 (1989).
- ²⁰U. V. Riss and H.-D. Meyer, *J. Phys. B* **26**, 4503 (1993).
- ²¹A. I. Kuleff and L. S. Cederbaum (unpublished).
- ²²R. Santra, L. S. Cederbaum, and H.-D. Meyer, *Chem. Phys. Lett.* **303**, 413 (1999).
- ²³J. Schirmer, L. S. Cederbaum, and O. Walter, *Phys. Rev. A* **28**, 1237 (1983).
- ²⁴L. S. Cederbaum, in *Encyclopedia of Computational Chemistry*, edited by P. von Ragué Schleyer, P. R. Schreiner, H. F. Schaefer, III, W. L. Jorgensen, W. Thiel, and R. C. Glen (Wiley, Chichester, 1998), p. 1.
- ²⁵Y. Öhrn and G. Born, *Adv. Quantum Chem.* **13**, 1 (1981).
- ²⁶J. Schirmer, *Phys. Rev. A* **43**, 4647 (1991).
- ²⁷F. Mertins and J. Schirmer, *Phys. Rev. A* **53**, 2140 (1996).
- ²⁸A. L. Fetter and J. D. Walecka, *Quantum Theory of Many-Particle Systems* (Dover, New York, 2003).
- ²⁹J. Schirmer and A. B. Trofimov, *J. Chem. Phys.* **120**, 11449 (2004).
- ³⁰H. Hennig, J. Breidbach, and L. S. Cederbaum, *J. Phys. Chem.* **109**, 409 (2005).
- ³¹R. Weinkauff, P. Aicher, G. Wesley, J. Grotemeyer, and E. W. Schlag, *J. Phys. Chem.* **98**, 8381 (1994).
- ³²R. Weinkauff, P. Schanen, D. Yang, S. Soukara, and E. W. Schlag, *J. Phys. Chem.* **99**, 11255 (1995).
- ³³R. Weinkauff, P. Schanen, A. Metsala, E. W. Schlag, M. Bürgle, and H. Kessler, *J. Phys. Chem.* **100**, 18567 (1996).
- ³⁴R. Weinkauff, E. W. Schlag, T. J. Martinez, and R. D. Levine, *J. Phys. Chem. A* **101**, 7702 (1997).
- ³⁵GAMESS UK, v6.2.1: Package of *ab initio* programs written by M. F. Guest, J. H. van Lenthe, J. Kendrick *et al.* The package is derived from the original GAMESS code due to M. Dupuis, D. Spangler, and J. Wendoloski, NRCC software catalog, Vol. 1, Program No. QG01 (GAMESS), 1980. Used module: MCSCF/CASSCF; P. J. Knowles, G. J. Sexton, and N. C. Handy, *Chem. Phys.* **72**, 337 (1982); P. J. Knowles and H.-J. Werner, *Chem. Phys. Lett.* **115**, 259 (1985).
- ³⁶T. H. Dunning, Jr., *J. Chem. Phys.* **53**, 2823 (1970); T. H. Dunning, Jr. and P. J. Hay, in *Methods of Electronic Structure Theory*, edited by H. F. Schaefer III (Plenum, New York, 1977), Vol. 2.
- ³⁷W. T. Pollard and R. A. Friesner, *J. Chem. Phys.* **100**, 5054 (1994).
- ³⁸A. I. Kuleff and L. S. Cederbaum (to be published).
- ³⁹A. Szabo and N. S. Ostlund, *Modern Quantum Chemistry* (McGraw-Hill, New York, 1989).
- ⁴⁰L. S. Cederbaum, W. Domcke, J. Schirmer, and W. von Niessen, *Adv. Chem. Phys.* **65**, 115 (1986).

Tracing Ultrafast Interatomic Electronic Decay Processes in Real Time and Space

Alexander I. Kuleff* and Lorenz S. Cederbaum

Theoretische Chemie, Universität Heidelberg, Im Neuenheimer Feld 229, 69120 Heidelberg, Germany

(Received 28 August 2006; published 23 February 2007)

Advances in laser pump-probe techniques open the door for observations in real time of ultrafast *electronic processes*. Particularly attractive is the visualization of interatomic processes where one can follow the energy transfer from one atom to another. The interatomic Coulombic decay (ICD) provides such a process which is abundant in nature. A wave packet propagation method now enables us to trace fully *ab initio* the electron dynamics of the process in real time and space, taking into account *all* electrons of the system and their correlations. The evolution of the electronic cloud during the ICD process in NeAr following Ne2s ionization is computed and analyzed. The process takes place on a femtosecond time scale, and a surprisingly strong response is found already in the attosecond regime.

DOI: [10.1103/PhysRevLett.98.083201](https://doi.org/10.1103/PhysRevLett.98.083201)

PACS numbers: 34.30.+h, 31.70.Hq, 82.33.Fg

In recent years tremendous developments of laser pump-probe experimental techniques made possible a direct observation in real time of different kinds of ultrafast processes with subfemtosecond resolution [1–4]. This opened the door for the investigation of electronic processes in the attosecond or femtosecond time scale that take place before the nuclear dynamics comes into play. Processes like the rearrangement of the electronic system following an excitation of an inner-shell electron can now be traced in time and space and analyzed. These capabilities promise a revolution in our microscopic knowledge and understanding of matter.

The excitation of an electron from an atomic shell other than the outermost valence orbital creates a transient hole state. This hole is not stable and the system tends to minimize its energy by filling the vacancy with an electron from an outer shell, the excess binding energy being either carried away by an extreme uv or x-ray fluorescence photon or transferred via Coulomb forces to another electron, which subsequently escapes from the atomic binding. When possible energetically, the latter nonradiative mechanism of deexcitation is extremely efficient in comparison to the competing photon emission. Indeed, the characteristic times are typically less than 100 fs ($1 \text{ fs} = 10^{-15} \text{ s}$) to even well less than a femtosecond entering the attosecond regime ($1 \text{ asec} = 10^{-18} \text{ s}$), compared to radiative decay lifetimes which, except for core levels of heavy elements, belong to the nanosecond range ($1 \text{ ns} = 10^{-9} \text{ s}$).

The nonradiative decay processes can be divided into two major categories depending on whether the electrons involved in the process belong to the same or different subunits of the system. The former are referred to as intratomic (intramolecular) decay processes and the latter as interatomic (intermolecular) decay processes. An example of intra-atomic decay is the well-known Auger effect, following a core ionization of atoms, which besides its fundamental importance has a wide range of applications. Depending on the energy of the core hole and the strength of the electronic coupling, the Auger lifetimes range from a

few femtoseconds to a few hundreds attoseconds (in the so-called super-Coster-Kronig transitions). That is why the observation in real time of the electron dynamics of such processes became possible only recently. Few years ago, Drescher *et al.* [1] using a subfemtosecond x-ray pulse for excitation and a few-cycle light pulse for probing the emission traced the electron rearrangement during the $M_{4,5}N_1N_{2,3}$ Auger decay in Kr, with a lifetime of the *M*-shell vacancy of about 8 fs, giving birth to time-resolved atomic inner-shell spectroscopy.

Contrary to core ionization, the ionization of inner-valence electrons usually produces ions in excited states lying energetically below the second ionization threshold, thus making the slow radiative decay the only possible deexcitation mechanism as long as the resulting ions are isolated. It has been shown recently [5] that the situation is fundamentally different if the ions are embedded in an environment or have neighbors like in a cluster. Then, the possibility to distribute the positive charges between cluster subunits substantially lowers the double ionization threshold of the cluster compared to that of the isolated subunit giving rise to an interatomic (intermolecular) decay mechanism, where the excess energy of the ion with the inner-valence hole is utilized to ionize a neutral neighbor. The process is ultrafast, in the femtosecond time scale, and the emitted electron has a kinetic energy of a few electron volts. This process, called interatomic (or intermolecular) Coulombic decay (ICD), was predicted theoretically and shown to follow a general decay mechanism, taking place in both hydrogen bonded and van der Waals clusters [5–7]. Very recently, the theoretical findings have been confirmed in a series of spectacular experiments carried out by several groups [8–12]. Other experimental groups are engaged in the preparation of time-resolved ICD experiments using novel attosecond pulse techniques [13,14].

The goal of the present work is to provide for the first time a theoretical description of an interatomic decay process in real time and space. Such a description requires

accurate *ab initio* calculations of the time evolution of the electronic cloud including explicitly the correlations among all the electrons; i.e., it requires *multielectron wave packet dynamics*. Here, we present such a computational method and apply it for tracing in time and space the ICD process in NeAr following the $2s$ ionization of Ne. It should be noted that the method is equally suitable for calculating in real time all kinds of ultrafast electron relaxation processes following an ionization of a system. The technical details of the method are given elsewhere [15], where it is used to compute electron dynamics of *nondecaying* states. Here, only the theoretical foundations of the method as well as some subtleties concerning its application to decaying states will be sketched. We stress that treating the dynamics of a decay process represents a much higher degree of complexity.

The starting point of our investigation is a neutral system $|\Psi_0\rangle$. The ionization of the system generates a nonstationary state $|\Phi_i\rangle$. The resulting hole charge then is traced in time and space; i.e., the time-dependent hole density is calculated. For convenience we assume that the initial state is created by the sudden removal of an electron. The hole density of the ionized system is defined by

$$\begin{aligned} Q(\vec{r}, t) &= \langle \Psi_0 | \hat{\rho}(\vec{r}, t) | \Psi_0 \rangle - \langle \Phi_i | \hat{\rho}(\vec{r}, t) | \Phi_i \rangle \\ &= \rho_0(\vec{r}) - \rho_i(\vec{r}, t), \end{aligned} \quad (1)$$

where $\hat{\rho}$ is the local density operator and $|\Phi_i\rangle$ is the generated initial cationic state. The first term in Eq. (1) is the time-independent ground state density of the neutral system, ρ_0 , and the second one, ρ_i , is the density of the cation which is time dependent, since $|\Phi_i\rangle$ is not an eigenstate of the cation. The quantity $Q(\vec{r}, t)$ describes the density of the hole at position \vec{r} and time t and by construction is normalized at all times t . In the Heisenberg picture, the time-dependent part $\rho_i(\vec{r}, t)$ reads

$$\begin{aligned} \rho_i(\vec{r}, t) &= \langle \Phi_i | e^{i\hat{H}t} \hat{\rho}(\vec{r}, 0) e^{-i\hat{H}t} | \Phi_i \rangle \\ &= \langle \Phi_i(t) | \hat{\rho}(\vec{r}, 0) | \Phi_i(t) \rangle, \end{aligned} \quad (2)$$

where $|\Phi_i(t)\rangle = e^{-(i/\hbar)\hat{H}t} |\Phi_i\rangle$ is the propagating multielectron wave packet.

Using the standard representation of the density operator in a one-particle basis $\{\varphi_p(\vec{r})\}$, often called orbitals, and occupation numbers $\{n_p\}$, Eq. (1) can be rewritten in the following form:

$$Q(\vec{r}, t) = \sum_{p,q} \varphi_p^*(\vec{r}) \varphi_q(\vec{r}) N_{pq}(t), \quad (3)$$

where the matrix $\mathbf{N}(t) = \{N_{pq}(t)\}$ with elements

$$N_{pq}(t) = \delta_{pq} n_p - \sum_{M,N} \langle \Phi_i(t) | \tilde{\Psi}_M \rangle \rho_{MN} \langle \tilde{\Psi}_N | \Phi_i(t) \rangle \quad (4)$$

is referred to as the hole density matrix. The second term of Eq. (4) is obtained by inserting in Eq. (2) a resolution of

identity of a complete set of appropriate ionic eigenstates $|\tilde{\Psi}_M\rangle$. The matrix ρ_{MN} is the representation of the density operator within this basis.

Diagonalization of the matrix $\mathbf{N}(t)$ for fixed time points t leads to the following expression for the hole density:

$$Q(\vec{r}, t) = \sum_p |\tilde{\varphi}_p(\vec{r}, t)|^2 \tilde{n}_p(t), \quad (5)$$

where $\tilde{\varphi}_p(\vec{r}, t)$ are called *natural charge orbitals*, and $\tilde{n}_p(t)$ are their *hole occupation numbers*. The hole occupation number, $\tilde{n}_p(t)$, contains the information which part of the created hole charge is in the natural charge orbital $\tilde{\varphi}_p(\vec{r}, t)$ at time t . Because of the conservation of hole charge, one finds that $\sum_p \tilde{n}_p(t) = 1$ at any time. The hole occupation numbers, together with the hole density, are central quantities in the observation and interpretation of the multi-electron dynamics taking place after the removal of an electron.

For calculating the hole density matrix [Eq. (4)], we have used *ab initio* methods only. The description of the nonstationary ionic state was done by means of the formalism of Green's functions, using the so-called algebraic diagrammatic construction scheme [16,17], and the direct time propagation of the electronic wave packet was performed through the short iterative Lanczos technique (see, e.g., Ref. [18]). For more details, see Ref. [15] and references therein. An important point should be addressed. Since the formalism is used for tracing the evolution of decaying states, i.e., a second hole is created in the system and an electron is ejected into the continuum, special care must be taken in constructing an appropriate basis set in order to have a good description of the continuum electron at least in some volume around the origin.

We have applied the above sketched methodology to describe in real time the interatomic decay of the Ne $2s$ vacancy in NeAr. The choice of the system is motivated by the availability of Ne $_n$ Ar $_m$ clusters [11], and by the fact that the lifetime of the Ne $2s$ hole (35 fs, see below) is short compared to the nuclear motion (vibrational and rotational periods of NeAr are 1.2 and 180 ps, respectively), justifying the use of clamped nuclei. The internuclear distance is taken to be 3.5 Å, the equilibrium geometry of the NeAr cluster. To simulate an experiment, one would have to compute the process at various internuclear distances and then average over the weighted distribution of these distances. Nevertheless, such an averaging should only induce some smoothing of the curves presented below and a small shift of the predicted decay time.

The electron dynamics calculations on NeAr have been performed using a combination of atomic and distributed Gaussian basis sets. The atomic basis set was chosen to be d-aug-cc-pVDZ on Ne and aug-cc-pVDZ on Ar. The distributed Gaussian basis consisted of (6s, 4p, 3d) Kaufmann *et al.* [19] diffuse functions centered between the Ne and Ar and the 36 s-functions placed on a grid on the x, y, and z axes. The positions and the exponents of the latter are

optimized to approximate up to 15 \AA from the system the radial part of the Coulomb s -wave with a kinetic energy of the ICD electron.

In Fig. 1 we show the results for the hole occupation numbers [see Eq. (5)] as a function of time for NeAr after sudden removal of a Ne $2s$ electron. This implies that $\bar{n}_{\text{Ne}2s} = 1$ at $t = 0$ and all other hole occupation numbers are zero. As time proceeds, the initial hole (black curve) is gradually filled up, and two other holes are opened (the two ascending curves). This is accompanied by the creation of an electron (“negative” hole) in the virtual orbital space (the lowest curve). For transparency, the hole occupations corresponding to the p_x , p_y , and p_z components of the orbitals are grouped together, as well as all negative occupations contributing to the description of the continuum electron. The time evolution of the hole occupations reflects the time scale of the ICD process. After about 35 fs, the initial hole on Ne $2s$ is filled by an electron from the Ne $2p$ orbitals, and an electron from the Ar $3p$ orbitals is ejected into the continuum, represented in our treatment by a vast number of virtual orbitals. The ICD lifetime is thus about 35 fs, in very good agreement with the result obtained by elaborate *ab initio* calculations of the decay width [20]. Several decay channels participate (see below), and therefore the shape of the Ne $2s$ hole occupation curve is not purely single exponential, but rather a linear combination of several exponential functions. In principle, one may think of another process—the hole on Ne $2s$ is filled by an electron from the Ar $3p$, and an electron from the Ne $2p$ is ejected. However, our numerical analysis of the electronic wave packet shows that the decay probability of this pathway is negligible, being several orders of magnitude smaller than that of the ICD process.

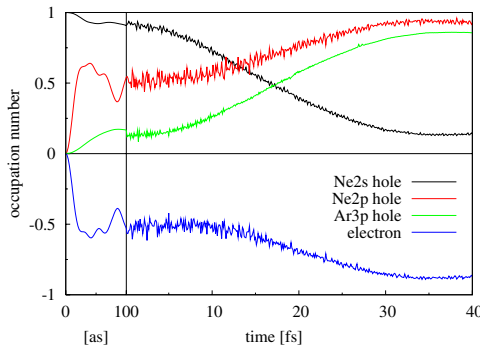


FIG. 1 (color online). Time-dependent hole occupation numbers of NeAr after Ne $2s$ ionization. Note the different time scale on the left part of the graphic. The initially ionized Ne $2s$ orbital, plotted in black, loses more than 80% of its hole charge in about 35 fs. In the same time, two other holes are opened—one on Ne $2p$ [upper ascending (red) curve], and one on Ar $3p$ [lower ascending (green) curve]—and more than 90% of an electron is created in the continuum [the lowest (blue) curve].

It is worth mentioning that, due to the finite basis set used, after some time the hole occupation numbers cease to reflect the physical reality when dealing with decaying states, since the so-described continuum electron actually cannot leave the system. When the ICD electron reaches the spatial end of the basis set it can be reflected back yielding unphysical oscillations of the hole occupation numbers. In the present study such oscillations appear after about 50 fs. That is why the size of the space covered by the basis set is of crucial importance for the proper description of decaying states.

An interesting phenomenon is observed in the ultrashort time scale after the sudden ionization. On the left-hand side of Fig. 1 the first 100 asec of the process are presented on an expanded scale. Besides the fast drop of the initial occupancy for about 50 asec, shown to be universal for multielectron systems and related to the filling of the exchange-correlation hole [21], one observes an extremely strong response of the system to the creation of the Ne $2s$ hole. In just 30 asec, more than half of a full hole is opened on Ne $2p$ and more than half of an electron is already in the continuum. In such a short time the system is already “prepared” for the consecutive ICD process which is completed 35 fs later. The removal of a Ne $2s$ electron is seen to introduce an enormous disturbance of the electronic cloud yielding an extremely fast hole-particle excitation. We mention that at such short times a local “violation” of the energy conservation is possible. Indeed, following the Heisenberg uncertainty relation, $\Delta E \Delta t \sim \hbar$, one finds for times ~ 30 asec an energy dispersion $\Delta E \sim 220$ eV. This is by far more than the energy involved in the whole ICD process.

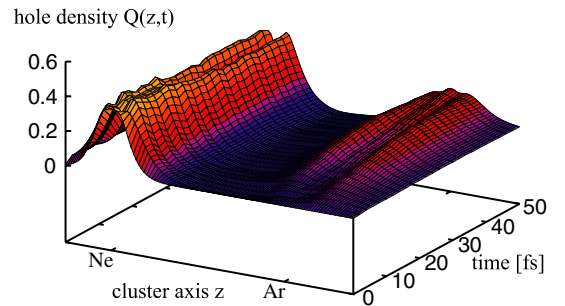


FIG. 2 (color online). Hole density $Q(z, t)$ plotted against the Ne-Ar axis z as a function of time after Ne $2s$ ionization of NeAr. $Q(z, t)$ is obtained by integrating the total charge over the coordinates perpendicular to the z axis. The initial hole density changes its character from a one- to a two-ridge surface, corresponding to the filling of the Ne $2s$ hole predominantly by a Ne $2p_z$ electron. In the same time a Ar $3p$ hole is created (right-hand side of the plot), which also has mainly p_z character up to about 40 fs. One clearly sees that the dominant ICD channel is $\text{Ne}^+(2s^{-1})\text{Ar} \rightarrow \text{Ne}^+(2p_z^{-1})\text{Ar}^+(3p_z^{-1})$.

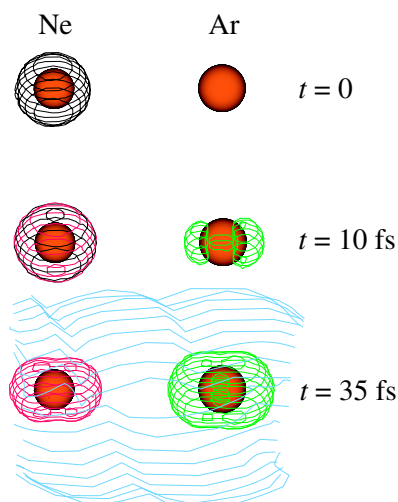


FIG. 3 (color online). The contribution of the holes [$\bar{n}_p(t) \geq 0$ in Eq. (5)] to the hole density $Q(\vec{r}, t)$ at times 0, 10, and 35 fs. For completeness, at $t = 35$ fs the electron density in the continuum [$\bar{n}_p(t) < 0$ in Eq. (5)] is also given [space-filling opened (light blue) curves]. The colors used correspond to those utilized in Fig. 1.

More insight into the process is gained by inspecting the time evolution of the hole density, Eq. (5). In Fig. 2 the charge $Q(z, t)$ obtained by integrating $Q(\vec{r}, t)$ over the coordinates perpendicular to the Ne-Ar axis (z axis) is plotted. The displayed results support the conclusion that the dominant decay is to $\text{Ne}^+(2p_z^{-1})\text{Ar}^+(3p_z^{-1})$; see also Ref. [20]. Indeed, the initial hole density (left-hand side of the surface in Fig. 2) changes its character from a one- to a two-ridge surface, corresponding to the filling of the initial $\text{Ne}2s$ hole predominantly by a $\text{Ne}2p_z$ electron. The second hole opened on Ar (right-hand side of the surface) displays predominantly p_z character up to about 40 fs. The channel ending with $\text{Ar}^+(3p_{x,y}^{-1})$, seen as a tiny, steadily increasing ridge situated between the two wide humps on the right-hand side of the surface, becomes important after that time indicating a slower decay channel.

The surface in Fig. 2 represents the total charge density obtained by summing over both positive and negative occupancies, i.e., over hole and electron charges. Because of the mutual cancellations in some spatial regions, it is insightful to separate the hole and electron charges, i.e., to show separately the positive and negative occupancies. In Fig. 3 the so-determined hole charge density $Q(\vec{r}, t)$ is shown in three dimensions for the three different times $t = 0, 10$, and 35 fs. One clearly sees the stages of the ICD process. After 10 fs the initial $2s$ hole on Ne is already a mixture of s and p_z character, and at the

same time the p_z hole on Ar is already partly formed. After 35 fs the decay via the faster channel of the ICD process is essentially completed and we see $\text{Ne}2p_z$ and $\text{Ar}3p_z$ holes, while the $\text{Ar}3p_{x,y}$ orbitals have just started to contribute to the formation of the $\text{Ar}3p$ hole. For completeness, the electron density in the continuum at $t = 35$ fs is also displayed in Fig. 3.

Let us summarize. A fully *ab initio* methodology for calculating in real time ultrafast electron relaxation dynamics processes after ionization of a system is proposed. The method gives the possibility to trace in time and space the electron dynamics throughout different nonradiative decays taking into account *all* electrons of the system and their correlations. We have presented the first study of the multielectron dynamics of the interatomic Coulombic decay in NeAr following $\text{Ne}2s$ ionization. The results disclose many microscopic details of the decay process in space as time proceeds. To trace the dynamics of the decay directly in the time domain with attosecond resolution, a pump-probe experiment can be done in analogy to that described in Ref. [1]. We hope that the present research will stimulate future experimental and theoretical studies.

Financial support by the DFG is acknowledged.

*Electronic address: alexander.kuleff@pci.uni-heidelberg.de

- [1] M. Drescher *et al.*, Nature (London) **419**, 803 (2002).
- [2] H. Niikura *et al.*, Nature (London) **417**, 917 (2002).
- [3] H. Niikura *et al.*, Nature (London) **421**, 826 (2003).
- [4] H. Niikura *et al.*, Phys. Rev. Lett. **94**, 083003 (2005).
- [5] L. S. Cederbaum *et al.*, Phys. Rev. Lett. **79**, 4778 (1997).
- [6] R. Santra and L. S. Cederbaum, Phys. Rev. Lett. **90**, 153401 (2003).
- [7] V. Averbukh and L. S. Cederbaum, Phys. Rev. Lett. **96**, 053401 (2006).
- [8] S. Marburger *et al.*, Phys. Rev. Lett. **90**, 203401 (2003).
- [9] T. Jahnke *et al.*, Phys. Rev. Lett. **93**, 163401 (2004).
- [10] G. Öhrwall *et al.*, Phys. Rev. Lett. **93**, 173401 (2004).
- [11] S. Barth *et al.*, Phys. Chem. Chem. Phys. **8**, 3218 (2006).
- [12] Y. Morishita *et al.*, Phys. Rev. Lett. **96**, 243402 (2006).
- [13] S. Leone and D. Neumark (private communication).
- [14] H. Kapteyn (private communication).
- [15] A. I. Kuleff *et al.*, J. Chem. Phys. **123**, 044111 (2005).
- [16] L. S. Cederbaum, in *Encyclopedia of Computational Chemistry*, edited by P. v. R. Schleyer *et al.* (Wiley, Chichester, 1998).
- [17] J. Schirmer *et al.*, J. Chem. Phys. **109**, 4734 (1998).
- [18] C. Leforestier *et al.*, J. Comput. Phys. **94**, 59 (1991).
- [19] K. Kaufmann *et al.*, J. Phys. B **22**, 2223 (1989).
- [20] S. Scheit *et al.*, J. Chem. Phys. **124**, 154305 (2006).
- [21] J. Breidbach and L. S. Cederbaum, Phys. Rev. Lett. **94**, 033901 (2005).

Available online at www.sciencedirect.com

Chemical Physics 338 (2007) 320–328

Chemical
Physicswww.elsevier.com/locate/chemphys

Charge migration in different conformers of glycine: The role of nuclear geometry

Alexander I. Kuleff ^{*,1}, Lorenz S. Cederbaum*Theoretische Chemie, PCI, Universität Heidelberg, Im Neuenheimer Feld 229, 69120 Heidelberg, Germany*

Received 5 February 2007; accepted 18 April 2007

Available online 25 April 2007

Abstract

The migration of hole charge created via ionization of the main conformers of the gaseous amino acid glycine is studied. The migration is ultrafast and is mediated solely by many-electron effects, i.e. electronic correlation and relaxation. The influence of the nuclear geometry is investigated by studying the three most abundant conformers of glycine. It is shown that the electron dynamics following ionization can be dramatically different for the different conformers. To facilitate the discussion of the charge migration, the ionization spectra of the conformers are computed as well.

© 2007 Elsevier B.V. All rights reserved.

Keywords: Ultrafast charge migration; Glycine conformers; Ionization spectra

1. Introduction

Charge transfer is a fundamental phenomenon in nature and also plays an essential role in many chemical, biological and even physical processes. Hence, it is not surprising, that it is a subject of a vast number of scientific investigations. The concept “charge transfer”, however, is not attributed to an elementary process step or mechanism, but rather to variety of phenomena where, in general, an electron (or a hole charge) is transported from one site of a molecular system, usually termed a donor site, to another – an acceptor site. One special source of examples of charge transfer is supplied by biophysics. A classical example here is the photosynthesis, where the charge transfer is of central importance for the development of the process after the absorption of a photon by the chlorophyll molecule [1].

Traditionally it is assumed that the nuclear dynamics play an essential role in the course of the charge transfer process. In particular, that the process of charge transfer occurs through the non-adiabatic coupling between the nuclear and electronic motion. Usually, a weak non-adiabatic coupling is supposed (allowing a perturbative treatment), which leads to a relatively slow timescale of the transfer (see, e.g. Ref. [2] and references therein). We remark that nuclear dynamics through a conical intersection of potential energy surfaces is ultrafast [3–5]. Indeed, recent measurements and theoretical investigations showed that charge transfer mediated by conical intersections can take place [6–12]. This mechanism leads to an intramolecular [6,7] and even intermolecular [8,10–12] charge transfer. Typically one expects in those cases a timescale of about 100 fs (1 fs = 10⁻¹⁵ s).

An important question arises. Is it possible that the charge transfer is mediated also purely electronically, i.e. without the influence of the nuclear motion? It was shown [13] that the answer to this question is yes and a very efficient charge transfer can be driven solely by many-electron effects (electron correlation and relaxation) [14–18]. In order to distinguish this mechanism from the conventional

* Corresponding author.

E-mail addresses: alexander.kuleff@pci.uni-heidelberg.de (A.I. Kuleff), lorenz.cederbaum@pci.uni-heidelberg.de (L.S. Cederbaum).

¹ On leave from Institute for Nuclear Research and Nuclear Energy, BAS, 72, Tzarigradsko Chaussee Blvd., 1784 Sofia, Bulgaria.

charge transfer it was termed *charge migration*. This migration takes place on an ultrafast timescale (usually few femtoseconds) and thus it can be calculated neglecting the nuclear motion as long as one studies the relevant time interval during which this ultrafast migration takes place. Clearly, if we wish to know precisely what happens at later times, nuclear motion must be considered. However, since several or even many electronic states participate, an adequate description of the nuclear motion is rather involved.

It should be mentioned that Remacle and Levine [19] proposed a model for a description of charge migration along a molecular backbone. The authors used a Hückel–Hubbard Hamiltonian with one orbital per molecular site to describe the charge hopping between different molecular sites of an n -site chain. An on-site Coulomb repulsion of electrons of opposite spin is included in the model, which can suppress the hopping (or the charge migration) and is thus an indication for the importance of many-body effects.

In the present work we study the migration of a hole charge initiated by a sudden ionization of the amino acid glycine. Emphasis is put on the dependence of the charge migration on the nuclear geometry of the studied system. For this purpose three different conformers of glycine, the most abundant ones in gas phase, are investigated. Glycine ($\text{NH}_2\text{—CH}_2\text{—COOH}$) is the simplest amino acid and is one of the most biologically important compounds known to exist in the gas phase in a non-ionized form [20–22], and often serves as a prototype structural unit in the investigation of more complex composites like peptides or proteins.

The paper is organized as follows. In Section 2 the multi-electron wavepacket propagation methodology for studying electron dynamics following a sudden removal of an electron from a system is briefly reviewed. Section 3 is devoted to the application of the method to three of the glycine conformers. The differences in the ionization spectra and in the evolution of the electronic cloud after a removal of an electron out of three different orbitals is analyzed and discussed for all three glycine conformers. We summarize the results and conclude in Section 4.

2. Theory: multi-electron wavepacket propagation

In what follows we briefly review the theoretical foundations of the methodology used to study charge migration following ionization of a system, referring the reader to Refs. [14,17,18] for technical details.

The starting point of our investigation is a neutral system in its ground state $|\Psi_0\rangle$. The ionization of the system generates a non-stationary state $|\Phi_i\rangle$. For convenience we assume that the initial ionic state is created by the sudden removal of an electron. The density of the initially created hole, or briefly the *hole density*, then can be defined by the following expression:

$$\begin{aligned} Q(\vec{r}, t) &:= \langle \Psi_0 | \hat{\rho}(\vec{r}, t) | \Psi_0 \rangle - \langle \Phi_i | \hat{\rho}(\vec{r}, t) | \Phi_i \rangle \\ &= \rho_0(\vec{r}) - \rho_i(\vec{r}, t), \end{aligned} \quad (1)$$

where $\hat{\rho}$ is the local density operator. The first term on the right-hand side of Eq. (1), ρ_0 , is the ground state density of the neutral system and is time-independent, while the second one, ρ_i , is the density of the cation and is time-dependent, since $|\Phi_i\rangle$ is not an eigenstate of the cation. The quantity $Q(\vec{r}, t)$ describes the density of the hole at position \vec{r} and time t and by construction is normalized at all times t . In the Heisenberg picture, the time-dependent part $\rho_i(\vec{r}, t)$ reads

$$\rho_i(\vec{r}, t) = \langle \Phi_i | e^{i\hat{H}t} \hat{\rho}(\vec{r}, 0) e^{-i\hat{H}t} | \Phi_i \rangle = \langle \Phi_i(t) | \hat{\rho}(\vec{r}, 0) | \Phi_i(t) \rangle, \quad (2)$$

where $|\Phi_i(t)\rangle = e^{-i\hat{H}t} |\Phi_i\rangle$ is the propagating multi-electron wavepacket.

Using the standard representation of the density operator in an one-particle basis $\{\varphi_p(\vec{r})\}$ and occupation numbers $\{n_p\}$, Eq. (1) can be rewritten as follows:

$$Q(\vec{r}, t) = \sum_{p,q} \varphi_p^*(\vec{r}) \varphi_q(\vec{r}) N_{pq}(t), \quad (3)$$

where the matrix $\mathbf{N}(t) = \{N_{pq}(t)\}$ with elements

$$N_{pq}(t) = \delta_{pq} n_p - \sum_{M,N} \langle \Phi_i(t) | \Psi_M \rangle \rho_{MN} \langle \Psi_N | \Phi_i(t) \rangle \quad (4)$$

is referred to as the hole density matrix. The last term of Eq. (4) is obtained by inserting in Eq. (2) a resolution of identity of a complete set of appropriate ionic states $|\Psi_M\rangle$. The matrix ρ_{MN} is the representation of the density operator within this basis.

Diagonalization of the matrix $\mathbf{N}(t)$ for fixed time points t yields the following expression for the hole density:

$$Q(\vec{r}, t) = \sum_p |\tilde{\varphi}_p(\vec{r}, t)|^2 \tilde{n}_p(t), \quad (5)$$

where $\tilde{\varphi}_p(\vec{r}, t)$ are called *natural charge orbitals*, and $\tilde{n}_p(t)$ are their *hole occupation numbers*. The hole occupation number, $\tilde{n}_p(t)$, contains the information which part of the created hole charge is in the natural charge orbital $\tilde{\varphi}_p(\vec{r}, t)$ at time t . Because of the conservation of hole charge, one finds that $\sum_p \tilde{n}_p(t) = 1$ at any time. The hole occupation numbers, together with the hole density, are central quantities in the observation and interpretation of the multi-electron dynamics taking place after the removal of an electron.

For calculating the hole density and its constituents we use *ab initio* methods only. The calculation consists of the following steps. First, the ground state geometry of the corresponding conformer of neutral glycine is optimized on the Hartree–Fock level using the standard *ab initio* program package GAMESS-UK [23], with the DZP basis set [24]. This basis set is also used in all the remaining calculations.

The next step is the calculation of the cationic eigenstates. For this purpose we use a Green’s function formalism. A computationally very successful approach to obtain

the Green's function is the *algebraic diagrammatic construction* (ADC(n)) scheme which represents infinite partial summations being exact up to n th order of perturbation theory [25,26]. In the present calculation the non-Dyson ADC(3) approximation scheme [27] implemented by Breidbach [16,18] was utilized. Since the effects we want to study take place on an ultrashort timescale, the fixed equilibrium geometry of the system studied was used. It is worth to mention that in the present calculations nearly 9700 cationic eigenstates are taken into account in constructing the hole density matrix (Eq. (4)) which clearly shows the advantage of the Green's function based approaches, where all the eigenstates are obtained in a single run, over many other standard methods, where one has to compute each state separately.

The third step of the computation consists of the direct propagation of the multielectron wavepacket of the ionized system [17]. This is done by propagating the initial cationic state using thereby the short iterative Lanczos technique (see, e.g. Ref. [28]).

The last step of the calculation procedure is building the matrix $\mathbf{N}(t)$ through Eq. (4), the subsequent diagonalization of which yields the natural charge orbitals $\tilde{\varphi}_p(\vec{r}, t)$ and the hole occupation numbers $\tilde{n}_p(t)$ (see Eq. (5)). With the aid of these quantities we can now trace in time and space the response of the electronic cloud of the system to the sudden removal of one of its electrons.

3. Results: charge migration in glycine

In the present study we focus on the three lowest-energy glycine ($\text{NH}_2\text{CH}_2\text{COOH}$) conformers. All of them possess mirror symmetry with all heavy atoms lying in the mirror plane, i.e. they belong to the C_s symmetry group with irreducible representations a' and a'' . Throughout the text the conformers are denoted as Gly I, Gly II and Gly III, a nomenclature commonly used in the literature [29,30]. The abundance of these conformers depends on the temperature, and for 165° is as follows: Gly I $\sim 53\%$, Gly II $\sim 9\%$ and Gly III $\sim 30\%$ [29,31]. The geometrical parameters of all the three conformers were optimized on the Hartree–Fock level and are in a good agreement with both experimental results and previous theoretical predictions. Both bond lengths and angles deviate by less than 1.5% from the experimental data [21], and by less than 1% from other calculations using higher level of approximation [30,31].

As we will see, the evolution of the electronic cloud following an ionization out of the inner and outer valence shell of glycine is conformer dependent. Since the difference in the time evolution is encoded in the cationic eigenstates, a careful analysis of the ionization spectrum is needed for proper understanding of the underlying mechanisms. We shall, therefore, first discuss the ionization spectra of the glycine conformers which are also of interest by themselves and subsequently the charge migration.

3.1. Ionization spectra of glycine conformers

The energetics of the ionized glycine conformers, calculated through the non-Dyson ADC(3) approach, together with sketches of the corresponding conformers are presented in Fig. 1. For comparison, in the uppermost panel

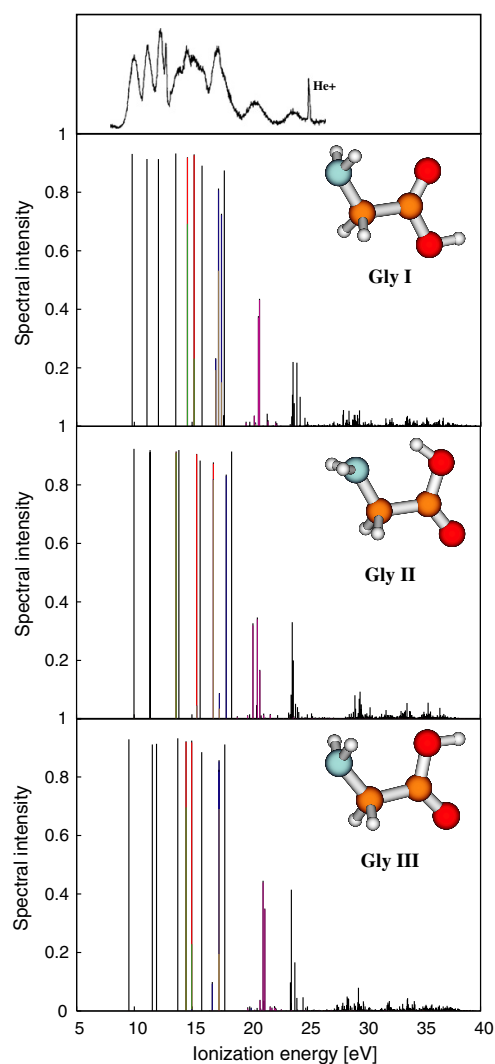


Fig. 1. The ionization spectra of the glycine conformers Gly I, Gly II and Gly III computed in this work (lower three panels), together with the experimental photoelectron He(II) spectrum taken from Ref. [32] (uppermost panel). In each panel with a calculated spectrum a sketch of the nuclear geometry of the corresponding conformer is given. The contributions to the cationic eigenstates of the $1h$ -configurations involved in the studied cases of charge migration are given in colors, all other contributions are given in black. The contributions of the $(14a')^{-1}$ configuration are given in green, those of $(13a')^{-1}$ in red, $(12a')^{-1}$ in brown, $(11a')^{-1}$ in blue, and $(10a')^{-1}$ in violet. (For interpretation of the references in colour in this figure legend, the reader is referred to the web version of this article.)

of the figure the experimental He(II) photoelectron spectrum of glycine (a mixture of all conformers) taken from Ref. [32] is reproduced. It is seen that the calculated spectra are in a very good agreement with the experimental results. The calculated spectra, however, allow a deeper analysis of the electronic structure of glycine conformers.

Each line in the calculated spectrum represents an eigenstate of the cation. The position of the line is given by the corresponding ionization energy, while the height represents the spectral intensity (related to the ionization cross section, see Ref. [33]). An exact cationic state $|I\rangle$ can be expanded in a series of electronic configurations, as is traditionally done in the CI calculations [34]

$$|I\rangle = \sum_j c_j^{(I)} \hat{a}_j |\Phi_0\rangle + \sum_{a,k < l} c_{akt}^{(I)} \hat{a}_a^\dagger \hat{a}_k \hat{a}_l |\Phi_0\rangle + \dots, \quad (6)$$

where $|\Phi_0\rangle$ is some approximation to the ground state of the neutral molecule, e.g. Hartree–Fock, $c^{(I)}$'s are the expansion coefficients, and \hat{a}_p^\dagger and \hat{a}_p are creation and annihilation operators, respectively. In Eq. (6) the indices i, j, k, \dots denote occupied orbitals, or holes, whereas a, b, c, \dots denote unoccupied (virtual) orbitals, or particles. Thus, the sum is over one-hole ($1h$) configurations, as well as over two-hole–one-particle ($2h-1p$) and higher excitations. The $2h-1p$ and higher terms represent actually the electronic correlation and relaxation. Without correlation effects, the spectra in Fig. 1 will be a series of lines, one for each occupied orbital with intensity equal to 1. When going deeper into the electronic shells, the correlation among the electrons typically increases. Thus, with the increase of the ionization energy the spectra become more and more complicated and the one-particle picture ceases to be a good approximation. From some energy on, a general phenomenon known as the *breakdown of the molecular orbital picture* [35] occurs where the ionization out of an orbital leads to the appearance of a multitude of ionic states.

Despite the overall similarity, the spectra of the different conformers show some important differences. First, the ordering of the electronic orbitals is different. For Gly I and Gly III the electronic configuration is

$$\begin{aligned} &(\text{core})(6a')^2(7a')^2(8a')^2(9a')^2(10a')^2(1a'')^2(11a')^2(12a')^2 \\ &(2a'')^2(13a')^2(14a')^2(3a'')^2(4a'')^2(15a')^2(16a')^2, \end{aligned}$$

while for Gly II the orbitals $14a'$ and $3a''$ are swapped and the orbitals $4a''$ and $15a'$ are energetically degenerate. Second, the character of the eigenstates can differ substantially.

Let us concentrate on three cases, namely what happens after ionization out of orbitals $14a'$, $11a'$ and $10a'$. The two former cases are analyzed in Ref. [17] where only the conformer Gly I is studied. In Fig. 1 the contribution to the eigenstates corresponding to the orbitals from $10a'$ to $14a'$ are shown in color. For conformers I and III there are two states in the spectra which are mainly a mixture of $(14a')^{-1}$ and $(13a')^{-1}$ $1h$ -configurations, while all other

configurations have very small weight (see Eq. (6)). These are typical hole-mixing cases [14]. Except for a small energy shift these states are very similar for Gly I and Gly III thus predetermining similar electron dynamics. In contrast, the hole mixing between $14a'$ and $13a'$ is completely missing in Gly II. Instead, there is a hole mixing between the configurations $(13a')^{-1}$ and $(12a')^{-1}$ (shown in brown in Fig. 1).

The differences are even more pronounced if we consider the ionization out of orbital $11a'$. The $(11a')^{-1}$ configuration is given in blue in Fig. 1 and mainly mixes with the $(12a')^{-1}$ configuration. In the case of Gly I there appear three cationic states – the corresponding two main lines at 17.55 eV and 17.29 eV, respectively, and one satellite at 17.04 eV. In the case of Gly III there is a negligible contribution of the $(11a')^{-1}$ configuration to the satellite at 16.75 eV, whose population comes mainly from ionization out of orbital $12a'$. In addition, the two main lines are nearly degenerate and indistinguishable in the figure. For Gly II the configurations $(11a')^{-1}$ and $(12a')^{-1}$ mix only in the satellite state at 17.38 eV, while, as was mentioned above, the configuration $(12a')^{-1}$ mixes also with configuration $(13a')^{-1}$.

The ionization out of orbital $10a'$ represents a case of a breakdown of the molecular orbital picture. The contribution to the eigenstates corresponding to the orbital $10a'$ is shown in violet in Fig 1. Again, the situation is similar in the cases of Gly I and Gly III, and substantially different for Gly II.

All these differences in the spectra of the studied glycine conformers naturally predetermine the different electron dynamics following ionization out of these orbitals.

3.2. Charge migration in glycine conformers

In the following we shall discuss how the positive charge created via an ionization out of the orbitals $14a'$, $11a'$ and $10a'$ evolves in time. Before going into details let us remark that one does not observe charge migration after ionization out of each orbital of the system and the charge simply stays where it is created (the HOMO is for instance such an example). Furthermore, ionization out of not all orbitals of the studied conformers show different electron dynamics.

As was mentioned above, the charge migrations in Gly I and Gly III are quite similar to each other in the case of ionization out of orbital $14a'$. The only difference is the time scale. Since in these two cases the charge migration represent a pure hole-mixing mechanism, one observes an oscillation of the charge between the two involved orbitals, namely $14a'$ and $13a'$. For Gly I (see Figs. 5–8 in Ref. [17]) at time $t = 0$, the hole is on orbital $14a'$, which is spread over the entire molecule, but has its most significant part located on the N-terminal moiety. After 3.5 fs more than 90% of the hole are transferred to orbital $13a'$, which is localized mainly on the carboxyl (COOH) group. After that time, the process continues in reverse order up to

$t \approx 7$ fs when the charge has returned back to its initial position. In the case of Glycine III one finds (not shown) the same situation, but the whole process lasts approximately 9 fs. Thus, in these two cases we encounter a very efficient and ultrafast mechanism of charge transfer from essentially one part of the molecule to another part.

What happens in the case of Glycine II? There, 99.4% of the corresponding cationic state is built from the $(14a')^{-1}$ configuration and, hence, no charge migration occurs. In Fig. 2 the evolution of hole occupation numbers (see Eq. (5)) for the first 20 fs are depicted. As one can see, except for the extremely fast drop of the initial occupancy for about 50 asec, shown to be universal for multielectron systems and related to the filling of the exchange-correlation hole [36], one observes no change of the hole occupation number as time proceeds. Thus, the charge stays where it is created. The hole-particle excitations, represented by the other positive and negative occupations, describe the many-body effects present in the cation. Obviously, the ionization out of orbital $14a'$ leads to completely different behaviors of the different glycine conformers – ultrafast charge migration with a cycle of 7–9 fs in the case of Glycine I and Glycine III, and no charge migration at all in the case of Glycine II.

Let us now examine the electron dynamics following an ionization out of orbital $11a'$. The hole occupation numbers of the natural charge orbitals relevant to the process are presented in Fig. 3 for the three different conformers. For conformer Glycine I (top panel of Fig. 3) we have a combination of hole-mixing and dominant-satellite mechanisms [14] which leads to a nearly complete flow of the charge from the initially ionized orbital $11a'$ to the orbital

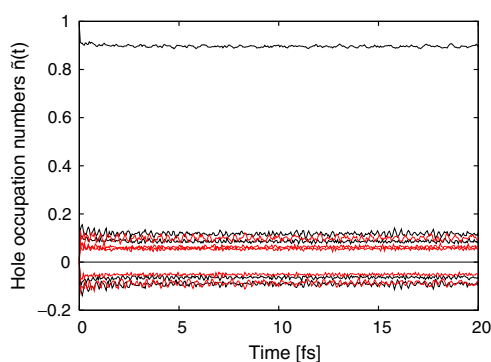


Fig. 2. Time-dependent hole occupation numbers of the glycine conformer Glycine II after ionization out of orbital $14a'$. The curves corresponding to hole occupations of the natural charge orbitals belonging to irrep a' are given in black, while those belonging to a'' in red. Except for the extremely fast drop of the initial occupancy (the uppermost black curve), a general phenomenon discussed elsewhere [36], there is no change of the occupation numbers as time proceeds. The hole-particle excitations, represented by the other positive and negative occupations, describe the many-body effects present in the cation. (For interpretation of the references in colour in this figure legend, the reader is referred to the web version of this article.)

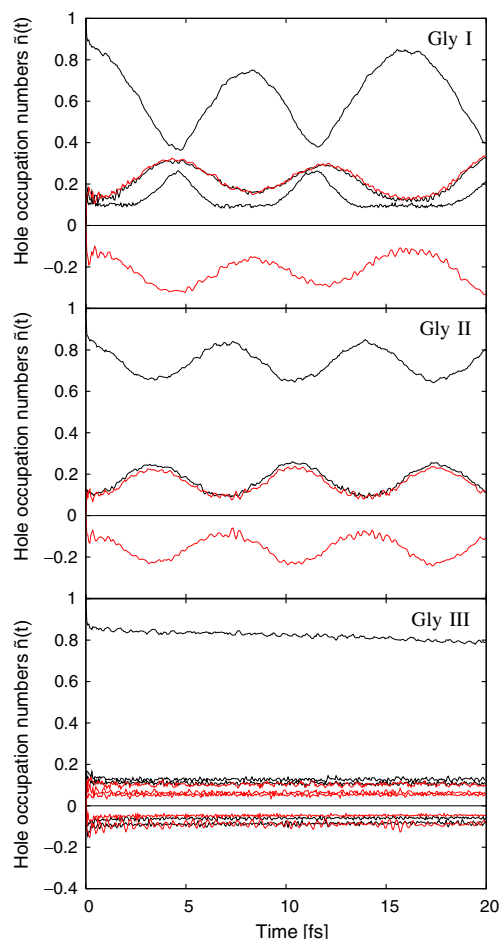


Fig. 3. Time-dependent hole occupation numbers of the studied glycine conformers after ionization out of orbital $11a'$. Occupations of Glycine I are presented in the top panel (taken from Ref. [17]), those for Glycine II in the middle panel, and those for Glycine III in the bottom panel. The curves corresponding to hole occupations of natural charge orbitals belonging to irrep a' are given in black, while those belonging to a'' in red. For Glycine I a combination of hole-mixing and dominant-satellite cases appears, for Glycine II we observe a pure dominant-satellite mechanism, while for Glycine III a pure hole mixing takes place, but in nearly degenerate ionic states thus yielding a very slow electron dynamics. (For interpretation of the references in colour in this figure legend, the reader is referred to the web version of this article.)

$12a'$ in about 8.3 fs. After that time the process continues in reverse order. Note that an avoided crossing appears at about 4.7 fs and again at about 11.2 fs between two of the hole occupations (the uppermost and the lowermost black curves in the top panel of Fig. 3) and the character of the natural charge orbitals corresponding to these hole occupations is swapped there. In space the whole process represents a fast delocalization of the charge – in the beginning it is localized on the carboxyl group and after 8.3 fs it is spread over almost the whole molecule, but having its

maximal density on the C-CH₂ and CH₂-NH₂ groups (see Fig. 4 in Ref. [17]).

For Gly II the ionization out of orbital 11a' leads to a pure dominant-satellite mechanism of charge migration (see the middle panel of Fig. 3). The initially ionized orbital 11a', having hole occupation equal to 1 at time 0, loses its hole charge to the natural charge orbital having more than 85% overlap with orbital 16a' (the lower black curve in the middle panel of Fig. 3). This process is accompanied by an excitation of nearly 0.25 of an electron from 4a'', or HOMO-2, to the initially unoccupied orbital 5a'', or LUMO (the positive and negative red curves in the middle panel of Fig. 3, respectively). The whole process is again cyclic with a period of about 7.4 fs (note that no avoided crossings appear in this case). In space the process also represents a delocalization of the initial charge, but less pronounced than in the case of Gly I.

For Gly III the situation is fundamentally different. The evolution of the hole occupation numbers within the first 20 fs following an ionization out of orbital 11a' in the case of conformer Gly III is shown in the lowest panel of Fig. 3. The mechanism here is a pure hole mixing between orbitals 11a' and 12a', but the two cationic eigenstates built essentially by these 1h configurations are nearly degenerate, the energy difference being only 0.02 eV. Thus, the usual oscillations in the corresponding hole occupations are with a period of about 207 fs, much beyond the timescale where one can treat the electron dynamics separately from the nuclear one. That is why one cannot speak about charge migration here, at least not within the definition of this term discussed in the introduction as a phenomenon of charge transfer entirely due to the many-electron effects and decoupled from the nuclear dynamics.

As our calculations show, the different behavior of different conformers is already evident at short times where the nuclear dynamics is not yet relevant. Nevertheless, it is interesting to see the electron dynamics also at longer times. May be one day it will be possible to also accurately compute the impact of nuclear dynamics on charge migration.

Let us now turn to the electron dynamics following ionization out of orbital 10a'. As was mentioned in Section 3.1, in all three conformers the ionization out of orbital 10a' yields a breakdown of the molecular orbital picture, where one cannot distinguish between main and satellite states. It should be mentioned that this ionization does not lead to a decaying electronic state. The double ionization threshold is several electronvolts higher in all three conformers. In Fig. 4 the hole occupation numbers of the natural charge orbitals relevant to the process are depicted for the three different conformers up to 30 fs.

For Gly I (top panel of Fig. 4) the initially ionized orbital 10a' loses nearly 97% of its charge in about 21.5 fs (note that there are two avoided crossings occurring around 11 and 15 fs). This charge is almost entirely transferred to orbital 15a' accompanied by an excitation from orbital 3a'' to orbital 5a'' (the upper positive and the negative red

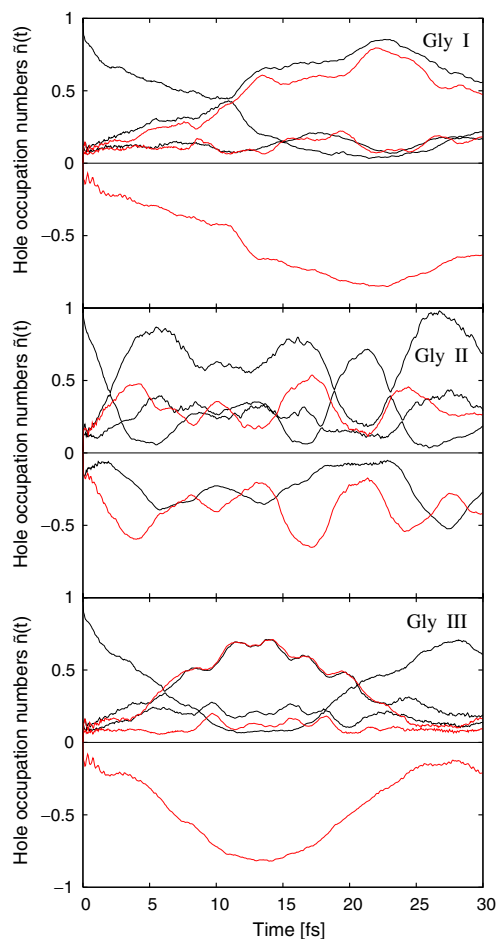


Fig. 4. Time-dependent hole occupation numbers of the studied glycine conformers (Gly I – top panel, Gly II – middle panel, Gly III – bottom panel) after ionization out of orbital 10a'. The curves corresponding to hole occupations of natural charge orbitals belonging to irrep a' are given in black, while those belonging to a'' in red. In all three conformers the ionization out of orbital 10a' leads to a breakdown of the molecular orbital picture. The initially ionized orbital loses almost entirely its charge in about 22, 5 and 13 fs for Gly I, Gly II and Gly III, respectively. Note that in all three cases nearly a full electron is promoted to the virtual orbitals. (For interpretation of the references in colour in this figure legend, the reader is referred to the web version of this article.)

curves in the upper panel of Fig. 4). This excitation promotes more than 85% of an electron to the LUMO orbital of Gly I. After about 24 fs the process continues in reverse order, till nearly 75% of the charge migrates back to its initial position after ~49 fs (not shown in the figure). However, since many ionic states participate in the dynamics, the process is not purely repetitive.

In order to see how the charge transfer takes place in real space, we examine the evolution of the hole density, Eq. (5). In Fig. 5 the hole density is shown for four different

326

A.I. Kuleff, L.S. Cederbaum / Chemical Physics 338 (2007) 320–328

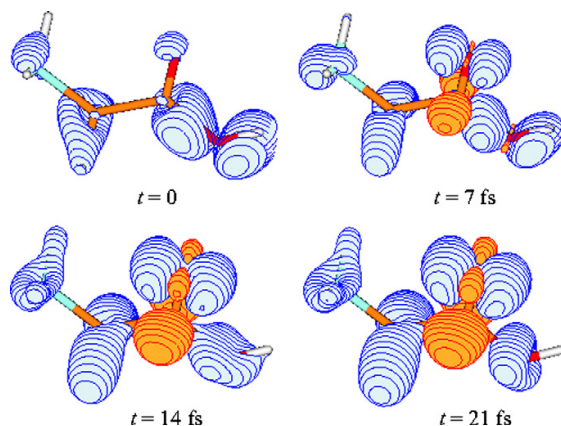


Fig. 5. Hole density $Q(\vec{r}, t)$ of conformer Gly I at four different times $t = 0, 7, 14,$ and 21 fs after ionization out of orbital $10a'$. The “negative” hole density, or the electron density is given in orange. At $t = 0$ the charge is mainly located on the COH group and a smaller part on the CH_2 group. After 21 fs the charge has migrated to the amino (NH_2) group and to the carbonyl oxygen. In addition, almost a full electron is formed mainly around the carbon and a small part on the carbonyl oxygen of the carboxyl group as a result of an excitation mainly from the CH_2 group. (For interpretation of the references in colour in this figure legend, the reader is referred to the web version of this article.)

times: $t = 0, 7, 14$ and 22 fs. As it is seen, at time 0 the hole charge is mainly localized on the COH group and a smaller part on the CH_2 group. As time proceeds the charge migrates to the amino group and to the carbonyl oxygen. In the same time, almost a full electron (given in orange in Fig. 5) is formed mainly around the carbon and a small part on the carbonyl oxygen of the carboxyl group. The excitation is mainly from the CH_2 group, as well as from the amino group and the carboxyl oxygen.

For Gly III (bottom panel of Fig. 4) the electron dynamics is similar, but the process develops nearly twice faster. The initially ionized orbital $10a'$ again loses almost entirely its charge, but now in about 13 fs. During this period of time the charge migrates to orbital $14a'$ and an excitation promotes almost an electron from orbital $4a''$ to the LUMO, $5a''$ (the upper positive and the negative red curves in the bottom panel of Fig. 4). Then, the process continues in reverse order and after about 27 fs more than 70% of the charge is in its initial position on orbital $10a'$. The evolution of the process in space is given in Fig. 6, where the corresponding hole density is depicted for four different times: $t = 0, 4, 8$ and 12 fs. At time 0 the charge is localized mainly on COH and on CH_2 groups. After 4 fs a substantial part of this charge has already migrated to the amino group and to the carbonyl oxygen. In the same time an electron (depicted in orange in Fig. 6) has started to be formed around the carbon of the carboxyl group. After 12 fs a substantial part of the charge is already also on the CN bond and almost an entire electron is formed after an excitation from the carbonyl oxygen to the carbon of

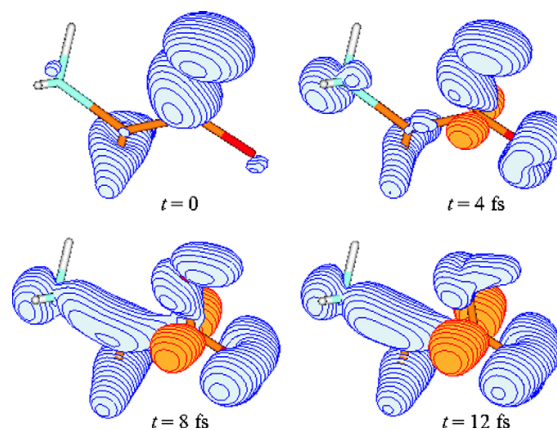


Fig. 6. Hole density $Q(\vec{r}, t)$ of conformer Gly III at four different times $t = 0, 4, 8,$ and 12 fs after ionization out of orbital $10a'$. The “negative” hole density, or the electron density is given in orange. At $t = 0$ the charge is mainly located on the COH and CH_2 groups. After 12 fs the charge has migrated to the amino group and to the carbonyl oxygen. In addition, almost a full electron is formed around the carbon of the carboxyl group, as a result of excitation from orbital $4a''$ (localized mainly on carbonyl oxygen) to orbital $5a''$. (For interpretation of the references in colour in this figure legend, the reader is referred to the web version of this article.)

the carboxyl group (note the symmetry of the corresponding electron and hole densities with respect to the symmetry plane). Thus, the whole process can be divided into two processes proceeding in parallel – a charge migration from hydroxyl group to the aminomethyl group, and an excitation from the carbonyl oxygen to the carbon of the carboxyl group.

For Gly II (middle panel of Fig. 4) the situation is very different. The initially ionized orbital $10a'$ loses more than 96% of its charge in only 5 fs. During that time the hole charge migrates to the orbital $15a'$, or the HOMO. This process is accompanied by mainly two excitations – from orbital $4a''$ to orbital $5a''$, or the LUMO, (the positive and the negative red curves in the middle panel of Fig. 4), and from orbital $14a'$ to orbital $17a'$, or LUMO + 1, (the middle positive and the negative black curves in the middle panel of Fig. 4). Beyond 5 fs the electron dynamics has become quite complicated because many electronic states participate. The process is nevertheless quasicyclic (the main part of the charge returns to its initial position) with a period of about 21 fs. It should be mentioned, however, that after each cycle less and less of the charge returns to its initial position on orbital $10a'$. After the first cycle we find only 70% of the charge back on orbital $10a'$, and after the second one – a little more than 60%.

Let us see how the process develops in real space during the first 6 fs. The hole density is depicted in Fig. 7 for four different times: $t = 0, 2, 4$ and 6 fs. It is seen that at $t = 0$ the hole charge is mainly localized on the COH moiety with a small fraction on the carbonyl oxygen. As time proceeds

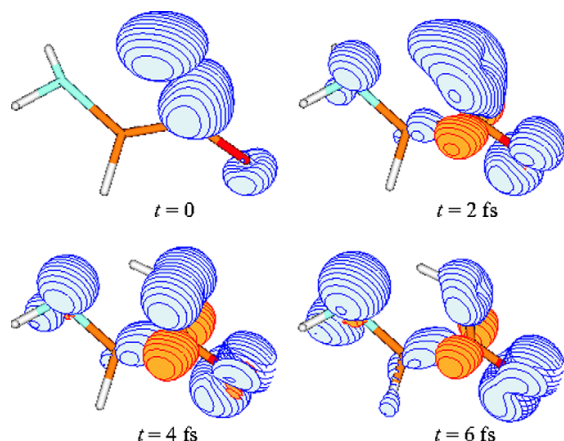


Fig. 7. Hole density $Q(\vec{r}, t)$ of conformer Gly II at four different time points $t = 0, 2, 4,$ and 6 fs after ionization out of orbital $10a'$. The “negative” hole density, or the electron density is given in orange. At $t = 0$ the charge is mainly located on the COH group and a small part on the carbonyl oxygen. After 6 fs the charge has migrated mainly to the nitrogen, carbonyl oxygen and smaller part to the CC bond. In addition, a fraction of an electron is formed around the carbon of the carboxyl group, as a result of an excitation from orbital $4a''$ (localized mainly on carbonyl oxygen) to orbital $5a''$. (For interpretation of the references in colour in this figure legend, the reader is referred to the web version of this article.)

the charge migrates mainly to the nitrogen and carbonyl oxygen, and a smaller part to the CC bond. In addition, an electron starts to be formed around the carbon of the carboxyl group (shown in orange in Fig. 7) and on the amino group, where, due to the mutual cancellation of the positive and “negative” densities, it results mainly in diminution of the hole charge localized on the nitrogen. Thus, in this case we observe an ultrafast charge migration of about 5 fs from the COH group mainly to the two ends of the Gly II molecule, namely to the nitrogen and the carbonyl oxygen. In addition, a fraction of an electron is formed around the carbon of the carboxyl group.

Despite of the differences found, the formation of an electron around the carbon of the carboxyl group is present in the electron dynamics following the ionization out of orbital $10a'$ in all three conformers. It is a result of an excitation from orbital $4a''$ to orbital $5a''$ for Gly II and Gly III, and from orbital $3a''$ to orbital $5a''$ for Gly I. These orbitals are antisymmetric with respect to reflection about the molecular plane and are very little affected by the conformational changes along the nodal plane (see also Ref. [31]). In all three glycine conformers the orbital $3a''$ is localized on CH_2 and smaller parts on NH_2 and carboxyl oxygen, the orbital $4a''$ is on the $\text{C}=\text{O}$ moiety and on the carboxyl oxygen, while the orbital $5a''$ is mainly on the carbon of the carboxyl group and smaller parts on the two oxygens. The presence of positive and negative charges at the same time will strongly affect the subsequent nuclear dynamics, since the nuclei will tend to relax and stabilize the charge.

4. Brief summary

In this paper we have studied the charge migration following ionization out of three different orbitals of three different glycine conformers. The results show that in all three cases the migration is conformer dependent, and can vary from an ultrafast migration of the hole charge (few femtoseconds) to a very slow migration, or even to no migration at all. In the case of ionization out of orbital $14a'$ we observe an ultrafast charge migration with a cycle of 7 and 9 fs in the case of Gly I and Gly III, respectively, and no charge migration at all in the case of Gly II. The ionization out of orbital $11a'$ again leads to a different charge-migration mechanism in the conformers – fast delocalization of the initial charge in less than 10 fs in the case of Gly I and Gly II, and very slow migration of more than 200 fs in the case of Gly III. Finally, the ionization out of orbital $10a'$ gives rise to a different charge migration pattern in all three conformers with timescales varying from about 5 to 20 fs in the various conformers.

Such dissimilarities in the electron dynamics following ionization are surprisingly strong in view of the fact that the studied glycine conformers differ mainly in the mutual orientation of the hydrogen atoms. This clearly shows that the subsequent nuclear dynamics will play an important role, since the movement of the nuclei can trap the charge and block the migration process.

Finally, we remark that strong differences in the electronic dynamics following ionization can be expected to also lead to strong differences in the behavior of the nuclear dynamics because, at least within the Born–Oppenheimer approximation, the electronic motion governs the effective potential seen by the nuclei.

Acknowledgments

This work is dedicated to Jörn Manz on the occasion of his 60th birthday. One of us (L.S.C.) expresses his gratitude for a very long-term friendly relationship. Financial support by the DFG is gratefully acknowledged.

References

- [1] J. Jortner, B. Pullmann (Eds.), *Perspectives in Photosynthesis*, Kluwer, Dordrecht, 1990.
- [2] P.F. Barbara, T.J. Meyer, M.A. Ratner, *J. Phys. Chem.* 100 (1996) 13148.
- [3] H. Köppel, W. Domcke, L.S. Cederbaum, *Adv. Chem. Phys.* 35 (1984) 59.
- [4] W. Domcke, D. Yarkony, H. Köppel (Eds.), *Conical Intersections*, *Advanced Series in Physical Chemistry*, vol. 15, World Scientific, NJ, Singapore, 2004.
- [5] G.A. Worth, L.S. Cederbaum, *Annu. Rev. Phys. Chem.* 55 (2004) 127.
- [6] M. Garavelli, P. Celani, F. Bernardi, M.A. Robb, M. Olivucci, *J. Am. Chem. Soc.* 119 (1997) 6891.
- [7] A. Sanchez-Galvez, P. Hunt, M.A. Robb, M. Olivucci, T. Vreven, H.B. Schlegel, *J. Am. Chem. Soc.* 122 (2000) 2911.
- [8] G.A. Worth, L.S. Cederbaum, *Chem. Phys. Lett.* 338 (2001) 219.

- [9] W. Fuß, K.K. Pushpa, W. Rettig, W.E. Schmid, S.A. Trushin, *Photochem. Photobiol. Sci.* 1 (2002) 255.
- [10] A. Dreuw, G.A. Worth, M. Head-Gordon, L.S. Cederbaum, *J. Phys. Chem. B* 108 (2004) 19049.
- [11] T. Schultz, E. Samoylova, W. Radloff, I.V. Hertel, A.L. Sobolewski, W. Domcke, *Science* 306 (2004) 1765.
- [12] A.L. Sobolewski, W. Domcke, *Chem. Phys. Chem.* 7 (2006) 561.
- [13] L.S. Cederbaum, J. Zobeley, *Chem. Phys. Lett.* 307 (1999) 205.
- [14] J. Breidbach, L.S. Cederbaum, *J. Chem. Phys.* 118 (2003) 3983.
- [15] H. Hennig, J. Breidbach, L.S. Cederbaum, *J. Phys. Chem.* 109 (2005) 409.
- [16] H. Hennig, J. Breidbach, L.S. Cederbaum, *J. Chem. Phys.* 122 (2005) 134104.
- [17] A.I. Kuleff, J. Breidbach, L.S. Cederbaum, *J. Chem. Phys.* 123 (2005) 044111.
- [18] J. Breidbach, L.S. Cederbaum, *J. Chem. Phys.* 126 (2007) 034101.
- [19] F. Remacle, R.D. Levine, *J. Chem. Phys.* 110 (1999) 5089.
- [20] R.D. Suenram, F.J. Lovas, *J. Mol. Spectrosc.* 72 (1978) 372.
- [21] K. Iijima, K. Tanaka, S. Onuma, *J. Mol. Struct.* 246 (1991) 257.
- [22] S.G. Stepanian, I.D. Reva, E.D. Radchenko, M.T.S. Rosado, M.L.T.S. Duarte, R. Fausto, L. Adamowicz, *J. Phys. Chem.* 102 (1998) 1041.
- [23] GAMESS UK, v6.2.1: Package of *ab initio* programs written by M.F. Guest, J.H. van Lenthe, J. Kendrick, et al., The package is derived from the original GAMESS code due to M. Dupuis, D. Spangler, J. Wendoloski, NRCC software Catalog, vol. 1, Program No. QG01 (GAMESS), 1980. Used module: MCSCF/CASSCF;
- P.J. Knowles, G.J. Sexton, N.C. Handy, *Chem. Phys.* 72 (1982) 337;
- P.J. Knowles, H.-J. Werner, *Chem. Phys. Lett.* 115 (1985) 259.
- [24] T.H. Dunning Jr., *J. Chem. Phys.* 53 (1970) 2823;
- T.H. Dunning Jr., P.J. Hay, in: H.F. SchaeferIII (Ed.), *Methods of Electronic Structure Theory*, vol. 2, Plenum Press, New York, 1977.
- [25] J. Schirmer, L.S. Cederbaum, O. Walter, *Phys. Rev. A* 28 (1983) 1237.
- [26] L.S. Cederbaum, in: P. von Ragué Schleyer et al. (Eds.), *Encyclopedia of Computational Chemistry*, Wiley, Chichester, 1998.
- [27] J. Schirmer, A.B. Trofimov, G. Stelter, *J. Chem. Phys.* 109 (1998) 4734.
- [28] C. Leforestier, R.H. Bisseling, C. Cerjan, M.D. Feit, R. Friesner, A. Guldberg, A. Hammerich, G. Jolicard, W. Karrlein, H.-D. Meyer, N. Lipkin, O. Roncero, R. Kosloff, *J. Comp. Phys.* 94 (1991) 59.
- [29] J.J. Neville, Y. Zheng, C.E. Brion, *J. Am. Chem. Soc.* 118 (1996) 10533.
- [30] A.G. Császár, *J. Am. Chem. Soc.* 114 (1992) 9568.
- [31] C.T. Falzon, F. Wang, *J. Chem. Phys.* 123 (2005) 214307.
- [32] P.H. Cannington, N.S. Ham, *J. Electron. Spectrosc. Relat. Phenom.* 32 (1983) 139.
- [33] L.S. Cederbaum, W. Domcke, *Adv. Chem. Phys.* 36 (1977) 205.
- [34] A. Szabo, N.S. Ostlund, *Modern Quantum Chemistry*, McGraw-Hill, New York, 1989.
- [35] L.S. Cederbaum, W. Domcke, J. Schirmer, W. von Niessen, *Adv. Chem. Phys.* 65 (1986) 115.
- [36] J. Breidbach, L.S. Cederbaum, *Phys. Rev. Lett.* 94 (2005) 033901.

Available online at www.sciencedirect.com

Chemical Physics Letters 450 (2008) 232–235

**CHEMICAL
PHYSICS
LETTERS**www.elsevier.com/locate/cplett

Ultrafast charge migration in 2-phenylethyl-*N,N*-dimethylamine

Siegfried Lünemann^{*}, Alexander I. Kuleff¹, Lorenz S. Cederbaum*Theoretische Chemie, PCI, Universität Heidelberg, Im Neuenheimer Feld 229, 69120 Heidelberg, Germany*

Received 29 August 2007; in final form 13 November 2007

Available online 19 November 2007

Abstract

Electron correlation can be the driving force for ultrafast charge migration. Using *ab initio* calculations this is demonstrated in the present paper for the first time as a consequence of ionizing the *outer-valence* shell. The example studied is 2-phenylethyl-*N,N*-dimethylamine (PENNA) on which exciting pump–probe measurements have been recently carried out.
© 2007 Elsevier B.V. All rights reserved.

Charge transfer (CT) is a fundamental phenomenon in nature, playing an essential role in many chemical and biological processes. Traditionally it is assumed that the nuclear dynamics is the mediator of the CT process. However, it was shown [1] that after a localized ionization the created positive charge can migrate throughout the system solely driven by many-electron effects – i.e., by electron correlation and relaxation effects [2–5]; see also [6] for the importance of Coulomb repulsion between the electrons. This phenomenon was termed *charge migration*. The migration mechanism can be extremely fast, typically in the femtosecond time regime. In this letter we present a theoretical study on 2-phenylethyl-*N,N*-dimethylamine (PENNA) for which we find an ultrafast charge migration. The amount of charge that migrates from the initially ionized chromophore site to the N-terminal site in just 4 femtoseconds (fs) increases along the dissociation pathway of the molecule, indicating a mechanism of coupled electron-nuclear dynamics. These findings may give a clue for understanding the results of recent measurements on that system [7].

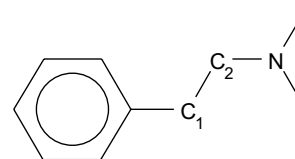
We have studied charge migration in different molecules [2–5] and found that it usually takes place after ionization

in the inner-valence shell, and, depending on the system and ionized orbital, may last just a few fs. Being usually much faster than the nuclear motion, charge migration following inner-valence ionization can thus be calculated neglecting the nuclear dynamics, as long as one studies the time interval during which this ultrafast mechanism takes place. Clearly, if we wish to know precisely what happens at later times, nuclear motion has to be considered. However, since many electronic states participate, an adequate description of the nuclear motion is rather involved.

The main motivation of this work is to identify beyond doubt charge migration following ionization in the *outer-valence* shell of an interesting system. We decided to study the process in PENNA (see Sketch) because of the recent exciting experiment by Weinkauff and Schlag on this molecule [7]. In these laser pump–probe measurements it was observed that after a local ionization of the chromophore site [8,9] a breaking of the C₁–C₂ bond occurs accompanied by a transfer of the positive charge to N-terminal fragment. The time of this CT dynamics was reported to be 80 ± 28 fs. However, this time has to be regarded as an upper limit for the duration of the CT.

E-mail addresses: siegfried.luennemann@pci.uni-heidelberg.de (S. Lünemann), alexander.kuleff@pci.uni-heidelberg.de (A.I. Kuleff), lorenz.cederbaum@pci.uni-heidelberg.de (L.S. Cederbaum).

¹ On leave from: Institute for Nuclear Research and Nuclear Energy, BAS, 72, Tzarigradsko Chaussee Blvd., 1784 Sofia, Bulgaria.



Let us see what happens after a localized ionization of the chromophore site in PENNA. In order to trace in time and space the migration of the positive charge, the so-called *hole density* has to be calculated. The hole density is defined as the difference between the electronic density of the neutral and that of the cation:

$$Q(\vec{r}, t) = \langle \Psi_0 | \hat{\rho}(\vec{r}, t) | \Psi_0 \rangle - \langle \Phi_i | \hat{\rho}(\vec{r}, t) | \Phi_i \rangle \\ = \rho_0(\vec{r}) - \rho_i(\vec{r}, t), \quad (1)$$

where $\hat{\rho}$ is the density operator, $|\Psi_0\rangle$ is the ground state of the neutral, and $|\Phi_i\rangle$ is the initially prepared cationic state. The second term in Eq. (1), ρ_i , is time-dependent, since $|\Phi_i\rangle$ is not an eigenstate of the cation. The quantity $Q(\vec{r}, t)$ describes the density of the hole at position \vec{r} and time t and by construction is normalized at all times t . For calculating the hole density we use *ab initio* methods only. The cationic Hamiltonian, represented in an effective many-body basis using the Green's function method, is used for directly propagating in the electronic space an initial state via the Lanczos technique [3]. The electronic wavepacket thus obtained is then utilized to construct the hole density at each time point via Eq. (1). Theoretical and technical details concerning construction and analysis of the hole density are given in [2–5].

We are not aiming here at simulating a given experiment, but rather at investigating what happens once the initial state with the localized hole on the phenyl site is prepared. For this purpose the initial cationic state $|\Phi_i\rangle$ is prepared by a sudden removal of an electron from the highest occupied Hartree–Fock orbital which is localized on the chromophore (see below). Experimentally, utilizing attosecond pulses could be helpful in approaching this limit. For attosecond pulses, see e.g. [10].

To better understand the underlying mechanisms of electron dynamics following ionization, we will first analyze the valence part of the ionization spectrum. In Fig. 1a the ionization energies obtained via a Hartree–Fock (HF) calculation and Koopmans' theorem together with the corresponding orbitals are presented [11]. In Fig. 1b the ionization spectrum computed using Green's functions (GF) [12] is shown. The height of the lines refers to the spectral intensities of the cationic states and is related to the ionization cross section. The colors in the spectrum show the contributions of the one-hole configurations corresponding to the removal of an electron from one of the HF-orbitals shown in Fig. 1a. Note that the HF calculation predicts a different ordering of the cationic states than found by the GF calculation and experimental data [8,13]. Thus, PENNA provides an example of the breakdown of Koopmans' theorem, where relaxation and correlation effects in the valence part are sufficiently strong to interchange the ordering of the ionization energies. The first cationic state (7.96 eV) is clearly the state where the hole is created on the nitrogen. The second (8.49 eV) and third (8.78 eV) states correspond to holes on the π -orbitals of the benzene ring. These three states are well separated

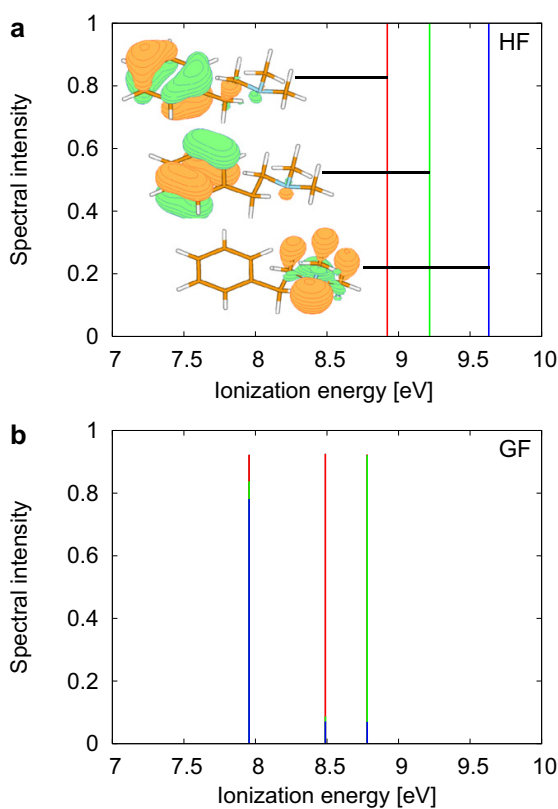


Fig. 1. Ionization spectrum of PENNA. (a) Hartree–Fock (HF)–Koopmans' theorem results. (b) Green's function (GF) results. The corresponding HF-orbitals are also plotted in (a).

from the fourth cationic state (not shown) at 11.41 eV. As one can see in the spectrum (Fig. 1b) the three states are mixed, i.e., each of them has contributions coming from ionization out of all of the three orbitals. This leads to a charge migration mechanism due to *hole mixing* where the created hole charge is mainly oscillating between the corresponding orbitals [2–5]. The stronger the mixing of the states, the more efficient will be the transfer of charge among the orbitals involved.

In order to see how the positive charge created on the benzene ring evolves in time we calculated the hole density $Q(\vec{r}, t)$. The initial state is prepared by a removal of an electron from the highest occupied HF-orbital (the uppermost in Fig. 1a). In Fig. 2 the quantity $Q(z, t)$ is plotted, which is obtained from $Q(\vec{r}, t)$ after integration over the two remaining perpendicular axes. The axis z is chosen to pass through the longest spatial extension of the molecule and is denoted as 'molecular axis'. The relative positions of the atoms along this axis are indicated. Fig. 2a shows the evolution of the hole density calculated using the equilibrium geometry of the neutral molecule. At time 0 the charge is localized on the benzene ring. After only 4 fs a fraction of it has

234

S. Linnemann et al. / Chemical Physics Letters 450 (2008) 232–235

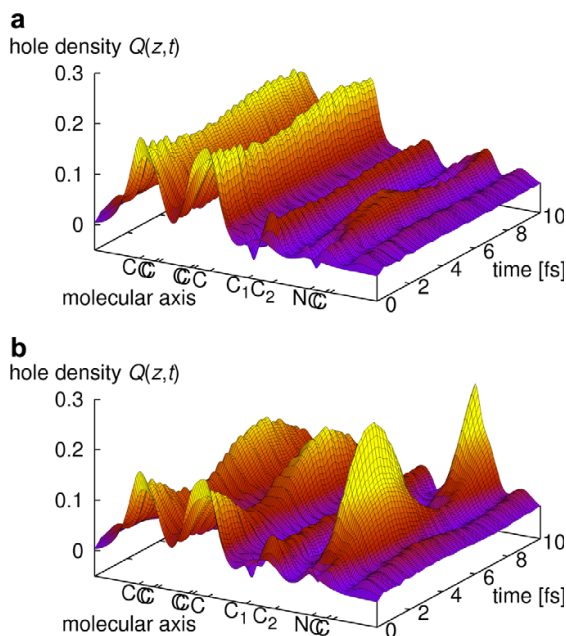


Fig. 2. Hole density of PENNA. (a) At the ground state geometry of the neutral. (b) At the geometry with C_1-C_2 bond elongated by 20 pm.

already migrated to the nitrogen (the hump on the right-hand side of the surface). Afterwards the charge returns mainly to its initial position and the whole process starts again. However, since many ionic states participate in the dynamics, the process is not purely repetitive.

First principles molecular dynamics simulations of the cationic ground state at DFT (BP86/SV(P)) level starting with the equilibrium geometry of the neutral indicate a stretching of the C_1-C_2 bond of 5 pm within the first 5 fs. This is the bond which was observed to break in the experiments of Weinkauff et al. [7,13]. To gain an idea on the impact of this stretching on the charge migration, we calculated the hole density and traced its migration at several different geometries along the dissociation path. It was observed that more and more charge migrates to the N-terminal as the C_1-C_2 bond elongates. In Fig. 2b the hole density is shown for a geometry where the C_1-C_2 bond is elongated by 20 pm. One clearly sees that in this case almost the entire charge is transferred from the chromophore to the N-terminal, and this again within 4 fs.

To further trace the evolution of the hole charge in real space we present in Fig. 3 $Q(\vec{r}, t)$ in 3D for the two discussed geometries at three different times $t = 0, 2$ and 4 fs. The results suggest the following conceivable scenario of coupled electron-nuclear dynamics. The localized initial ionization of the chromophore triggers ultrafast charge migration and some part of the positive charge starts to bounce between the chromophore and the N-terminal. As time proceeds, nuclear dynamics enters the picture and with the elongation of the C_1-C_2 bond more and more charge oscillates between the two sites. These oscillations are not perfect, due to dissipation caused by the participation of many electronic states and nuclear dynamics, and when the bond breaks the charge is trapped at the energetically more favorable N-terminal fragment, i.e. the molecule dissociates into $C_6H_5CH_2$ radical and $H_2CN(CH_3)_2$ cation. This is confirmed by calculations on the CC2 level which predict that dissociation into $C_6H_5CH_2 +$

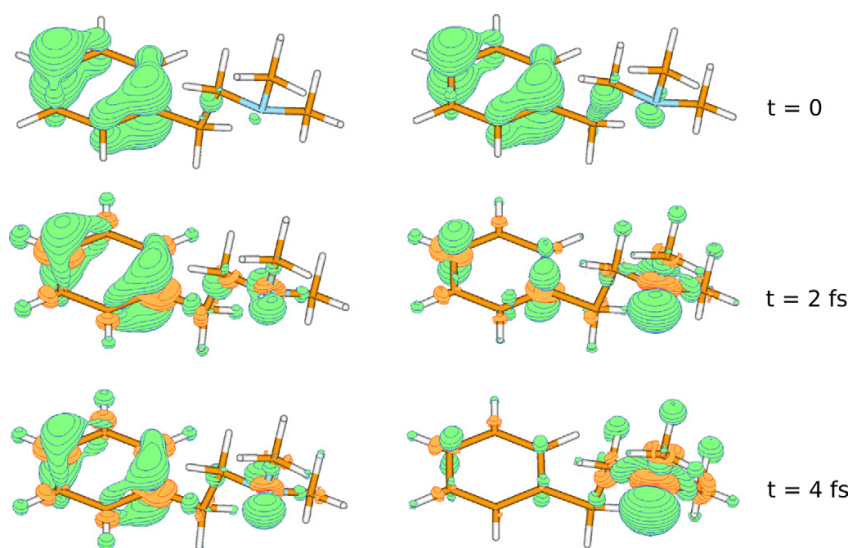


Fig. 3. 3D-hole density of PENNA at three different time steps (0, 2, 4 fs). The 'negative' hole density, or the electron density is given in orange. Left-hand side for the ground state geometry, right-hand side for the geometry with C_1-C_2 bond elongated by 20 pm. (For interpretation of the references to colour in this figure legend, the reader is referred to the web version of this Letter.)

$[\text{H}_2\text{CN}(\text{CH}_3)_2]^+$ is energetically more favorable than that into $[\text{C}_6\text{H}_5\text{CH}_2]^+ + \text{H}_2\text{CN}(\text{CH}_3)_2$ by about 1.4 eV.

According to our findings there is an electronic beat of around 4 fs between the chromophore and the nitrogen site of PENNA. Although the initial conditions in our calculations differ substantially from these used in the available experiments of PENNA, we propose an interpretation of the reported experimental CT time of 80 ± 28 fs in the light of our computations. The determination of the CT time scale in this ingenious pump–probe experiments is based on the fact that the probe pulse used is resonantly absorbed by the charged chromophore only. Consequently, the system is transparent to the probe pulse once the charge has moved to the nitrogen moiety. On the other hand, the nuclear dynamics involved in the bond breaking are much slower than the purely electronic step of 4 fs and several to many oscillations are necessary until the charge is trapped and the system becomes transparent to the probe pulse. We argue that the reported experimental time may not correspond to the purely electronic CT time, but rather to the time at which the charge is finally trapped at the N-moiety. This is further supported by Cheng et al., who, using Rydberg fingerprint spectroscopy, infer an ultrafast CT dynamics in PENNA with time scale of 1 fs as a lower limit [8]. Of course, in order to fully clarify the experimental results calculations using the corresponding initial conditions would be necessary.

Let us summarize. Our calculations on PENNA demonstrate that after ionization of an outer-valence electron at the phenyl site an ultrafast charge migration to the nitrogen takes place entirely due to many-electron effects. The charge oscillates between the two sites in only 4 fs and its amount increases with the elongation of the $\text{C}_1\text{--C}_2$ bond, i.e. along the dissociation pathway.

References

- [1] L.S. Cederbaum, J. Zobeley, *Chem. Phys. Lett.* 307 (1999) 205.
- [2] J. Breidbach, L.S. Cederbaum, *J. Chem. Phys.* 118 (2003) 3983.
- [3] A.I. Kuleff, J. Breidbach, L.S. Cederbaum, *J. Chem. Phys.* 123 (2005) 044111.
- [4] H. Hennig, J. Breidbach, L.S. Cederbaum, *J. Phys. Chem. A* 109 (2005) 409.
- [5] J. Breidbach, L.S. Cederbaum, *J. Chem. Phys.* 126 (2007) 034101.
- [6] F. Remacle, R.D. Levine, *J. Chem. Phys.* 110 (1999) 5089.
- [7] L. Lehr, T. Horneff, R. Weinkauff, E.W. Schlag, *J. Phys. Chem. A* 109 (2005) 8074.
- [8] W. Cheng, N. Kuthirummal, J.L. Gosselin, T.I. Sølling, R. Weinkauff, P.M. Weber, *J. Phys. Chem. A* 109 (2005) 1920.
- [9] R. Weinkauff, F. Lehrer, E.W. Schlag, A. Metsala, *Faraday Discuss.* 115 (2000) 363.
- [10] P.B. Corkum, F. Krausz, *Nature Phys.* 3 (2007) 381.
- [11] We have used standard DZ basis set and a geometry optimized on RIMP2/TZVP level.
- [12] J. Schirmer, A.B. Trofimov, G. Stelter, *J. Chem. Phys.* 109 (1998) 4734.
- [13] R. Weinkauff, L. Lehr, A. Metsala, *J. Phys. Chem. A* 107 (2003) 2787.

THE JOURNAL OF CHEMICAL PHYSICS 129, 104305 (2008)

Charge migration following ionization in systems with chromophore-donor and amine-acceptor sites

Siegfried Lünemann,^{a)} Alexander I. Kuleff, and Lorenz S. Cederbaum*Theoretische Chemie, PCI, Universität Heidelberg, Im Neuenheimer Feld 229, 69120 Heidelberg, Germany*

(Received 19 June 2008; accepted 22 July 2008; published online 9 September 2008)

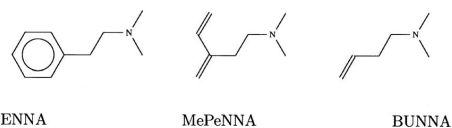
The ultrafast charge migration following outer-valence ionization in three different but related molecules, namely, 2-phenylethyl-*N,N*-dimethylamine (PENNA), and its butadiene (MePeNNA) and ethylene (BUNNA) derivatives, is studied in detail. The molecules have different chromophore-donor sites, but nearly identical amine-acceptor sites. The results show that the charge migration process depends strongly on the particular donor site, varying from ultrafast migration of the charge from the donor to the acceptor site (4 fs for MePeNNA) to no migration at all (for BUNNA). The influence of the geometrical structure of the molecule on the charge migration is also investigated. It is shown that energetically closely lying conformers may exhibit dramatically different charge migration behaviors. The basic mechanism of the charge migration process in the studied molecules is analyzed in detail and is demonstrated to be due to electron correlation and relaxation effects. © 2008 American Institute of Physics. [DOI: 10.1063/1.2970088]

I. INTRODUCTION

About ten years ago in a first work¹ it was shown that the positive charge created after ionization can migrate throughout the system solely driven by the many-body effects. It was shown also that this charge migration is ultrafast and the charge can reach a remote site of the system typically in just few femtoseconds. Although representing a transportation of a charge from one site of the molecule to another, this phenomenon differs from processes traditionally termed “charge transfer” by the underlying basic mechanism. Indeed, it is assumed that nuclear dynamics play an essential role in the course of the charge transfer process, in particular, that the process of charge transfer occurs through the nonadiabatic coupling between the nuclear and electronic motions.^{2–4} Contrary to that the charge migration appears *only* due to the electron correlation and relaxation effects and thus can take place even if the nuclear skeleton of the molecule is fixed during the process. The different timescales of the electronic and nuclear motions explain why the charge migration is typically orders of magnitude faster even from the fastest known charge transfer processes, i.e., those mediated by the so-called conical intersections of the potential energy surfaces (see, e.g., Refs. 5–7). Thus, the charge migration can be calculated neglecting the nuclear motion as long as one is concerned with the relevant time interval during which this ultrafast process takes place. Clearly, if we wish to know precisely what happens at later times, nuclear motion must be considered. However, since several or even many electronic states participate, an adequate description of the nuclear motion is rather involved. It should be noted that very recently a time-dependent Born–Oppenheimer approximation for treating quantum mechanically coupled electron–nuclear dynamics was proposed.^{8,9}

We have studied the charge migration in different molecules^{10–14} and found that it usually takes place after ionization in the inner-valence shell where the electron correlation effects are typically much stronger than in the outer-valence shell. However, very recently we have shown that the charge migration phenomenon is not inherent only to the inner-valence ionized states but can take place also after an outer-valence ionization.¹⁵ In the system studied in Ref. 15 after ionization of the chromophore-donor site, the created hole charge migrates to the amine-acceptor site in just 4 fs.

In the present study we aim at obtaining a deeper understanding on the mechanism underlying the charge migration following an outer-valence ionization of a molecule and to investigate also the dependence of the process on the donor site. For this purpose we compare the evolution of the electronic cloud after a localized ionization of three molecules differing only in the initially ionized chromophore site. The molecules chosen are 2-phenylethyl-*N,N*-dimethylamine (PENNA) and its butadiene [3-methylene-4-penten-*N,N*-dimethylamine (MePeNNA)] and ethylene [3-buten-*N,N*-dimethylamine (BUNNA)] derivatives (see the sketch).



We mention here that there were recent experiments on the PENNA molecule^{16,17} showing that after a localized ionization of the chromophore site a fast charge transfer to the nitrogen site takes place. The time scale of this process was reported to be 80 ± 28 fs (for a discussion on the timescale of the process, see also Ref. 15).

The paper is organized as follows. In Sec. II the theoretical background of the methodology used for calculating the charge migration is briefly reviewed. In Sec. III we present

^{a)}Electronic mail: siegfried.luenemann@pci.uni-heidelberg.de.

the results of our calculations. In Sec. III A the computed outer-valence ionization spectra of the three investigated molecules are presented and briefly discussed. These spectra serve as a tool to analyze charge migration and are also of interest by themselves. The similarities and differences of the charge migration behavior are discussed in Sec. III B. The influence of the geometrical structure of the molecule on the charge migration is studied in Sec. III C. Section IV is devoted to the analysis of the mechanism of charge migration. We summarize the results and conclude in Sec. V.

II. THEORETICAL BACKGROUND

In this section we briefly review the theoretical background of the methodology used to study charge migration following ionization of a system. For technical details, we refer the reader to Refs. 10, 11, and 14.

The starting point of our investigation is a neutral molecule in its ground state $|\Psi_0\rangle$. The ionization of the system brings it into a nonstationary state $|\Phi_i\rangle$. A convenient quantity then for tracing the succeeding electron dynamics is the density of the so created initial hole which can be defined by the following expression:

$$Q(\vec{r}, t) := \langle \Psi_0 | \hat{\rho}(\vec{r}, t) | \Psi_0 \rangle - \langle \Phi_i | \hat{\rho}(\vec{r}, t) | \Phi_i \rangle = \rho_0(\vec{r}) - \rho_i(\vec{r}, t), \quad (1)$$

where $\hat{\rho}$ is the electron density operator. The first term on the right-hand side of Eq. (1), ρ_0 , is the ground-state density of the neutral system and is time independent. The second term, ρ_i , is the density of the cation and hence is time dependent, since $|\Phi_i\rangle$ is not an eigenstate of the cationic system. The quantity $Q(\vec{r}, t)$, referred hereafter as the *hole density*, describes the density of the hole at position \vec{r} and time t and by construction is normalized at all times t .

In the Heisenberg picture, the time-dependent part $\rho_i(\vec{r}, t)$ reads

$$\rho_i(\vec{r}, t) = \langle \Phi_i | e^{i\hat{H}t} \hat{\rho}(\vec{r}, 0) e^{-i\hat{H}t} | \Phi_i \rangle = \langle \Phi_i(t) | \hat{\rho}(\vec{r}, 0) | \Phi_i(t) \rangle, \quad (2)$$

where $|\Phi_i(t)\rangle = e^{-i\hat{H}t} |\Phi_i\rangle$ is the propagating multielectron wavepacket.

Using the standard representation of the density operator in a one-particle basis $\varphi_p(\vec{r})$ and occupation numbers n_p , Eq. (1) can be rewritten as follows:

$$Q(\vec{r}, t) = \sum_{p,q} \varphi_p^*(\vec{r}) \varphi_q(\vec{r}) N_{pq}(t), \quad (3)$$

where the matrix $\mathbf{N}(t) = \{N_{pq}(t)\}$ with elements

$$N_{pq}(t) = \delta_{pq} n_p - \sum_{M,N} \langle \Phi_i(t) | \tilde{\Psi}_M \rangle \rho_{MN} \langle \tilde{\Psi}_N | \Phi_i(t) \rangle \quad (4)$$

is referred to as the hole density matrix. The second term of Eq. (4) is obtained by inserting in Eq. (2) a resolution of identity of a complete set of appropriate ionic eigenstates $|\tilde{\Psi}_M\rangle$. The matrix ρ_{MN} is the representation of the density operator within this basis.

Diagonalization of the matrix $\mathbf{N}(t)$ for fixed time points t yields the following expression for the hole density:

$$Q(\vec{r}, t) = \sum_p |\tilde{\varphi}_p(\vec{r}, t)|^2 \tilde{n}_p(t), \quad (5)$$

where $\tilde{\varphi}_p(\vec{r}, t)$ are called *natural charge orbitals* and $\tilde{n}_p(t)$ are their *hole occupation numbers*. The hole occupation number $\tilde{n}_p(t)$ contains the information what part of the created hole charge is in the natural charge orbital $\tilde{\varphi}_p(\vec{r}, t)$ at time t . Because of charge conservation, one finds that $\sum_p \tilde{n}_p(t) = 1$ at any time t .

For calculating the hole density and its constituents we use *ab initio* methods only. The whole calculation consists of four steps. After determining the molecular geometry, the first step is a Hartree–Fock (HF) self-consistent field calculation. The second step is the calculation of the cationic eigenstates via Green’s function (GF) formalism. A computationally very successful approach to obtain GF is the *algebraic diagrammatic construction* [ADC(n)] scheme.^{18,19} In the present calculation we used the non-Dyson ADC(3) method²⁰ realized within the so-called intermediate-state representation,^{21,22} an effective many-body basis serving as $|\tilde{\Psi}_M\rangle$ introduced in Eq. (4). The third step is the propagation of the multielectron wavepacket of the ionized system¹¹ with the help of the short iterative Lanczos technique. The fourth and last step is to build through Eq. (4) the matrix $\mathbf{N}(t)$ and to diagonalize it in order to obtain the natural charge orbitals $\tilde{\varphi}_p(\vec{r}, t)$ and the hole occupation numbers $\tilde{n}_p(t)$, see Eq. (5). With the help of these quantities we can now trace the evolution of the hole density of a system after suddenly removing one of its electrons.

At this point we would like to comment briefly on the choice of the initial state $|\Phi_i\rangle$. The above sketched methodology is independent of the particular choice and the way of preparation of the initial state as long as the ionized electron is removed from the system on a shorter time scale than that of the charge migration. In our numerical calculations to be discussed in this paper the initial state is prepared through a sudden removal of an electron from a particular HF orbital. More precisely, by acting with the corresponding annihilation operator on the correlated ground state of the neutral system. This choice is justified by the fact that the canonical HF orbital appears to be the best one-particle approximation to describe well the hole created via single photon ionization. The initial state can, of course, be constructed such that it corresponds to a removal of an electron from a linear combination of HF orbitals. This liberty allows one to reproduce the hole density of practically every particular initial vacancy. However, to avoid investigating many linear combinations of HF orbitals of interest we concentrate on specific HF orbitals. In this way we can unambiguously identify the basic mechanisms leading to charge migration. Since the time-dependent Schrödinger equation which governs the electron dynamics is a linear equation, these mechanisms are also operative when other choices of the initial state are used.

III. RESULTS

We have applied the above sketched methodology to the molecules PENNA, MePeNNA, and BUNNA in order to trace in real time and space the response of the electronic

104305-3 Controlling factors in charge migration

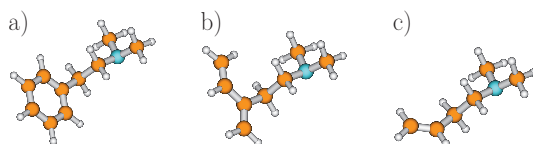
J. Chem. Phys. **129**, 104305 (2008)

FIG. 1. (Color) Structure of the three molecules (a) PENNA, (b) MePeNNA, and (c) BUNNA.

cloud of these systems to the sudden removal of an electron from their chromophore site. Throughout the calculations standard DZ basis sets²³ were used.

The three studied molecules differ at their chromophore site but are nearly identical at their nitrogen site (see Fig. 1). The geometries were obtained using density functional theory (DFT) methodology [BP86/SV(P)]. All three molecules have more than one conformer. For the purposes of our study we took the conformer which is the lowest in energy for PENNA and BUNNA. Since we are interested in how the replacement of the chromophore influences the charge migration, we took for MePeNNA the conformer where the nitrogen site has a similar geometry compared to PENNA and BUNNA. According to our calculations, it is not the lowest in energy conformer but the second lowest one lying only about 0.5 kcal/mol higher. We shall address the charge migration in the lowest energy conformer in Sec. III C.

The geometries of the lowest in energy conformers of PENNA have been studied before,¹⁷ and the results obtained are similar to ours. Since, to the best of our knowledge, the molecule MePeNNA has not been studied until now, some more information about the conformational search performed by us is probably needed. The conformational search was done via standard molecular mechanics methods²⁴ using the MMFF94 force field.²⁵ These computations showed that the molecule MePeNNA possesses two energetically close conformers ($\Delta E < 1$ kcal/mol) which lie 3–4 kcal/mol lower in energy than the other ones. The geometry of these two lowest in energy conformers was subsequently optimized at BP86/SV(P) level. Single point energy calculations at the higher BP86/TZVP level show that these two conformers are nearly degenerate in energy, differing by only 0.5 kcal/mol which is smaller than the expected accuracy of the employed methods. Although known from the literature, to the best of our knowledge, no conformational study has been published also for the molecule BUNNA. Thus, to BUNNA we applied the same conformational-search methodology as to MePeNNA. We found three energetically close conformers all showing very similar ionization spectra and charge migration behavior. Thus, in this paper we present the results only for the lowest in energy conformer.

In what follows we present and analyze *ab initio* many-body results. We will start our discussion by a comparison of the outer-valence ionization spectra of the studied molecules (Sec. III A). In Sec. III B we will investigate the evolution of the hole charge created via localized ionization of the chromophore site of the three molecules. The impact of the nuclear geometry on the electron dynamics following ionization of the chromophore site is studied in Sec. III C.

A. Ionization spectra and the nature of the cationic states

Let us first analyze the outer-valence ionization spectra of the studied molecules. The simplest approximation to the ionization spectrum of a system consists of applying Koopmans' theorem. In this approach the electrons are treated as independent particles and the ionic states are given by the following simple expression:

$$|I\rangle = \hat{a}_i |\Phi_0\rangle, \quad (6)$$

where \hat{a}_i is the usual annihilation operator of an electron in the occupied orbital φ_i and $|\Phi_0\rangle$ is the HF ground-state determinant. Within this approach the ionization spectrum will be a series of lines, one for each occupied orbital φ_i with spectral intensity equal to 1. However, as we will see, even for the outer-valence part of the spectrum, where Koopmans' theorem is expected to be a reasonable approximation, for the molecules studied here this approach is not only unable to describe the electron dynamics following ionization but even gives an incorrect ordering of the ionic states.

The process of charge migration we want to describe is entirely due to electronic correlation and relaxation effects, and one has to employ many-body approaches to calculate the participating cationic states. In such approaches, the exact cationic state $|I\rangle$ can be expanded in a series of electronic configurations.²⁶ For the ease of interpretation we can use the traditional configuration interaction (CI) expansion, where the cationic state is given by

$$|I\rangle = \sum_i c_i^{(I)} \hat{a}_i |\Phi_0\rangle + \sum_{a,j < k} c_{ajk}^{(I)} \hat{a}_a^\dagger \hat{a}_j \hat{a}_k |\Phi_0\rangle + \dots, \quad (7)$$

where $|\Phi_0\rangle$ is again the HF ground state of the molecule and \hat{a} and \hat{a}^\dagger the annihilation and creation operators, respectively. In the above equation we have used the following index convention: i, j, \dots denote occupied orbitals (or holes), whereas a, b, \dots denote unoccupied (virtual) orbitals (or particles). Thus, the exact cationic state consists of one-hole ($1h$) $a_i |\Phi_0\rangle$, two-hole one particle ($2h1p$) $\hat{a}_a^\dagger \hat{a}_j \hat{a}_k |\Phi_0\rangle$, and higher configurations. A $2h1p$ $\hat{a}_a^\dagger \hat{a}_j \hat{a}_k |\Phi_0\rangle$ configuration means that on top of the removal of an electron from orbital j , another electron is excited from orbital k to the virtual orbital a .

In principle, any post HF method giving a proper description of the electron correlation effects can be used for calculating the cationic states. However, in practice, GF based methodologies are clearly well suited in the cases where the calculation of many cationic states is needed for understanding the underlying physical phenomena. Indeed, within the GF approaches *all* the eigenstates are obtained in a single run, while employing standard wavefunction based methods one has to compute each state separately.

In the present work we have used the non-Dyson ADC(3) approach to the GF to obtain the many-body cationic basis $|\tilde{\Psi}_M\rangle$ used in constructing the time-dependent hole density [see Eq. (4)]. Note that although the ADC(3) expansion is up to $2h1p$ configurations, it accounts for much more electron correlation than the CI expansion up to $2h1p$ [Eq. (7)]. This is because in the ADC expansion the corre-

104305-4 Lünemann, Kuleff, and Cederbaum

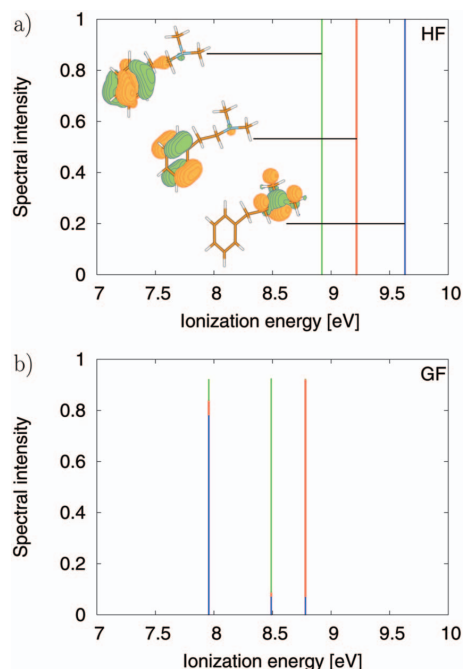
J. Chem. Phys. **129**, 104305 (2008)

FIG. 2. (Color) Ionization spectrum of PENNA. The upper panel shows the results obtained by employing the HF-Koopmans' theorem. The corresponding HF orbitals are also displayed. The lower panel shows the results of the GF calculation (the colors on the lines indicate the individual contributions of the respective $1h$ configurations shown in the upper panel). The latter results are in agreement with experiments (Ref. 27).

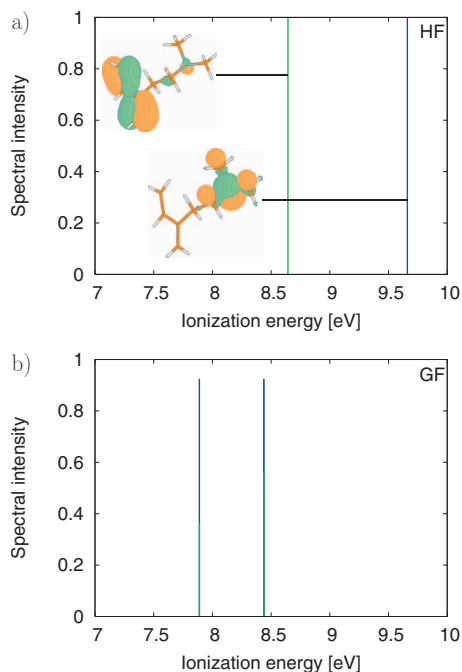


FIG. 3. (Color) Ionization spectrum of MePeNNA. The upper panel shows the results obtained by employing the HF-Koopmans' theorem. The corresponding HF orbitals are also displayed. The lower panel shows the results of the GF calculation (the colors on the lines indicate the individual contributions of the respective $1h$ configurations shown in the upper panel). Experimental spectra are not available.

lated neutral ground state rather than the uncorrelated HF one is used, and in addition the ADC scheme includes infinite partial summations of certain terms in the perturbation expansion. For details, see Refs. 18–20.

In Figs. 2–4 we present the outer-valence part of the ionization spectra of the molecules PENNA, MePeNNA, and BUNNA, respectively, calculated via the HF-Koopmans' approach and via the GF ADC(3) approach.²⁰ Each line in these spectra represents an eigenstate of the cation, the position being given by the energy of the corresponding eigenstate, i.e., the ionization energy, and the height, corresponding to the spectral intensity (related to the ionization cross section), given by the square of the transition amplitudes $\langle I | \Phi_i \rangle$.

The upper panels of Figs. 2–4 show the results obtained applying HF-Koopmans' theorem together with the corresponding HF orbitals. On this level of approximation we have only pure $1h$ states, i.e., one electron is removed out of the orbital shown. Each of the ionization spectra consists of a single level related to the nitrogen lone-pair site and of other levels related to the chromophore site. As seen, within the HF-Koopmans' approach the ionization out of the nitrogen lone-pair orbital requires nearly the same energy (9.4–9.7 eV) in all three molecules. In contrast, the energies of the localized ionization on the chromophore site vary more strongly and the number of the resulting states may

even differ—in PENNA we observe two states at 9.0 and 9.2 eV, in MePeNNA one state at 8.6 eV, and in BUNNA one state at 9.8 eV.

The picture changes dramatically if one includes the many-body effects. These effects lead to characteristic shifts of the ionization energies and to strongly varying mixing of the configurations. The ionization energy of the state with the main contribution from the nitrogen lone-pair orbital shifts to lower energies by about 1.6–1.8 eV in all three molecules, while the states with dominant contributions from the chromophore orbitals undergo displacements only by about 0.2–0.4 eV. Importantly, the many-body effects lead to a reordering of the ionic states in the cases of PENNA and MePeNNA. In all three molecules the cationic ground state is now the state stemming from the ionization of the nitrogen lone-pair electron (the $1h$ configuration from the nitrogen lone-pair orbital has the largest contribution to the state) and all have essentially the same ionization energy of 7.9 (± 0.1 eV). The second cationic state has an ionization energy of about 8.5 eV in PENNA and MePeNNA, and 9.4 eV in BUNNA, and arises from the ionization of the chromophore.

In all three molecules we observe a *hole mixing* of the cationic states. In the case of hole mixing two (or more) lines in the spectrum are superpositions of two (or more) $1h$ configurations [see Eq. (7)]. A strong hole mixing is observed in MePeNNA (Fig. 3) where the nitrogen lone-pair $1h$ configu-

104305-5 Controlling factors in charge migration

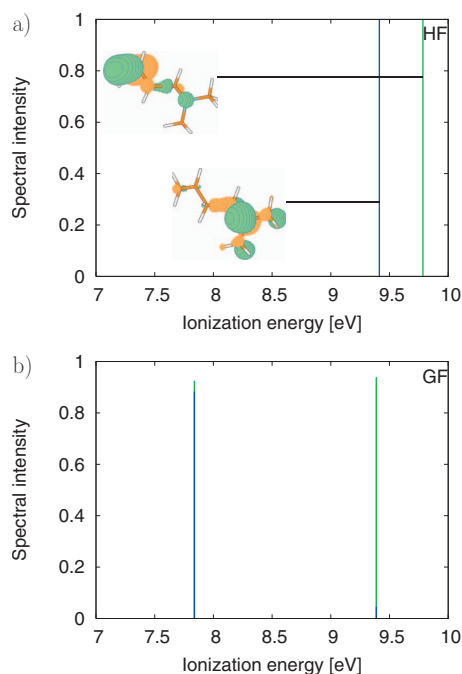
J. Chem. Phys. **129**, 104305 (2008)

FIG. 4. (Color) Ionization spectrum of BUNNA. The upper panel shows the results obtained by employing the HF-Koopmans' theorem. The corresponding HF orbitals are also displayed. The lower panel shows the results of the GF calculation (the colors on the lines indicate the individual contributions of the respective $1h$ configurations shown in the upper panel). Experimental spectra are not available.

ration contributes 56% and the chromophore $1h$ configuration 36% to the first cationic state. The contributions to the second cationic state from the nitrogen lone pair and the chromophore are inverted. In the other two molecules, PENNA and BUNNA, the hole mixing is less pronounced. In PENNA the nitrogen $1h$ configuration contributes 78% to the first cationic state, while the weights of the two chromophore $1h$ configurations (see Fig. 2) are only 8% and 6%. In BUNNA this mixing is even less—the first cationic state holds 88% from the nitrogen lone-pair $1h$ configuration and 4% from the chromophore $1h$ configuration. In all three molecules the missing contributions of approximately 8% to the cationic state arise from other $1h$ configurations and, in particular, from a large number of $2h1p$ configurations.

Already at this point it is clear that including or not the electron correlation and relaxation effects will lead to entirely different electron dynamics following ionization. Within the independent particle picture (HF-Koopmans' approach) the ionization out of any of the HF orbitals will not trigger followup processes, i.e., the hole will stay where it is originally created. The situation is fundamentally different if we include the many-body effects. In this case, due to the participation of the other states (through the hole-mixing mechanism in our particular case), the initially created hole will not be stationary and will evolve in time, e.g., can migrate throughout the system. Thus, the charge migration that can follow the ionization of a molecular system is solely due

to the many-body effects. In the concrete examples, the larger the hole mixing, the richer the ensuing electron dynamics. We stress, however, that the hole mixing is mediated by the $2h1p$ and higher configurations, i.e., it vanishes if the $2h1p$ configurations are not included in the calculation. For a detailed discussion, see Sec. IV.

B. Charge migration in the outer-valence shell

Let us now examine the charge migration following ionization of the outer-valence shell of the molecules PENNA, MePeNNA, and BUNNA. We want to investigate the influence of the donor site on the charge migration mechanism tracing the electron dynamics following a localized ionization on the chromophore site of all three molecules. The initial cationic state is thus prepared by a sudden removal of an electron from the HF orbital localized on the chromophore. In the molecules PENNA and MePeNNA this is the highest occupied molecular orbital (HOMO) and in the case of BUNNA—the HOMO-1 one (see the upper panels of Figs. 2–4).

In order to analyze the electron dynamics following the ionization, it is illuminating to trace the time evolution of the hole occupation numbers $\tilde{n}_p(t)$ and the corresponding natural charge orbitals $\tilde{\varphi}_p(\vec{r}, t)$ defined in Eq. (5). In Fig. 5 we present the evolution of the hole occupation numbers during the first 10 fs after the ionization of the chromophores of PENNA, MePeNNA, and BUNNA. In order not to overburden the figure, only five of the hole occupation numbers (those which contribute the most) are depicted. At time $t=0$ all the occupation numbers are equal to zero except the one which carries the whole charge.

We will start our closer look with the molecule PENNA (see also Ref. 15). There, after about 2 fs, nearly 20% of the initial charge is transferred to other natural charge orbitals [see the uppermost curve in Fig. 5(a)]. After that time, the process is reversed and the charge flows back such that 4 fs after the ionization more than 90% of the hole charge is again on the natural charge orbital populated by the initial ionization. However, this does not mean that the charge has returned to its initial spatial position since the natural charge orbitals also change with time. Technically speaking, at each time point the natural charge orbitals are different linear combinations of the original HF molecular orbitals (virtual and occupied), coinciding with them only at time $t=0$. In order to demonstrate this we show in Fig. 6 snapshots of the natural charge orbital corresponding to the hole occupation number bearing most of the charge [the uppermost curve in Fig. 5(a)]. As we see, after 2 fs the charge continues to flow to the nitrogen moiety of the system. However, after 4 fs this process is reversed, and in the following 4 fs the charge migrates back to the chromophore. Although from Fig. 5(a) it seems that the charge performs perfect oscillations with a period of 8 fs, the participation of a large number of ionic states in the process actually introduce a dissipation effect. Thus, after 8 fs the charge does not return exactly to its initial spatial position.

A final comment on Fig. 5(a) is in order. The hole occupation numbers with negative sign correspond to particles

104305-6 Lünemann, Kuleff, and Cederbaum

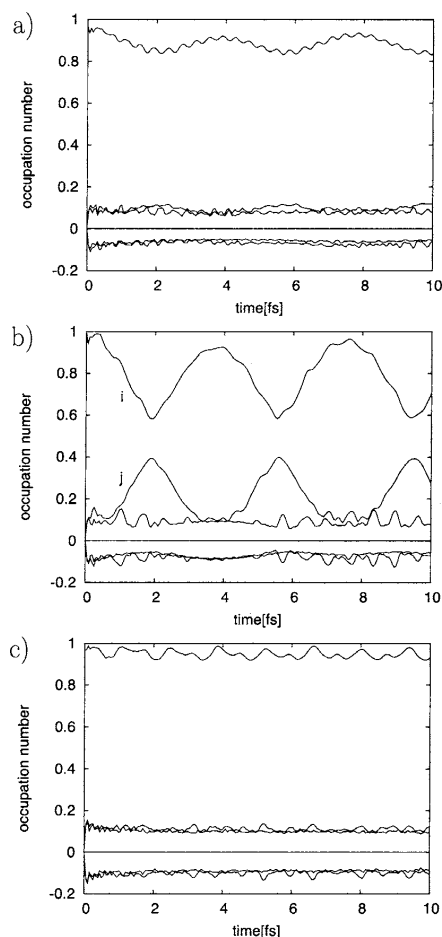
J. Chem. Phys. **129**, 104305 (2008)

FIG. 5. Hole occupation numbers as a function of time for the first 10 fs after ionization of the chromophore of (a) PENNA, (b) MePeNNA, and (c) BUNNA. The five most important occupation numbers are shown in each panel. At $t=0$ all occupation numbers are equal to 0 except of the one which relates to the ionized chromophore.

(electrons). It is seen that after the ultrafast (about 50 as) response of the system, a phenomenon discussed elsewhere,²⁸ the hole occupation numbers corresponding to particles are nearly constant in time (apart from the small wiggles seen in the figure). Because, by construction, the hole density is normalized to 1 at any time point, these negative hole occupations have their positive counterparts. These positive and negative occupations represent hole-particle excitations, originating from the $2h1p$ configurations, and describing many-body effects present in the cation.

Let us now see what happens after ionizing the chromophore of the molecule MePeNNA. The hole occupation numbers that contribute most to the succeeding electron dynamics are shown in Fig. 5(b). As in the case of PENNA, the initial state is constructed such that it corresponds to a sudden removal of an electron from the HF molecular orbital localized on the chromophore, i.e., at $t=0$ the entire hole charge is carried by the HF-HOMO (see Fig. 3). As was

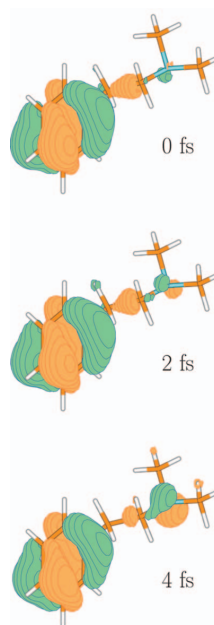


FIG. 6. (Color) The most occupied time-dependent natural charge orbital of the molecule PENNA at times $t=0$, 2, and 4 fs after ionizing the HF-HOMO. At time of 0 the natural charge orbital is equivalent to the HF-HOMO.

discussed in the previous subsection on the ionization spectrum, we encounter for MePeNNA the situation of strong hole mixing. From Fig. 5(b) we see that at $t \approx 2$ fs about 40% of the hole charge have migrated to the natural charge orbital denoted by j , which consists mainly of the HF-HOMO-1 located predominantly on the nitrogen site of the molecule. After that time an avoided crossing between natural charge orbitals i and j occurs, and the characters of the two orbitals are swapped, i.e., the orbital i is now mainly the HF-HOMO-1 and the orbital j mainly HF-HOMO. Thus, after 2 fs the charge continues to flow from the natural charge orbital constructed mainly by HF-HOMO to the natural charge orbital constructed mainly by HF-HOMO-1 until at $t \approx 4$ fs more than 90% of the charge has migrated to the orbital localized on the nitrogen moiety of the molecule. The full cycle of oscillation lasts about 7.5 fs, with a second avoided crossing at around 5.5 fs. After that time the whole process starts again. As in the case of PENNA, these oscillations are not perfect due to the participation of a large number of ionic states.

Snapshots of the natural charge orbital corresponding to the hole occupation number bearing the initial charge [the uppermost curve in Fig. 5(b)] are presented in Fig. 7 for the first half cycle of the process. It is seen that almost the entire charge migrates from the chromophore to the nitrogen site of the molecule in only about 4 fs.

What happens in the case of BUNNA? As was noted in the previous subsection, the ionization of the chromophore site in BUNNA is not expected to lead to a migration of the created positive charge since the other valence ionic states

104305-7 Controlling factors in charge migration

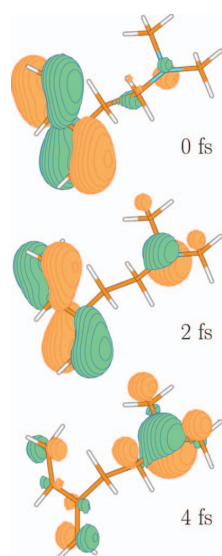
J. Chem. Phys. **129**, 104305 (2008)

FIG. 7. (Color) The most occupied time-dependent natural charge orbital of the molecule MePeNNA at times $t=0$, 2, and 4 fs after ionizing the HF-HOMO. At time of 0 the natural charge orbital is equivalent to the HF-HOMO.

are nearly entirely build from a single $1h$ configuration each. In Fig. 5(c) the evolution of the hole occupation numbers for the first 10 fs is depicted. One can see that apart from small fluctuations, the hole occupation number of the natural charge orbital which carries the initial charge [the uppermost curve in Fig. 5(c)] does not change as time proceeds. The natural charge orbital itself (not shown) also does not evolve and overlaps at all times nearly 100% with the HF-HOMO. Consequently, the charge stays where it is initially created. As discussed above, the hole-particle excitations, represented by the other curves of positive and negative occupations in Fig. 5(c), describe the many-body effects present in the cation after removing an electron from the chromophore.

To complete the visualization of electron dynamics following localized ionization on the chromophore sites of the molecules PENNA, MePeNNA, and BUNNA, the hole density $Q(z,t)$ is calculated [see Eq. (5)]. The quantity $Q(z,t)$ was obtained by integrating $Q(\vec{r},t)$ over the remaining x and y components, perpendicular to z , while the axis z was chosen to pass through the longest spatial extension of each of the molecules, thus called “molecular axis.” The results are shown in Fig. 8. For convenience, the relative positions of the atoms along the molecular axis are indicated.

At time of 0 the hole charge is located on the chromophore site in all three molecules. After only about 4 fs nearly the complete hole charge in MePeNNA has migrated to the nitrogen site [see humps on the right-hand side of the $Q(z,t)$ landscape in Fig. 8(b)]. After that time the charge flows back mainly to its initial position and the whole process starts again. For PENNA the same time scale holds, but only a small fraction of the hole charge migrates at all. In the case of BUNNA the ionization of the chromophore does not lead to succeeding electron dynamics and the charge stays where it was initially created.

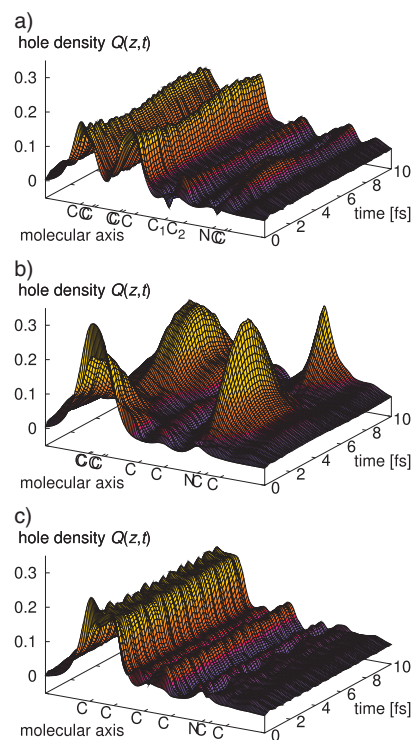


FIG. 8. (Color) Hole density $Q(z,t)$ along the molecular axis as a function of time for the three molecules: (a) PENNA, (b) MePeNNA, and (c) BUNNA.

In conclusion, although the molecules are very similar and differ only at their chromophore site, they exhibit completely different electron dynamics. In MePeNNA we observe a strong and directed charge migration from the initially ionized chromophore site to the nitrogen site. In PENNA the migration is again between these sites, but only a small fraction of the charge migrates. An interesting point is that the time scale of this migration is nearly identical to

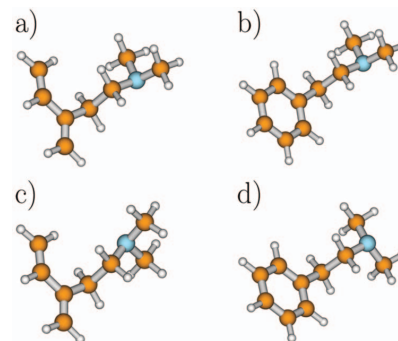


FIG. 9. (Color) Structures of the two conformers low in energy of MePeNNA and PENNA. (a) The previously discussed conformer of the molecule MePeNNA, (b) the previously discussed conformer of PENNA, (c) the second conformer of MePeNNA, called MePeNNA', and (d) the second conformer of PENNA, called PENNA'.

104305-8 Lünemann, Kuleff, and Cederbaum

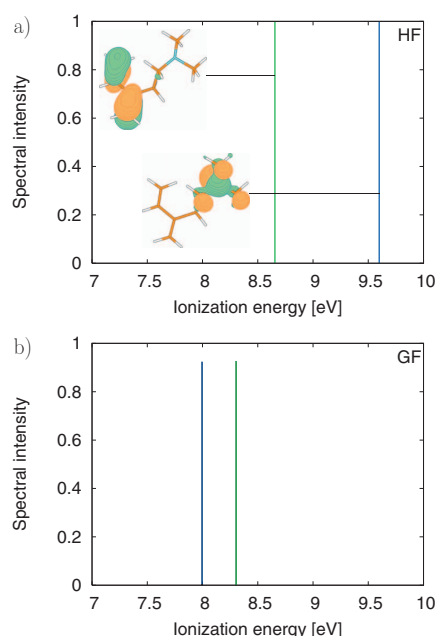
J. Chem. Phys. **129**, 104305 (2008)

FIG. 10. (Color) Ionization spectrum of MePeNNA'. The upper panel shows the results obtained by employing the HF-Koopmans' theorem. The corresponding HF orbitals are also displayed. The lower panel shows the results of the GF calculation (the colors on the lines indicate the individual contributions of the respective $1h$ configurations shown in the upper panel).

that found for MePeNNA (≈ 4 fs). The third molecule discussed (BUNNA) does not show any charge migration, and within the time interval investigated the created charge is essentially stationary. Most importantly, the migration is *not* proceeding along the molecule: The hole charge which disappears from the chromophore site appears on the nitrogen site without showing up in between these two sites. This behavior is a typical signature of the many-body character of the underlying charge migration mechanism.

C. Impact of the geometrical structure on charge migration

Let us shed some light on the influence of the geometrical structure of the molecule on the charge migration. For this purpose, we have investigated two other conformers of the molecules PENNA and MePeNNA, denoted in what follows as PENNA' and MePeNNA', respectively. In both molecules the difference in the nuclear geometry compared to the cases discussed up to now is a change in the angle of torsion around the CN bond.

According to a theoretical study on PENNA,¹⁷ the conformer second lowest in energy is a symmetrical molecule differing from the ground-state geometry by a rotation around the CN bond, see Fig. 9 panels b and d. The energy difference between these two conformers is about 0.8 kcal/mol.¹⁷

As mentioned in the second paragraph of Sec. III, also MePeNNA possesses two low lying conformers separated by about 0.5 kcal/mol. The geometrical difference between

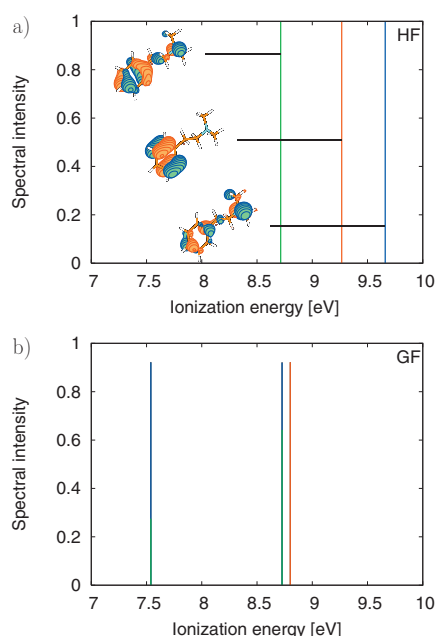


FIG. 11. (Color) Ionization spectrum of PENNA'. The upper panel shows the results obtained by employing the HF-Koopmans' theorem. The corresponding HF orbitals are also displayed. The lower panel shows the results of the GF calculation (the colors on the lines indicate the individual contributions of the respective $1h$ configurations shown in the upper panel).

these two conformers is comparable to that found in PENNA—just a change in the angle of torsion at the nitrogen site of the molecule, see Fig. 9, panels a and c.

In both cases, the energy difference between the conformers is less than 1 kcal/mol which is smaller than the typical error of the computational methodology used. (For errors of the DFT method see, e.g., Ref. 29 and references therein.) Thus, the computational methodology is not precise enough to predict unambiguously which is the lowest conformational state of the respective molecules. Nevertheless, one may expect that at room temperature both primed and unprimed conformers will be nearly equally populated.

The ionization spectrum of MePeNNA' is shown in Fig. 10, and that of PENNA' in Fig. 11. The upper panels show again the HF-Koopmans' results together with the corresponding HF orbitals. In MePeNNA' the ionization energies and HF orbitals are nearly identical to these of MePeNNA (see Fig. 3). In PENNA' the ionization energies are only slightly shifted but the corresponding HF orbitals differ more noticeably from those of PENNA. The HOMO and HOMO-2 in PENNA' are delocalized compared to those in PENNA where they are clearly localized on the chromophore and the nitrogen moieties, respectively (see Fig. 2).

Although the differences between the conformers are only slight at the HF level, the picture changes dramatically if we compare the ionization spectra including many-body effects (see the lower panels of Figs. 10 and 11). Whereas in the previously discussed systems we observed a strong hole mixing of two states in MePeNNA and a less pronounced

104305-9 Controlling factors in charge migration

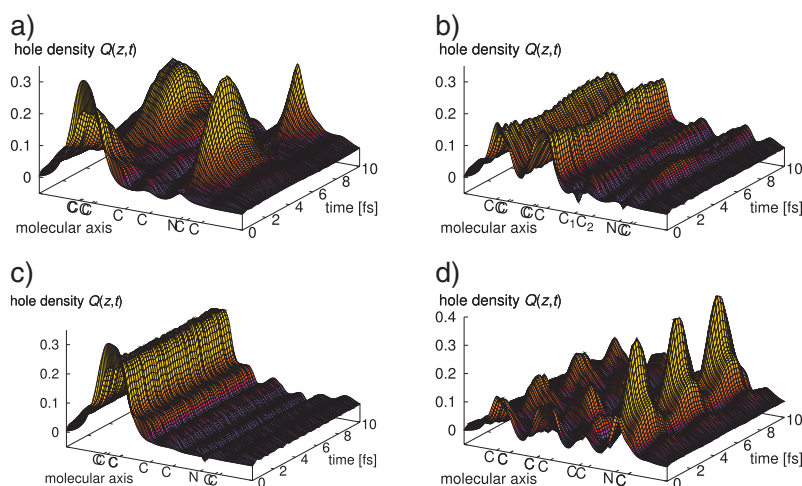
J. Chem. Phys. **129**, 104305 (2008)

FIG. 12. (Color) Hole density $Q(z,t)$ along the molecular axis as a function of time for the molecules: (a) MePeNNA, (b) PENNA, (c) MePeNNA', and (d) PENNA'.

hole mixing in PENNA, the situation reverses in their conformers. Now, in MePeNNA' no hole mixing is present, while PENNA' exhibits stronger hole mixing. The first cationic state of MePeNNA' at 8.0 eV is a state to which the hole on the nitrogen site contributes 92%. The second cationic state with ionization energy of 8.3 eV has a contribution of 93% from the hole on the chromophore. In PENNA' there is a 65% contribution from the HOMO-2 $1h$ configuration and a 28% contribution from the HOMO $1h$ configuration to the first ionic state at 7.5 eV. The contributions from the HOMO-2 and HOMO $1h$ configurations to the second ionic state at 8.7 eV are inverted. The missing 8%, respectively, 7%, of the cationic states is distributed over other small $1h$ and a large number of $2h1p$ configurations.

Again, including the many-body effects leads to a more substantial shift in energy of the state corresponding to the ionization of the nitrogen site than of the state corresponding to the ionization of the chromophore. However, the energy difference between the cationic states of MePeNNA' conformer is smaller (0.3 eV), compared to that in MePeNNA (0.5 eV), while we encounter the opposite situation in PENNA—the energy difference between the first and second cationic states in PENNA is 0.5 eV, whereas in PENNA' it is 1.2 eV.

The differences in the ionization spectra and, more importantly, the different natures of the cationic states in the primed and unprimed conformers naturally lead to different electron dynamics following the ionization out of the HF-HOMO. The results are shown in Fig. 12 where a comparison of the evolution of the hole density of the two conformers of the two molecules can be made. The hole densities of MePeNNA and MePeNNA' are shown on the left-hand side of Fig. 12 (panels a and c) and those of PENNA and PENNA' on the right-hand side of Fig. 12 (panels b and d). One observes a completely different behavior in the primed conformers compared to the unprimed ones. Whereas in MePeNNA we have a strong and fast (4 fs) charge migrations to the nitrogen site following ionization of the chromophore, no charge migration is observed from the corre-

sponding initial state in MePeNNA', i.e., the initially created charge there is stationary. In PENNA and PENNA' the differences start already at the initial state. In PENNA we have a localized charge at time of 0, whereas in PENNA' the initial hole is somewhat delocalized (the two conformers have different HF-HOMOs). Particularly interesting is the finding that the amount of charge which migrates throughout the system is very different. In PENNA only a small fraction of the charge flows to the nitrogen site, while in PENNA' nearly the whole charge initially localized on the chromophore migrates to the nitrogen. Another difference is the

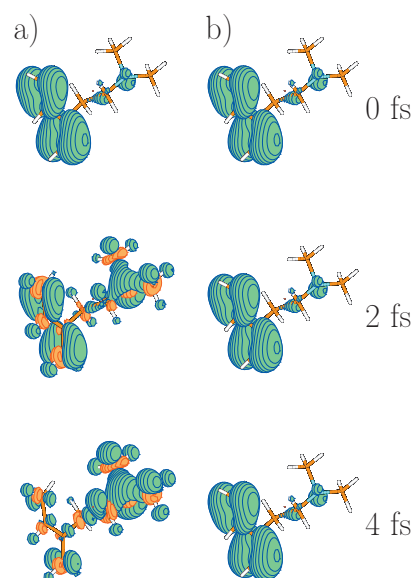


FIG. 13. (Color) Time-dependent hole density of MePeNNA at times $t=0$, 2, and 4 fs after ionizing the HF-HOMO. The “negative” hole density or electron density is given in orange. Shown are the results for (a) the complete hole density and (b) the hole density computed without the mediating excitations.

time scale of the charge migration. Because of the relatively large energy difference between the two mixed cationic states in PENNA' (1.2 eV), the electron dynamics are ultrafast. Only about 1.7 fs are needed for the charge on the chromophore to reach the nitrogen site.

Clearly, the electron dynamics following the ionization are extremely sensitive to the nuclear geometry of the ionized system (see also Ref. 13). Thus, if a reliable experimental measurement of the charge migration phenomenon is achieved, it can be used to probe the concrete nuclear geometry of the investigated system at the time of ionization. In addition, it is clear that the nuclear dynamics will start to play an important role at later times. The movement of the nuclei may block the migration process, trapping the charge on a particular site, or, on the contrary, may facilitate it. One also has to keep in mind that the electron dynamics can influence the nuclear dynamics since, at least within the Born–Oppenheimer approximation, the electronic motion governs the effective potential seen by the nuclei.

IV. DISCUSSION AND ANALYSIS

Let us now come to the analysis of the results obtained. Two important observations can be immediately made. First, the results clearly show that the charge migration depends strongly on the type of the chromophore-donor site and, second, that electron dynamics are very sensitive to the particular geometry of the ionized system. In all investigated molecules we observe strong and fast charge migration in the cases of strong hole mixing in the cationic states, and not so pronounced (or lack of) charge migration when the mixing of the states is weak (or negligible). The natural question that arises is what is the mechanism of this mixing and is there a simple analytical measure of it?

Since the charge migration phenomenon is entirely due to the many-body effects, it is natural to suppose that the hole mixing is governed by the electron correlation and electron relaxation effects. In CI language [see Eq. (7)] this means that the $2h1p$ configurations are the mediator of the mixing in the $1h$ space. To clarify this we performed calcu-

lations on the molecule MePeNNA (where a strong hole mixing is observed) neglecting the contribution of the $2h1p$ configurations. The results are shown in Fig. 13. On the left-hand side we display snapshots of the full hole density at times $t=0, 2$, and 4 fs, and on the right-hand side the hole density calculated neglecting the $2h1p$ configurations.

One clearly sees that without the mediating $2h1p$ configurations no charge migration appears. The analysis of the concrete cationic states show that in order to have strong hole mixing in two (or more) states, the most important contribution of the $2h1p$ space to these states has to come from the same $2h1p$ configurations. That is why we say that the $2h1p$ configurations appear as the *mediator* of the hole mixing and thus of the charge migration caused by it.

However, since many $2h1p$ configurations may be admixed with comparable weights and the coupling can have a very complicated structure, this analysis can become very tedious and sometimes even impossible. That is why, to acquire an additional insight and to describe the underlying mechanisms in a simple and transparent way, it is useful to replace the interaction of the numerous configurations by the effective interaction of only those that are relevant to the problem. This can be done by the so-called exact effective Hamiltonian (EEH) method,³⁰ based on the block-diagonalization technique for Hermitian matrices developed in Ref. 31, and successfully used to analyze eigenvectors with a complicated structure. For details of the method and its applications, we refer the reader to Refs. 30, 32, and 33. In brief, the method consists in constructing a small EEH matrix that exhibits the energies and interactions between the configurations dressed by the interaction with all the remaining configurations of the underlying huge secular problem.

The procedure of the EEH method can be well exemplified if we make use of a model CI Hamiltonian having 2×2 $1h$ block and a large $2h1p$ block, and we are interested in the effective interaction of the two $1h$ configurations in the first two eigenvectors. The EEH procedure brings the CI matrix to the following block-diagonal form:

$$\begin{array}{c}
 \begin{array}{cc|ccc}
 \overbrace{\varepsilon_1} & 0 & \overbrace{x_{11}} & \cdots & \overbrace{x_{1n}} \\
 \varepsilon_2 & & \overbrace{x_{21}} & \cdots & \overbrace{x_{2n}} \\
 \hline
 & & \overbrace{a_{11}} & \cdots & \overbrace{a_{1n}} \\
 & & & \ddots & \vdots \\
 & & & & \overbrace{a_{nn}}
 \end{array} \\
 H_{\text{CI}}
 \end{array}
 \rightarrow
 \begin{array}{c}
 \begin{array}{c|ccc}
 \tilde{E}_1 & V_{12} & 0 & \cdots & 0 \\
 & \tilde{E}_2 & 0 & \cdots & 0 \\
 \hline
 & & \tilde{a}_{11} & \cdots & \tilde{a}_{1n} \\
 & & & \ddots & \vdots \\
 & & & & \tilde{a}_{nn}
 \end{array} \\
 H_{\text{eff}}
 \end{array}
 \quad (8)$$

In the CI Hamiltonian H_{CI} the $1h$ configurations do not couple directly but through the $2h1p$ configurations. In the

block-diagonal effective Hamiltonian H_{eff} produced by the EEH procedure the coupling through this large number of

$2h1p$ configurations is replaced by a single effective coupling term V_{12} . Of course, the EEH procedure can be applied when studying the effective interaction of more than two configurations.

The EEH procedure was applied to all molecules studied in the present work, calculating the effective coupling between the $1h$ configurations, corresponding to a hole on the chromophore or a hole on the nitrogen site, in the first two cationic states. The results are the following (all matrix elements are given in eV):

$$\begin{pmatrix} \text{PENNA} \\ 8.00 & 0.15 \\ \cdots & 8.44 \\ \Delta E=0.53 \text{ eV} \end{pmatrix}, \begin{pmatrix} \text{MePeNNA} \\ 8.13 & 0.30 \\ \cdots & 8.20 \\ \Delta E=0.55 \text{ eV} \end{pmatrix}, \begin{pmatrix} \text{BUNNA} \\ 7.91 & 0.32 \\ \cdots & 9.32 \\ \Delta E=1.55 \text{ eV} \end{pmatrix}, \quad (9)$$

$$\begin{pmatrix} \text{PENNA}' \\ 7.90 & 0.54 \\ \cdots & 8.37 \\ \Delta E=1.19 \text{ eV} \end{pmatrix}, \begin{pmatrix} \text{MePeNNA}' \\ 8.00 & 0.001 \\ \cdots & 8.30 \\ \Delta E=0.31 \text{ eV} \end{pmatrix}. \quad (10)$$

In addition, we display the energy difference ΔE between the cationic states. Note that the numbers on the diagonal of the effective matrices are not the ionization energies but effective (or dressed) energies, and thus their difference is not equal to ΔE . When we compare the hole mixing in the different molecules, we have to take into account two quantities—the coupling matrix element between the dressed $1h$ configurations [V_{12} in Eq. (8)] and the energy difference between the effective energies. Large coupling and small effective energy difference will lead to a strong hole mixing in the cationic states, and vice versa—small coupling and large effective energy difference will lead to a negligible hole mixing. Situations with large coupling and large energy difference, as well as with small coupling and small energy difference, will lead to a small to moderate hole mixing.

Inspecting the numbers in Eqs. (9) and (10), we see that they explain well the different behaviors in the electron dynamics we have observed in the studied molecules. In MePeNNA we have a moderate coupling but small effective energy difference yielding strong hole mixing and thus strong charge migration. In PENNA' we have a relatively large energy gap but a strong coupling giving rise also to a strong hole mixing and hence charge migration. In PENNA the small coupling is combined with a relatively small energy gap, and thus we observe that only a small fraction of the charge migrates to the nitrogen site. In BUNNA there is a moderate coupling, but a large energy gap predetermining the very small hole mixing and thus the lack of charge migration. Finally, even though the energy gap in MePeNNA' is relatively small, the coupling is so negligible that no hole mixing appears and the charge stays where it is originally created.

It should be noted that a single number as a measure of the effective coupling between the $1h$ configurations we are interested in can be obtained by dividing the effective coupling matrix element V_{12} by the energy difference ΔE . In fact, the quantity obtained in that way is exactly the first order perturbation correction to the transition amplitude $\langle \Phi_i | I \rangle$. For the molecules studied this quantity gives 0.28 for PENNA, 0.54 for MePeNNA, 0.19 for BUNNA, 0.003 for

MePeNNA', and 0.45 for PENNA'. Obviously these numbers are in accord with our observations for the charge migration in the different molecules. However, this quantity $|V_{12}/\Delta E|$ alone cannot establish an absolute scale for the “strength” of the hole mixing. It can give only an indication for the expected electron dynamics, in particular, when comparing related molecules.

An important advantage of the analysis through the EEH method is that we do not need to know the full eigenvectors of the system Hamiltonian in order to construct the EEH. It is sufficient to know only the components of the $1h$ configurations in the eigenvectors we want to analyze and the corresponding eigenvalues. This is a valuable feature when performing a full diagonalization of the Hamiltonian matrix is prohibitively expensive. In those cases one can, for instance, perform a filter diagonalization to obtain the eigenvectors only within a given energy range and then use the EEH method for analysis.

V. SUMMARY

In the present paper we have studied the ultrafast charge migration following outer-valence ionization in three different but related molecules, namely, 2-phenylethyl-*N,N*-dimethylamine (PENNA), and its butadiene (MePeNNA) and ethylene (BUNNA) derivatives. The molecules have different chromophore sites, but nearly identical nitrogen sites. In all three molecules we have investigated the evolution of the charge density after creating a localized hole on the chromophore-donor site of the molecules. The results show that the charge migration process depends strongly on the particular donor site. We observe that in the case of MePeNNA molecule the created positive charge migrates to the amine-acceptor site in just 4 fs. In PENNA the charge migration has the same time scale, but in this case only a small fraction of the charge flows to the amine-acceptor site. The third investigated molecule, BUNNA, shows no electron dynamics after ionization of its chromophore, and within the studied time interval, the charge stays at its initial position.

In order to investigate the influence of the geometrical structure on the charge migration process, we have investigated two conformers of the molecules PENNA and MePeNNA, denoted in our study as PENNA' and MePeNNA', respectively. In both cases the primed conformers are energetically very close to the unprimed ones and differ in their nuclear geometry by a rotation of the amine site around the CN bond. Although the differences in the nuclear geometry are small, the electron dynamics following ionization of the respective chromophores change dramatically. In contrast to MePeNNA, where we have observed a very strong charge migration, the ionization of the chromophore does not trigger any electron dynamics in MePeNNA' and the created charge is stationary. At the same time, in the case of PENNA' the removal of an electron from the chromophore is followed by an ultrafast charge migration and the positive charge reaches the amine-acceptor site in only 1.7 fs. These results clearly show that the charge migration is very sensitive to the nuclear geometry of the ionized

104305-12 Lünnemann, Kuleff, and Cederbaum

J. Chem. Phys. **129**, 104305 (2008)

system and thus probably can be used for probing the momentary nuclear positions at the time of ionization.

The calculations performed in the present work allow also to shed some light on the underlying physical mechanisms of the charge migration phenomenon. It is shown that in the studied molecules, the charge migration appears due to the so-called hole mixing in the cationic states. Our analysis shows that the hole mixing is a result of a coupling through the $2h1p$ configurations. This means that the admixture of the two $1h$ configurations, corresponding to localized holes on the chromophore-donor and amine-acceptor sites, in the cationic states is not due to a direct coupling between these configurations but via, in general, a large number of $2h1p$ configurations reflecting the electron correlation present in the cation.

A final comment on our results is in order. As we have seen, the electron dynamics following localized ionization of the chromophore site in the molecules PENNA, MePeNNA, and BUNNA are completely different. Thus, if the mechanism leading to the experimentally observed fragmentation after localized ionization of the chromophore in the molecule PENNA (Refs. 16 and 17) is a result of a coupled electron-nuclear dynamics, as we have suggested in a recent publication,¹⁵ one may expect also a completely different behavior and time scale of this fragmentation in the case of MePeNNA, and even no fragmentation in the case of BUNNA. However, the different electron dynamics in the different conformers have also to be taken into account.

We hope that our work will stimulate further experimental and theoretical studies on the fascinating subject of charge migration.

ACKNOWLEDGMENTS

Financial support by the DFG is gratefully acknowledged.

- ¹L. S. Cederbaum and J. Zobeley, *Chem. Phys. Lett.* **307**, 205 (1999).
- ²P. F. Barbara, T. J. Meyer, and M. A. Ratner, *J. Phys. Chem.* **100**, 13148 (1996).
- ³J. Jortner and A. M. Ratner, *Molecular Electronics* (Blackwell Science,

- Oxford, 1997).
- ⁴V. May and O. Kühn, *Charge and Energy Transfer Dynamics in Molecular Systems* (Wiley-VCH, Weinheim, 2004).
- ⁵M. Garavelli, P. Celani, F. Bernardi, M. A. Robb, and M. Olivucci, *J. Am. Chem. Soc.* **119**, 6891 (1997).
- ⁶A. Dreuw, G. A. Worth, L. S. Cederbaum, and M. Head-Gordon, *J. Phys. Chem. B* **108**, 19049 (2004).
- ⁷T. Schultz, E. Samoylova, W. Radloff, I. V. Hertel, A. L. Sobolewski, and W. Domcke, *Science* **306**, 1765 (2004).
- ⁸L. S. Cederbaum, *J. Chem. Phys.* **128**, 124101 (2008).
- ⁹J. Müller, *Phys. Today* **61**(5), 15 (2008).
- ¹⁰J. Breidbach and L. S. Cederbaum, *J. Chem. Phys.* **118**, 3983 (2003).
- ¹¹A. I. Kuleff, J. Breidbach, and L. S. Cederbaum, *J. Chem. Phys.* **123**, 044111 (2005).
- ¹²H. Hennig, J. Breidbach, and L. S. Cederbaum, *J. Phys. Chem. A* **109**, 409 (2005).
- ¹³A. I. Kuleff and L. S. Cederbaum, *Chem. Phys.* **338**, 320 (2007).
- ¹⁴J. Breidbach and L. S. Cederbaum, *J. Chem. Phys.* **126**, 034101 (2007).
- ¹⁵S. Lünnemann, A. I. Kuleff, and L. S. Cederbaum, *Chem. Phys. Lett.* **450**, 232 (2008).
- ¹⁶L. Lehr, T. Horneff, R. Weinkauff, and E. W. Schlag, *J. Phys. Chem. A* **109**, 8074 (2005).
- ¹⁷R. Weinkauff, L. Lehr, and A. Metsala, *J. Phys. Chem. A* **107**, 2787 (2003).
- ¹⁸J. Schirmer, L. S. Cederbaum, and O. Walter, *Phys. Rev. A* **28**, 1237 (1983).
- ¹⁹L. S. Cederbaum, in *Encyclopedia of Computational Chemistry* (Wiley, Chichester, 1998), Vol. 1, p. 1202.
- ²⁰J. Schirmer, A. B. Trofimov, and G. Stelter, *J. Chem. Phys.* **109**, 4734 (1998).
- ²¹J. Schirmer, *Phys. Rev. A* **43**, 4647 (1991).
- ²²F. Mertins and J. Schirmer, *Phys. Rev. A* **53**, 2140 (1996).
- ²³T. H. Dunning, *J. Chem. Phys.* **53**, 2823 (1970).
- ²⁴MACROMODEL, version 9.1, Schrödinger, LLC, New York, NY, 2005.
- ²⁵T. Halgren, *J. Comput. Chem.* **17**, 490 (1996).
- ²⁶A. Szabo and N. S. Ostlund, *Modern Quantum Chemistry: Introduction to Advanced Electronic Structure Theory* (Dover, Mineola, New York, 1989).
- ²⁷L. N. Domelsmith, L. L. Munchausen, and K. N. Houk, *J. Am. Chem. Soc.* **99**, 4311 (1977).
- ²⁸J. Breidbach and L. S. Cederbaum, *Phys. Rev. Lett.* **94**, 033901 (2005).
- ²⁹S. Grimme, *Angew. Chem.* **118**, 4571 (2006).
- ³⁰N. V. Dobrodey, L. S. Cederbaum, and F. Tarantelli, *Phys. Rev. B* **57**, 7340 (1998).
- ³¹L. S. Cederbaum, J. Schirmer, and H.-D. Meyer, *J. Phys. A* **22**, 2427 (1989).
- ³²N. V. Dobrodey, A. I. Streltsov, and L. S. Cederbaum, *Phys. Rev. A* **65**, 022501 (2002).
- ³³A. I. Streltsov, N. V. Dobrodey, and L. S. Cederbaum, *J. Chem. Phys.* **119**, 3051 (2003).

Theoretical description of charge migration with a single Slater-determinant and beyond

Alexander I. Kuleff^{1,a)} and Andreas Dreuw^{2,b)}

¹*Institute of Physical Chemistry, Ruprecht Karls-University Heidelberg, Im Neuenheimer Feld 229, 69120 Heidelberg, Germany*

²*Institute of Physical and Theoretical Chemistry, Goethe-University Frankfurt, Max von Laue-Strasse 7, 60438 Frankfurt, Germany*

(Received 16 July 2008; accepted 9 December 2008; published online 15 January 2009)

Triggered by the interest to study charge migration in large molecular systems, a simple methodology has recently been proposed based on straightforward density functional theory calculations. This approach describes the time evolution of the initially created hole density in terms of the time evolution of the ionized highest occupied molecular orbital (HOMO). Here we demonstrate that this time-dependent analog of Koopmans' theorem is not valid, and instead of the time evolution of the HOMO, the time evolution of the orbitals that remain occupied in the cation determines the evolution of the initially created hole in the framework of time-dependent single-determinant theories. Numerical examples underline that for a proper description of charge migration processes, an explicit treatment of the electron correlation is indispensable. Moreover, they also demonstrate that the attempts to describe charge migration based on Kohn-Sham density functional theory using conventional exchange-correlation functionals are doomed to fail due to the well-known self-interaction error. © 2009 American Institute of Physics. [DOI: 10.1063/1.3058899]

I. INTRODUCTION

Transfer of charge is a fundamental process in nature and plays important roles in physics, chemistry, and biology.¹ A vast number of experimental and theoretical works have thus been dedicated to the investigation of charge transfer in molecular systems (see, e.g., Ref. 2 and references therein). In the traditional picture of charge transfer from one place in a molecular system to another, the motion of the nuclei is required. Moreover, the charge transfer occurs through the nonadiabatic couplings between nuclear and electronic motions, i.e., the charge transfer is mediated by the nuclear dynamics.³ In other words, if the nuclei do not move, charge is not transferred. The time scales of charge or equivalently electron transfer can vary drastically. In cases when the nonadiabatic coupling is weak, electron or charge transfer is usually slow compared to the time scale of nuclear motion of picoseconds.² Nevertheless, nuclear-dynamics-mediated charge transfer can also be ultrafast occurring on a time scale of only a few hundred femtoseconds when conical intersections dominate the process,^{4–6} where the nonadiabatic coupling elements are infinitely large.

However, only recently it has been demonstrated theoretically that charge can be transferred through molecules with frozen nuclei driven just by electron correlation alone on time scales of only a few femtoseconds.⁷ To differentiate the nuclear-dynamics-driven charge transfer from the purely electronically driven one, we will refer to the latter as *charge migration*. The concept of charge migration is as follows. At initial time, a hole is instantaneously created in the electron

density of the molecule, for example, a molecule is suddenly ionized⁸ at one particular site. The electron density reacts upon the sudden ionization and the created charge, or hole, may start to travel through the molecule due to the correlated motion of all electrons.

In real molecular systems, both mechanisms are hardly separable and individually observable in typical time-resolved experiments, since electronic and nuclear motions are always strongly coupled in ultrafast processes. With the help of attosecond laser pulses, though, it may become possible to monitor the motion of the electrons separately from that of the nuclei. However, although ultrafast charge transfer and charge migration are very similar, the important difference is the underlying concept. In the first, the charge transfer is triggered by the nuclear dynamics, while in the latter, the charge migration triggers some nuclear motion.

Meanwhile, charge migration has been demonstrated theoretically to occur in various relatively small molecules.^{9–14} It has been shown in great detail that the many-body effects, i.e., the electron correlation and electron relaxation are the driving forces of charge migration.⁹ For these studies, high-level theoretical methods based on the algebraic diagrammatic construction (ADC) scheme^{15–17} for the one-particle Green's function have been employed taking orbital relaxation and electron correlation into account. Recent time-resolved experiments by Schlag and Weinkauff on oligopeptide radical ions triggered interest to study ultrafast charge migration in these systems and, in general, in larger molecules.^{18–20} Questions of whether charge migration still occurs on ultrafast time scales in larger molecules over larger distances and whether it remains relevant are of general interest. However, large molecular systems cannot be studied with computationally expensive high-level *ab initio* methods.

^{a)}Electronic mail: alexander.kuleff@pci.uni-heidelberg.de.

^{b)}Electronic mail andreas@theochem.uni-frankfurt.de.

Thus, less demanding theoretical approaches are needed for the description of charge migration in, for example, oligopeptides. We note here that several useful models for describing charge migration in peptides are known from the literature.^{21,22} Although these models give qualitative results, they are based on a representation of the peptide as an n -site chain, where each site stands for an amino acid, which is insufficient for quantitative description of charge migration processes. That is why it appears almost natural to turn toward density functional theory (DFT), since in many applications DFT yields reasonably accurate results at moderate computational cost. Remacle and Levine²³ thus applied standard ground-state Kohn–Sham (KS) DFT with the B3LYP exchange–correlation (xc) functional to study charge migration in oligopeptides and later also in the water dimer and other small molecule complexes.²⁴ They also developed an easy and straightforward applicable theoretical methodology²³ based on the KS orbitals and orbital energies of the neutral parent molecule and that of the cationic one to compute and trace charge migration. It has to be noted, however, that all single-determinant approaches (DFT makes no exception) by definition cannot describe certain classes of charge migration phenomena, in particular, those stemming from the participation in the process of the so-called satellite or shake-up states, since these kinds of ionic states are simply missing in the single-particle picture. It is thus clear already at this point that single-determinant approaches and DFT, in particular, would have a limited applicability when treating charge migration processes.

In this work, we review possible approaches to describe charge migration in molecular systems and evaluate their applicability. Moreover, it is demonstrated that DFT cannot be generally applied to study charge migration since the orbitals are corrupted by electron self-interaction. The paper is organized as follows. First, we outline the theoretical methodology required to study charge migration within a single-determinant approach and make connection to the simple theory of Remacle and Levine (Sec. II A). Furthermore, we show that for the proper description of the evolution of the density of the initially created charge within a single-determinant approximation, one has to take into account the relaxation of *all* occupied orbitals. Section II B is devoted to a brief outline of a fully correlated methodology for calculation of the time-dependent charge density. Computational details are given in Sec. III. In Sec. IV we present and discuss the numerical tests performed. We summarize and conclude in Sec. V.

II. THEORETICAL BACKGROUND

A. Time evolution of the hole density in TDHF or time-dependent KS

For simplicity and ease of argumentation, let us assume that a neutral molecule exists for which a single Hartree–Fock (HF) Slater determinant $|\Phi_n\rangle$ is the correct electronic wave function. In that case, the energies ϵ_i of the occupied orbitals correspond to the ionization potentials owing to Koopmans’ theorem and the orbitals ϕ_i themselves are related to the hole density via

$$\rho_h(\vec{r}) = |\phi_i|^2. \quad (1)$$

This is the well-known frozen-orbital approximation, since the orbitals remain unchanged upon removal of an electron. It is clear that the created cationic state $|\Phi_c^n\rangle$ (a cation with all electrons in the frozen orbitals of the neutral) is nonstationary and will immediately start evolving in time. The time evolution of this initially created nonstationary state is governed by the time-dependent HF (TDHF) equation,

$$i\hbar \frac{\partial}{\partial t} \Phi_c^n(\vec{r}, t) = \hat{F}_c^{\text{HF}} \Phi_c^n(\vec{r}, t). \quad (2)$$

The Fock operator of Eq. (2) should be an approximation of the *full* $N-1$ (or cationic) Hamiltonian which, in principle, will govern the evolution of the initially prepared nonstationary cationic state $|\Phi_c^n\rangle$. Since we want to use a standard single-determinant approach, a reasonable choice for this Fock operator will be that of the cationic ground state, i.e., the Fock operator must be built from the self-consistent orbitals of the cation. We point out here that within the time-independent DFT framework, this is even the only possible choice, since DFT is formulated only for ground states. Since the Fock operator is a one-particle operator, it acts on one electron at a time, and we have to solve $N-1$ single-orbital equations of the form

$$i\hbar \frac{\partial}{\partial t} \phi_i^n(r, t) = \hat{f}_c^{\text{HF}} \phi_i^n(r, t), \quad i = 1, 2, \dots, N-1. \quad (3)$$

The orbitals of the neutral ϕ_i^n are not eigenfunctions of \hat{f}_c^{HF} , but one can expand them in the complete set of the self-consistent, time-independent cationic orbitals making the expansion coefficients time dependent,

$$\phi_i^n(\vec{r}, t) = \sum_j c_{ij}(t) \phi_j^c(\vec{r}). \quad (4)$$

By substitution of Eq. (4) into Eq. (3) one arrives at

$$\frac{\partial}{\partial t} \phi_i^n(\vec{r}, t) = -\frac{i}{\hbar} \hat{f}_c^{\text{HF}} \sum_j c_{ij}(t) \phi_j^c(\vec{r}) = -\frac{i}{\hbar} \sum_j c_{ij}(t) \epsilon_j \phi_j^c(\vec{r}), \quad (5)$$

finally yielding an expression for the time evolution of the orbitals of the neutral in the potential of the cation,

$$\phi_i^n(\vec{r}, t) = \sum_j c_{ij}(0) e^{-(i/\hbar)\epsilon_j t} \phi_j^c(\vec{r}). \quad (6)$$

Now, knowing the time evolution of the orbitals, let us analyze how an initially created hole density evolves in time. Assume that a hole is created in the highest occupied molecular orbital (HOMO) of the neutral molecule with the initial orbitals being time dependent according to Eq. (6). This approximation would be a time-dependent analog of Koopmans’ theorem, and, assuming for now its validity, this results in a time-dependent hole density given by

$$\rho_h(\vec{r}, t) = |\phi_{\text{HOMO}}(\vec{r}, t)|^2 \quad (7)$$

$$= \sum_{jj'} c_{Nj}^*(0) c_{Nj'}(0) e^{(i/\hbar)(\epsilon_j - \epsilon_{j'})t} \phi_j^{c*}(\vec{r}) \phi_{j'}^c(\vec{r}),$$

with $N = \text{HOMO}$. (8)

Equation (8) is the basic working equation of the scheme proposed by Remacle and Levine²³ for the description of the time evolution of the initially created hole density. It is seen that within this approximation the time-dependent change of the hole density depends only on the relaxation of the HOMO and does not account for the relaxation of the remaining occupied orbitals. Thus, an obvious question to answer is whether this time-dependent analog of the Koopmans' theorem is valid within the time-dependent single-determinant approaches.

The true time-dependent hole density $\rho_h^{\text{true}}(\vec{r}, t)$ is defined as the difference between the static electron density of the neutral $\rho_n(\vec{r})$ and the time-dependent density of the initially created cation, $\rho_c^n(\vec{r}, t)$, where one electron is removed from the HOMO,

$$\rho_h^{\text{true}}(\vec{r}, t) = \rho_n(\vec{r}) - \rho_c^n(\vec{r}, t). \quad (9)$$

In the latter equation, the electron density of the neutral, $\rho_n(\vec{r})$, is given by

$$\rho_n(\vec{r}) = \sum_i^N |\phi_i^n(\vec{r})|^2, \quad (10)$$

and the nonstationary electron density of the cation by

$$\rho_c^n(\vec{r}, t) = \sum_i^{N-1} |\phi_i^c(\vec{r}, t)|^2. \quad (11)$$

For each orbital of the neutral, one has an expression similar to Eq. (8), which yields

$$\rho_c^n(\vec{r}, t) = \sum_i^{N-1} \sum_{jj'} c_{ij}^*(0) c_{ij'}(0) e^{(i/\hbar)(\epsilon_j - \epsilon_{j'})t} \phi_j^{c*}(\vec{r}) \phi_{j'}^c(\vec{r}). \quad (12)$$

Inserting of Eqs. (10) and (12) into Eq. (9), one arrives at an expression for the true time-dependent hole density

$$\rho_h^{\text{true}}(\vec{r}, t) = \sum_i^N |\phi_i^n(\vec{r})|^2 - \sum_i^{N-1} \sum_{jj'} c_{ij}^*(0) c_{ij'}(0) e^{(i/\hbar)(\epsilon_j - \epsilon_{j'})t} \phi_j^{c*}(\vec{r}) \phi_{j'}^c(\vec{r}). \quad (13)$$

Using the expansion of the orbitals of the neutral in the orbitals of the cation, Eq. (4) yields

$$\begin{aligned} \rho_h^{\text{true}}(\vec{r}, t) &= \sum_i^N \sum_{jj'} c_{ij}^*(0) c_{ij'}(0) \phi_j^{c*}(\vec{r}) \phi_{j'}^c(\vec{r}) \\ &\quad - \sum_i^{N-1} \sum_{jj'} c_{ij}^*(0) c_{ij'}(0) e^{(i/\hbar)(\epsilon_j - \epsilon_{j'})t} \phi_j^{c*}(\vec{r}) \phi_{j'}^c(\vec{r}) \\ &= \sum_i^N \sum_{jj'} c_{ij}^*(0) c_{ij'}(0) \phi_j^{c*}(\vec{r}) \phi_{j'}^c(\vec{r}) (1 - e^{(i/\hbar)(\epsilon_j - \epsilon_{j'})t}) \\ &\quad + |\phi_{\text{HOMO}}^n(\vec{r}, 0)|^2. \end{aligned} \quad (14)$$

The latter equation tells us now how the true hole density changes in time starting from a suddenly ionized neutral state, which is described by one single Slater determinant. At the initial time $t=0$, the hole density corresponds to $|\phi_{\text{HOMO}}^n(\vec{r}, 0)|^2$, which is in agreement with Koopmans' theorem. However, the time evolution of the hole density depends only on the relaxation of the $N-1$ orbitals of the neutral that remain occupied in the cation, since only those acquire a time dependence, which is described by the first term of the right-hand side of Eq. (14). This can already be seen in a completely static picture where the change in the hole density is given by

$$\begin{aligned} \Delta\rho_h &= |\phi_{\text{HOMO}}^n|^2 - \sum_i^N |\phi_i^n|^2 + \sum_j^{N-1} |\phi_j^c|^2 \\ &= \sum_i^{N-1} (|\phi_i^c|^2 - |\phi_i^n|^2), \end{aligned} \quad (15)$$

where ϕ_i^n and ϕ_j^c correspond to the converged self-consistent field (SCF) orbitals of the neutral and cationic ground states, respectively. Thus, at the level of Hartree-Fock theory, the change of the hole density corresponds to the relaxation of the occupied orbitals only. In other words, even if it is true that the initial hole density is well described by the HOMO of the neutral via $\rho_h^{\text{true}}(0) = |\phi_{\text{HOMO}}^n(\vec{r}, 0)|^2$, it will forever stay that density unless the remaining orbitals relax. Nevertheless, the time evolution of the ionized HOMO of the neutral, or equivalently the lowest unoccupied molecular orbital (LUMO) of the cation, would still correspond to the time evolution of the hole density when the relaxation of all occupied orbitals in the cationic state is simultaneously reflected by the relaxation of the single cationic LUMO. This can only be fulfilled when the electron density of the parent neutral is conserved at all times as the electron density of the cation plus the density of its LUMO $|\phi_{\text{LUMO}}^c|^2$, i.e.,

$$\sum_i^N |\phi_i^n(\vec{r})|^2 = \sum_i^{N-1} |\phi_i^c(\vec{r}, t)|^2 + |\phi_{\text{LUMO}}^c(\vec{r}, t)|^2. \quad (16)$$

This is certainly not guaranteed within the SCF procedure and it is demonstrated numerically using the water dimer as example. Since Eq. (16) has to be fulfilled for all times, it must also hold for the neutral and cationic ground states, i.e., when $t=0$. In Fig. 1 the difference between the electron densities on the left- and right-hand sides of Eq. (16) is plotted for the water dimer at the level of HF/6-311++G(d,p). If the assumption (16) is correct, this difference has to be zero,

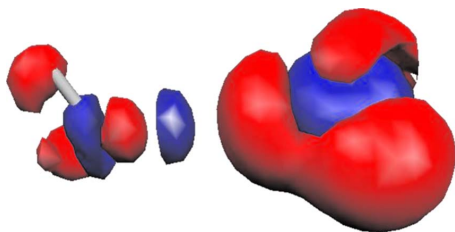


FIG. 1. (Color online) Difference of the electron densities of the neutral water dimer constructed from the self-consistent orbitals of the neutral and from the self-consistent orbitals of the cation plus the LUMO at the theoretical level of HF/6-311++G(*d,p*) according to Eq. (16). The isosurface is drawn at values of +0.003 (blue) and -0.003 (red).

but it is clearly apparent that it is not zero. In HF theory, Eq. (16) may still be a reasonable assumption due to the existence of Koopmans' theorem, which ensures in the frozen-orbital picture that the LUMO corresponds to the one-electron wave function of an attached electron. Thus, the cationic HF ground state together with the LUMO is a zeroth order approximation to the ground state of the neutral parent molecule. However, if orbital relaxation is taken into account, this equality is no longer strictly valid as demonstrated by our numerical example.

In summary, the assumption that a simple time-dependent analog of Koopmans' theorem exists [Eq. (7)] resulting in the derivation of Eq. (8) is not correct because the time-dependent change in the HOMO itself is irrelevant for the description of the time-dependent change in the hole density of the initially prepared nonstationary cation. The simple methodology proposed by Remacle and Levine is thus not a valid theory to describe the time evolution of the hole density, i.e., to describe charge migration.

Toward the end of this section, we would like to note that although our derivations have focused on HF and time-dependent HF, it is obvious that all arguments and equations can be directly transferred to KS DFT and time-dependent KS-DFT, since no assumption on the explicit form of the Fock operator has been made. Moreover, when going to DFT, further conceptual problems arise since Koopmans' theorem is valid only for the HOMO of the neutral. In particular, the LUMO of the cation does not correspond to the wave function of an additional electron but to the one of an excited electron of the cation,^{25,26} and it is thus not at all related to the initially ionized orbital of the neutral parent state. Hence, Eq. (16) is even conceptually wrong in the case of DFT with approximate xc functionals. As a consequence, the expansion of the ionized HOMO in the virtual orbitals of the cation [Eq. (8)] is not physically sound. Less conceptually and more fundamentally, when using conventional functionals, KS-DFT is corrupted by electron self-interaction^{27,28} which spoils the description of open-shell cations, in general.²⁹ This aspect will be discussed in detail later in Sec. IV.

B. Time evolution of the correlated hole density

In Sec. II A, we have restricted our discussion to the description of electronic ground states of the neutral and the

corresponding cation with a single Slater determinant, that is, to the description of the time evolution of the hole density by TDHF. Then only orbital-relaxation effects are described and electron correlation is, by definition, missing. However, the latter can be, and usually is, critically important. To capture electron correlation effects one needs to resort to *ab initio* many-body theories, which have been recently demonstrated to be feasible and very successful in this aspect.^{9,11,12} In a many-body description of the time-dependent hole density, one starts again from Eq. (9), but now the electronic densities of the neutral and cationic system are computed from many-body wave functions according to

$$\rho_n(\vec{r}) = \langle \Psi_n(\vec{r}) | \hat{\rho} | \Psi_n(\vec{r}) \rangle, \quad (17)$$

$$\rho_c(\vec{r}, t) = \langle \Psi_c(\vec{r}, t) | \hat{\rho} | \Psi_c(\vec{r}, t) \rangle, \quad (18)$$

where $\hat{\rho}$ is the density operator, $\Psi_n(\vec{r})$ is the stationary many-body wave function of the neutral, and $\Psi_c(\vec{r}, t) = e^{-i(\hat{H}-\epsilon_c)t} \Psi_c(\vec{r}, 0)$ is the propagating multielectron wavepacket of the initially created cationic state. The latter is not an eigenstate of the cation but can be described as a superposition of cationic states. These expressions can, in general, be transferred to a density matrix formulation when the density operators are represented in a one-particle basis $\{\phi_p(\vec{r})\}$ and occupation numbers $\{n_p\}$. The hole density matrix is then given as the difference between the density matrices of the neutral and cationic systems,

$$\mathbf{P}_h(t) = \mathbf{P}_n - \mathbf{P}_c(t). \quad (19)$$

The eigenvectors and eigenvalues of the hole density matrix $\mathbf{P}_h(t)$ obtained by diagonalization represent the so-called *natural charge orbitals* $\{\tilde{\phi}_p^h(\vec{r}, t)\}$ and *hole occupation numbers* $\{\tilde{n}_p^h(t)\}$. The time-dependent hole density is then obtained via⁹

$$\rho_h(\vec{r}, t) = \sum_p \tilde{n}_p^h(t) |\tilde{\phi}_p^h(\vec{r}, t)|^2. \quad (20)$$

The hole occupation numbers determine what part of the initial charge is in which natural charge orbital at a certain time t . Because of charge conservation, it is clear that $\sum_p \tilde{n}_p^h(t) = 1$ at all times. The natural charge orbitals and hole occupation numbers have proven to be very useful tools in the observation and interpretation of multielectron dynamics upon ionization (see, e.g., Refs. 9–13). This concept is closely related to the interpretation of complicated excited electronic states via *natural transition orbitals* obtained by diagonalization of the difference density matrix between ground and excited electronic states.³⁰

The accuracy of the description of the time-dependent hole density is determined by the level of theory that is employed for the computation of the many-body wave functions of neutral and cationic states in Eqs. (17) and (18). One can use any quantum chemical method to compute the neutral ground state and the required cationic states; however, it is worth to note that, in principle, all and, in practice, very many cationic states are needed calling for efficient theoretical approaches.

III. COMPUTATIONAL DETAILS

The calculations of the time-dependent hole density within the approach of Remacle and Levine, Eq. (8), are straightforward, once the neutral HOMO, as well as the cationic orbitals and orbital energies are provided by some standard quantum chemical program package. In all calculations reported here, the HF and DFT data were obtained via the GAUSSIAN03 package. Unrestricted HF and DFT schemes were used for the single-determinant cationic ground state. The standard B3LYP potential was utilized within the DFT calculations in combination with the 6-311++G(*d,p*) basis set.

For the ease of interpretation it will be useful to represent the true time-dependent hole density, Eq. (14), within orbitals and occupation numbers, e.g., in a form similar to Eq. (20). For this purpose we can rearrange Eq. (14) as follows:

$$\rho_h^{\text{true}}(\vec{r}, t) = \sum_{jj'} \phi_j^{c*}(\vec{r}) \phi_{j'}^c(\vec{r}) \left\{ c_{Nj'}^*(0) c_{Nj'}(0) + \sum_i^{N-1} c_{ij}^*(0) c_{ij'}(0) (1 - e^{(i/\hbar)(\epsilon_j - \epsilon_{j'})t}) \right\}. \quad (21)$$

Without loss of generality, one can assume that all the quantities are real, thus, the last equation becomes

$$\rho_h^{\text{true}}(\vec{r}, t) = \sum_{jj'} \phi_j^c(\vec{r}) \phi_{j'}^c(\vec{r}) \left\{ c_{Nj}(0) c_{Nj'}(0) + c_{ij}(0) c_{ij'}(0) \times \left[1 - \cos\left(\frac{\epsilon_j - \epsilon_{j'}}{\hbar} t\right) \right] \right\} = \sum_{jj'} \phi_j^c(\vec{r}) \phi_{j'}^c(\vec{r}) N_{jj'}(t), \quad (22)$$

where the matrix in braces, denoted by $N_{jj'}(t)$, is referred to as the hole density matrix. The diagonalization of that matrix for each point in time leads to the following expression for the hole density:

$$\rho_h^{\text{true}}(\vec{r}, t) = \sum_j |\tilde{\phi}_j^c(\vec{r}, t)|^2 \tilde{n}_j(t). \quad (23)$$

We will refer to $\tilde{n}_j(t)$ as the hole occupation numbers and to $\tilde{\phi}_j^c(\vec{r}, t)$ as the natural charge orbitals. By construction, at each point in time the natural charge orbitals represent different linear combinations of the time-independent cationic orbitals $\phi_j^c(\vec{r})$.

Finally, we would like to briefly sketch the large scale *ab initio* many-body computational methodology used by us for obtaining the time-dependent hole density taking electron correlation and orbital-relaxation explicitly into account. For details, the reader is referred to Refs. 9, 11, and 12. Within this methodology, the cationic Hamiltonian, represented in an effective many-body basis using Green's function method, is used for direct propagation of a cationic initial state via the Lanczos technique (see Ref. 12). The electronic wavepacket thus obtained is then utilized to construct the hole density at each point in time via Eqs. (17), (18), and (9). The hole

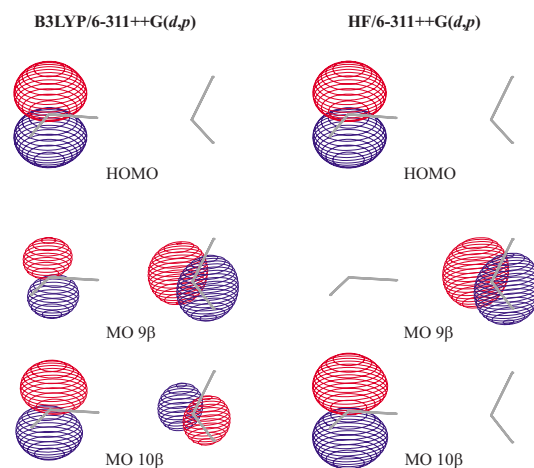


FIG. 2. (Color online) The neutral HOMO, together with the cationic HOMO (MO 9 β) and LUMO (MO 10 β) of the water dimer in its equilibrium geometry calculated via B3LYP/6-311++G(*d,p*) and HF/6-311++G(*d,p*). The picture is very similar when the water molecules are 20 Å apart (see text).

density can then be cast into a one-particle basis representation, i.e., into a superposition of time-dependent natural charge orbitals and time-dependent hole occupation numbers [Eq. (20)], in analogy with the procedure outlined above [Eqs. (22) and (23)]. The cationic Hamiltonian matrix was constructed via the ADC approach,^{15,16} in particular, via the non-Dyson ADC(3) method¹⁷ that is correct up to the third order of perturbation theory in the electron-electron interaction.

IV. RESULTS AND DISCUSSION

Let us now examine how the single-determinant approach for evaluation of the time-dependent hole density works in practice. For this purpose we have chosen a simple system, that of the water dimer, where an ultrafast migration of the positive charge created after a sudden ionization of the HOMO was recently reported by Remacle and Levine.²⁴ Their calculations at the level of DFT/B3LYP suggest that the initially created hole, localized on the proton donor water molecule, will oscillate between the two water molecules with a period of about 4 fs.

Before going any further, it is worth to analyze in some detail these calculations. The methodology used by Remacle and Levine consists in expanding the HOMO of the neutral in the molecular orbitals (MOs) of the cation and expressing the time-propagating hole orbital as a sum of the expansion coefficients multiplied by time-dependent phase factors, see Eq. (8). The modulus squared of an expansion coefficient gives the weight with which the corresponding cationic MO contributes to the time-propagating hole. In the case of the water dimer, it turns out that the initially ionized HOMO of the neutral is well represented by a linear combination of the HOMO and the LUMO of the cation, i.e., orbitals 9 β and 10 β , with weights of 0.29 and 0.71, respectively. These cationic MOs are shown on the left column in Fig. 2. It is

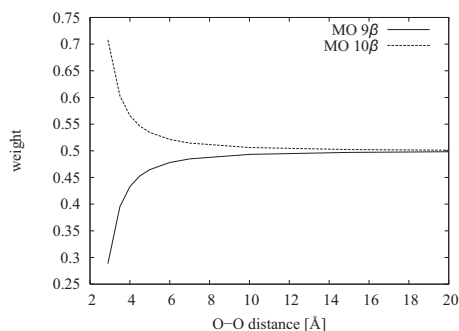


FIG. 3. The weights of the cationic HOMO (MO 9β) and LUMO (MO 10β) of the water dimer in the expansion of the neutral HOMO as a function of the intermolecular distance, defined as the distance between the oxygens. The calculations are done at B3LYP/6-311++G(d,p) level.

obvious that the orbitals are delocalized and the positive and negative linear combination out of them will produce orbitals localized on one or the other water molecule. Technically, this is exactly what leads to the charge oscillation reported by Remacle and Levine, the oscillation period being determined by the energy difference between the two cationic orbitals.

It is clear that if the two water molecules do not interact, no charge migration has to be observed. However, if one separates the two water molecules by 20 Å, the neutral HOMO is again a linear combination of the cationic MOs 9β and 10β , which are still delocalized. The weights of these two cationic MOs in the expansion of the neutral HOMO as a function of the interoxygen separation of the two water molecules are presented in Fig. 3. It is seen that increasing the intermolecular separation, the two cationic orbitals tend to contribute equally in the expansion of the neutral HOMO. Since the cationic orbitals are delocalized at each intermolecular distance, the application of the methodology proposed by Remacle and Levine leads to oscillation of the entire charge between the two water molecules even when the latter are 20 Å apart and practically do not interact. The period of oscillations in the latter case is 28.7 fs, reflecting the reduced energy splitting between MO 9β and MO 10β (0.14 eV compared to 1.05 eV at the equilibrium). However, as has been pointed out in Sec. II A, this approach for describing charge migration is not physically sound and based on an invalid assumption, since the relaxation of all occupied orbitals of the neutral determines the process.

Let us now see whether the physically correct approach and thereby accounting for the relaxation of all orbitals of the neutral that remain occupied in the cation, i.e., using Eqs. (14) and (20), will alleviate this unphysical behavior. We will start by comparing the results at equilibrium geometry. In Fig. 4 the hole occupation numbers, as defined in Eq. (23), are plotted for the equilibrium geometry of the water dimer. Again, all calculations are done at B3LYP/6-311++G(d,p) level. At $t=0$ the whole charge is in the natural charge orbital denoted by “ i ” in Fig. 4, which is localized on the proton donor water molecule and coincide at that time with the neutral HOMO. As time proceeds, the natural

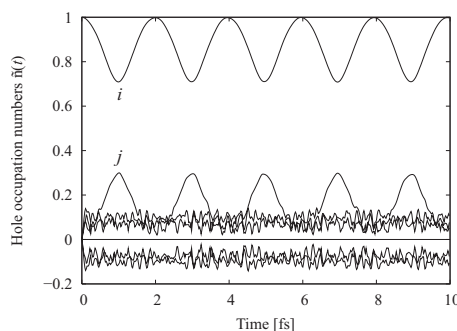


FIG. 4. Time-dependent hole occupation numbers of water dimer in its equilibrium geometry after ionization out of the HOMO obtained via Eq. (23). The charge is initially in the natural charge orbital i localized on the proton donor water molecule and as time proceeds migrates to the natural charge orbital j localized on the proton acceptor water molecule. When curves i and j face each other there is an avoided crossing and the characters of the two orbitals are swapped. The sawtoothlike curves around zero correspond to particle-hole excitations representing orbital-relaxation effects.

charge orbital i “loses” its hole charge which is transferred to the natural charge orbital denoted by “ j ” in the figure which is localized on the proton acceptor water molecule. At about 1 fs, when the minimum of the curve i faces the maximum of curve j , there is an avoided crossing and the characters of the natural charge orbitals i and j are swapped, i.e., after that point the orbital i is localized on the proton acceptor water molecule and the orbital j on the proton donor one. Thus, after about 2 fs, the whole charge has flown to the proton acceptor molecule. After that time, the process continues in reverse order and the charge migrates back to its initial position in another 2 fs. Note that each time the minima of curve i face the maxima of curve j , there are avoided crossings and the characters of the orbitals i and j are swapped. Thus, at the equilibrium geometry the correct single-determinant approach within DFT/B3LYP also predicts oscillations of the initially created hole density with a period of about 4 fs.

Furthermore, the correct single-determinant construction of the time-dependent hole density does not remove the unphysical behavior in the case when the two waters are 20 Å apart from each other—the charge again bounces between the two water molecules with a period of about 29 fs. From these results, it is clear that the single-determinant approach has a wrong asymptotic behavior and leads to an artificial charge migration when the two moieties of the system are far apart and do not interact.

Before analyzing this nonphysical behavior at large distances, it is worth to examine whether the single-determinant approach gives at least qualitatively correct results at the equilibrium. For this purpose we have calculated the electron dynamics following ionization of the HOMO orbital of the water dimer using the correlated many-body approach sketched in Secs. II B and III. The evolution of the hole occupation numbers obtained within this elaborated methodology, using the same equilibrium geometry and 6-311++G(d,p) basis set, is presented in Fig. 5. It is seen that apart

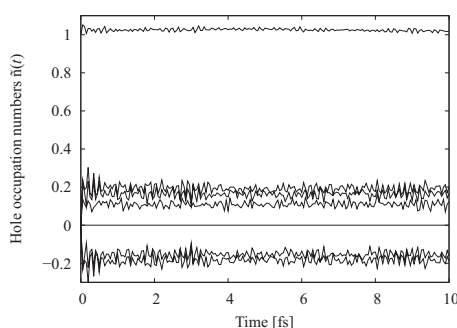


FIG. 5. Time-dependent hole occupation numbers of water dimer in its equilibrium geometry after ionization out of HOMO obtained via correlated many-body approach. The uppermost curve shows the time evolution of the initially created positive charge. The hole-particle excitations, represented by the other positive and negative occupations, describe the many-body effects present in the cation.

from the small wiggles due to the correlation effects present in the cation, the charge stays where it is initially created and no oscillations are observed.

From the above analysis we conclude that the single-determinant ansatz employing DFT methods fails in giving a physically correct description of the evolution of the electronic cloud following a sudden ionization. The natural question arises: what is the origin of the wrong physical behavior of the single-determinant approach? To answer this question it is instructive to investigate the performance of HF SCF methodology. In this case, one observes no oscillations at all at every intermolecular distance. The simple reason is that the HF calculations produce localized cationic HOMO and LUMO orbitals (see right column of Fig. 2) at any intermolecular distance, and thus the ionized neutral HF HOMO is well represented ($\approx 95\%$) by a single cationic MO, namely MO 10β .

The difference in the cationic MOs obtained via HF and KS-DFT methodologies is a result of the well-known self-interaction error of the conventional DFT schemes. Although the exact ground-state density functional is self-interaction-free, the approximate xc functionals used in practice lead to an incomplete cancellation of the electron self-interaction included in the electron-electron repulsion energy.²⁷ This serious flaw of DFT methods is especially pronounced when treating odd-electron systems. In these cases the SCF procedure tries to reduce the self-repulsion of the unpaired electron by delocalization of the orbitals.²⁹ Today, several xc functionals are available that are particularly designed to reduce self-interaction, for example, MYC3 (Ref. 31) or TPSS.^{32,33} However, employing the TPSS functional for the investigation of charge migration in the water dimer, the neutral HOMO is still a linear combination of the strongly delocalized cationic HOMO and LUMO, and one still observes artificial oscillations of the charge. For the equilibrium geometry of the water dimer these oscillations are with a period of 138 fs. The longer period of the oscillation compared to B3LYP is due to the decreased energy gap between the occupied and virtual orbitals in the TPSS calculation which appears to be only 0.03 eV. Obviously, the quality of a DFT

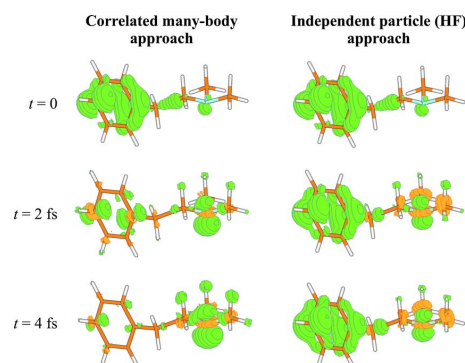


FIG. 6. (Color online) The evolution of the hole density of the molecule PENNA after ionization of the HF HOMO. The “negative” hole density or the electron density is given in orange. On the left-hand side the density calculated through a correlated many-body approach (Ref. 14); on the right-hand side the density calculated through the single-determinant approach using HF SCF methodology. Note that the molecule shown is not in its ground-state geometry (for details see Ref. 14).

description of charge migration depends heavily on the choice of the xc functional leading to results with essentially no predictive power. This drawback of the DFT methodologies makes them inappropriate for describing odd-electron cationic systems and yields spurious ultrafast charge migration following the ionization of the water dimer.

The fact that the HF methodology gives the correct physical picture in this particular case, since in the HF approach the self-interaction is exactly canceled, does not mean, however, that it is well suited for investigating electron dynamics following sudden ionization. For a proper description of such processes it is crucial to take electron correlation effects into account, which are, by definition, lacking in the HF approach. For illustration, we have calculated the electron dynamics following the ionization of the HF HOMO of the molecule 2-phenylethyl-*N,N*-dimethylamine (PENNA), see also Ref. 14. The results are shown in Fig. 6. On the left-hand side we display snapshots of the evolution of the hole density calculated through a correlated many-body approach,¹⁴ and on the right-hand side, using single-determinant approach [Eq. (14)] based on HF SCF. As seen, within the independent-particle HF picture the large amount of the charge stays where it is initially created and only a small portion of it migrates to the other end of the molecule due to orbital relaxation. On contrary, when we include correlation effects almost the entire charge migrates to the other end of the molecule within only 4 fs. This example clearly demonstrates that a proper account of the many-body effects is indispensable for the correct description of electron dynamics following ionization. Moreover, the charge migration phenomenon is *solely* due to electron correlation and orbital relaxation.⁹ That is why, when choosing the theoretical methodology to study such processes, special care has to be taken to include and treat correctly the many-body effects.

V. SUMMARY AND CONCLUSIONS

In the present paper, we have reviewed the possibility to employ single-determinant approaches for the description of

034102-8 A. I. Kuleff and A. Dreuw

J. Chem. Phys. **130**, 034102 (2009)

electron dynamics following outer-valence ionization. Our analysis shows that the time evolution of the hole density depends on the relaxation of all neutral orbitals that remain occupied in the cation, and not on the time evolution of the HOMO alone. A time-dependent analog to Koopmans' theorem does not exist.

Moreover, our numerical examples show that the conventional KS-DFT methods are inherently inapt to describe such processes due to the well-known self-interaction error. The incomplete cancellation of the self-interaction in the conventional xc functionals leads to an unphysical delocalization of the orbital of the unpaired electron and thus to spurious charge oscillations between different moieties of the ionic system even when these moieties do not interact. We would like to note that even though various schemes for construction of self-interaction-free functionals exist in the literature, single-determinant approaches based on DFT appear to be not adequate for describing electron dynamics following ionization owing to the unclear physical meaning of the KS orbitals. The correct time propagation of the hole density implies the use of exact (or reasonable approximation of) cationic electronic states as a basis rather than cationic or neutral SCF orbitals.

Therefore, also the self-interaction-free HF method is not a suitable approach for studying charge migration phenomena. Charge migration is predominantly due to electron correlation, and accounting only for the orbital relaxation does not allow for a proper description of the process. In addition, the single-determinant methods are by definition unable to describe an important class of ionic states, like the so-called satellites or shake-up states, which further reduces their applicability. Thus, our conclusion is that for a meaningful investigation of electron dynamics following ionization, the inclusion of many-body effects is indispensable.

ACKNOWLEDGMENTS

The authors thank Anthony Dutoi for valuable discussions. Financial support by the Deutsche Forschungsgemeinschaft (DFG) is gratefully acknowledged, A.D. as a DFG Emmy Noether-fellow.

¹A. M. Kuznetsov, *Charge Transfer in Physics, Chemistry and Biology: Physical Mechanisms of Elementary Processes and an Introduction to the Theory* (Gordon and Breach, Luxembourg, 1995).

²P. F. Barbara, T. J. Meyer, and M. A. Ratner, *J. Phys. Chem.* **100**, 13148 (1996).

³V. May and O. Kühn, *Charge and Energy Transfer Dynamics in Molecu-*

lar Systems (Wiley-VCH, Weinheim, 2004).

⁴M. Garavelli, P. Celani, F. Bernardi, M. A. Robb, and M. Olivucci, *J. Am. Chem. Soc.* **119**, 6891 (1997).

⁵A. Dreuw, G. A. Worth, M. Head-Gordon, and L. S. Cederbaum, *J. Phys. Chem. B* **108**, 19049 (2004).

⁶T. Schultz, E. Samoylova, W. Radloff, I. V. Hertel, A. L. Sobolewski, and W. Domcke, *Science* **306**, 1765 (2004).

⁷L. S. Cederbaum and J. Zobeley, *Chem. Phys. Lett.* **307**, 205 (1999).

⁸The sudden approximation concept used in this construction simply supposes that the ionization process is done fast enough, e.g., by a high-energy photon, such that the final state of the ionized system is described by a wavefunction where the interaction between the ionized electron and the remaining core is neglected.

⁹J. Breidbach and L. S. Cederbaum, *J. Chem. Phys.* **118**, 3983 (2003); **126**, 034101 (2007).

¹⁰H. Hennig, J. Breidbach, and L. S. Cederbaum, *J. Phys. Chem. A* **109**, 409 (2005).

¹¹H. Hennig, J. Breidbach, and L. S. Cederbaum, *J. Chem. Phys.* **122**, 134104 (2005).

¹²A. I. Kuleff, J. Breidbach, and L. S. Cederbaum, *J. Chem. Phys.* **123**, 044111 (2005).

¹³A. I. Kuleff and L. S. Cederbaum, *Chem. Phys.* **338**, 320 (2007).

¹⁴S. Lünemann, A. I. Kuleff, and L. S. Cederbaum, *Chem. Phys. Lett.* **450**, 232 (2008).

¹⁵J. Schirmer, L. S. Cederbaum, and O. Walter, *Phys. Rev. A* **28**, 1237 (1983).

¹⁶L. S. Cederbaum, in *Encyclopedia of Computational Chemistry*, edited by P. von Ragué Schleyer, P. R. Schreiner, H. F. Schaefer III, W. L. Jorgensen, W. Thiel, and R. C. Glen (Wiley, Chichester, 1998), Vol. 1, p. 1202.

¹⁷J. Schirmer, A. B. Trofimov, and G. Stelter, *J. Chem. Phys.* **109**, 4734 (1998).

¹⁸L. Lehr, T. Horneff, R. Weinkauff, and E. W. Schlag, *J. Phys. Chem. A* **109**, 8074 (2005).

¹⁹R. Weinkauff, L. Lehr, and A. Metsala, *J. Phys. Chem. A* **107**, 2787 (2003).

²⁰E. W. Schlag, S.-Y. Sheu, D.-Y. Yang, H. L. Selzle, and S. H. Lin, *Angew. Chem., Int. Ed.* **46**, 3196 (2007).

²¹F. Remacle and R. D. Levine, *J. Chem. Phys.* **110**, 5089 (1999).

²²F. Remacle and R. D. Levine, *J. Phys. Chem. A* **104**, 2341 (2000).

²³F. Remacle and R. D. Levine, *Proc. Natl. Acad. Sci. U.S.A.* **103**, 6793 (2006).

²⁴F. Remacle and R. D. Levine, *J. Chem. Phys.* **125**, 133321 (2006).

²⁵O. Gritsenko and J. E. Baerends, *J. Chem. Phys.* **121**, 655 (2004).

²⁶A. Savin, C. J. Umrigar, and X. Gonze, *Chem. Phys. Lett.* **288**, 391 (1998).

²⁷J. P. Perdew and A. Zunger, *Phys. Rev. B* **23**, 5048 (1981).

²⁸A. D. Dutoi and M. Head-Gordon, *Chem. Phys. Lett.* **422**, 230 (2006).

²⁹Y. A. Mantz, F. L. Gervasio, T. Laino, and M. Parrinello, *J. Phys. Chem. A* **111**, 105 (2007).

³⁰R. L. Martin, *J. Chem. Phys.* **118**, 4775 (2003).

³¹A. J. Cohen, P. Mori-Sánchez, and W. Yang, *J. Chem. Phys.* **126**, 191109 (2007).

³²J. Tao, J. P. Perdew, V. N. Staroverov, and G. E. Scuseria, *Phys. Rev. Lett.* **91**, 146401 (2003).

³³V. N. Staroverov, G. E. Scuseria, J. Tao, and J. P. Perdew, *J. Chem. Phys.* **119**, 12129 (2003).

THE JOURNAL OF CHEMICAL PHYSICS **130**, 154305 (2009)

Ultrafast electron dynamics following outer-valence ionization: The impact of low-lying relaxation satellite states

Siegfried Lünemann,^{a)} Alexander I. Kuleff,^{b)} and Lorenz S. Cederbaum
Theoretische Chemie, PCI, Universität Heidelberg, Im Neuenheimer Feld 229, 69120 Heidelberg, Germany

(Received 24 November 2008; accepted 12 March 2009; published online 16 April 2009)

Low-lying relaxation satellites give rise to ultrafast electron dynamics following outer-valence ionization of a molecular system. To demonstrate the impact of such satellites, the evolution of the electronic cloud after sudden removal of an electron from the highest occupied molecular orbital (HOMO) of the organic unsaturated nitroso compound 2-nitroso[1,3]oxazolo[5,4-*d*][1,3]oxazole is traced in real time and space using *ab initio* methods only. Our results show that the initially created hole charge remains stationary but on top of it the system reacts by an ultrafast π - π^* excitation followed by a cyclic excitation-de-excitation process which leads to a redistribution of the charge. The π - π^* excitation following the removal of the HOMO electron takes place on a subfemtosecond time scale and the period of the excitation-de-excitation alternations is about 1.4 fs. In real space the processes of excitation and de-excitation represent ultrafast delocalization and localization of the charge. The results are analyzed by simple two- and three-state models. © 2009 American Institute of Physics. [DOI: 10.1063/1.3112567]

I. INTRODUCTION

With the advent of the attosecond pulse techniques (see, e.g., Refs. 1 and 2 and the references therein) the scientific community obtained a powerful tool to monitor the electron dynamics in atomic and molecular systems and to study processes that take place on a time scale in which the electronic motion is still disentangled from the slower nuclear dynamics. Such kind of processes are, for example, the response of the electronic cloud to an ultrafast perturbation, such as ultrafast excitation or ionization.³⁻⁷ About ten years ago in a first work⁸ it was shown that after a sudden ionization the electronic many-body effects alone can beget rich ultrafast electron dynamics. The positive charge created after the ionization can migrate throughout the system solely driven by the electron correlation and electron relaxation.^{8,9} Since this charge migration is ultrafast, typically few femtoseconds,⁹⁻¹³ it can be calculated neglecting the nuclear motion as long as one is concerned with the relevant time interval during which this ultrafast process takes place. Clearly, at later times the nuclear dynamics will come into play and will perturb the picture. Thus, if we wish to know precisely what happens at this later stage, the nuclear motion must be considered. However, since several or even many electronic states participate, an adequate description of the nuclear motion is rather involved. It should be noted, in this respect, that very recently a time-dependent Born–Oppenheimer approximation for treating quantum mechanically coupled electron-nuclear dynamics was proposed,^{14,15} which might provide a possibility to attack such complicated problems. This becomes especially important in the light of the series of pioneering ex-

periments by Schlag, Weinkauff, and co-workers (see, e.g., Refs. 16–18 and references therein) showing site-selective reactivity of the electronically excited ionic states in oligopeptides appearing on the time scale of tens of femtoseconds.

We have studied the charge migration in different molecules⁹⁻¹³ and found that it usually takes place after ionization in the inner-valence shell where the electron correlation effects are typically much stronger than in the outer-valence shell. However, very recently we have shown that the charge migration phenomenon is not inherent only to the inner-valence ionized states but can take place also after an outer-valence ionization.¹⁹ The system studied in Ref. 19 possesses a chromophore-donor site which is initially ionized and the created hole charge migrates throughout the system to the amine-acceptor site within just 4 fs. Further analysis²⁰ then showed that the mechanism underlying this ultrafast migration is the so-called hole mixing,²¹ which is one of several ways of the manifestation of electronic many-body effects in the ionization process.²²

In the present work we want to continue the investigation of ultrafast electron dynamics following ionization of the outer-valence shell focusing on a different mechanism, namely, the so-called dominant satellite mechanism. It is known from the early days of the photoelectron spectroscopy that the correlation and relaxation effects can lead to the appearance of additional weak bands in the photoelectron spectrum, the so-called shake-up or satellite bands, which correspond to excitation processes accompanying the ionization.²³ This kind of shake-up states are typical for the inner valence and core ionization and appear in the ionization spectra of nearly every atom or molecule. However, numerous theoretical and experimental studies showed that there are certain classes of compounds where satellites can appear also in the outer-valence region. These are systems

^{a)}Electronic mail: siegfried.luenemann@pci.uni-heidelberg.de.

^{b)}Electronic mail: alexander.kuleff@pci.uni-heidelberg.de. On leave from: Institute for Nuclear Research and Nuclear Energy, BAS, 72, Tzarigradsko Chaussee Blvd., 1784 Sofia, Bulgaria.

containing heavier atoms, like transition-metal complexes,^{24,25} or π -electron systems,^{26–30} which have low-energy virtual orbitals. Here we will concentrate on the latter class of systems and will investigate the impact of the low-lying satellites on the electron dynamics following outer-valence ionization of some organic unsaturated nitroso compounds.³⁰

The paper is organized as follows. In Sec. II the theoretical background of the methodology used for calculating the ultrafast electron dynamics is briefly outlined (Sec. II A) and the different mechanisms of charge migration are briefly discussed (Sec. II B). In Sec. III we present the results of our calculations including the ionization spectrum of the molecule 2-nitroso[1,3]oxazolo[5,4-*d*][1,3]oxazole and the electron dynamics following ionization of its highest occupied molecular orbital (HOMO). Section IV is devoted to the discussion and analysis of the results obtained via simple two- and three-state models.

II. THEORETICAL BACKGROUND

A. Basic equations

In this section we briefly review the theoretical background of the methodology used to study ultrafast electron dynamics following ionization of a system. For technical details we refer the reader to Refs. 9, 11, and 13.

The starting point of our investigation is a neutral molecule in its ground state $|\Psi_0\rangle$. The ionization of the system brings it into a nonstationary state $|\Phi_i\rangle$. A convenient quantity then for tracing the succeeding electron dynamics is the density of the so created initial hole which can be defined by the following expression:

$$Q(\vec{r}, t) := \langle \Psi_0 | \hat{\rho}(\vec{r}, t) | \Psi_0 \rangle - \langle \Phi_i | \hat{\rho}(\vec{r}, t) | \Phi_i \rangle = \rho_0(\vec{r}) - \rho_i(\vec{r}, t), \quad (1)$$

where $\hat{\rho}$ is the electron density operator. The first term on the right-hand side of Eq. (1), ρ_0 , is the ground state density of the neutral system and is time independent. The second term, ρ_i , is the density of the cation and hence is time dependent since $|\Phi_i\rangle$ is not an eigenstate of the cationic system. The quantity $Q(\vec{r}, t)$, referred hereafter as the *hole density*, describes the density of the hole at position \vec{r} and time t and by construction is normalized at all times t .

In the Heisenberg picture, the time-dependent part $\rho_i(\vec{r}, t)$ reads

$$\rho_i(\vec{r}, t) = \langle \Phi_i | e^{i\hat{H}t} \hat{\rho}(\vec{r}, 0) e^{-i\hat{H}t} | \Phi_i \rangle = \langle \Phi_i(t) | \hat{\rho}(\vec{r}, 0) | \Phi_i(t) \rangle, \quad (2)$$

where $|\Phi_i(t)\rangle = e^{-i\hat{H}t} |\Phi_i\rangle$ is the propagating multielectron wavepacket.

Using the standard representation of the density operator in a one-particle basis $\varphi_p(\vec{r})$ and occupation numbers n_p , Eq. (1) can be rewritten as follows:

$$Q(\vec{r}, t) = \sum_{p,q} \varphi_p^*(\vec{r}) \varphi_q(\vec{r}) N_{pq}(t), \quad (3)$$

where the matrix $\mathbf{N}(t) = \{N_{pq}(t)\}$ with elements

$$N_{pq}(t) = \delta_{pq} n_p - \sum_{M,N} \langle \Phi_i(t) | \tilde{\Psi}_M \rangle \rho_{MN} \langle \tilde{\Psi}_N | \Phi_i(t) \rangle \quad (4)$$

is referred to as the hole density matrix. The second term of Eq. (4) is obtained by inserting in Eq. (2) a resolution of identity of a complete set of appropriate ionic eigenstates $|\tilde{\Psi}_M\rangle$ before and after the density operator $\hat{\rho}(\vec{r}, 0)$. The matrix ρ_{MN} is thus the representation of the density operator within this basis.

Diagonalization of the matrix $\mathbf{N}(t)$ for fixed time points t yields the following expression for the hole density:³¹

$$Q(\vec{r}, t) = \sum_p |\tilde{\varphi}_p(\vec{r}, t)|^2 \tilde{n}_p(t), \quad (5)$$

where $\tilde{\varphi}_p(\vec{r}, t)$ are called *natural charge orbitals* and $\tilde{n}_p(t)$ are their *hole occupation numbers*. The hole occupation number $\tilde{n}_p(t)$ contains the information about which part of the created hole charge is in the natural charge orbital $\tilde{\varphi}_p(\vec{r}, t)$ at time t . Because of the charge conservation, one finds that $\sum_p \tilde{n}_p(t) = 1$ at any time t .

For calculating the hole density and its constituents we use *ab initio* methods only. The whole calculation consists of four steps. After determining the molecular geometry, the first step is a Hartree–Fock (HF) calculation. The second step is the calculation of the relevant part of the ionization spectrum via Green’s function (GF) formalism. A computationally very successful approach to obtain the GF is the *algebraic diagrammatic construction* [ADC(*n*)] scheme.³² In the present calculation we used the non-Dyson ADC(3) method^{33,34} realized within the so-called intermediate-state representation,^{35,36} an effective many-body basis serving as $|\tilde{\Psi}_M\rangle$ introduced in Eq. (4). The third step is the propagation of the multielectron wavepacket of the ionized system¹¹ with the help of the short iterative Lanczos technique.³⁷ The fourth and last step is to build through Eq. (4) the matrix $\mathbf{N}(t)$ and to diagonalize it in order to obtain the natural charge orbitals $\tilde{\varphi}_p(\vec{r}, t)$ and the hole occupation numbers $\tilde{n}_p(t)$, see Eq. (5). With the help of these quantities we can now trace the evolution of the hole density of a system after suddenly removing one of its electrons.

At this point we would like to comment briefly on the choice of the initial state $|\Phi_i\rangle$. The above sketched methodology is independent of the particular choice and the way of preparation of the initial state as long as the ionized electron is removed from the system on a shorter time scale than that of the charge migration. The assumption made is that the initially created ionic state can be described by a separable many electron wave function, i.e., the interaction between the ionized electron and the remaining core is neglected—sudden approximation (see, e.g., Ref. 38). Within this approximation the initial hole is described by the so-called Dyson orbital, i.e., the overlap between the N -electron initial and $(N-1)$ -electron final wave functions. However, in the outer-valence region the Dyson orbitals differ very little from the canonical HF-orbitals.^{39,40} That is why, in the numerical calculations to be discussed in this paper the initial state is prepared through a sudden removal of an electron from a particular HF-orbital. The initial state can, of course, be constructed such that it corresponds to a removal of an electron

from a linear combination of HF-orbitals. This liberty allows one to reproduce the hole density of practically every particular initial vacancy. However, to avoid investigating many linear combinations of HF-orbitals of interest we concentrate on specific HF-orbitals. In this way we can unambiguously identify the basic mechanisms leading to charge migration. Since the time-dependent Schrödinger equation which governs the electron dynamics is a linear equation, these mechanisms are also operative when other choices of the initial state are used.

B. Ionic states and mechanisms of charge migration

Here we will briefly review the basic mechanisms of charge migration referring the interested reader to Ref. 9 for more details.

For proper understanding of the basic mechanisms of ultrafast charge migration following ionization it is illuminative to analyze a typical ionization spectrum. The calculated cationic spectrum consists of vertical lines, where each line represents a cationic eigenstate $|I\rangle$. The position of the line is given by the ionization energy, and its height—by the square of the transition amplitude $\langle\Phi_i|I\rangle$, a quantity related to the ionization cross section. For the ease of interpretation we will expand the exact cationic state $|I\rangle$ in a series of electronic configurations, as is traditionally done in configuration interaction (CI) calculations (see, e.g., Ref. 41),

$$|I\rangle = \sum_j c_j^{(I)} \hat{a}_j |\Psi_0\rangle + \sum_{a,k < l} c_{akl}^{(I)} \hat{a}_a^\dagger \hat{a}_k \hat{a}_l |\Psi_0\rangle + \dots, \quad (6)$$

where $|\Psi_0\rangle$ is the exact ground state of the neutral system, \hat{a} and \hat{a}^\dagger are the annihilation and creation operators, respectively, and $c^{(I)}$'s are the expansion coefficients. The indices a, b, \dots refer to unoccupied (virtual) orbitals (or particles), whereas the indices i, j, \dots indicate occupied orbitals (or holes). Throughout the whole text p, q, \dots will be used as general indices. Accordingly, the terms $\hat{a}_j |\Psi_0\rangle$ are called one-hole ($1h$) configurations since one electron has been removed from the corresponding occupied orbital, the terms $\hat{a}_a^\dagger \hat{a}_k \hat{a}_l |\Psi_0\rangle$ are referred to as two-hole-one-particle ($2h1p$) configurations, indicating that in addition to the removal of one electron another one is excited to a virtual orbital, and so forth. Note that in the spirit of the GF approach, which accounts also for the ground state correlations, in Eq. (6) the expansion is applied on the exact ground state $|\Psi_0\rangle$, rather than the uncorrelated HF one $|\Phi_0\rangle$ as in the usual CI calculations.

As was noted above, in our study the initially prepared nonstationary ionic state is created by suddenly removing an electron from a particular HF-orbital, i.e., by acting with the corresponding annihilation operator on the ground state of the neutral, $|\Phi_i\rangle = \hat{a}_i |\Psi_0\rangle$. Thus, only the $1h$ configurations contribute to the transition amplitude $\langle\Phi_i|I\rangle$, i.e., to the spectral intensity. Without correlation effects, the spectrum will consist of lines, one for every occupied orbital φ_i , with intensities equal to 1. If correlation effects are weak, the ionization spectrum will consist of *main lines* which have large overlap with the $1h$ configurations. This is typical when ionizing the outer-valence shell of a system. In this case the molecular orbital picture is still valid. If the correlation ef-

fects are stronger, beside the main line *satellite lines* will appear. The intensities of the satellite lines are weaker than those of the main lines since they correspond to cationic states that are dominated by $2h1p$ configurations and have only small or moderate overlap with the $1h$ configurations. Three types of satellites can be distinguished:²² *relaxation satellites* where at least one of the two holes in the $2h1p$ configuration is identical to the $1h$ orbital of the main line, *correlation satellites* where both holes differ from the $1h$ orbital of the main line, and *ground-state-correlation satellites* stemming from the correlation effects present in the ground state of the neutral. In the inner valence, where the correlation effects are strong, the distinction between the main lines and the satellites cease to exist and the spectrum becomes a quasicontinuum of lines with small to moderate intensities. This phenomenon is known as breakdown of the molecular orbital picture.²²

Depending on the structure of the ionic states involved, three basic mechanisms of charge migration have been identified:⁹ the hole mixing case, the dominant satellite case, and the breakdown of the molecular orbital picture case. In what follows we will briefly describe them.

- (i) Hole mixing case. For simplicity, we will consider the two-hole mixing, i.e., the situation when two lines in the spectrum correspond to ionic states which are linear combinations of two $1h$ configurations $\hat{a}_j |\Psi_0\rangle$ and $\hat{a}_k |\Psi_0\rangle$. In this idealized case, if we create the initial hole in one of the orbitals, say φ_j , then the hole will oscillate between the two orbitals φ_j and φ_k with a frequency determined by the energy difference between the two ionic states. If the two orbitals are localized on two different sites of the system, the hole mixing mechanism will lead to an oscillation of the initially created positive charge between these two sites. The hole mixing mechanism was identified as the driving force of the ultrafast charge migration following outer- and inner-valence ionizations in many different molecular systems (see, e.g., Refs. 10, 11, 19, and 20).
- (ii) Dominant satellite case. Let us consider the situation when we have two ionic states, a main state and a satellite, both having overlap with the original $1h$ configuration. In CI language these states can be written as

$$|I_m\rangle = c_1 \hat{a}_i |\Psi_0\rangle + c_2 \hat{a}_a^\dagger \hat{a}_k \hat{a}_l |\Psi_0\rangle,$$

$$|I_s\rangle = c_2 \hat{a}_i |\Psi_0\rangle - c_1 \hat{a}_a^\dagger \hat{a}_k \hat{a}_l |\Psi_0\rangle,$$

where the two coefficients c_1 and c_2 satisfy the equation $c_1^2 + c_2^2 = 1$. In this idealized case, assuming that all involved orbitals φ_i , φ_k , φ_l , and φ_a are different, i.e., the case of a correlation satellite, we will observe the following electron dynamics succeeding the ionization out of orbital φ_i . The hole initially localized on orbital φ_i will migrate to the orbital φ_k (or φ_l) accompanied by an excitation from orbital φ_l (or φ_k) to the virtual orbital φ_a . Again the dynamics will be oscillatory with a period determined by the energy differ-

154305-4 Lünemann, Kuleff, and Cederbaum

J. Chem. Phys. **130**, 154305 (2009)

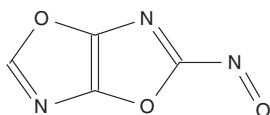
ences between the states $|I_m\rangle$ and $|I_s\rangle$. This type of mechanism was identified to be responsible for the ultrafast electron dynamics taking place after inner-valence ionization in several systems.^{11,12,42} We note at this point that there is also a dominant *relaxation* satellite mechanism which is not discussed so far and will be investigated for the first time in the present paper.

- (iii) Breakdown of the molecular orbital picture case. In the inner-valence region of the spectrum, where the quasicontinuum of lines appears, one can distinguish two general cases depending on whether the states are below or above the double ionization threshold of the system. Supposing that the quasicontinuum of states has a Lorentzian shape, in both cases the initially ionized orbital will “lose” its positive charge exponentially with time. If the states are below the double ionization threshold, the charge will be typically shared among many other orbitals and at the end of the process will be spread more or less uniformly over the whole cation. This situation was studied in Refs. 9 and 42. If the states are above the double ionization threshold, i.e., an electronic decay channel is open, this mechanism will describe the process of emission of a secondary electron. This situation was studied in Ref. 43.

In the present work we will concentrate on the dominant relaxation satellite mechanism of charge migration, and will discuss for the first time the manifestation of this mechanism after ionization of the outer-valence shell.

III. RESULTS

We applied the methodology sketched in Sec. II A to several molecules known to possess low-lying satellites in order to trace in real time and space the response of the electronic cloud of these systems to the sudden removal of an electron from their outer-valence shell. The systems studied were organic unsaturated nitroso compounds theoretically investigated by Wardermann and von Niessen.³⁰ The molecular geometries were optimized using density functional theory (DFT) methodology [BP86/SV(P)]. Throughout the remaining calculations standard DZ basis sets⁴⁴ were used. All studied molecules show very similar behavior, thus in this paper we will present only one of them, namely the molecule 2-nitroso[1,3]oxazolo[5,4-*d*][1,3]oxazole (see sketch).



The molecule is planar and belongs to the C_s symmetry point group having 29 occupied orbitals in the a' irreducible representation (irrep) and 6 occupied orbitals in the irrep a'' . The computed outer-valence ionization spectrum of the molecule is shown in Fig. 1. The calculations were performed

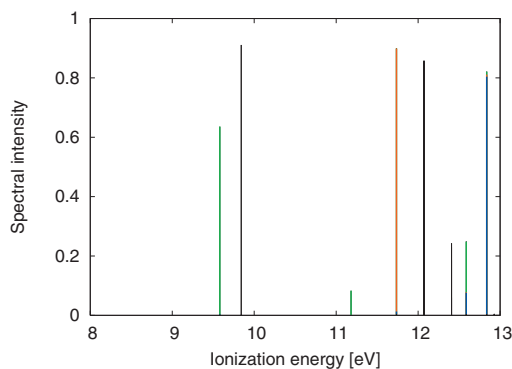


FIG. 1. (Color) Outer-valence part of the ionization spectrum of the molecule 2-nitroso[1,3]oxazolo[5,4-*d*][1,3]oxazole calculated via the non-Dyson ADC(3) GF method. Each vertical line shown is related to a final cationic state and is located at the corresponding ionization energy. The states belonging to the a' irrep are plotted in black. All other colors are related to different $1h$ -configurations resulting from the removal of an electron out of a specific HF-orbital belonging to the a' irrep.

via GF based approach, namely the non-Dyson ADC(3) method.³³ The states belonging to the a' irrep are plotted in black. All other colors are related to different $1h$ -configurations resulting from the removal of an electron out of a specific HF-orbital belonging to the a' irrep. It is seen that the main line at 9.6 eV, the satellite at 11.2 eV, and the larger contribution to the satellite at 12.6 eV come from the same $1h$ configuration, namely, the $29a'^{-1}$ configuration which is given in green in the figure. The orbital $29a'$ is the HOMO of the molecule.

Let us take a closer look at the cationic states corresponding to these three lines in the spectrum, the main line and the two satellites. The first cationic state, corresponding to the line at 9.6 eV, is constructed mainly from the $29a'^{-1}$ $1h$ configuration (63%) and from the $29a'^{-1}6a''^{-1}7a''$ $2h1p$ configuration (25%). The second state, corresponding to the satellite line at 11.2 eV, is also mainly constructed from the $29a'^{-1}$ and $29a'^{-1}6a''^{-1}7a''$ configurations but their weights are inverted compared to the first cationic state. The third state at 12.6 eV consists of 17% $29a'^{-1}$, 10% of $27a'^{-1}$, and 43% of $29a'^{-1}6a''^{-1}7a''$. In all states the missing contributions are distributed over many other $1h$ and $2h1p$ configurations.

Obviously, we encounter the situation of a main line stemming from the ionization out of the HOMO and two relaxation satellites corresponding to an excitation of an electron from HOMO-1 to the lowest unoccupied molecular orbital (LUMO). The three involved HF-orbitals (the HOMO, orbital $29a'$, the HOMO-1, orbital $6a''$, the LUMO, orbital $7a''$) are displayed in Fig. 2. It is seen that the HOMO is localized on the nitroso site (N=O site) of the molecule, while the HOMO-1 and LUMO are delocalized π orbitals.

Let us now see what happens after a sudden removal of an electron out of the HOMO. In order to analyze the electron dynamics following the ionization it is illuminating to trace the time evolution of the hole occupation numbers $\tilde{n}_p(t)$. In Fig. 3 we present the evolution of the hole occupation numbers during the first 5 fs after the ionization. The

154305-5 Ultrafast electron dynamics

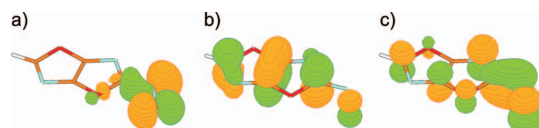
J. Chem. Phys. **130**, 154305 (2009)

FIG. 2. (Color) HF-orbitals of the molecule 2-nitroso[1,3]oxazolo[5,4-*d*][1,3]oxazole: (a) orbital $29a'$, or the HOMO; (b) orbital $6a''$, or the HOMO-1; and (c) orbital $7a''$, or the LUMO.

occupation numbers corresponding to orbitals belonging to irrep a' are shown in black, while those corresponding to orbitals belonging to a'' in red. Only five of the occupation numbers from each irrep (those who contribute the most) are shown. At the beginning of the process all occupation numbers are equal to zero except one which corresponds to the initially ionized natural charge orbital $\tilde{\varphi}_i$, indicated by i in the figure. At that time the natural charge orbital $\tilde{\varphi}_i$ has 100% overlap with the HF-orbital $29a'$. We see that apart from the very fast drop during the first 50 as, which is a universal response of a system upon sudden ionization (see Ref. 45), the initially created hole charge stays in orbital $\tilde{\varphi}_i$ throughout the whole studied period. One should keep in mind that the natural charge orbitals also change with time, but in this case the orbital $\tilde{\varphi}_i$ varies very little and at any time point has more than 95% overlap with the HF-HOMO. Thus, the positive charge practically stays where it is initially created.

However, another process takes place. We see that for approximately 0.7 fs more than 80% of another hole appears on the natural charge orbital denoted by k in Fig. 3, and in the same time more than 80% of an electron is promoted to the natural charge orbital denoted by a in the figure (note that negative hole occupation number describes a particle, i.e., an electron in a virtual orbital). The analysis shows that at all time points the natural charge orbital $\tilde{\varphi}_k$ overlaps more than 80% with HF-orbital $6a''$, while the natural charge orbital $\tilde{\varphi}_a$ overlaps more than 60% with HF-orbital $7a''$. Thus, the removal of an electron from the HF-HOMO leads to an ul-

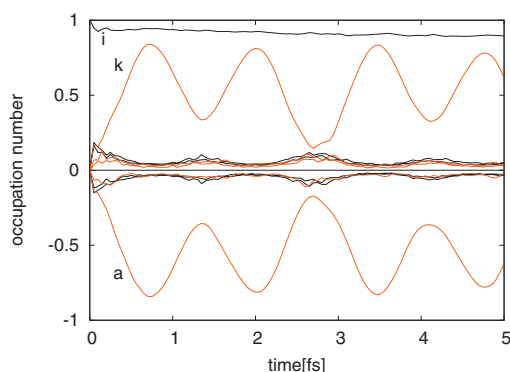


FIG. 3. (Color) Hole occupation numbers as a function of time for the first 5 fs after ionization of the HOMO (orbital $29a'$) of the molecule 2-nitroso[1,3]oxazolo[5,4-*d*][1,3]oxazole. The five most important occupation numbers of each irreducible representation are shown. At $t=0$ all occupation numbers are equal to 0 except for the one which relates to the initially ionized orbital. The negative hole occupations have to be interpreted as the corresponding fraction of an electron filling the respective virtual orbital.

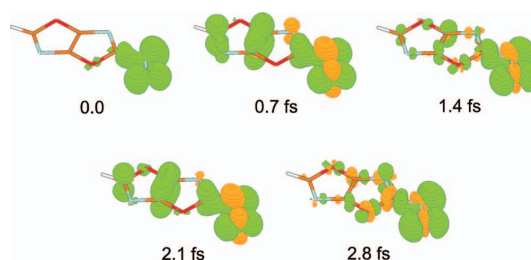


FIG. 4. (Color) Three-dimensional hole density $Q(\vec{r}, t)$ at times $t=0, 0.7, 1.4, 2.1,$ and 2.8 fs after ionization of the HOMO of 2-nitroso[1,3]oxazolo[5,4-*d*][1,3]oxazole. The negative hole density, or the electron density, is shown in orange.

trafast (less than a femtosecond) $\pi \rightarrow \pi^*$ excitation from orbital $6a''$ to orbital $7a''$. From Fig. 3 we see also that this excitation process is cyclic, i.e., one observes alternating excitations and de-excitations with two beating periods one nearly twice as long as the other.

Before analyzing in more detail the mechanism underlying this ultrafast electron dynamics, let us see how the process develops in space. For that purpose in Fig. 4 we display snapshots of the evolution of the hole density, Eq. (5), at different time points covering the time of a full oscillation cycle. The points chosen are $t=0, 0.7, 1.4, 2.1,$ and 2.8 fs, which correspond to the minima and maxima of the curves k and a in Fig. 3. We see that at $t=0$ the charge is localized on the nitroso side of the molecule (N=O group). As time proceeds a second hole starts to open at the left oxazole ring and an electron starts to appear at the nitroso group (shown in orange in Fig. 4). One has to keep in mind that, since the orbitals $6a''$ and $7a''$ are delocalized, at the places of overlap we have a mutual cancellation between the electronic and hole densities. Thus, the process represents alternating ultrafast delocalization and localization of the charge. However, due to the large number of electronic states involved these alternations are not purely repetitive. From Fig. 4 it is clear that the charge tends to delocalize more and more as time proceeds.

IV. ANALYSIS AND DISCUSSION

Here we would like to analyze in more detail the underlying mechanism of the ultrafast electron dynamics observed after sudden ionization of the HOMO of 2-nitroso[1,3]oxazolo[5,4-*d*][1,3]oxazole. The dominant satellite mechanism studied in Ref. 9 and described briefly in Sec. II B provides an understanding for the impact of a *correlation* satellite on the electron dynamics following ionization. It leads to the migration of the initially created hole charge and a simultaneous excitation on top of it. However, as we saw in the previous section, in the case of dominant *relaxation* satellite we observe only the excitation while the initially created charge remains stationary (see the red and black curves, denoted as $k, a,$ and $i,$ respectively in Fig. 3).

This behavior can be understood with the help of a simple model.

Suppose we have only two cationic states—a main state and a relaxation satellite. In CI language these states can be written as

$$|I_m\rangle = c_1|\Psi_i\rangle + c_2|\Psi_{aik}\rangle,$$

$$|I_s\rangle = c_2|\Psi_i\rangle - c_1|\Psi_{aik}\rangle,$$

where $|\Psi_i\rangle \equiv \hat{a}_i|\Psi_0\rangle$ and $|\Psi_{aik}\rangle \equiv \hat{a}_a^\dagger \hat{a}_i \hat{a}_k|\Psi_0\rangle$. After some trivial algebra (see Ref. 9) one arrives at the following analytical expression for the hole density matrix [Eq. (4)]:

$$\mathbf{N}(t) = \begin{pmatrix} 1 & 0 & 0 \\ 0 & -2(c_1c_2)^2[1 - \cos(\omega t)] & -c_1c_2(c_1^2 - c_2^2)[1 - \cos(\omega t)] \\ 0 & -c_1c_2(c_1^2 - c_2^2)[1 - \cos(\omega t)] & 2(c_1c_2)^2[1 - \cos(\omega t)] \end{pmatrix}, \quad (7)$$

where $\omega = (E_i - E_{I_m})/\hbar$.

The diagonalization of this matrix gives the time-dependent hole occupation numbers (using that $c_1^2 + c_2^2 = 1$)

$$\begin{aligned} \tilde{n}_i(t) &= 1, \\ \tilde{n}_{k/a}(t) &= \pm 2c_1c_2 \sin^2(\omega t/2). \end{aligned} \quad (8)$$

We see that indeed the initially created hole is stationary and the occupations of the two other natural charge orbitals involved in the $2h1p$ configuration oscillate such that the total charge is equal to 1 at any time.

The time evolution of the three hole occupation numbers in this model are shown in Fig. 5. In order to compare with the full calculation presented in Fig. 3, the parameters used in the model are $c_1 = \sqrt{0.7}$, $c_2 = \sqrt{0.3}$, and $\omega = 2.4 \text{ fs}^{-1}$, which corresponds to the situation realized in the studied molecule taking only the main state at 9.6 eV and the first relaxation satellite at 11.2 eV. It is seen that this simple two-state model reproduces the overall behavior of the cyclic excitation and de-excitation with a period of about 2.6 fs. The more involved beating pattern observed in Fig. 3 can be explained easily by the influence of the third state at 12.6 eV.

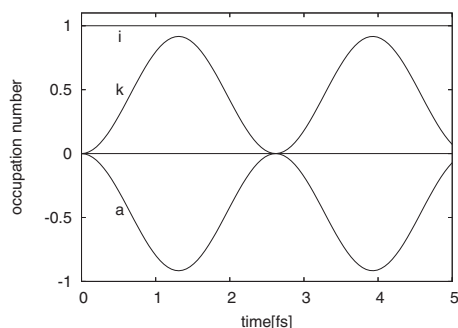


FIG. 5. Model time-dependent occupation numbers of the three natural charge orbitals (i, k, a) in the case of a dominant relaxation satellite. The initially created hole (i) remains stationary, while an excitation from the occupied orbital (k) to the virtual orbital (a) is observed. The following parameters were used in the model: $c_1 = \sqrt{0.7}$, $c_2 = \sqrt{0.3}$, and $\omega = 2.4 \text{ fs}^{-1}$ [see Eq. (8)].

It is straightforward to show that in the case of a main state and two relaxation satellites having the form

$$\begin{aligned} |I_m\rangle &= c_1^{(m)}|\Psi_i\rangle + c_2^{(m)}|\Psi_j\rangle + c_3^{(m)}|\Psi_{aik}\rangle, \\ |I_{s1}\rangle &= c_1^{(s1)}|\Psi_i\rangle + c_2^{(s1)}|\Psi_j\rangle + c_3^{(s1)}|\Psi_{aik}\rangle, \\ |I_{s2}\rangle &= c_1^{(s2)}|\Psi_i\rangle + c_2^{(s2)}|\Psi_j\rangle + c_3^{(s2)}|\Psi_{aik}\rangle, \end{aligned}$$

and supposing that $c_2^{(m)} = c_2^{(s1)} = 0$, i.e., the $1h$ configuration $|\Psi_j\rangle$ does not contribute to the main state and one of the two satellites, the hole occupation numbers describing the excitation $k \rightarrow a$ will be proportional to $[\sin^2(\omega_1 t/2) + \sin^2(\omega_2 t/2)]$, where $\omega_2 = (E_{I_{s1}} - E_{I_m})/\hbar$ and $\omega_1 = (E_{I_{s2}} - E_{I_m})/\hbar$, while the orbital j will get no occupancy, i.e., $\tilde{n}_j(t) = 0$. This is exactly the case realized in the example studied in the present paper where the $1h$ configuration $|\Psi_j\rangle$ corresponds to $27a'^{-1}$, which contributes only to the second satellite state at 12.6 eV. It is seen that this second relaxation satellite will then just introduce an additional frequency $\omega_2 = 4.6 \text{ fs}^{-1}$ corresponding to an oscillation period of about 1.4 fs and we will get the beating oscillation behavior observed in Fig. 3.

The following comment is in order. Although the relaxation satellite does not affect the dynamics of the initial hole charge itself (the initial hole remains stationary), depending on the spatial distribution of the orbitals involved the dominant relaxation satellite mechanism can lead to a charge migration via hole screening. If the electron is ejected from a localized orbital i and the unoccupied orbital a is localized in the same region of space, then promoting an electron to the orbital a will cancel out in physical space the initially created hole in orbital i , i.e., the initial hole will be “screened” by the excitation $k \rightarrow a$. Thus, in the idealized case when the orbitals i and a are localized on one site of the system, while the orbital k is localized on a different site, the dominant relaxation satellite mechanism will lead to oscillations in the real space of the total hole charge between these two parts of the system. It has to be noted that the unoccupied orbitals are often delocalized and the realization of this simple mechanism of charge migration from one site to another is not very likely in such systems. This is also seen in the example pre-

sented in this work where the process represents rather an ultrafast delocalization and localization of the charge. However, in larger and/or strongly correlated systems where many orbitals can be mixed in the ionic states, the hole-screening charge migration mechanism may be operative. We note that there do exist many systems with localized unoccupied orbitals, e.g., *para*-nitroaniline.^{46,47} Furthermore, in large systems even σ^* orbitals are likely to be located on individual moieties. In all these kinds of systems one could expect ultrafast charge migration from one part of the system to another via the hole-screening excitation mechanism.

Let us summarize. In the present work we studied the ultrafast electron dynamics following outer-valence ionization of a molecular system concentrating on the impact of low-lying relaxation satellites. For that purpose we traced the evolution of the electronic cloud after sudden removal of an electron from the HOMO of some organic unsaturated nitro compounds known to possess low-lying satellites. Our results show that in all cases the initially created hole charge remains stationary but the system reacts by an ultrafast cyclic excitation-de-excitation process, which leads to severe changes in the charge. In the presented example, the molecule 2-nitroso[1,3]oxazolo[5,4-*d*][1,3]oxazole, the π - π^* excitation following the removal of the HOMO electron takes place on a subfemtosecond time scale, the period of the excitation-de-excitation alternations being about 1.4 fs. In real space the processes of excitation and de-excitation represent ultrafast delocalization and localization of the charge. In other systems with more localized π^* or σ^* orbitals one could anticipate by the same mechanism directed ultrafast charge migration from one site to another.

At the end we would like to comment on the relation between the purely electronic phenomenon of ultrafast charge migration and the slower processes of charge transfer or charge transport which involve the nuclear dynamics. The ultrafast redistribution of the electronic cloud can, of course, influence the nuclear dynamics which will come into play at later times since at least within the Born–Oppenheimer approximation, the electronic motion governs the effective potential seen by the nuclei. We have reasons to believe^{12,20} that although the pure electron dynamics often represents an ultrafast oscillation of the charge within the molecule, the coupling to the nuclear motion at later times could lead to trapping of the charge and thus achieving irreversibility of the process, i.e., an effective transfer of the charge from one moiety of the system to another.

ACKNOWLEDGMENTS

Financial support by the DFG is gratefully acknowledged.

¹P. B. Corkum and F. Krausz, *Nat. Phys.* **3**, 381 (2007).

²G. A. Reider, *J. Phys. D* **37**, R37 (2004).

³M. Drescher, R. Kienberger, M. Uiberacker, V. Yakovlev, A. Scrinzi, Th. Westerwalbesloh, U. Kleineberg, U. Heinzmann, and F. Krausz, *Nature (London)* **419**, 803 (2002).

⁴F. Remacle, M. Nest, and R. D. Levine, *Phys. Rev. Lett.* **99**, 183902

(2007).

⁵M. Nest, F. Remacle, and R. D. Levine, *New J. Phys.* **10**, 025019 (2008).

⁶A. D. Bandrauk and S. Barmaki, *Chem. Phys.* **350**, 175 (2008).

⁷X. Xie, M. Wickenhauser, W. Boutu, H. Merdji, P. Salières, and A. Scrinzi, *Phys. Rev. A* **76**, 023426 (2007).

⁸L. S. Cederbaum and J. Zobeley, *Chem. Phys. Lett.* **307**, 205 (1999).

⁹J. Breidbach and L. S. Cederbaum, *J. Chem. Phys.* **118**, 3983 (2003).

¹⁰H. Hennig, J. Breidbach, and L. S. Cederbaum, *J. Phys. Chem. A* **109**, 409 (2005).

¹¹A. I. Kuleff, J. Breidbach, and L. S. Cederbaum, *J. Chem. Phys.* **123**, 044111 (2005).

¹²A. I. Kuleff and L. S. Cederbaum, *Chem. Phys.* **338**, 320 (2007).

¹³J. Breidbach and L. S. Cederbaum, *J. Chem. Phys.* **126**, 034101 (2007).

¹⁴L. S. Cederbaum, *J. Chem. Phys.* **128**, 124101 (2008).

¹⁵J. Miller, *Phys. Today* **61**(5), 15 (2008).

¹⁶R. Weinkauff, P. Aicher, G. Wesley, J. Grotemeyer, and E. W. Schlag, *J. Phys. Chem.* **98**, 8381 (1994).

¹⁷R. Weinkauff, E. W. Schlag, T. J. Martinez, and R. D. Levine, *J. Phys. Chem. A* **101**, 7702 (1997).

¹⁸E. W. Schlag, S.-Y. Sheu, D.-Y. Yang, H. L. Selzle, and S. H. Lin, *Angew. Chem., Int. Ed.* **46**, 3196 (2007).

¹⁹S. Lünemann, A. I. Kuleff, and L. S. Cederbaum, *Chem. Phys. Lett.* **450**, 232 (2008).

²⁰S. Lünemann, A. I. Kuleff, and L. S. Cederbaum, *J. Chem. Phys.* **129**, 104305 (2008).

²¹W. von Niessen, G. Bieri, J. Schirmer, and L. S. Cederbaum, *Chem. Phys.* **65**, 157 (1982).

²²L. S. Cederbaum, W. Domcke, J. Schirmer, and W. von Niessen, *Adv. Chem. Phys.* **65**, 115 (1986).

²³K. Siegbahn, *Rev. Mod. Phys.* **54**, 709 (1982).

²⁴W. von Niessen and L. S. Cederbaum, *Mol. Phys.* **43**, 897 (1981).

²⁵D. Moncrieff, I. H. Hillier, V. R. Saunders, and W. von Niessen, *Mol. Phys.* **24**, 4247 (1985).

²⁶S. Masuda, M. Aoyama, K. Ohno, and Y. Harada, *Phys. Rev. Lett.* **65**, 3257 (1990).

²⁷H.-G. Weikert and L. S. Cederbaum, *Chem. Phys. Lett.* **237**, 1 (1995).

²⁸M. S. Deleuze, M. G. Giuffreda, J.-P. François, and L. S. Cederbaum, *J. Chem. Phys.* **112**, 5325 (2000).

²⁹M. Ehara, M. Nakata, and H. Nakatsuji, *Mol. Phys.* **104**, 971 (2006).

³⁰W. Wardermann and W. von Niessen, *Chem. Phys.* **159**, 11 (1992).

³¹Note that since we want to obtain real natural charge orbitals, only the diagonalization of the real part of the matrix $\mathbf{N}(t)$ is needed. The natural choice to use real orbitals enforces cancellation of the imaginary part of the matrix $\mathbf{N}(t)$.

³²J. Schirmer, L. S. Cederbaum, and O. Walter, *Phys. Rev. A* **28**, 1237 (1983).

³³J. Schirmer, A. B. Trofimov, and G. Stelter, *J. Chem. Phys.* **109**, 4734 (1998).

³⁴A. B. Trofimov and J. Schirmer, *J. Chem. Phys.* **123**, 144115 (2005).

³⁵F. Mertins and J. Schirmer, *Phys. Rev. A* **53**, 2140 (1996).

³⁶J. Schirmer, *Phys. Rev. A* **43**, 4647 (1991).

³⁷C. Leforestier, R. H. Bisseling, C. Cerjan, M. D. Feit, R. Friesner, A. Gulberg, A. Hammerich, G. Jolicard, W. Karrlein, H.-D. Meyer, N. Lipkin, O. Roncero, and R. Kosloff, *J. Comput. Phys.* **94**, 59 (1991).

³⁸B. T. Pickup, *Chem. Phys.* **19**, 193 (1977).

³⁹R. J. F. Nicholson, I. E. McCarthy, and W. Weyrich, *J. Phys. B* **32**, 3873 (1999).

⁴⁰C. E. Brion, G. Cooper, Y. Zheng, I. V. Litvinyuk, and I. E. McCarthy, *Chem. Phys.* **270**, 13 (2001).

⁴¹A. Szabo and N. S. Ostlund, *Modern Quantum Chemistry* (McGraw-Hill, New York, 1989).

⁴²H. Hennig, J. Breidbach, and L. S. Cederbaum, *J. Chem. Phys.* **122**, 134104 (2005); **122**, 249901(E) (2005).

⁴³A. I. Kuleff and L. S. Cederbaum, *Phys. Rev. Lett.* **98**, 083201 (2007).

⁴⁴T. H. Dunning, *J. Chem. Phys.* **53**, 2823 (1970).

⁴⁵J. Breidbach and L. S. Cederbaum, *Phys. Rev. Lett.* **94**, 033901 (2005).

⁴⁶W. Domcke, L. S. Cederbaum, J. Schirmer, and W. von Niessen, *Chem. Phys.* **39**, 149 (1979).

⁴⁷A. C. O. Guerra, G. B. Ferreira, S. P. Machado, and C. C. Turci, *Int. J. Quantum Chem.* **108**, 2340 (2008).

Ultrafast Charge Migration Following Valence Ionization of 4-Methylphenol: Jumping over the Aromatic Ring[†]

Alexander I. Kuleff,^{*,‡} Siegfried Lünemann, and Lorenz S. Cederbaum

Theoretische Chemie, PCI, Universität Heidelberg, Im Neuenheimer Feld 229, 69120 Heidelberg, Germany

Received: February 9, 2010; Revised Manuscript Received: April 20, 2010

Electronic many-body effects alone can be responsible for the migration of a positive charge created upon ionization in molecular systems. Here, we report an ultrafast charge migration taking place after valence ionization of the molecule 4-methylphenol. The results obtained by a fully ab initio methodology show that the positive charge localized initially on the methyl group can migrate to the hydroxyl group in less than 2 fs jumping over the whole aromatic ring.

I. Introduction

The rapid development during the past decade of very intense light sources with an extreme short pulse duration opened a new era in the study of matter. With the availability of attosecond laser pulses, the scientific community obtained a powerful tool to monitor the electron dynamics in atomic and molecular systems and to study processes that take place on a time scale in which the electronic motion is still disentangled from the slower nuclear dynamics (for recent reviews see, e.g., refs 1 and 2). Thus, the response of the electronic cloud to an ultrafast perturbation, like ultrafast excitation or ionization, can now be monitored and analyzed. First steps in this direction were already undertaken: Drescher et al. have traced the evolution of a decaying ionic state after core ionization of Kr atom,³ whereas Smirnova et al. monitored the ultrafast electron dynamics after outer-valence ionization of CO₂ molecule.^{4,5} In both cases, an attosecond precision was achieved.

About ten years ago in a first work,⁶ it was shown that after a sudden ionization the electronic many-body effects alone can beget rich electron dynamics. The positive charge created after the ionization can migrate throughout the system solely driven by the electron correlation and electron relaxation.^{6,7} This charge migration is ultrafast, typically a few femtoseconds,^{7–13} and, thus, it can be described neglecting the nuclear motion, as long as one is concerned with the relevant time interval during which this ultrafast process takes place. That is why we refer to this process as charge migration in order to distinguish it from the conventional charge transfer where the nuclear dynamics play the role of the mediator for the transportation of the charge through space making the process much slower.

We have studied the charge migration in various molecules and found that this phenomenon can take place both after inner-^{7–11} and after outer-valence^{12–14} ionization. In most of the studied cases, the molecules possessed a chain-like structure and it was observed that the created positive charge can jump over one or even few C–C or C–N bonds. In this respect it is important to know whether the charge migration phenomenon is inherent only to chain-like molecules. In the present paper we report an ultrafast charge migration in the molecule 4-methylphenol where the hole charge jumps over the whole

aromatic ring showing that the “bridge” between the two sites involved in the migration process does not need to possess a chain-like structure.

The paper is organized as follows. In section II, the theoretical background of the methodology used for calculating the ultrafast electron dynamics following ionization is briefly outlined. In section III, we present the results of our calculations including the ionization spectrum of the molecule 4-methylphenol and the electron dynamics following ionization out of one of its inner-valence molecular orbitals. We summarize and conclude in section IV.

II. Theoretical Background

In this section we briefly review the theoretical background of the methodology used to study ultrafast electron dynamics following ionization of a system. For technical details we refer the reader to refs 7, 9, and 11.

The starting point of our investigation is a neutral molecule in its ground state $|\Psi_0\rangle$. The ionization of the system brings it into a nonstationary state $|\Phi_i\rangle$. A convenient quantity then for tracing the succeeding electron dynamics is the density of the so created initial hole which can be defined by the following expression:

$$Q(\vec{r}, t) := \langle \Psi_0 | \hat{\rho}(\vec{r}, t) | \Psi_0 \rangle - \langle \Phi_i | \hat{\rho}(\vec{r}, t) | \Phi_i \rangle = \rho_0(\vec{r}) - \rho_i(\vec{r}, t) \quad (1)$$

where $\hat{\rho}$ is the electron density operator. The first term on the right-hand side of eq 1, ρ_0 , is the ground state density of the neutral system, and hence, it is time-independent. The second term, ρ_i , is the density of the cation which is time dependent, since $|\Phi_i\rangle$ is not an eigenstate of the cationic system. The quantity $Q(\vec{r}, t)$, referred hereafter as the hole density, describes the density of the hole at position \vec{r} and time t and by construction is normalized at all times t .

In the Heisenberg picture, the time-dependent part $\rho_i(\vec{r}, t)$ reads

$$\rho_i(\vec{r}, t) = \langle \Phi_i | e^{i\hat{H}t} \hat{\rho}(\vec{r}, 0) e^{-i\hat{H}t} | \Phi_i \rangle = \langle \Phi_i(t) | \hat{\rho}(\vec{r}, 0) | \Phi_i(t) \rangle \quad (2)$$

where $|\Phi_i(t)\rangle = e^{-i\hat{H}t} |\Phi_i\rangle$ is the propagating multielectron wavepacket.

[†] Part of the “Klaus Ruedenberg Festschrift”.

* Corresponding author. E-mail: alexander.kuleff@pci.uni-heidelberg.de.

[‡] On leave from: Institute for Nuclear Research and Nuclear Energy, BAS, 72, Tzarigradsko Chaussee Blvd., 1784 Sofia, Bulgaria.

Ultrafast Charge Migration

Using the standard second quantization representation of the density operator in one particle basis $\varphi_p(\vec{r})$ and occupation numbers n_p , eq 1 can be rewritten as follows:

$$Q(\vec{r}, t) = \sum_{p,q} \varphi_p^*(\vec{r}) \varphi_q(\vec{r}) N_{pq}(t) \quad (3)$$

where the matrix $\mathbf{N}(t) = \{N_{pq}(t)\}$ with elements

$$N_{pq}(t) = \delta_{pq} n_p - \sum_{M,N} \langle \Phi_M(t) | \tilde{\Psi}_M \rangle \rho_{MN}^{pq} \langle \tilde{\Psi}_N | \Phi_i(t) \rangle \quad (4)$$

is referred to as the hole density matrix. The second term of eq 4 is obtained by inserting in eq 2 a resolution of identity of a complete set of appropriate ionic eigenstates $|\tilde{\Psi}_M\rangle$ before and after the density operator $\hat{\rho}(\vec{r}, 0)$. The matrix ρ_{MN}^{pq} is thus the representation of the density operator in its second quantization form within this basis, $\rho_{MN}^{pq} = \langle \tilde{\Psi}_M | \hat{\rho} | \tilde{\Psi}_N \rangle$.

Diagonalization of the matrix $\mathbf{N}(t)$ for fixed time points t yields the following expression for the hole density:¹⁵

$$Q(\vec{r}, t) = \sum_p |\tilde{\varphi}_p(\vec{r}, t)|^2 \tilde{n}_p(t) \quad (5)$$

where $\tilde{\varphi}_p(\vec{r}, t)$ are called natural charge orbitals, and $\tilde{n}_p(t)$ are their hole occupation numbers. The hole occupation number $\tilde{n}_p(t)$ contains the information on which part of the created hole charge is in the natural charge orbital $\tilde{\varphi}_p(\vec{r}, t)$ at time t . Because of the charge conservation, one finds that $\sum_p \tilde{n}_p(t) = 1$ at any time t .

For calculating the hole density and its constituents we use ab initio methods only. The one-particle basis introduced in eq 3 is obtained via a standard Hartree–Fock (HF) calculation. This step also provides the orbital energies and the two-electron integrals which are used to construct the many-electron cationic Hamiltonian within Green’s function formalism by the use of the algebraic diagrammatic construction [ADC(n)] scheme.¹⁶ In the present calculation, we use the non-Dyson ADC(3) method^{17,18} realized within the so-called intermediate-state representation,^{19,20} an effective many-body basis serving as $|\tilde{\Psi}_M\rangle$ introduced in eq 4. The propagation of the multielectron wavepacket of the ionized system⁹ is done with the help of the short iterative Lanczos technique.²¹ At the end, the matrix $\mathbf{N}(t)$, eq 4, is built and diagonalized in order to obtain the natural charge orbitals $\tilde{\varphi}_p(\vec{r}, t)$ and the hole occupation numbers $\tilde{n}_p(t)$, see eq 5. With the help of these quantities we can now trace the evolution of the hole density of a system after suddenly removing one of its electrons.

At this point we would like to comment on the choice of the initial state $|\Phi_i\rangle$. The above sketched methodology is independent of the particular choice and the way of preparation of the initial state as long as the ionized electron is removed from the system on a shorter time scale than that of the charge migration. The assumption made is that the initially created ionic state can be described by a separable many-electron wave function, i.e. the interaction between the ionized electron and the remaining ionic core is neglected. This assumption is also an important part of the so-called sudden approximation (see, e.g., ref 23), where the ionization of a system is described as a sudden removal of one of its electrons. With the available ultrashort pulses nowadays, the realization of an ionization where the use of the sudden approximation is justified is conceivable. Within

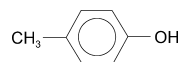
J. Phys. Chem. A, Vol. 114, No. 33, 2010 **8677**

this approximation the initial cationic state is thus constructed by acting with the corresponding annihilation operator on the neutral ground state, i.e., $|\Phi_i\rangle = \tilde{a}_i |\Psi_0\rangle$. The annihilation operator \tilde{a}_i destroys an electron from a particular molecular orbital k . The molecular orbitals can be a result of any one-particle theory. However, the Hartree–Fock approximation provides the best one-particle theory to describe the ionization, since the many-body corrections to the ionization energies begin to contribute at a higher order of perturbation theory than with other choices of approximations.²² Consequently, the initial hole is described favorably by a HF orbital.

If the ionization populates only a single cationic state then the initial hole is represented by the so-called Dyson orbital, given by the overlap between the N -electron initial and $(N - 1)$ -electron final wave functions. When the electronic many-body effects are weak, which is typically the case in the outer-valence region, the Dyson orbitals differ very little from the canonical HF orbitals.^{24,25} In the cases when the many-body effects are strong, the Dyson orbitals represent linear combinations of HF orbitals. Depending on the particular experimental conditions, e.g., the energy and temporal profiles of the ionizing pulse, the initial state can be a superposition of few ionic states, i.e. the initial hole can be a superposition of few Dyson orbitals (see, e.g., refs 4 and 5), or, equivalently, of a few HF orbitals.²⁶ However, in order to avoid investigating many linear combinations of HF-orbitals of interest, in the numerical calculations to be discussed in this paper the initial state is prepared through a sudden removal of an electron from a particular HF orbital. In this way, we can unambiguously identify the basic mechanisms leading to charge migration. Since the time-dependent Schrödinger equation which governs the electron dynamics is a linear equation, these mechanisms are also operative when other choices of the initial state are used.

III. Results

We applied the methodology outlined in section II to the molecule $(\text{CH}_3)\text{C}_6\text{H}_4(\text{OH})$, known as 4-methylphenol or *p*-cresol (see the sketch). The system is often used as a molecular model of more complex aromatic amino acids as tyrosine.²⁷



The molecular geometry of 4-methylphenol was optimized on the HF level with standard DZP basis sets²⁸ (the same basis sets were used throughout all calculations presented). The equilibrium geometry obtained is in a very good agreement with the experimentally determined one.²⁹ The molecule belongs to the C_s symmetry point group having 24 occupied orbitals in the a' irreducible representation (irrep) and 5 occupied orbitals in the irrep a'' .

The computed valence ionization spectrum of the molecule is shown in Figure 1. The calculations were performed via Green’s functions based approach, namely the non-Dyson ADC(3) method.¹⁷ Each line in the calculated spectrum represents an eigenstate of the cation. The position of the line is given by the corresponding ionization energy, whereas the height represents the spectral intensity (related to the ionization cross section, see ref 26). The calculated spectrum is in a good agreement with a previously reported experimental data obtained by photoelectron spectroscopy.³⁰

Let us now take a closer look at the two cationic states located at 13 and 14.1 eV, respectively. The analysis of these states

8678 *J. Phys. Chem. A, Vol. 114, No. 33, 2010*

Kuleff et al.

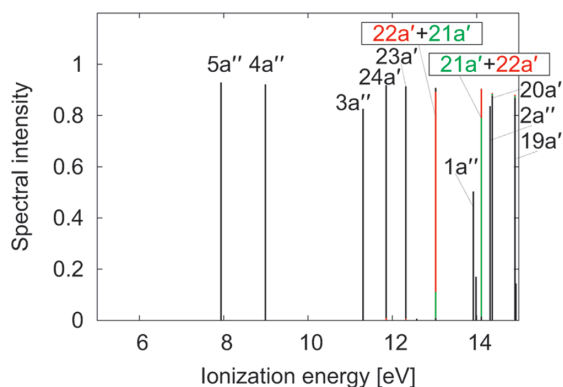


Figure 1. Valence part of the ionization spectrum of the molecule 4-methylphenol calculated via the non-Dyson ADC(3) Green's function method. Each vertical line shown corresponds to a final cationic state and is located at the respective ionization energy. The colors represent the contributions of the one-hole configurations to the corresponding states: the removal of an electron out of orbitals $21a'$ is shown in green and that out of $22a'$ in red. The assignment of the states is also given.

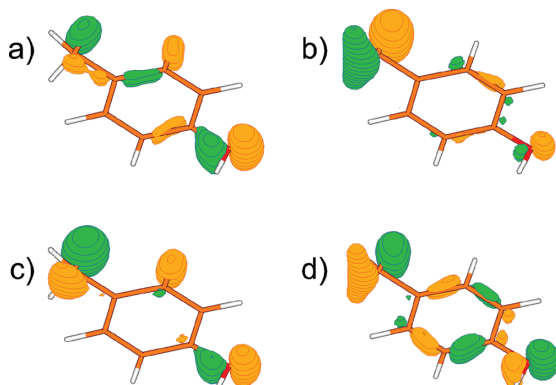


Figure 2. Hartree-Fock and Dyson orbitals of the molecule 4-methylphenol: (a) HF orbital $21a'$, (b) HF orbital $22a'$, (c) Dyson orbital corresponding to creation of the ionic state at 14.1 eV (see Figure 1), and (d) Dyson orbital corresponding to creation of the ionic state at 13 eV (see Figure 1). The methyl and hydroxyl groups are located in the upper-left and lower-right ends of the molecule sketches, respectively.

shows that they are built mainly from two one-hole (1h) configurations: one that corresponds to the removal of an electron from orbital $21a'$ and one that corresponds to the removal of an electron from orbital $22a'$. In Figure 1 the contributions of these 1h configurations are depicted in green and red, respectively. Thus, we encounter the situation known as hole mixing³¹ where two (or more) lines in the spectrum are linear combinations of two (or more) 1h configurations. This means that, if we prepare an initial state by taking out an electron from orbital $22a'$, we will create a state which can be represented as a linear combination of the two states at 13 and 14.1 eV, with a much bigger overlap with the state at 13 eV.

Before analyzing the electron dynamics following preparation of such an initial state it is illuminating to see how the two orbitals participating in the hole mixing, i.e., orbitals $21a'$ and $22a'$, look like. In Figure 2 [panels a and b] the two orbitals are depicted using different colors for the opposite signs. We see that the orbital $22a'$ is mainly localized on the methyl group

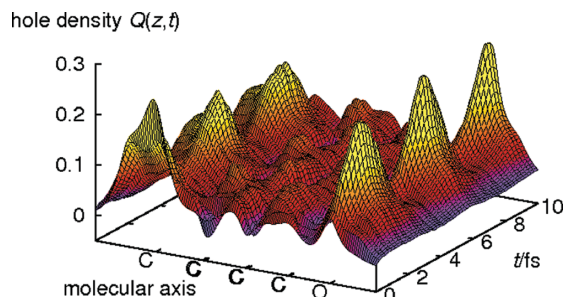


Figure 3. Hole density $Q(z, t)$ along the molecular axis as a function of time for the molecule 4-methylphenol. Nearly the whole charge, initially located at the CH_3 group, migrates back and forth between the CH_3 and OH groups with a period of less than 4 fs. Note that the charge jumps over the whole aromatic ring.

while the orbital $21a'$ is rather delocalized with its main contributions located at the hydroxyl and methyl groups. For completeness the Dyson orbitals corresponding to the cationic states at 14.1 and 13 eV are shown in panels c and d of Figure 2, respectively. It is seen that due to the many-body effects the Dyson orbitals differ from the HF ones being clearly more delocalized. If the ionization is performed with a very short pulse, which, as we will see shortly, is a necessary prerequisite for observing the ultrafast electron dynamics we are discussing in the present paper, several cationic states will be populated and the initial hole created will be a linear combination of several Dyson orbitals. In other words, several ionization channels can interfere resulting in a localization of the initial hole on different parts of the molecule, e.g., on the methyl group. This is exactly the situation realized in the recent study of the electron dynamics following outer-valence ionization of CO_2 reported in refs 4 and 5. In our case, a constructive interference between the ionization channels at 13 and 14.1 eV will create an initial state in which the hole looks exactly like the HF orbital shown in Figure 2b (orbital $22a'$). Therefore, the practical realization of the situation where the initial hole is represented by a single orbital is conceivable.

Let us now see how the system reacts upon a sudden removal of an electron out of orbital $22a'$. For visualizing this response we have calculated the hole density $Q(\vec{r}, t)$, eq 5. In Figure 3 the quantity $Q(z, t)$ is plotted, which is obtained from $Q(\vec{r}, t)$ after integration over the two remaining perpendicular axes. The axis z is chosen to pass through the longest spatial extension of the molecule and is denoted as "molecular axis". The relative positions of the atoms along this axis are indicated. At time 0 the charge is localized mainly on the methyl group. After only about 2 fs nearly the whole charge has already migrated to the hydroxyl group, located on the opposite side of the aromatic ring. During the next 2 fs the charge returns mainly to its initial position and the whole process starts again. However, since many ionic states participate in the dynamics, the process is not purely repetitive. For more clarity, in Figure 4 we show cuts through the 3D presentation at different times up to 4 fs for which time the charge makes an entire cycle migrating from methyl to hydroxyl group and back.

Note also that in the course of its migration from the CH_3 to the OH group the charge does not flow throughout the molecule (the charge density on the benzene ring stays small) but rather jumps from side to side without showing up in between. This behavior is a typical signature of the many-body character of the underlying charge migration mechanism, namely the hole-mixing mechanism. Here two single hole configurations are

Ultrafast Charge Migration

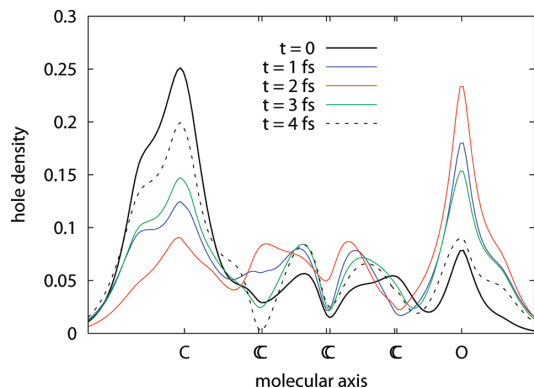


Figure 4. Cuts through the hole density $Q(z, t)$ shown in Figure 3 at times 0, 1, 2, 3, and 4 fs.

indirectly coupled to each other by interacting directly to a common set of two-hole-one-particle configurations, describing excitations on top of ionizations (for more detailed analysis of the hole mixing mechanism see ref 14). This indirect coupling is responsible for the quantum beating behavior of the hole density.

IV. Summary and Conclusions

In the present work, we studied the ultrafast electron dynamics following inner-valence ionization of the molecule 4-methylphenol. For that purpose we traced the evolution of the electronic cloud after sudden removal of an electron from an inner-valence orbital localized on the methyl group. Our results show that the charge localized on the methyl group migrates over the whole aromatic ring to reach the hydroxyl group in only 2 fs. Most importantly, the migration is *not* proceeding along the molecule: the hole charge which disappears from the methyl site appears on the hydroxyl site without showing up in between these two sites. This behavior is a typical signature of the many-body character of the underlying charge migration mechanism. Moreover, this phenomenon is entirely due to the many-body effects (electronic correlation and electronic relaxation). It can be easily shown analytically⁷ that without taking into account electron correlation and electron relaxation the charge will stay at its initial position.

In the end we would like to comment on the relation between the purely electronic phenomenon of ultrafast charge migration and the slower processes of charge transfer or charge transport which involve the nuclear dynamics. The ultrafast redistribution of the electronic cloud can, of course, influence the nuclear dynamics which will come into play at later times, since, at least within the Born–Oppenheimer approximation, the electronic motion governs the effective potential seen by the nuclei. We have reasons to believe^{10,14} that, although the pure electron dynamics often represent an ultrafast oscillation of the charge within the molecule, the coupling to the nuclear motion at later

J. Phys. Chem. A, Vol. 114, No. 33, 2010 **8679**

times could lead to trapping of the charge and thus achieving irreversibility of the process, i.e., an effective transfer of the charge from one part of the system to another.

We hope that our results will inspire future theoretical and experimental studies on the fascinating subject of ultrafast charge migration.

Acknowledgment. Financial support by the DFG is gratefully acknowledged.

References and Notes

- (1) Krausz, F.; Ivanov, M. *Rev. Mod. Phys.* **2009**, *81*, 163.
- (2) Nisoli, M.; Sansone, G. *Prog. Quantum Electron.* **2009**, *33*, 17.
- (3) Drescher, M.; Kienberger, R.; Uiberacker, M.; Yakovlev, V.; Scrinzi, A.; Westerwalbesloh, Th.; Kleineberg, U.; Heinzmann, U.; Krausz, F. *Nature* **2002**, *419*, 803.
- (4) Smirnova, O.; Mairesse, Y.; Patchkovskii, S.; Dudovich, N.; Villeneuve, D.; Corkum, P.; Ivanov, M. Yu. *Nature* **2009**, *460*, 972.
- (5) Smirnova, O.; Patchkovskii, S.; Mairesse, Y.; Dudovich, N.; Ivanov, M. Yu. *Proc. Natl. Acad. Sci. U.S.A.* **2009**, *106*, 16556.
- (6) Cederbaum, L. S.; Zobeley, J. *Chem. Phys. Lett.* **1999**, *307*, 205.
- (7) Breidbach, J.; Cederbaum, L. S. *J. Chem. Phys.* **2003**, *118*, 3983.
- (8) Hennig, H.; Breidbach, J.; Cederbaum, L. S. *J. Phys. Chem. A* **2005**, *109*, 409.
- (9) Kuleff, A. I.; Breidbach, J.; Cederbaum, L. S. *J. Chem. Phys.* **2005**, *123*, 044111.
- (10) Kuleff, A. I.; Cederbaum, L. S. *Chem. Phys.* **2007**, *338*, 320.
- (11) Breidbach, J.; Cederbaum, L. S. *J. Chem. Phys.* **2007**, *126*, 34101.
- (12) Lünemann, S.; Kuleff, A. I.; Cederbaum, L. S. *Chem. Phys. Lett.* **2008**, *450*, 232.
- (13) Lünemann, S.; Kuleff, A. I.; Cederbaum, L. S. *J. Chem. Phys.* **2009**, *130*, 154305.
- (14) Lünemann, S.; Kuleff, A. I.; Cederbaum, L. S. *J. Chem. Phys.* **2008**, *129*, 104305.
- (15) Note that, since we want to obtain real natural charge orbitals, only the diagonalization of the real part of the matrix $N(t)$ is needed. The natural choice to use real orbitals enforces cancellation of the imaginary part of the matrix $N(t)$.
- (16) Schirmer, J.; Cederbaum, L. S.; Walter, O. *Phys. Rev. A* **1983**, *28*, 1237.
- (17) Schirmer, J.; Trofimov, A. B.; Stelter, G. *J. Chem. Phys.* **1998**, *109*, 4734.
- (18) Trofimov, A. B.; Schirmer, J. *J. Chem. Phys.* **2005**, *123*, 144115.
- (19) Mertins, F.; Schirmer, J. *Phys. Rev. A* **1996**, *53*, 2140.
- (20) Schirmer, J. *Phys. Rev. A* **1991**, *43*, 4647.
- (21) Leforestier, C.; Bisseling, R. H.; Cerjan, C.; Feit, M. D.; Friesner, R.; Gulberg, A.; Hammerich, A.; Jolicard, G.; Karrlein, W.; Meyer, H.-D.; Lipkin, N.; Roncero, O.; Kosloff, R. *J. Comp. Phys.* **1991**, *94*, 59.
- (22) Szabo, A.; Ostlund, N. S. *Modern Quantum Chemistry*; McGraw-Hill: New York, 1989.
- (23) Pickup, B. T. *Chem. Phys.* **1977**, *19*, 193.
- (24) Nicholson, R. J. F.; McCarthy, I. E.; Weyrich, W. *J. Phys. B* **1999**, *32*, 3873.
- (25) Brion, C. E.; Cooper, G.; Zheng, Y.; Litvinyuk, I. V.; McCarthy, I. E. *Chem. Phys.* **2001**, *270*, 13.
- (26) Cederbaum, L. S.; Domcke, W. *Adv. Chem. Phys.* **1977**, *36*, 205.
- (27) Arp, Z.; Autrey, D.; Laane, J.; Overman, S. A.; Thomas, G. J. *Biochemistry* **2001**, *40*, 2522.
- (28) Dunning, T. H.; Hay, P. J. In *Methods of electronic structure theory*; Schaefer, H. F., III, Ed.; Plenum Press: New York, 1977; Vol. 2.
- (29) Myszkiewicz, G.; Meerts, W. L. *J. Chem. Phys.* **2005**, *123*, 044304.
- (30) Palmer, M. H.; Moyes, W.; Speirs, M.; Ridyard, J. N. A. *J. Mol. Struct.* **1979**, *52*, 293.
- (31) von Niessen, W.; Bieri, G.; Schirmer, J.; Cederbaum, L. S. *Chem. Phys.* **1982**, *65*, 157.

JP101256N

Radiation Generated by the Ultrafast Migration of a Positive Charge Following the Ionization of a Molecular System

Alexander I. Kuleff^{1,2,*} and Lorenz S. Cederbaum^{1,2}

¹*Theoretische Chemie, Universität Heidelberg, Im Neuenheimer Feld 229, 69120 Heidelberg, Germany*

²*Kavli Institute for Theoretical Physics, University of California, Santa Barbara, California 93106-4030, USA*

(Received 23 November 2010; published 31 January 2011)

Electronic many-body effects alone can be the driving force for an ultrafast migration of a positive charge created upon ionization of molecular systems. Here we show that this purely electronic phenomenon generates a characteristic IR radiation. The situation when the initial ionic wave packet is produced by a sudden removal of an electron is also studied. It is shown that in this case a much stronger UV emission is generated. This emission appears as an ultrafast response of the remaining electrons to the perturbation caused by the sudden ionization and as such is a universal phenomenon to be expected in every multielectron system.

DOI: 10.1103/PhysRevLett.106.053001

PACS numbers: 33.20.-t, 42.65.Re, 82.39.Jn

If a multielectron system is ionized, a question of fundamental importance is, how do the remaining electrons react? How does the created hole change its form and position as time proceeds due to the interaction with the remaining electrons, and, of course, what is the time scale of these changes? More than 10 years ago it was shown [1] that after ionizing a molecule the many-body effects alone can beget rich ultrafast electron dynamics such that the hole created upon ionization can migrate throughout the system on the time scale of only few femtoseconds. Since the mediator of the process is the electron correlation and the electron relaxation, in order to distinguish it from the nuclear-dynamics-driven charge transfer, this phenomenon was termed charge migration. The charge migration after ionization of the valence shell has been theoretically studied in different molecules [2–5]. In some specific, but not rare, cases the hole initially created on one end of the molecule was found to oscillate to the other one and back within just a few femtoseconds. Being usually much faster than the nuclear motion, the charge migration following ionization can thus be computed neglecting the nuclear dynamics, as long as one is interested in what happens within the time interval during which this ultrafast process takes place. Clearly, at later times the coupling to the nuclear dynamics will start to play a role and it has to be considered. However, before the nuclear dynamics start to perturb the picture, the charge migration represents a charge oscillating throughout the molecule and, thus, the molecule itself can be seen as an oscillating dipole. It is well known that an oscillating dipole emits radiation. The natural question is then, what is the emitted radiation and how strong is it?

In this Letter we show that the charge migration phenomenon generates a characteristic infrared (IR) radiation and compute the spectrum of this emission. In addition, we study the fundamental question of what will happen if the ionization is performed extremely fast and obtain surprising

results. We would like to note here that although it might appear academic, approaching the limit of sudden ionization is conceivable in view of the rapid development of the attosecond laser pulse techniques (see, e.g., Refs. [6,7]).

The total power of the radiation emitted by a moving charge as a function of time can be calculated via the well-known Larmor formula (see, e.g., Ref. [8]), which in atomic units reads

$$P(t) = \frac{2}{3c^3} |\ddot{\vec{D}}(t)|^2, \quad (1)$$

where $\ddot{\vec{D}}(t)$ is the second time derivative of the dipole moment

$$\vec{D}(t) = \langle \Psi(t) | \hat{D} | \Psi(t) \rangle \quad (2)$$

and c is the speed of light. The spectrum of the emitted radiation can be obtained by substituting in Eq. (1) $\ddot{\vec{D}}(t)$ by its Fourier transform.

Let us take a realistic showcase example, the molecule 3-methylen-4-penten-*N,N*-dimethylamine (MePeNNA), for which we showed in a recent work that after an outer-valence ionization a strong charge migration takes place [5]. Our many-body calculations showed that the outer-valence part of the ionization spectrum of the molecule consists of two ionic states, one at about 7.9 eV and one at about 8.4 eV (see Ref. [5] and Fig. 3 below). These two states can be simultaneously populated via a laser pulse with photon energy centered between the two states and a bandwidth sufficient to embrace both of them. Since the states are about 0.5 eV apart, one needs a pulse with duration of about 1 fsec, ideally even shorter. Subfemtosecond pulses are already available (see, e.g. [9]), and, thus, a simultaneous population of the two states is experimentally achievable. Of course, if the two ionization channels are open, they will interfere. A similar situation was realized experimentally and discussed in

Refs. [10,11]. Our calculations showed [5] (see also Fig. 3 below) that, due to the many-body effects, each of the two ionic states is a strong mixture of two one-hole (1h) configurations, $(\text{HOMO})^{-1}$ and $(\text{HOMO} - 1)^{-1}$ (here the superscript “-1” denotes that the corresponding molecular orbital has one fewer electron). The highest occupied molecular orbital (HOMO) of MePeNNA is localized on the chromophore moiety of the molecule, while the $\text{HOMO} - 1$ on the N terminal (see Fig. 1). A constructive interference between the two ionization channels will lead to a localization of the initial hole on the chromophore, while a destructive one will lead to a localization of the charge on the N terminal. Let us take the ionic state prepared by the constructive interference, i.e., a hole localized on the chromophore, and see what will be the succeeding electron dynamics. Such an initial state can be prepared, e.g., by an intense positively chirped broadband laser pulse [12] or by a π pulse. For computing the charge migration we use elaborated many-body *ab initio* methods only. A detailed description of the methodology is given elsewhere [2,4].

The hole density of the molecule MePeNNA after creating the initial hole on the chromophore is shown in Fig. 1. The hole density is given by the difference between the electronic densities of the system before and after the ionization [1,2]. It is clearly seen that immediately after the ionization the hole starts to oscillate between the “left” and the “right” moiety of the system with a period of about 7.5 fsec. These oscillations will be gradually distorted by the coupling to the nuclear degrees of freedom. The slower nuclear dynamics will eventually trap the charge on one of the two sites. However, the nuclear dynamics time scale is such that the hole will have time to perform a few, nearly perfect oscillations before the nuclear motion will distort

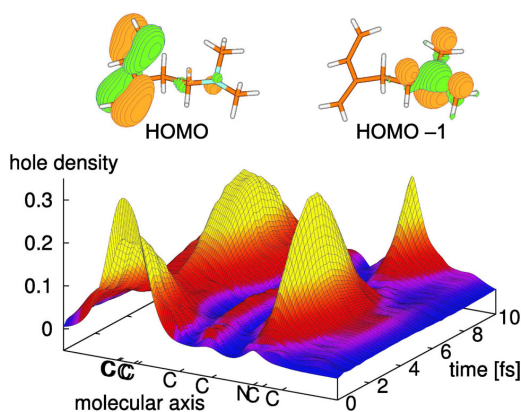


FIG. 1 (color online). Hole density along the molecular axis of the molecule MePeNNA as a function of time after a localized ionization of the chromophore. The molecular axis is chosen to pass through the longest spatial extension of the molecule. The Hartree-Fock HOMO and $\text{HOMO} - 1$ of the molecule are also shown.

the picture. Thus, within the first few periods this charge migration process will represent an oscillating dipole.

In order to compute the time-dependent dipole moment of the cationic MePeNNA after the ionizing pulse is over, one can use the following, in principle exact, expansion of Eq. (2):

$$\vec{D}(t) = \sum_{I,J} x_I^* \langle I | \hat{D} | J \rangle x_J e^{-i\omega_{IJ}t}, \quad (3)$$

where $|I\rangle$ is a complete set of cationic eigenstates, $x_I = \langle I | \Phi_i \rangle$ is the transition amplitude with respect to the initially prepared nonstationary cationic state $|\Phi_i\rangle$, and $\omega_{IJ} = E_J - E_I$ is the difference between the corresponding cationic eigenenergies. If the parameters of the ionizing pulse are chosen as discussed above, only the first two states will be populated and will give a nonzero contribution to the expansion (3). The components of the time-dependent dipole moment computed via Eq. (3) are shown in the upper panel of Fig. 2. By taking the second time derivative of the dipole moment and Fourier transforming it, one obtains the spectrum of the emission generated by the oscillating charge shown in the lower panel of Fig. 2.

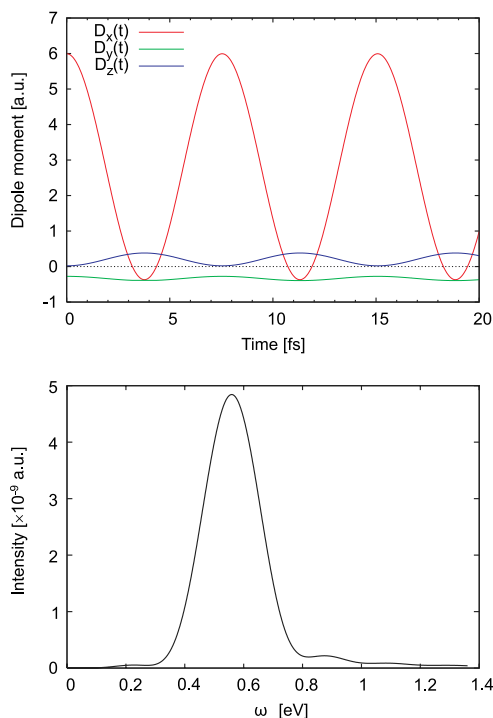


FIG. 2 (color online). Components of the time-dependent dipole moment (upper panel) and the emission spectrum (lower panel) generated by the charge migration process initiated by a localized ionization of the chromophore site of the molecule MePeNNA.

We see that the spectrum consists of a single peak at about 0.55 eV corresponding to the oscillation period of 7.5 fsec. This emission is probably measurable. The total energy emitted during 10 fsec radiation from a single molecule is $\sim 2.3 \times 10^{-9}$ eV. For density of $\sim 10^{18}$ molecules/cm³, a typical density used in high-harmonic generation gas chambers [13], and interaction volume of $\sim 10^{-7}$ cm³ [13], the charge migration will generate ~ 115 IR photons. Not long ago, the IR emission caused by the charge separation step of the phototransduction process of bacteriorhodopsin was successfully measured [14]. We would like to note that since the charge migration generates a characteristic radiation, the experimental observation of such an emission will be a direct proof for existence of the phenomenon of charge migration.

Let us now discuss the situation when the ionization is performed extremely fast, ideally infinitely fast. Of course, one cannot in practice remove an electron suddenly in the literal sense, but we have to note that attosecond laser pulses are already available and maybe in the not-so-distant future one will be able to approach this limit also experimentally in the following sense. It will suffice that the electron is removed such that during the process of ionization the other electrons do not have time to react. The time needed for the other electrons to respond to a sudden creation of a hole is about 50 asec [15] (see also Ref. [16]). It was shown [15] that this time is universal, i.e., it does not depend on the particular system, and as such appears as the time scale of the electron correlation. Thus, in practice, sudden ionization is equivalent to ionization performed faster than the electron correlation. If the ionization is performed faster than the electron correlation, one may assume that the electron is removed from a single molecular orbital, being a result of an independent particle model. The Hartree-Fock (HF) approximation provides the best independent particle theory to describe the ionization since the many-body corrections to the ionization energies begin to contribute at a higher order of perturbation theory than with other choices of approximations [17]. That is why we may assume that the initial hole created upon sudden ionization is described favorably by a HF orbital. On the other hand, if the sudden ionization has to be performed with a laser pulse, it has to be extremely short, ideally shorter than 50 asec. We would like to note that isolated pulses with duration of about 80 asec are already available [18]. Such pulse will have a very broad band allowing the population of a large number of ionic states of the system. Thus, many ionic states $|I\rangle$ will contribute to the expansion (3). In addition, with such pulses one will probably not be able to address a particular HF orbital. In principle, all valence HF orbitals will participate, and one will have to know how to separate the signal coming from the ionization out of the desired orbital.

Let us assume, for the moment, that one can remove an electron from a particular HF orbital and see what will happen. As an example we will take again the molecule

MePeNNA and will remove an electron from its HOMO, which, as we discussed above, is localized on the chromophore (see Fig. 1). The ionization spectrum of the molecule, calculated via Green's function methodology [19], is shown in Fig. 3. The $(\text{HOMO})^{-1}$ contributions to the ionic states are shown in dark gray (red) in the figure. We see that apart from the two states already discussed above, the configuration $(\text{HOMO})^{-1}$ contributes also to a large number of ionic states spread over a large energy range (see the inset of Fig. 3). Thus, a sudden removal of an electron from the HF HOMO will create a superposition of a large number of ionic states weighted by the corresponding transition matrix elements. The time-dependent dipole moment created by such initial wave packet is shown in the upper panel of Fig. 4.

We see that apart from the strong oscillation with a period of about 7.5 fsec, the components of the dipole moment show small wiggles on a time scale of only few tens of attoseconds. These, of course, come from the coupling between states separated by tens of eV. Although small, these variations of the dipole moment generate a strong emission in the UV range. This can be clearly seen in the lower panel of Fig. 4, where the emission generated by the charge migration following sudden ionization of the HF HOMO of the molecule is shown. We see that the spectrum spreads up to about 50 eV with the most intense emission in the range 10–25 eV. The intensity of this UV emission is 2 orders of magnitude stronger than the IR radiation produced by the 7.5 fsec oscillations of the charge between the two ends of the molecule. The latter is shown in the inset of the lower panel of Fig. 4 together with the emission produced by the initial state constructed as a superposition of the two lowest in energy states, as discussed above and shown in Fig. 2. Interestingly, the white noise generated by the contribution of a large number of ionic states

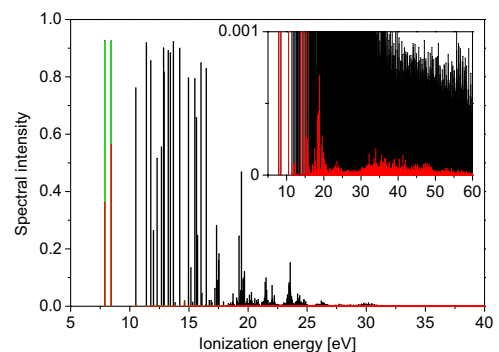


FIG. 3 (color online). Ionization spectrum of the molecule MePeNNA computed using the *ab initio* many-body Green's function method. The contributions of the 1h configuration $(\text{HOMO})^{-1}$ to the cationic states is given in dark gray (red). The contribution of the $(\text{HOMO} - 1)^{-1}$ configuration in the first two ionic states is shown in light gray (green). The inset is a zoom of the same plot.

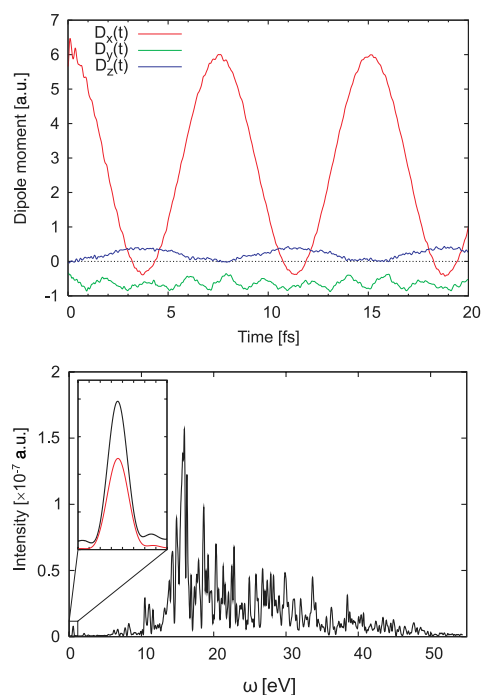


FIG. 4 (color online). Components of the time-dependent dipole moment (upper panel) and the emission spectrum (lower panel) after sudden removal of an electron from the HF HOMO of the molecule MePeNNA. Comparison with the emission spectrum reported in Fig. 2 is shown in the inset.

introducing a superposition of a large number of different frequencies gives rise to a substantial increase of the IR emission produced by the 7.5 fsec charge oscillation.

We have to emphasize that the UV emission generated by the attosecond variations of the hole charge is not inherent only to the cases when a strong charge migration within the molecule is observed. These variations appear as a result of the electronic correlation present in the cation and as such will accompany any sudden ionization of a many-electron system, irrespective of the succeeding dynamics. Removing an electron from each valence HF orbital will lead to an emission in the UV range similar to the one shown in Fig. 4. Thus, exposing the system to an ultrashort pulse will generate an UV emission which will be a superposition of the emission spectra coming from the ionization of each individual HF orbital.

In conclusion, we demonstrated that the purely electronic phenomenon of ultrafast charge migration following ionization of a molecular system generates a characteristic radiation. Since the charge migration typically represents charge oscillations with a few femtoseconds period, the generated emission is in the IR range. Encouraged by the successful measurement of the emission produced by the nuclear-dynamics-driven charge transfer in

bacteriorhodopsin [14], we believe that the emission generated by a purely electron-correlation-driven charge migration could be measurable. That is why we advocate here experimental efforts in this direction. Because of the fact that the charge migration produces a characteristic radiation, the observation of such IR emission would be a direct experimental proof for the charge migration phenomenon. We also studied the situation when the initial ionic wave packet is produced by a sudden removal of an electron and found out that in this case a much stronger UV emission is generated. Moreover, this emission appears as an ultrafast response of the remaining electrons to the perturbation caused by the sudden ionization and as such is a universal phenomenon to be expected in every multielectron system irrespective of the succeeding electron dynamics.

We hope that our results will trigger future experimental studies on the fascinating subject of ultrafast charge migration and ultrafast ionization.

The authors thank André Bandrauk for enlightening discussions. This research was supported in part by the National Science Foundation under Grant No. NSF PHY05-51164 and by the DFG.

*alexander.kuleff@pci.uni-heidelberg.de

- [1] L. S. Cederbaum and J. Zobeley, *Chem. Phys. Lett.* **307**, 205 (1999).
- [2] J. Breidbach and L. S. Cederbaum, *J. Chem. Phys.* **118**, 3983 (2003).
- [3] H. Hennig, J. Breidbach, and L. S. Cederbaum, *J. Phys. Chem. A* **109**, 409 (2005).
- [4] A. I. Kuleff, J. Breidbach, and L. S. Cederbaum, *J. Chem. Phys.* **123**, 044111 (2005).
- [5] S. Lünemann, A. I. Kuleff, and L. S. Cederbaum, *J. Chem. Phys.* **129**, 104305 (2008).
- [6] F. Krausz and M. Ivanov, *Rev. Mod. Phys.* **81**, 163 (2009).
- [7] M. Nisoli and G. Sansone, *Prog. Quantum Electron.* **33**, 17 (2009).
- [8] J. D. Jackson, *Classical Electrodynamics* (Wiley, New York, 1999), 3rd ed.
- [9] G. Sansone *et al.*, *Science* **314**, 443 (2006).
- [10] O. Smirnova *et al.*, *Nature (London)* **460**, 972 (2009).
- [11] O. Smirnova *et al.*, *Proc. Natl. Acad. Sci. U.S.A.* **106**, 16 556 (2009).
- [12] J. Cao, C. J. Bardeen, and K. R. Wilson, *Phys. Rev. Lett.* **80**, 1406 (1998).
- [13] B. Shan, A. Cavalieri, and Z. Chang, *Appl. Phys. B* **74**, S23 (2002).
- [14] G. I. Groma *et al.*, *Proc. Natl. Acad. Sci. U.S.A.* **101**, 7971 (2004).
- [15] J. Breidbach and L. S. Cederbaum, *Phys. Rev. Lett.* **94**, 033901 (2005).
- [16] A. I. Kuleff and L. S. Cederbaum, *Phys. Rev. Lett.* **98**, 083201 (2007).
- [17] A. Szabo and N. S. Ostlund, *Modern Quantum Chemistry* (McGraw-Hill, New York, 1989).
- [18] E. Goulielmakis *et al.*, *Science* **320**, 1614 (2008).
- [19] J. Schirmer, A. B. Trofimov, and G. Stelter, *J. Chem. Phys.* **109**, 4734 (1998).



Contents lists available at SciVerse ScienceDirect

Chemical Physics

journal homepage: www.elsevier.com/locate/chemphys

Ultrafast reorganization of the hole charge created upon outer-valence ionization of porphyrins

Alexander I. Kuleff*, Siegfried Lünemann, Lorenz S. Cederbaum

Theoretische Chemie, PCI, Universität Heidelberg, Im Neuenheimer Feld 229, 69120 Heidelberg, Germany

ARTICLE INFO

Article history:
Available online xxx

Keywords:
Porphyrins
Ionization spectra
Ultrafast electron dynamics
Charge migration

ABSTRACT

Based on elaborated *ab initio* calculations we first study the ionization spectra of the free-base porphyrin (H2-P) and Mg(II) porphyrin (Mg-P). Then we investigate the ultrafast electron dynamics following outer-valence ionization of these systems which constitutes the highlight of this paper. It is shown that the electron correlation effects are very strong in these systems giving rise to pronounced shake-down satellites in the outer-valence part of the ionization spectra. We show that due to these strong correlation effects the removal of an electron from the $3b_{1g}$ orbital of H2-P and Mg-P leads to an ultrafast reorganization of the electronic cloud. After being initially localized on the B and D pyrrole rings, the hole charge created upon ionization spreads throughout the molecule in only few femtoseconds. In both systems the electron dynamics triggered by the ionization represent alternating ultrafast delocalizations and localizations of the charge. The results may also give a hint on the nuclear dynamics in the free-base and Mg(II) porphyrin radical cations that will follow the ultrafast charge migration.

© 2011 Elsevier B.V. All rights reserved.

1. Introduction

Porphyrins play an important role in a large variety of biological and chemical processes. They are one of the key structures in photosynthesis, oxygen transport, or charge transfer, to name only a few. Although when performing their functions the porphyrins are embedded in protein matrices, these protein scaffolds typically have very slight effect on their electron binding energies. That is why the electronic structure of isolated porphyrins and metalloporphyrins have been a subject of intensive research, both theoretical and experimental, over the past decades [1–14]. Of particular importance are the cation radicals of porphyrin-type molecules, known to be involved, for example, in the chemistry of the photosynthetic reaction center, explaining the efforts to compute or measure the ionization spectra of such kind of species.

In order to study the reactivity of the cationic porphyrin radicals, it is crucial to know how does the positive charge created upon ionization distribute throughout the molecular backbone. Usually this analysis is done using a single-particle picture assuming that the charge density can be obtained from the molecular orbital from which the electron has been removed. More than ten years ago, it was shown [15] that removing an electron from a molecular orbital can trigger ultrafast electron dynamics. Due to the many-body effects of electron correlation and relaxation, the created positive charge can migrate throughout the system

on a time scale of only few femtoseconds [16–22]. This ultrafast redistribution of the electronic cloud can, of course, influence the nuclear dynamics which will come into play at later times, since, at least within the Born–Oppenheimer approximation, the electronic motion governs the effective potential seen by the nuclei. To draw conclusions on the reorganization of the molecular structure and, from there, on the reactivity of the cationic system, it is thus of high importance to study this initial step of electron dynamics that follows the ionization.

In this paper we study fully *ab initio* the electron dynamics during the first few femtoseconds after outer-valence ionization of free-base porphyrin (H2-P) and Mg(II) porphyrin (Mg-P), see the sketch in Fig. 1. The outer-valence part of the ionization spectra of these system is also reported and analyzed.

The paper is organized as follows. In the next section we briefly present the computational methods used to compute the ionization spectra of the studied species and the electron dynamics triggered by ionization. The results are presented and discussed in Section 3. We summarize and conclude in Section 4.

2. Computational methods

2.1. Calculation of the ionization spectra

For computing the ionization spectra of the studied species we utilize a Green's functions formalism. A big advantage of the Green's function approach, compared to the much more frequently used wave function based methods, is that it provides the entire

* Corresponding author.
E-mail address: alexander.kuleff@pci.uni-heidelberg.de (A.I. Kuleff).

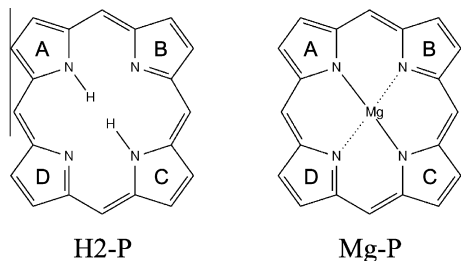


Fig. 1. Free-base porphyrin (H2-P) and Mg(II) porphyrin (Mg-P) structures and ring labeling.

ionization spectrum in a single run. Considering an N -electron system with a ground state $|\Psi_0^N\rangle$ and energy E_0^N , the one-particle Green's function in spectral representation can be expressed as [23]

$$G_{pq}(\omega) = \sum_n \frac{\langle \Psi_0^N | \hat{a}_p | \Psi_n^{N+1} \rangle \langle \Psi_n^{N+1} | \hat{a}_q^\dagger | \Psi_0^N \rangle}{\omega - (E_n^{N+1} - E_0) + i\eta} + \sum_n \frac{\langle \Psi_0^N | \hat{a}_q^\dagger | \Psi_n^{N-1} \rangle \langle \Psi_n^{N-1} | \hat{a}_p | \Psi_0^N \rangle}{\omega - (E_n^{N-1} - E_0) - i\eta}, \quad (1)$$

where $|\Psi_n^{N\pm 1}\rangle$ are complete sets of $(N \pm 1)$ -particle eigenstates with $E_n^{N\pm 1}$ being the corresponding eigenenergies, \hat{a}_p and \hat{a}_q^\dagger are the annihilation and creation operators, respectively, and η is a positive infinitesimal required to define the Fourier transformation between time and energy representations of the Green's function. Obviously, the first part of the Green's function describes the system with one extra electron, or the electron affinity, while the second term describes the system with one electron less, or the ionization.

Most of the methods for computing the Green's function rely on solving the so-called Dyson equation:

$$\mathbf{G}(\omega) = \mathbf{G}^0(\omega) + \mathbf{G}^0(\omega)\Sigma(\omega)\mathbf{G}(\omega), \quad (2)$$

relating $\mathbf{G}(\omega)$ with the so-called self energy $\Sigma(\omega)$ and free Green's function $\mathbf{G}^0(\omega)$.

The self energy can be divided in two parts:

$$\Sigma(\omega) = \Sigma(\infty) + \mathbf{M}(\omega), \quad (3)$$

where $\Sigma(\infty)$ is the static (energy independent) part and $\mathbf{M}(\omega)$ is the dynamic (energy depending) part.

The calculations reported in the present work were performed using the algebraic diagrammatic construction (ADC) approach [24]. More specifically we used the non-Dyson ADC(3) method [25], being exact up to the third order of perturbation theory. As the name suggests, the Green's function is not obtained directly via the solution of the Dyson equation, Eq. (2). This scheme rather uses the so-called *intermediate state representation* (ISR) [26,27] of the secular matrix, allowing the construction of a complete many-electron basis through a successive Gram–Schmidt orthogonalization of different classes of correlated excitations.

Two important features of this approach should be pointed out. First, contrary to the Dyson scheme, where the configuration space comprises of both $(N - 1)$ - and $(N + 1)$ -electron configurations, in the non-Dyson ADC one has a complete decoupling of the affinity and ionization blocks yielding, among others, a substantial reduction of the problem dimension. We note that a reduction of similar magnitude can also be obtained within the Dyson ADC approach if one wishes to restrict oneself to the $(N - 1)$ -electron space [28]. Second, and more importantly, the non-Dyson scheme is realized within a complete multielectron basis (the ISR basis) which makes it possible to calculate different physical properties [29], because

we can represent their operators in the ISR basis. These two advantages of the approach are especially important for computing the electron dynamics following ionization of the system, since they give the possibility to use direct propagation techniques [17].

In the Dyson, as well as in the non-Dyson, ADC hierarchy the static part of the self energy, $\Sigma(\infty)$, appears for the first time in third order. It accounts for the modification of the Hartree–Fock static exchange potential due to the ground-state electron correlation. In the cases when the ground-state correlation effects are weak, this term has a small contribution to the ionization energies and states. Its contribution to the ionization energies rarely exceeds few tenths of an eV [30,31]. Nevertheless, the computation of $\Sigma(\infty)$ represents a major numerical bottleneck of the approach. In view of the size of the systems treated in the present study, we did not include the static self energy in the calculation, which should result in a small but unknown shift of the cationic energies.

For the ease of interpretation of the results presented below, it is useful to formally represent the exact cationic state $|I\rangle \equiv |\Psi_n^{N-1}\rangle$ as an expansion in a series of electronic configurations, as this is traditionally done in configuration interaction (CI) calculations (see, e.g. Ref. [32]):

$$|I\rangle = \sum_j c_j^{(I)} \hat{a}_j | \Psi_0 \rangle + \sum_{a,k,l} c_{akl}^{(I)} \hat{a}_a^\dagger \hat{a}_k \hat{a}_l | \Psi_0 \rangle + \dots \quad (4)$$

In Eq. (4) $|\Psi_0\rangle$ is the exact ground state of the neutral system and $c^{(I)}$'s are the expansion coefficients. The indices a, b, \dots refer to unoccupied (virtual) orbitals (or particles), whereas the indices i, j, \dots indicate occupied orbitals (or holes). Throughout the whole text p, q, \dots will be used as general indices. Accordingly, the terms $\hat{a}_j | \Psi_0 \rangle$ are called one-hole (1h) configurations, since one electron has been removed from the corresponding occupied orbital, the terms $\hat{a}_i^\dagger \hat{a}_k \hat{a}_l | \Psi_0 \rangle$ are referred to as two-hole-one-particle (2h1p) configurations, indicating that in addition to the removal of one electron another one is excited to a virtual orbital, and so forth. Note that in the ADC approach used, which accounts also for the ground-state correlations, in Eq. (4) the expansion is applied on the exact ground state $|\Psi_0\rangle$, rather than on the uncorrelated Hartree–Fock one $|\Phi_0\rangle$ as in usual CI calculations.

The analysis in terms of configurations that the representation (4) of the cationic state allows is very useful for the proper understanding of the electron dynamics that follow the ionization of the system under study.

2.2. The calculation of the electron dynamics

Since we want to trace the electron dynamics triggered by the removal of an electron from a particular molecular orbital, it is convenient to construct and analyze the time-dependent hole density. This quantity can be defined by the following expression:

$$Q(\mathbf{r}, t) := \langle \Psi_0 | \hat{\rho}(\mathbf{r}, t) | \Psi_0 \rangle - \langle \Phi_i | \hat{\rho}(\mathbf{r}, t) | \Phi_i \rangle = \rho_0(\mathbf{r}) - \rho_i(\mathbf{r}, t), \quad (5)$$

where $\hat{\rho}$ is the electron density operator and the $|\Phi_i\rangle$ is the state prepared upon the removal of the electron. Correspondingly, the first term on the right-hand side of Eq. (5), ρ_0 , is the ground-state density of the neutral system and, hence, is time independent, while the second term, ρ_i , is the density of the cation which is time dependent, since $|\Phi_i\rangle$ is not an eigenstate of the cationic system. The quantity $Q(\mathbf{r}, t)$ describes the density of the hole at position \mathbf{r} and time t and by construction is normalized to 1 at all times t .

The time-dependent part of the hole density, $\rho_i(\mathbf{r}, t)$, can be expressed (using Heisenberg picture) as:

$$\rho_i(\mathbf{r}, t) = \langle \Phi_i | e^{i\hat{H}t} \hat{\rho}(\mathbf{r}, 0) e^{-i\hat{H}t} | \Phi_i \rangle = \langle \Phi_i(t) | \hat{\rho}(\mathbf{r}, 0) | \Phi_i(t) \rangle, \quad (6)$$

where $|\Phi_i(t)\rangle = e^{-i\hat{H}t} |\Phi_i\rangle$ is the propagating multielectron wavepacket.

For calculating the hole density we use *ab initio* methods only. The cationic Hamiltonian, represented in an effective many-body basis via the non-Dyson ADC(3) method, is used to directly propagate the initial state in the electronic space via the Lanczos technique [17]. The electronic wavepacket thus obtained is then utilized to construct the hole density at each time point via Eqs. (5) and (6). Theoretical and technical details concerning construction and analysis of the hole density are given in Refs. [16,17,33].

A comment on the preparation of the initial state is in order. The above sketched methodology for tracing the electron dynamics following ionization is independent of the particular choice and the way of preparation of the initial state as long as the ionized electron is removed from the system on a shorter time scale than that of the triggered electron dynamics. The assumption made is that the initially created ionic state can be described by a separable many-electron wavefunction, i.e. the interaction between the ionized electron and the remaining ionic core is neglected—sudden approximation (see, e.g., Ref. [34]). In the calculations to be discussed in this paper, the initial state is prepared through a sudden removal of an electron from a particular Hartree–Fock (HF) orbital; that is, $|\Phi_i\rangle = \hat{a}_i|\Phi_0\rangle$. The initial state can, of course, be constructed such that it corresponds to a removal of an electron from a linear combination of HF orbitals. This liberty allows one to reproduce the hole density of practically every particular initial vacancy. However, to avoid investigating many linear combinations of HF orbitals of interest we concentrate on specific HF orbitals. In this way we can unambiguously identify the basic mechanisms leading to charge migration. Since the time-dependent Schrödinger equation which governs the electron dynamics is a linear equation, these mechanisms are also operative when other choices of the initial state are used. A point to stress here is that as far as the coupling to the external field is described by a one-body operator, the concept of quasiparticles (or the molecular orbitals picture) appears naturally in the analysis of the ionization process. In this respect, the Hartree–Fock approximation provides the best independent-particle theory to describe the ionization, since the many-body corrections to the ionization energies begin to contribute at a higher order of perturbation theory than with other choices of single-particle approximations (see, e.g., [32]). Analysis of the sudden ionization and its implications can be found elsewhere [35].

3. Results and discussion

In the first part of this section we show the results for the ionization spectra of H2-P and Mg-P, computed using the methodology sketched in Section 2.1, and compare them to existing experimental results and other theoretical investigations. In the second part, we study the ultrafast electron dynamics following a sudden ionization of the same outer-valence orbital of both molecules calculated via the methodology briefly described in Section 2.2.

The molecular geometries of the H2-P and Mg-P were optimized using density functional theory methodology [BP86/SV(P)]. Throughout the remaining calculations Ahlrichs valence double-zeta basis sets (VDZ) [36] were used. Although the molecules belong to different symmetry groups, D_{2h} for H2-P and D_{4h} for Mg-P, we use the D_{2h} notation for both molecules in order to make the comparison between the two species easier.

We would like to note that the calculations presented are done within a full active space. Only the core orbitals were frozen. In the case of H2-P we have 220 active orbitals (56 occupied) and in the case of Mg-P 222 active orbitals (61 occupied). Thus, the electron dynamics computations, reported in the second part of this section, represent the response of 111 and of 121 correlated electrons to the outer-valence ionization of H2-P and Mg-P, respectively.

3.1. Ionization spectra

Let us first discuss H2-P. The ionization spectrum of H2-P obtained via non-Dyson ADC(3) approach is shown in Fig. 2. Each line in the calculated spectrum represents a cationic eigenstate $|I\rangle$ (see Eq. (4)). The position of the line is given by the ionization energy, and its height—by the square of the transition amplitude $\langle\Phi_i|I\rangle$. The latter is called pole strength, or spectral intensity, and is related to the ionization cross section (see Ref. [37]). As $|\Phi_i\rangle$ is obtained by removing an electron from a particular HF orbital ($|\Phi_i\rangle = \hat{a}_i|\Phi_0\rangle$), it is clear that only 1h configurations contribute to the spectral intensity. Due to the relatively small basis set used we concentrate on the outer-valence region of the ionization spectrum. The non-Dyson ADC(3) results for the ionic states up to 9 eV are summarized in Table 1 and compared to calculations reported by Dolgounitcheva et al. [12], and to experimental data from measurements performed on H2-P and H2-TPP (TPP = tetraphenylporphyrin) [2,4]. Tetraphenylporphyrins are easier to synthesize and are often used for gas phase experimental studies as replacements for the naturally-occurring porphyrins. Various Green's function based approaches were used by Dolgounitcheva et al. [12]. Here we show the results from the renormalized second-order approximation scheme (RN2) [38] as this is the most elaborated approach used by these authors.

The first two cationic states of H2-P stem from the ionization out of $5b_{3u}$ and $2a_u$ molecular orbitals (MOs), respectively, which are the HOMO – 1 and HOMO at the HF level (HOMO stands for “highest occupied molecular orbital”). Note that the HF calculation predicts different ordering of the first two ionization potentials. There are 3 states resulting from the ionization out of the $3b_{1g}$ orbital or HOMO – 2. The main state is at 8.33 eV and the two satellites are at 7.72 eV and 8.56 eV, respectively. These states are shown in red in Fig. 2 and are the states that we will concentrate on in the next subsection. A pronounced state at 8.31 eV and a small satellite at 7.79 eV are also found in this experimentally unresolved spectral region. The main state is identified as $(4b_{3u})^{-1}$ state, or (HOMO – 3) $^{-1}$ state, while the low-intensity state is a satellite of the $(3b_{2g})^{-1}$ state, or (HOMO – 4) $^{-1}$ state, located at 9.16 eV. We would like to note that in spite of the small basis set used and the neglect of the static self-energy, our computations are in a rather good agreement with the experimental and theoretical results of the displayed cationic states. Interestingly, our results are in better agreement with the available experimental data for H2-TPP (see Table 1). We note, however, that the experimental data have to

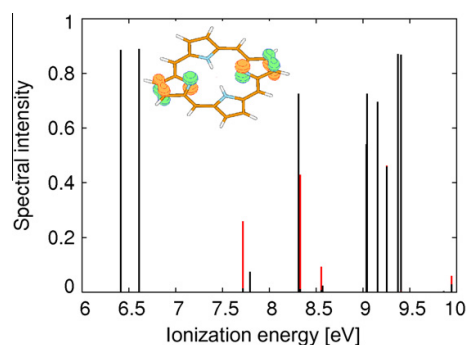


Fig. 2. Ionization spectrum of free-base porphyrin (H2-P), calculated via non-Dyson ADC(3) Green's function approach (see text, Section 2.1). The contributions of the (HOMO – 2) $^{-1}$ configuration to the eigenstates are given in red. The spatial distribution of HOMO – 2 is also shown. (For interpretation of the references to colour in this figure legend, the reader is referred to the web version of this article.)

Table 1

Ionization potentials of free-base porphyrin (H2-P) up to 9 eV. In the first column the symmetry assignments of the states are shown with those of the satellite states given in brackets. The next two columns display the ionization energies and pole strengths (given in brackets) for two different *ab initio* calculations denoted as “method/basis set”. States with pole strengths of less than 0.05 are not listed. The last two columns show experimental results for H2-P [4] and free-base tetraphenylporphyrin (H2-TPP) [2], respectively. By “sh” we denote a shoulder structure in the measured spectrum.

Ion.state	nD-ADC(3)/VDZ	NR2/6-311G** [12]	Exp.H2-P [4]	Exp.H2-TPP [2]
B_{3u}	6.41 (0.89)	6.68 (0.81)	6.9	6.4
A_u	6.61 (0.89)	6.78 (0.81)	7.1 sh	6.7
(B_{1g})	7.72 (0.26)	7.61 (0.31)		7.7
(B_{2g})	7.79 (0.07)	8.46 (0.10)		
B_{3u}	8.31 (0.73)	8.04 (0.67)	8.4	7.9
B_{1g}	8.33 (0.43)	8.10 (0.40)	8.8 sh	
(B_{1g})	8.56 (0.09)	9.83 (0.06)		

be taken only as tentative figures as they are extracted from low-resolution spectra.

Being the states of our interest in the next subsection, let us analyze in more details the B_{1g} states, in particular the main state at 8.3 eV and its dominant satellite at 7.7 eV. As mentioned above, the 1h parts of these two states are nearly exclusively built from the $(\text{HOMO} - 2)^{-1}$ configuration. This 1h configuration contributes with 42% and 25% to the main state and the satellite, respectively. Remember, that all 1h configurations form 43% and 26% of these states, respectively (see Table 1). There are two most prominent 2h1p configurations that participate in these B_{1g} states. One of them has holes in the HOMO and HOMO - 1 and a particle (electron) in the LUMO (LUMO stands for “lowest unoccupied molecular orbital”). It gives about 11% of the norm of the main state and about 22% of the norm of the satellite state. The other important 2h1p configuration has two holes in the HOMO and a particle in the LUMO + 1. It contributes to the main state with about 19% and to the satellite with about 27%. The remaining parts of these states are distributed among a large number of other configurations. According to this analysis, the satellite state at 7.7 eV is a correlation satellite [39].

Let us now have a look at Mg-P. The ionization spectrum of Mg-P, computed via non-Dyson ADC(3) approach, is shown in Fig. 3. The ionization energies and the pole strengths for the states up to 9 eV are given in Table 2 where the NR2 computations of Dolgouitcheva et al. [12] are also listed. To the best of our knowledge no measured ionization spectrum of Mg-P exists in the literature, thus we compare to experimental data for Mg-TPP [2].

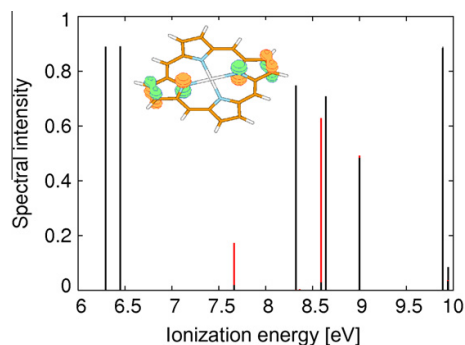


Fig. 3. Ionization spectrum of Mg(II) porphyrin (Mg-P), calculated via non-Dyson ADC(3) Green's function approach (see text, Section 2.1). The contributions of the $(\text{HOMO} - 3)^{-1}$ configuration to the eigenstates are given in red. The spatial distribution of HOMO - 3 is also shown. (For interpretation of the references to colour in this figure legend, the reader is referred to the web version of this article.)

Table 2

Ionization potentials of Mg(II) porphyrin (Mg-P) up to 9 eV. In the first column the symmetry assignments of the states are shown with those of the satellite states given in brackets. The next two columns display the ionization energies and pole strengths (given in brackets) for two different *ab initio* calculations denoted as “method/basis set”. States with pole strengths of less than 0.05 are not listed. As experiments on Mg-P have not been reported, we show in the last column the experimental results for Mg(II) tetraphenylporphyrin (Mg-TPP) [2]. By “sh” we denote a shoulder structure in the measured spectrum.

Ion.state	nD-ADC(3)/VDZ	NR2/6-311G** [12]	Exp.Mg-TPP [2]
B_{3u}	6.29 (0.89)	6.53 (0.81)	6.5
A_u	6.45 (0.89)	6.59 (0.81)	~6.6 sh
(B_{1g})	7.66 (0.17)	7.47 (0.17)	~7.6 sh
B_{3u}	8.32 (0.75)	7.93 (0.71)	7.8
(B_{1g})	8.36 (3×10^{-3})	8.36 (0.12)	~8-8.5
B_{1g}	8.59 (0.63)	8.14 (0.48)	~8-8.5
B_{3u}	8.64 (0.71)	8.64 (0.48)	~8-8.5
B_{2g}	9.00 (0.49)	9.38 (0.84)	8.9

The first two ionic states are again exclusively built from single 1h configurations. For the state at 6.29 eV this is the $(6b_{3u})^{-1}$ configuration, or $(\text{HOMO} - 1)^{-1}$, while for the state at 6.45 eV this is the $(2a_u)^{-1}$ configuration, or $(\text{HOMO})^{-1}$. Note that the HF calculation again predicts different ordering of the first two ionization potentials. The ionization out of the $(\text{HOMO} - 2)$, which is the orbital $5b_{3u}$, gives rise to the state at 8.32 eV. The ionization out of orbital $3b_{1g}$ is responsible for two pronounced states in the studied energy region, namely the main state at 8.59 eV and its satellite at 7.66 eV. The contribution of the $(3b_{1g})^{-1}$ configuration to the cationic states is shown in red in Fig. 3. Note that this orbital appears as $(\text{HOMO} - 3)$ in the case Mg-P, while, as we saw above, it appears as $(\text{HOMO} - 2)$ in the case of H2-P. However, these two orbitals are very similar, as it can be seen from the comparison between their sketches in Figs. 2 and 3. The ionization out of these orbitals also produces very similar structures in the ionization spectrum—a main line and a pronounced shake-down satellite. In the case of H2-P, however, a second satellite (a shake-up one) appears as well. This structure is also predicted for Mg-P by the NR2 computation. Although in our ADC results such a second satellite can also be found, its pole strength is negligible, see Table 2 where this state is listed for completeness.

The breakdown of the main state and the dominant satellite into electronic configurations shows the same structure as in the case of H2-P. The main 2h1p configurations contributing to both states are holes in HOMO and HOMO - 1 and a particle in LUMO, as well as two holes in HOMO and a particle in LUMO + 1. Thus, the shake-down state at 7.66 eV is again a correlation satellite.

Finally, we would like to note that the overall agreement between our data and the NR2 calculations of Dolgouitcheva et al. is relatively good. The discrepancies in the energy positions of the states are within 0.5 eV and the structure of the spectrum is well represented.

3.2. Electron dynamics triggered by outer-valence ionization

Let us now see how the electronic clouds of the studied systems react on a sudden removal of one of their outer-valence electrons; that is, we perform a sudden ionization out of the $3b_{1g}$ orbital, being $(\text{HOMO} - 2)$ and $(\text{HOMO} - 3)$ in H2-P and Mg-P, respectively, and trace the time evolution of the hole density, defined in Eq. (5). The spatial distribution of the corresponding orbitals is shown in Figs. 2 and 3.

We will first analyze the porphyrin molecule. As it was discussed in the previous subsection, the ionization out of HOMO - 2 populates mainly 3 more prominent cationic states. The main state at 8.33 eV and two satellites at 7.72 eV and 8.56 eV, respectively.

Thus, the removal of an electron from HOMO – 2 creates a wavepacket which is a coherent superposition mainly of these 3 states. Of course, the $(\text{HOMO} - 2)^{-1}$ configuration participates in, and thus couples, many other states, but their influence on the correlated dynamics is much weaker due to the small contribution of this 1h configuration to these states. This situation, when the ionization creates a coupling between a main state and a satellite was studied in details in Ref. [16] for the case of a correlation satellite and in Ref. [40] for the case of a relaxation satellite. In the idealized case when only one satellite is coupled an oscillatory dynamics is expected with a period of the oscillations determined by the energy difference between the coupled states. When more states are coupled, the electron dynamics become more involved exhibiting beating patterns of the different oscillating periods involved.

Snapshots of the hole density $Q(\mathbf{r}, t)$ following sudden ionization of the HOMO – 2 are shown in Fig. 4 for the first 7 fs. As seen, the hole is initially localized on the pyrrole rings B and D (see Fig. 1). As time proceeds, the charge starts to delocalize over the rest of the molecule (see the hole density after 2.8 fs) and then to localize again but now on the nitrogens of rings B and D, and on the carbons bridging the pyrrole rings (see the hole density after 4.2 fs). After about 7 fs the hole returns to the B and D rings. However, although the main oscillating period is about 6.8 fs, determined by the energy difference between the main state at 8.33 eV and the dominant satellite at 7.72 eV, since several states are coupled by the HOMO – 2 ionization, the electron dynamics are not purely repetitive and exhibit a beating pattern. Thus, after 7 fs the spatial distribution of the charge only barely resembles that of the initial hole.

We see that after the electron is removed from the HOMO – 2, the positive charge left behind reorganizes on an ultrafast time scale. The slower nuclear dynamics that will start to develop at some later time will be, of course, influenced by this charge reorganization, as it will predetermine the effective potential seen by the nuclei. We would like also to mention that the reorganization of the electronic cloud will also introduce ultrafast changes of the electric dipole moment of the system. It was recently shown that these fluctuations of the dipole moment in the few-femtosecond time scale generate a characteristic radiation in the infrared spectrum [35].

Let us now examine the situation in Mg-P molecule. The ionization out of the HOMO – 3 of Mg-P will create an initial wavepacket

which is a superposition of mainly two ionic states—the main state at 8.59 eV and its dominant correlation satellite at 7.66 eV. The large number of other states coupled by this 1h configuration have very small contribution and thus a weak influence on the electron dynamics. Therefore, here we encounter the typical situation of a dominant-satellite mechanism of charge migration [16] with a single oscillation period of the charge, determined by the energy gap between the coupled states. The relatively large energy gap of about 0.93 eV in Mg-P suggests faster electron dynamics (oscillation period of about 4.45 fs) compared to the case of H2-P.

This is indeed what we observe. In Fig. 5 we show snapshots of the hole density $Q(\mathbf{r}, t)$ during the first 4.5 fs after a sudden ionization of the HOMO – 3. We see that being initially localized on the B and D pyrrole rings the charge starts to spread over the molecule reaching its maximal delocalization after about 1.8 fs. After that time the process continues in a reverse order such that the charge essentially returns to its original position after about 4.5 fs. Without the nuclear dynamics this alternating localization and delocalization of the charge with a period of about 4.5 fs will continue. However, the coupling to the nuclear motion will certainly perturb this breathing process, eventually trapping the charge at some stage. We would like to note that even without the nuclear dynamics the charge migration is not purely repetitive. As we see, the charge density after 4.5 fs is slightly different as the density at time 0. Mainly, we see that some uncompensated “negative” hole charge, or electron charge (depicted in Fig. 5 in orange), appears on the pyrrole rings B and D. This comes as a result of the large number of other states participating in the construction of the wavepacket.

As we see, despite the overall similarity, the electron dynamics expected in H2-P and Mg-P show a few differences. The dynamics in the case of H2-P are more involved and not purely repetitive. This is mainly due to the second satellite state at 8.56 eV which introduces additional oscillation periods and is responsible for the beating pattern of the charge oscillations. In addition, owing to the different energy gaps between the states involved, the time scale of the charge reorganization is roughly 1.5 times faster in Mg-P. Finally, the amount of charge that spreads throughout the molecule is different. We observe less charge to migrate from its original position in the case of Mg-P molecule. All these findings suggest that the succeeding nuclear dynamics predetermined by these ultrafast charge reorganizations following the ionization

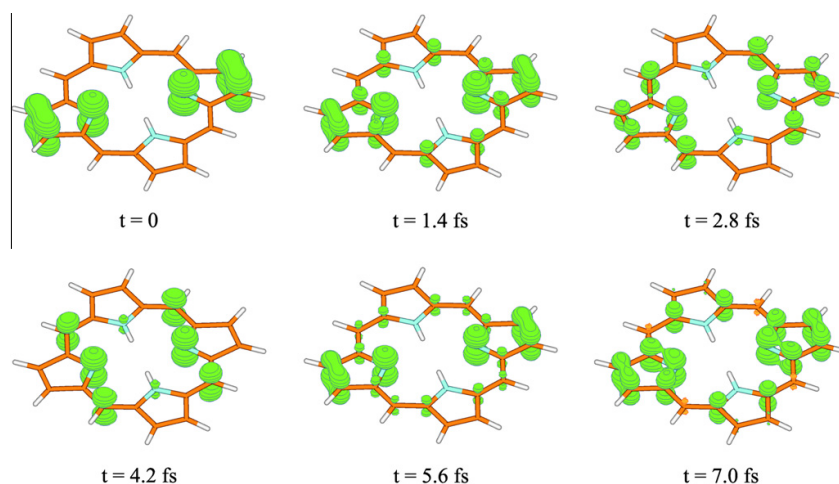


Fig. 4. 3D hole density $Q(\mathbf{r}, t)$ at times $t = 0, 1.4, 2.8, 4.2, 5.6,$ and 7 fs after ionization of the HOMO – 2 of the porphyrin molecule.

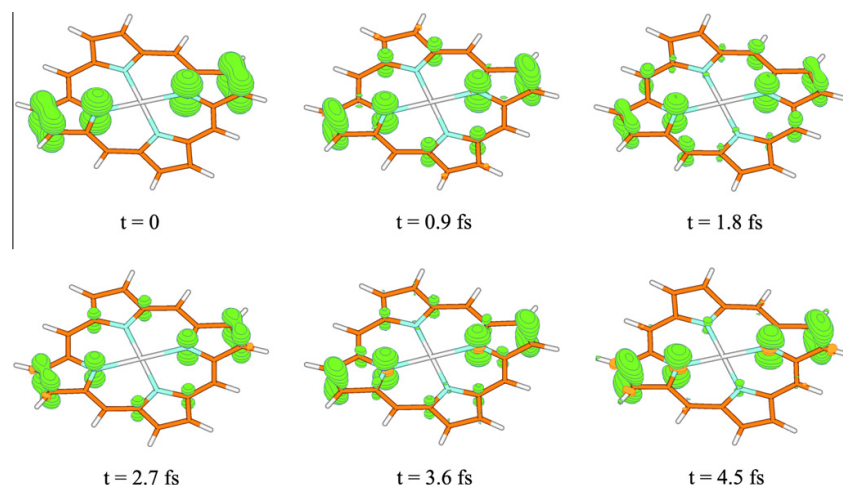


Fig. 5. 3D hole density $Q(\mathbf{r}, t)$ at times $t = 0, 0.9, 1.8, 2.7, 3.6,$ and 4.5 fs after ionization of the HOMO – 3 of the Mg(II) porphyrin molecule. The “negative” hole density, or the electron density, is shown in orange. (For interpretation of the references to colour in this figure legend, the reader is referred to the web version of this article.)

have to be different in the H2-P and Mg-P molecules. The nuclear dynamics induced by these purely electronic initial steps need a special careful investigation, which is far beyond the scope of the present paper.

Finally, we would like to comment briefly on the preparation of the initial state. In order to observe the electron dynamics discussed above, the initial state has to be prepared on an ultrashort time, ideally by using an attosecond pulse, as all states marked in red in Figs. 2 and 3 have to be populated, determining an energy dispersion of the pulse of about 1 eV. If such pumping pulses are centered around 8.2 eV and 8.5 eV for H2-P and Mg-P, respectively, they will, of course, populate also all the other states lying energetically below about 9 eV.

Let us examine more closely the situation in H2-P. In the case of H2-P the other states that will be populated are the B_{3u} state at 8.31 eV, the small satellite of the $(3b_{2g})^{-1}$ state at 7.79 eV and the two outermost ionic states. Thus, in reality, such a pulse will create an initial state being some linear combination of the one-hole configurations corresponding to ionization out of the first 5 MOs implying that the dynamical evolution of this state will be a superposition of the dynamics that one would expect if we were able to address each individual orbital separately. Our computations show that only after ionization out of HOMO – 2, or $4b_{3u}$ orbital, one observe more significant electron dynamics, while in all other cases the created charge is nearly stationary. We might, therefore, conclude that the electron dynamics triggered by the preparation of such more involved and realistic state will be predominantly governed by the dynamics triggered by $(3b_{1g})^{-1}$ alone and discussed above. The situation in the case of Mg-P is very similar. The dynamics triggered by creating holes in in all MOs other $3b_{1g}$ one show very weak variations of the initial charge and thus will only somewhat blur the $(3b_{1g})^{-1}$ component discussed above.

4. Conclusion

We have performed an *ab initio* study of the ultrafast electron dynamics following outer-valence ionization of the free-base porphyrin and Mg(II) porphyrin. In the course of our study we have computed the outer-valence ionization spectra of H2-P and Mg-P using Green's function based methodology, namely the non-Dyson ADC(3) approach. The results for the ionization potentials in the

studied species are in a good agreement with the available experimental data and other *ab initio* results, given the approximations made and the basis set used. We found that in both systems already the third cationic state is a pronounced shake-down satellite stemming from the ionization out of the $3b_{1g}$ orbital, being (HOMO – 2) and (HOMO – 3) in H2-P and Mg-P, respectively. The structure of the calculated spectra shows that the electron correlation effects are very strong already in the outer-valence. This explains the failure of the independent-particle approaches to predict reliable photoionization spectra of porphyrins. The Hartree-Fock approach (Koopmans' theorem) is unable to predict even the correct ordering of the first two ionic states. Thus, for studying the electronic structure and properties of porphyrins, high quality post Hartree-Fock methods have to be employed.

The strong electron correlation effects observed in porphyrins suggest that removing an electron from the outer-valence shell may trigger rich ultrafast electron dynamics. We found that indeed the removal of an electron from the $3b_{1g}$ orbital of H2-P and Mg-P leads to an ultrafast reorganization of the electronic cloud. Being localized initially on the B and D pyrrole rings, the hole charge spreads throughout the molecule in only a few femtoseconds. The electron dynamics in H2-P are more complicated, exhibiting a beating pattern of localizations and delocalizations, while in Mg-P the breathing motion of the charge density shows a single oscillation period.

Since the potential seen by the nuclei is determined also by the electron distribution, this strong reorganization of the charge is expected to influence the nuclear dynamics which will come into play at later times. The charge migration due to the electron correlation is also very sensitive to the momentary configuration of the nuclear skeleton [19,21], thus a complicated interplay between the electronic and the nuclear motion is expected to happen at later times.

Acknowledgment

Financial support by the DFG is gratefully acknowledged.

References

- [1] M.V. Zeller, R.G. Hayes, J. Am. Chem. Soc. 95 (1973) 3855.
- [2] S.C. Khandelwal, J.L. Roebber, Chem. Phys. Lett. 34 (1975) 355.

- [3] S. Kitagawa, I. Morishima, T. Yonezawa, N. Sato, *Inorg. Chem.* 18 (1979) 1345.
- [4] P. Dupuis, R. Roberge, C. Sandorfy, *Chem. Phys. Lett.* 75 (1980) 434.
- [5] D.P. Piet, D. Danovich, H. Zuilhof, E.J.R. Sudhölter, *J. Chem. Soc., Perkin Trans. 2* (1999) 1653.
- [6] N.E. Gruhn, D.L. Lichtenberger, H. Ogura, F.A. Walker, *Inorg. Chem.* 38 (1999) 4023.
- [7] B.L. Westcott, N.E. Gruhn, L.J. Michelsen, D.L. Lichtenberger, *J. Am. Chem. Soc.* 122 (2000) 8083.
- [8] S.I. Yang, S. Prathapan, M.A. Miller, J. Seth, D.F. Bocuian, J.S. Lindey, D. Holten, *J. Phys. Chem. B* 105 (2001) 8249.
- [9] L. Scudiero, D.E. Barlow, U. Mazur, K.W. Hipps, *J. Am. Chem. Soc.* 123 (2001) 4073.
- [10] L. Scudiero, D.E. Barlow, K.W. Hipps, *J. Phys. Chem. B* 106 (2002) 996.
- [11] J. Šeda, J.V. Burda, V. Brázdová, V. Kapsa, *Int. J. Mol. Sci.* 5 (2004) 196.
- [12] O. Dolgounitcheva, V.G. Zakrzewski, J.V. Ortiz, *J. Phys. Chem. A* 109 (2005) 11596.
- [13] I. Barth, J. Manz, Y. Shigeta, K. Yagi, *J. Am. Chem. Soc.* 128 (2006) 7043.
- [14] I. Barth, J. Manz, *Angew. Chem. Int. Ed.* 45 (2006) 2962.
- [15] L.S. Cederbaum, J. Zobeley, *Chem. Phys. Lett.* 307 (1999) 205.
- [16] J. Breidbach, L.S. Cederbaum, *J. Chem. Phys.* 118 (2003) 3983.
- [17] A.I. Kuleff, J. Breidbach, L.S. Cederbaum, *J. Chem. Phys.* 123 (2005) 044111.
- [18] H. Hennig, J. Breidbach, L.S. Cederbaum, *J. Phys. Chem. A* 109 (2005) 409.
- [19] A.I. Kuleff, L.S. Cederbaum, *Chem. Phys.* 338 (2007) 320.
- [20] S. Lünemann, A.I. Kuleff, L.S. Cederbaum, *Chem. Phys. Lett.* 450 (2008) 232.
- [21] S. Lünemann, A.I. Kuleff, L.S. Cederbaum, *J. Chem. Phys.* 129 (2008) 104305.
- [22] A.I. Kuleff, S. Lünemann, L.S. Cederbaum, *J. Phys. Chem. A* 114 (2010) 676.
- [23] A.L. Fetter, J.D. Walecka, *Quantum Theory of Many-Particle Systems*, Dover Publications, New York, 2003.
- [24] J. Schirmer, L.S. Cederbaum, O. Walter, *Phys. Rev. A* 28 (1983) 1237.
- [25] J. Schirmer, A.B. Trofimov, G. Stelter, *J. Chem. Phys.* 109 (1998) 4734.
- [26] J. Schirmer, *Phys. Rev. A* 43 (1991) 4647.
- [27] F. Mertins, J. Schirmer, *Phys. Rev. A* 53 (1996) 2140.
- [28] H.-G. Weikert, H.-D. Meyer, L.S. Cederbaum, F. Tarantelli, *J. Chem. Phys.* 104 (1996) 7122.
- [29] J. Schirmer, A.B. Trofimov, *J. Chem. Phys.* 120 (2004) 11449.
- [30] L.S. Cederbaum, *J. Phys. B* 8 (1975) 290.
- [31] A.B. Trofimov, J. Schirmer, *J. Chem. Phys.* 123 (2005) 144115.
- [32] A. Szabo, N.S. Ostlund, *Modern Quantum Chemistry*, McGraw-Hill, New York, 1989.
- [33] J. Breidbach, L.S. Cederbaum, *J. Chem. Phys.* 126 (2007) 34101.
- [34] B.T. Pickup, *Chem. Phys.* 19 (1977) 193.
- [35] A.I. Kuleff, L.S. Cederbaum, *Phys. Rev. Lett.* 106 (2011) 053001.
- [36] A. Schäfer, H. Horn, R. Ahlrichs, *J. Chem. Phys.* 97 (1992) 2571.
- [37] L.S. Cederbaum, W. Domcke, *Adv. Chem. Phys.* 36 (1977) 205.
- [38] J.V. Ortiz, *J. Chem. Phys.* 108 (1998) 1008.
- [39] L.S. Cederbaum, W. Domcke, J. Schirmer, W. von Niessen, *Adv. Chem. Phys.* 65 (1986) 115.
- [40] S. Lünemann, A.I. Kuleff, L.S. Cederbaum, *J. Chem. Phys.* 130 (2009) 154305.

DOI: 10.1002/cphc.201100528

Electron Correlation in Real Time

Giuseppe Sansone,^{*[a, b]} Thomas Pfeifer,^[c] Konstantinos Simeonidis,^[b] and Alexander I. Kuleff^[d]

Electron correlation, caused by the interaction among electrons in a multielectron system, manifests itself in all states of matter. A complete theoretical description of interacting electrons is challenging; different approximations have been developed to describe the fundamental aspects of the correlation that drives the evolution of simple (few-electron systems in atoms/molecules) as well as complex (multielectron wave functions in atoms, molecules, and solids) systems. Electron correlation plays a key role in the relaxation mechanisms that characterize excited states of neutral or ionized atoms and molecules populated by absorption of extreme ultraviolet (XUV) or X-ray radiation. The dynamics of these states can lead to different processes such as Fano resonance and Auger decay in atoms or interatomic Coulombic decay or charge migration in molecules and clusters. Many of these relaxation mechanisms are ubiquitous in nature and characterize the interaction of complex systems, such as biomolecules, adsorbates on surfaces,

and hydrogen-bonded clusters, with XUV light. These mechanisms evolve typically on the femtosecond ($1\text{ fs} = 10^{-15}\text{ s}$) or sub-femtosecond timescale. The experimental availability of few-femtosecond and attosecond ($1\text{ as} = 10^{-18}\text{ s}$) XUV pulses achieved in the last 10 years offers, for the first time, the opportunity to excite and probe in time these dynamics giving the possibility to trace and control multielectron processes. The generation of ultrashort XUV radiation has triggered the development and application of spectroscopy techniques that can achieve time resolution well into the attosecond domain, thereby offering information on the correlated electronic motion and on the correlation between electron and nuclear motion. A deeper understanding of how electron correlation works could have a large impact in several research fields, such as biochemistry and biology, and trigger important developments in the design and optimization of electronic devices.

1. Introduction

The latest developments in the generation and characterization of ultrashort extreme ultraviolet (XUV) pulses have recently made available pulses as short as $80\text{ as}^{[1]}$ and attosecond pulse trains with intensities higher than 10^{14} W cm^{-2} .^[2] The electron motion inside atoms and molecules evolves in the attosecond or few femtoseconds regime; this ultrafast timescale can be derived both in the classical picture of an electron moving inside an atom or a molecule and in the quantum description of a coherent superposition of eigenstates. The time resolution offered by the new XUV sources allows one, therefore, to initiate and probe electron dynamics on their natural timescale. In particular, the capability to characterize electron processes determined by electron correlations, that is, caused by the interaction between electrons, is attracting great interest. It was recently shown theoretically that if an electron is suddenly ejected from a many-electron system, the time needed for the other electrons to react is a few tens of attoseconds.^[3] This time does not depend on the particular system^[3] and as such appears as the timescale of the electron correlation. The XUV pulses available nowadays enter this time regime, thereby offering the possibility to follow in time and scrutinize the intertwined multielectron dynamics.

Electron correlation can dominate the dynamics initiated in a system by the interaction (single-photon or multiphoton absorption) with an external XUV field. Autoionization, population of excited ionic states, and energy exchange in small van der Waals or hydrogen-bonded clusters are just a few examples of processes governed by the energy exchange between

different electrons of the same system. So far these processes have been largely investigated in the energy domain, where access to the full quantum information (amplitude and phase) is often difficult; the possibility to generate attosecond pulses allows one to analyze such processes directly in the time domain, by applying advanced spectroscopic techniques, to uncover the full dynamical information.

At the same time, the theoretical description of a process involving electron correlation is extremely challenging; exact solutions exist only for the most simple systems and different approximations have been introduced to describe complex multi-electron systems. Comparison with experimental data will be

[a] Dr. G. Sansone
CNR-IFN Dipartimento di Fisica
Politecnico Milano
Piazza Leonardo da Vinci 32, 20133 Milano (Italy)
Fax: (+39) 0223996126
E-mail: giuseppe.sansone@polimi.it

[b] Dr. G. Sansone, Dr. K. Simeonidis
Max Planck Institut für Kernphysik
Saupfercheckweg 1, 69117 Heidelberg (Germany)

[c] Dr. T. Pfeifer
Center for Quantum Dynamics
Ruprecht-Karls-Universität Heidelberg
69120 Heidelberg (Germany)

[d] Dr. A. I. Kuleff
Theoretische Chemie
Universität Heidelberg
Im Neuenheimer Feld 229, 69120 Heidelberg (Germany)

important for validation of the different theoretical approaches.

In this minireview some of the new possibilities offered by femtosecond and attosecond XUV pulses to investigate how electron correlations can influence and drive multielectron dynamics in atoms and molecules are presented. The review is organized as follows. In Section 2 the theoretical methods applied for the description of dynamical electron correlation are reviewed. In Section 3 a few examples of processes driven by electron correlation that could be investigated using femtosecond and attosecond pulses are described. In Section 4 the fundamental aspects of the interaction of an intense infrared (IR) field with an atom are discussed by focusing the attention on the process of high-order harmonic generation (HHG). The attosecond spectroscopy techniques that have been applied or could be applied for the investigation of electron correlation are reviewed. Finally, in Section 5 the conclusions are presented.

2. Theoretical Approaches for Many-Electron Systems

In this section we would like to discuss briefly some of the theoretical methods for treating electron correlation in many-electron systems. We have to stress that we are not aiming at giving an overview of the various methods developed over the years. The literature on the theoretical methods designed to attack the problem of many interacting electrons is enormous and such an overview is far beyond the scope of this minireview. We would like rather to give some flavor of the general concepts used in the most widespread theoretical approaches and to point out some of the problems and challenges arising.

Let us discuss first a many-electron system (for example a molecule) in its ground state. All the properties of the system can be obtained from its wave function $\Psi(\underline{x};\underline{X})$ being the solution of the nonrelativistic time-independent Schrödinger equation [Eq. (1)]:

$$\hat{H}\Psi(\underline{x},\underline{X}) = E\Psi(\underline{x},\underline{X}) \quad (1)$$

where \underline{x} and \underline{X} denote all electronic and nuclear degrees of freedom, respectively, and \hat{H} is the Hamiltonian of the system. Even when the Hamiltonian operator has to describe only the Coulomb interaction between the charged particles, Equation (1) can be solved exactly only for systems containing two particles, for example, the hydrogen atom, which contains a single electron and a single nucleus. For three-body problems the exact mathematical solution of the Schrödinger equation is still unknown. Thus, in principle, even the treatment of the simplest molecule (H_2) relies on some approximation.

The first natural approximation is to decouple the nuclear and the electronic degrees of freedom, that is, to use the cornerstone of quantum chemistry—the Born–Oppenheimer approximation. Since the nuclei are much heavier than the electrons, they move much more slowly. Thus, to a good approximation, one can assume that the electrons are moving in the field created by the fixed nuclei and solve Equation (1) with

the following Hamiltonian (in atomic units) [Eq. (2)]:

$$\hat{H}_{\text{elec}} = -\sum_{i=1}^N \frac{\nabla_i^2}{2} - \sum_{i=1}^N \sum_{a=1}^M \frac{Z_a}{r_{ia}} + \sum_{i=1}^N \sum_{j>i}^N \frac{1}{r_{ij}} \quad (2)$$

where the first term is the electron kinetic energy operator, the second term represents the attraction between the electrons and the nuclei, and the third term the repulsion between the electrons. It is this last term that represents the electron interaction leading to correlation, and it is the one that constitutes probably the largest difficulty in modern electronic structure theory.

The simplest way to deal with this difficulty, suggested already in the early days of quantum theory, is the so-called orbital approximation, or the Hartree–Fock (HF) model (see, for example, refs. [4–6]), where each electron is assumed to move independently in the mean field of the remaining electrons. In the HF approximation the Hamiltonian of the system becomes a sum of one-electron Hamiltonians and the many-electron wave function a product of one-electron functions, known also as orbitals. To incorporate the indistinguishability of the electrons and the requirements of the Pauli exclusion principle, this product has to be antisymmetrized leading to the solution of the HF equations in the form of a Slater determinant, traditionally denoted as $|\Phi_0\rangle$. The incorporation of the Pauli exclusion principle actually represents the simplest form of electron correlation and is usually referred to as Fermi correlation. Although this partially correlates the electrons, the HF method does not take into account their correlated motion. Traditionally, in electronic structure theory the HF wave function is regarded as a fully uncorrelated one and that is why the electron correlation is defined as the difference between the exact and the HF solution of the many-electron problem. It is worth noting that even the HF model leads to integro-differential equations that are difficult to solve for polyatomic systems, and thus in practice the orbitals are expanded in finite basis sets.

The way the HF method addresses the many-electron problem leads to an overestimated electron–electron repulsion and, thus, to go beyond the HF picture, the manner in which the electron–electron interaction is treated has to be modified. The various methods developed for this purpose can fall into two broad classes. The first consists of approaches that can be called post-HF, or *ab initio* methods. These methods rely on the fact that the many-electron wave function can be improved by linearly combining eigenfunctions of the HF Hamiltonian. The second class comprises approaches that can be called semiempirical, since they rely on fitting some free parameters to experimental or *ab initio* data. The most prominent and widely used methods that fall into this category are the approaches based on density functional theory (DFT).^[7] In DFT the complicated many-electron wave function is replaced by a much simpler object, namely the electronic density, which leads to a great reduction of the computational costs. Although it is in principle an exact theory, DFT does not provide a recipe for constructing the exact exchange–correlation func-

tional; thus in practice it is subject to various approximation schemes. Although in recent years the DFT methods have become one of the most popular tools in quantum chemistry, the large variety of approximate exchange-correlation functionals proposed and the increasingly empirical method of their construction lend DFT methods not very much predictive power. That is why we will not discuss them further in the present review.

The various post-HF methods are generally based on two different approaches to the electron-correlation problem—configuration interaction (CI) and perturbation theory. In the CI approach (see, for example, refs. [4,6]), the single Slater determinant wave function is replaced by a linear combination of excited configurations [Eq. (3)]:

$$|\Psi\rangle = c_0|\Phi_0\rangle + \sum_{a,i} c_i^a|\Phi_i^a\rangle + \sum_{a<b,i<j} c_{ij}^{ab}|\Phi_{ij}^{ab}\rangle + \dots \quad (3)$$

where the standard ket notation for states is used. The first term, or the ground-state configuration, is the solution of the HF problem, while the remaining terms are generated by doing single, double, etc. excitations from the ground-state configuration. The CI approach consists of finding the expansion coefficients in Equation (3), which is done variationally. In principle, CI provides an exact solution of the many-electron problem (within the approximations discussed above), since the infinite set of excited configurations forms a complete basis. However, in practice, we can form only a finite number of configurations, related to the finite number of one-particle basis-set functions used for solving the HF problem. Nevertheless, being based on a variational principle, the CI approach is exact within the one-particle basis set used. Unfortunately, even for small molecules and moderate size basis sets, the number of configurations and the respective size of the CI matrix is enormous, thus making the so-called full CI (when all possible configurations within the basis set used are taken in expansion (3)) accessible only for few-electron systems. One usually has to truncate the expansion in Equation (3) after a certain excitation class which, unfortunately, leads to the so-called size-consistency problem, which makes the quality of the description decrease with the increase of the system size.

Fortunately, there are other approaches that do not have this drawback, such as the very successful coupled-cluster (CC) methods (for a recent review, see ref. [8]). The ansatz for the CC wave function is [Eq. (4)]:

$$|\Psi\rangle = e^{\hat{T}}|\Phi_0\rangle \quad (4)$$

where the so-called cluster operator $\hat{T} = \hat{T}_1 + \hat{T}_2 + \dots$ is a sum of single, double, etc. excitation operators which, when acting on the reference state $|\Phi_0\rangle$, produce singly, doubly, etc. excited Slater determinants. When all possible excitations within the one-particle basis set chosen are taken, the expansions in Equations (3) and (4) are, of course, equivalent. The exponential ansatz for the wave function, however, makes the truncated expansion (4) size-consistent. The price to pay is that con-

trary to the CI approach, the CC method is not variational, which means that the CC energy is not necessarily an upper bound of the exact one. Nevertheless, CC methods are one of the most accurate methods for molecular systems. Although relatively expensive, the CC methods can be used to obtain accurate results for small to medium size molecules.

In the other class of post-HF approaches, the perturbation approach, the Hamiltonian is divided into a zeroth-order Hamiltonian, \hat{H}_0 , with known eigenfunctions and eigenvalues, and a perturbation, \hat{H}' , that should be small compared to \hat{H}_0 . Then, the correlation energy can be expanded in correction terms to an arbitrary order in the perturbation. Especially useful is the possibility to represent the perturbation expansion in terms of pictorial diagrams. This allows the avoidance of cumbersome derivations and gives an intuitive way to classify and analyze the type of correlations included. An important aspect of the methods based on the perturbation expansion is that they are size-consistent at any order. The most widely used method based on perturbation theory is the Møller–Plesset (MP) method (see, for example, ref. [9]), in particular the so-called MP2 scheme, which is correct up to the second order of perturbation theory. Computationally MP2 is considerably cheaper than the CC approach and nowadays it can be routinely applied to systems containing a few hundred atoms.

Most of the methods discussed above (with the exception of the MP2 method) are applicable not only to systems in their neutral and charged ground states but also can be used to obtain excited states. However, in practice only the lowest few excited states can be obtained with a reasonable computational cost. A very successful alternative for obtaining properties of an excited or ionized system is the Green's function (GF) or propagator method. An important advantage of the GF-based methods, compared to the above-mentioned wave-function-based ones, is that they allow one to compute the entire spectrum of ionic or excited states of the system in a single run. Several GF approaches to the electronic problem are known in the literature.^[10] Here we would like to mention the class of GF methods known as algebraic diagrammatic construction (ADC) schemes.^[11,12] As the name suggests, the ADC schemes are based on perturbation expansion of the Hamiltonian, which can be directly compared to the diagrammatic series for the studied process (excitation or ionization). A point to stress in this context is that the perturbative character of the method applies only to the ground state of the system and *not* to the final states, which are treated nonperturbatively.^[13] Computationally the ADC methods are relatively inexpensive and can be used to treat systems with a few tens of atoms.

Now let us turn to the question of how to treat processes and, something which will be important for simulating experiments, how to describe the interaction of the system under study with an external laser field. In principle, the time evolution of a quantum system is governed by the time-dependent Schrödinger equation [Eq. (5)]:

$$i \frac{\partial}{\partial t} \Psi(\underline{x}, X; t) = \hat{H} \Psi(\underline{x}, X; t) \quad (5)$$

where the Hamiltonian \hat{H} can also be time-dependent and can include the interaction with an external field. Except in very simple cases, Equation (5) is not soluble exactly and thus one has to search for approximate solutions. As far as one is interested in the electron dynamics, the clamped-nuclei approximation can also be applied. Clearly, this is a reasonable approximation only for ultrafast electronic processes that transpire before the slower nuclear motion has started to play a significant role. Since the processes that we will focus on in the next sections are ultrafast electronic processes governed by the electron correlation, we will not discuss here methods for explicit description of the coupling between electron and nuclear dynamics.

Equation (5) has the following formal solution [Eq. (6)]:

$$\begin{aligned} |\Psi(t)\rangle &= \hat{U}(t, 0)|\Psi(0)\rangle \\ &= \hat{T} \exp\left(-i \int_0^t \hat{H}(t') dt'\right) |\Psi(0)\rangle \end{aligned} \quad (6)$$

where $\hat{T} \exp$ is the so-called chronological exponent which represents the evolution operator $\hat{U}(t, 0)$, and we have again used the standard ket vector notation for the time-dependent states. In the case of time-independent Hamiltonians, the operator describing the evolution of the system from time t to time $t + \Delta t$ is then given by [Eq. (7)]:

$$\hat{U}(t + \Delta t, t) = \exp(-i\hat{H}\Delta t) \quad (7)$$

Therefore, knowing the eigenstates of \hat{H} (which can be obtained by the steady-state approaches discussed above) makes the time propagation straightforward, since we always can expand $|\Psi(0)\rangle$ within the full set of the Hamiltonian eigenstates.

It may appear that this approach cannot be applied for treating experimentally realizable situations, since the Hamiltonian in Equation (7) is assumed to be time-independent and, hence, does not contain the interaction with the external time-dependent field. However, this approach can be used for studying electron dynamics triggered by an ultrashort pulse. If the system is brought by the pulse to a nonstationary state in a very short time, after the pulse is over, the electron dynamics of the system will be governed by the time-independent Hamiltonian describing the state of the system to which it is promoted by the interaction with the field. In this case, the time-dependent wave function can be represented as a linear combination of eigenstates of the Hamiltonian multiplied by time-dependent phase factors involving the corresponding eigenenergies. It is clear that since we are interested in processes governed by the electron correlation, high-precision stationary-state methods that account for as much correlation as possible have to be used. In addition, one needs as many eigenstates as possible to perform the propagation. For such purposes, the GF-based methods are especially appropriate since, as was mentioned above, they provide directly the full spectrum of the ionic or excited-state Hamiltonian, that is, the states in which the many-electron system can be found after

interacting with the external pulse. Thus, one can use those states to perform the time propagation or, alternatively, use the Hamiltonian matrix itself to directly propagate the initially prepared wave packet (see refs. [14, 15]).

In fact, the interaction with an external time-dependent field can also be included in the above approach. Equation (7) is approximately true also for time-dependent Hamiltonians if for a sufficiently small time increment Δt the variation of the Hamiltonian is negligible. In that way, we can represent the evolution operator as a product of operators that propagate the wave function from t to $t + \Delta t$ for which Equation (7) is valid. In other words, we can break up the time interval of interest into many small intervals with duration Δt and thus represent the evolution of the wave function as successive small steps. The expansion in eigenstates can also be used in this case by treating the time-dependent part of the Hamiltonian (the external field) as a perturbation. Obviously, this approach is applicable for many-electron systems interacting with weak fields.

To describe the evolution of a many-electron system in a strong laser field one has to solve the time-dependent Schrödinger equation with the full Hamiltonian. This can be done numerically, for example, by expanding $\Psi(\underline{x}, X; t)$ in a set of known time-independent functions. Although very accurate, this approach is computationally extremely demanding and currently possible only for two-electron systems (see, for example, ref. [16]). Another possibility is to also allow the basis functions to change in time. This is the idea behind the so-called multiconfigurational time-dependent Hartree-Fock (MCTDHF) approach (see refs. [17, 18]). MCTDHF is substantially cheaper computationally and can be applied to larger systems. However, the computational cost grows dramatically with the number of electrons, thus making the method prohibitively expensive for systems containing more than about ten electrons.

A popular approach to tackle time-dependent problems is also time-dependent density functional theory (TDDFT).^[19] However, the problems accompanying the construction of exchange-correlation potentials in the traditional DFT mentioned above are even more severe in its time-dependent formulation. In addition, although traditionally assumed as a formally exact theory, it was recently shown^[20] that there is a serious flaw in the TDDFT founding theorems^[19] and currently there is no rigorous proof that the TDDFT approach is in principle equivalent to solving the time-dependent Schrödinger equation. All this makes the predictive power of the TDDFT approach highly questionable.

3. Processes of Electron Correlation in Atoms and Molecules

3.1. Two-Electron System: Helium

Helium is a benchmark for the time-resolved investigation of electron correlation, as it represents the simplest multielectron system. Nevertheless, correlation is at the heart of different processes taking place in helium; in the following the processes of two-photon double ionization (TPDI) and of autoioniza-

tion will be analyzed in detail as prototypes of correlation-driven mechanisms.

3.1.1. Two-Photon Double Ionization

Experimental investigations of the TPDI process on the sub-femtosecond timescale have been missing so far because of the lack of intense attosecond pulses. Theoretical studies, however, have analyzed in great detail the correlated dynamics originating from the absorption of two XUV photons, which suggest possible approaches to characterize the motion of a two-electron wave packet. Depending on the energy of the XUV radiation, electron correlation can lead to different photoionization mechanisms. Considering that the first and second ionization potentials of helium are $I_{p1}=24.6$ eV and $I_{p2}=54.4$ eV, respectively, two photon-energy ranges can be identified for the generation of doubly ionized helium (He^{2+}).

1) $39.5 \text{ eV} \leq \hbar\omega \leq 54.4 \text{ eV}$

Generation of He^{2+} is possible only if two photons are absorbed simultaneously by the electrons according to the relation [Eq. (8)]:



where $\hbar\omega$ is the photon energy and e_1^- and e_2^- indicate the two photoionized electrons. This mechanism is usually referred to as nonsequential two-photon double ionization (NS-TPDI) and can be described by two different pictures as schematically shown in Figure 1 a₁, a₂. The two electrons absorb separately

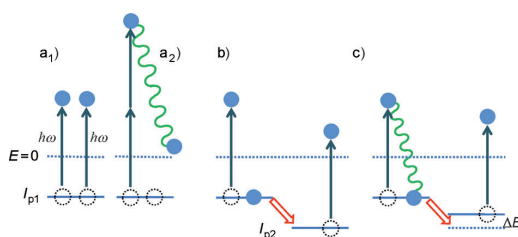


Figure 1. Schematic view of double ionization induced by absorption of two XUV photons $\hbar\omega$. a) NS-TPDI described by independent interaction of the two electrons with the external field (a₁) or by interaction of a single electron with the external field and involving electron correlation (a₂) (shown as a wavy line). b) S-TPDI described by independent interaction of the electrons with the external field at different time instants. c) S-TPDI characterized by electron correlation leading to the population of shake-up states. I_{p1} and I_{p2} are the first and second ionization potentials, respectively. ΔE is the energy difference between the shake-up state and the ionic ground state.

two photons and are emitted in the continuum (Figure 1 a₁). This process can be described by an independent-particle picture and does not imply electron correlation, in the sense indicated in Section 2. On the other hand, a single electron can absorb two photons (Figure 1 a₂) and give part of the energy to the second one that is emitted at the same time. This mechanism cannot be described by an independent-particle model and is based on the interaction between electrons.

2) $54.4 \text{ eV} \leq \hbar\omega$

In this energy range, besides the NS-TPDI mechanism, two additional pathways can lead to the formation of He^{2+} [Eq. (9)]:



and [Eq. (10)]:



The first mechanism (see Figure 1 b) represents a sequential process in which a first photon ejects one electron leaving the ion in the ground state $\text{He}^+(1s)$. At a later time a second photon is absorbed by the bound electron leading to a second ionization event. This process can be understood in an independent-particle picture and does not require electron correlation. The second mechanism (see Figure 1 c) is analogous but the intermediate ionic state is an excited state characterized by quantum numbers (nl). The process can be interpreted as a sequential process, but electron correlation plays a role as the first electron leaving the atom can exchange energy with the ionic core, thereby promoting the second one to an unoccupied electronic state (shake-up state). These two mechanisms are usually referred to as sequential two-photon double ionization (S-TPDI). It should be pointed out that for photon energy $\hbar\omega \geq I_{p1} + I_{p2} = 79.0$ eV, a mechanism for double ionization based on the absorption of a single XUV photon opens up. The process of single-photon double ionization requires electron correlation, but will not be further discussed in this mini-review.

The signature of S-TPDI and NS-TPDI can be identified in the probability energy distributions for the two electrons emitted by an intense attosecond pulse with central energy $\hbar\omega = 91.45$ eV and different pulse durations Δt , as shown in Figure 2 a–c.^[21] For a pulse duration of $\Delta t = 450$ as (see Figure 2 a), two strong contributions can be observed around $E_1 = 66.9$ eV and $E_2 = 37.1$ eV, which correspond to a sequential process in which the first electron is emitted with an energy $E_1 = \hbar\omega - I_{p1}$ and the second is ejected at a later time with an energy $E_2 = \hbar\omega - I_{p2}$. Besides these two main peaks, other peaks at energies of $E_{s1} = 25$ eV and $E_{s2} = 80$ eV are present (barely visible in Figure 2 a). These peaks correspond to a sequential ionization mechanism with excitation of a 2s or a 2p shake-up state, according to the relation $E_{s1} = \hbar\omega - I_{p1} - \Delta E$ and $E_{s2} = \hbar\omega - I_{p1} + \Delta E$, where ΔE indicates the energy difference between the ionic ground state and the shake-up state. The contribution of such a mechanism was also reported in Figure 1 of ref. [22].

The region between the two main peaks is characterized by a contribution that has been referred to as an “anomalous” component in ref. [21]. The relevance of this component increases upon reducing the pulse duration, as shown in Figure 2 b and c that report the two-electron energies for $\Delta t = 225$ as and 150 as, respectively. The increase of the anomalous

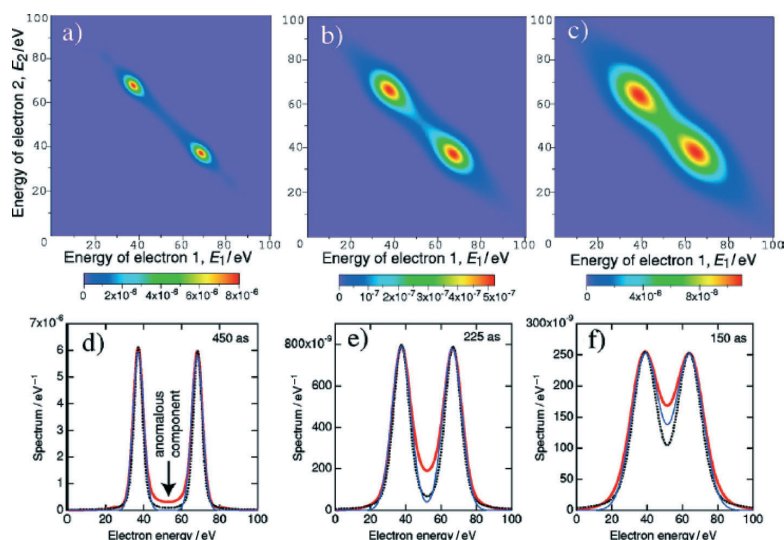


Figure 2. a–c) Probability distribution for the two electron energies E_1 and E_2 emitted by two-photon double ionization. d–f) Integration of the two-electron energy distribution over E_2 (red thick solid line), electron energy distribution based on an independent-particle model considering the Gaussian profile of the attosecond pulse (blue thin solid line), and the absorption profile of a single electron (black thin dotted lines) for the three different pulse durations Δt : 450 (a,d), 225 (b,e), and 150 as (c,f). Reprinted with permission from ref. [21]. Copyright (2005) by the American Physical Society.

component cannot be completely attributed to the larger pulse bandwidth associated with shorter attosecond pulses, as shown in Figure 2d–f. These figures report the integration of the two-electron energy distributions over the energy E_2 and the results of two independent-particle models considering the Gaussian profile of the attosecond pulses and the absorption profile of the helium electrons. Both models cannot fit the behavior of the anomalous component leading to the conclusion that the central part cannot be explained in the framework of an independent-particle approach.

The origin of this contribution has been discussed in several publications and different mechanisms have been suggested. Parker et al.^[23] have attributed this component to a nonsequential double above threshold ionization process (NS-DATI), in which the two electrons absorb simultaneously two photons and exchange energy escaping the atom. Ishikawa et al.^[21] argued that the anomalous component can be attributed to a sequential process and investigated two mechanisms involving electron correlation in the final or intermediate state:

- 1) Post-ionization energy exchange (PIEE). During the first ionization, the second electron leaves the ion when the first one is still in the proximity of the ion. In the continuum the two electrons can exchange energy by Coulomb interaction.
- 2) Second ionization during core relaxation (SICR). When the first electron is emitted, the ion is in a nonstationary state that can relax to the ionic ground state in a time determined by the difference between the two ionization potentials, $\hbar/(I_{p2}-I_{p1})$

= 22 as. The anomalous component can be attributed to ionization of the second electron during relaxation of the ionic core.

Considering the timescale for the core relaxation, it is clear that the distinction between NS-TPDI and S-TPDI has to be revisited when discussing photoionization induced by attosecond pulses. Indeed, the sequential mechanism is based on the assumption that the ion, after ejection of the first electron, can relax to a stationary state before the second electron is emitted. In the case of ionization by an attosecond pulse, the first electron is still close to the ion when the second is emitted, and an unambiguous distinction in time of the two ionization events is not straightforward. Therefore, sequential and nonsequential mechanisms

do not represent the most suitable physical picture to describe the TPDI in the attosecond domain. In this context it is more appropriate to distinguish between features that can be interpreted in an independent-particle picture and components that imply the relevance of the electron correlation. In particular, more physical understanding can be gained by identifying at which level the correlated electronic motion plays a key role.

In their work Feist et al.^[24] distinguished three different types of electron correlation:

- 1) Correlation in the ground state due to the Coulomb interaction in the helium atom;
- 2) Correlation in the intermediate state corresponding to the relaxation of the ionic core when the first electron is being ionized;
- 3) Correlation in the final state corresponding to the exchange of energy between the two electrons in the continuum.

It must be noted that no sharp boundaries between these three situations can be drawn. Nevertheless, their introduction allows us to deepen our physical understanding of the ongoing process.

Ishikawa et al.^[21] attributed the origin of the anomalous component mainly to the SICR process, fitting the correlated energy distributions for different pulse durations. Such a conclusion indicated that correlation in the intermediate state plays the most relevant role in explaining this component. The contribution of the PIEE (therefore correlation in the final state) cannot, however, be completely ruled out.

Electron Correlation in Real Time

Barna et al.^[22] analyzed the single-electron angular distribution $P(\theta)$ to identify the contributions of the different mechanisms to the TPDI. The photoelectron angular distribution can be expressed as [Eq. (11)]:

$$\frac{d\sigma}{d\Omega} = \frac{\sigma_0}{4\pi} [1 + \beta P_2(\cos\theta) + \gamma P_4(\cos\theta)] \quad (11)$$

where σ_0 is the total cross section, $P_{2,4}$ are the Legendre polynomials, and β and γ are the second-order ($k=2$) and fourth-order ($k=4$) anisotropy parameters, respectively. The coefficient β can take values between -1 and 2 ; a value of $\beta=2$ indicates a dipole transition given by the interaction of a single electron with the external field. The coefficient γ indicates the presence of a quadrupole component that can only arise from electron correlation. For the peaks shown in Figure 2 a, the angular distribution resembles that of a Hertz dipole that characterizes the interaction of a single electron with an external field (see Figure 3a). Deviations from the independent-particle model indicate the presence of correlation effects. For the angular distribution corresponding to the peaks, β is at least an order of magnitude larger than γ and is close to the maximum value of 2 ; for such peaks, the double-ionization process can be understood in terms of an independent-particle model. On

the other hand, for the anomalous component, β and γ have comparable values leading to a superposition of dipole and quadrupole contributions (as shown in Figure 3 b), thus indicating the relevance of electron correlation. The presence of the quadrupole component can be used to identify whether electron correlation affects the initial (both electrons are in a bound state), the intermediate (one electron is in a continuum state and the other is bound), or the final state (both electrons are in the continuum) of the two-electron dynamics. Referring to Equation (3), the two-electron wave function can be written in the CI form as [Eq. (12)]:

$$|\Psi\rangle = \sum_{n_j} a_s^{(n_j)} |s^n\rangle |s^j\rangle + \sum_{n_j} a_p^{(n_j)} |p^n\rangle |p^j\rangle + \sum_{n_j} a_d^{(n_j)} |d^n\rangle |d^j\rangle + \dots \quad (12)$$

Electron correlation in the initial state leads to the presence of non-s orbitals contributing to the ground state. A quadrupole component requires a contribution to the final state characterized by a total angular momentum $L_f=2$ as $k=2L_f$. This condition can be realized by a combination of single particle momentum orbitals in the final state, l_f and l'_f , such that $(l_f, l'_f) \in \{(s_f, d_f), (p_f, p_f), (d_f, d_f)\}$. The last configuration is negligible for the intensities used in the simulations. The peaks are dominated by the (p_f, p_f) configurations, while the anomalous component is dominated by the (s_f, d_f) component.

This final configuration can be reached along two pathways involving absorption of two XUV photons [Eq. (13)]:



While the first mechanism can be realized from the dominant configuration of the ground state (s_i, s_i) , the second one requires the contribution of a configuration (p_i, p_i) to the ground-state wave function and is only possible by considering electron correlation in the initial state. Barna and co-workers^[22] have verified that the anomalous component is reduced by an order of magnitude switching off the contribution of the initial configuration (p_i, p_i) , thereby indicating that correlation in the initial state may be more relevant than in the final state. The conclusion that electron correlation between the two outgoing electrons may play only a secondary role in the process is consistent with the observation of Ishikawa and co-workers^[21] that PIEE is only a secondary effect with respect to SICR. On the other hand, second ionization during core relaxation points towards correlation in the intermediate state, whereas the conclusion of Barna and co-workers indicates that initial-state correlation could be more relevant. These conclusions indicate that the interpretation of the different features of the TPDI process is still under discussion. Theoretical simulations will strongly benefit by comparison with experimental two-electron angular distributions that could be measured using the intense attosecond light sources available in the near future.

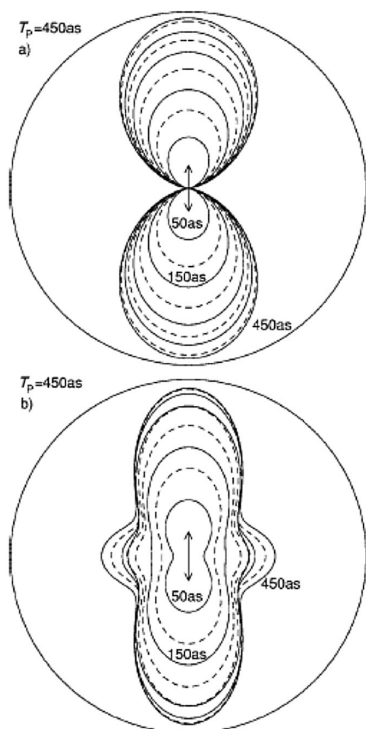


Figure 3. Angular distribution of the electrons emitted by an attosecond pulse with duration (T_p) 450 as for an energy of $E=37$ eV (a) and $E=52$ eV (b). The solid and dashed lines indicate surfaces of constant intensities at times 50 to 450 as in steps of 50 as. Reprinted with permission from ref. [22]. Copyright (2006) by the American Physical Society.

3.1.2. Autoionization and Fano Resonances

Quantum interference between bound and continuum states ubiquitously occurs in nature. An important example for such bound-continuum interference processes are non-Lorentzian-shaped resonance features—termed Fano resonances after they were explained by Ugo Fano in 1961^[25]—in spectra involving autoionization states.

The particular interest in Fano resonances arises not only from the fact that autoionization plays an important role in nature, in fields as diverse as chemistry, biology, earth/atmospheric science, and astrophysics. Fano resonances are also a prototypical example of correlated multielectron interaction processes, in which typically two electrons exchange energy leading to the relaxation of one and the ionization of the other (Figure 4). As the study of multielectron dynamics and correlation is a core theme in attosecond science, Fano resonances and the direct time-resolved observation of their electron–electron interaction dynamics represent a main focus of current research. Fano resonances have been observed and explored in multiple systems, including atoms (where they were first observed by Beutler^[26] in 1935), molecules, condensed-phase systems, and in particular nanoscale solid structures.^[27] In the latter, by using “artificial-atom” quantum dots or other nanostructures, Fano resonances and their underlying physical mechanisms can be studied and controlled.

Ugo Fano’s approach to describing the shape of the autoionization-state resonance, now named after him, is based on the initial assumption of one bound multielectron configura-

tion quantum state ψ embedded in a continuum of states $\phi(E)$ with energy E that are orthogonal eigenstates of the Hamiltonian $H_0 = H - V_{e-e}$ in the absence of electron–electron interaction V_{e-e} . In the presence of CI (due to electron–electron repulsion) the matrix element $\langle \psi | H | \phi(E) \rangle = V_{e-e}$ is nonzero, thus mediating a coupling between the continuum states $\phi(E)$ and the bound state ψ . Fano managed to find new eigenstates $\Psi(E) = a\psi + \int dE' b_{E'} \phi(E')$ as a linear combination (interference) of the initial continuum with the bound configuration states that diagonalize the full H . From these states, the (photo-) excitation cross section [Eq. (14)]:

$$\sigma \propto \frac{(\varepsilon + q)^2}{\varepsilon^2 + 1} \quad (14)$$

can be derived, which contains the asymmetry parameter q , and where ε is a scaled-energy parameter [Eq. (15)]:

$$\varepsilon = 2(E - E_0)/\Gamma \quad (15)$$

with Γ being an effective lifetime width (caused by the “decay” into the continuum) of the autoionizing state at an effective resonance energy E_0 of the resonant transition. An example of such a line shape is shown in Figure 4.

It is perhaps instructive to point out the difference between Fano resonances and Auger-autoionizing resonances that appear when exciting electrons from inner-valence or core states to outer-valence states. Even though the nature of both processes is characterized by autoionization, the observed line shapes of the energy-dependent cross sections in the latter, Auger, case would be Lorentzian, not of the Fano type. This is due to the fact that in Auger decay, the autoionization channel typically ends in a different continuum (leaving behind an ion with an outer-valence excitation after relaxation of the “core” or inner-valence excitation), while in the Fano case the final state is the same continuum with the same bound configuration as that reached by direct (single photon) ionization from the ground state. Therefore, interference between the direct ionization and the autoionization process is only possible in the Fano scenario and not (or only to a small fractional extent) in the resonant case.

The characteristic line shapes are observed both in absorption spectroscopy, which measures the spectrally resolved light transmitted through a dense-

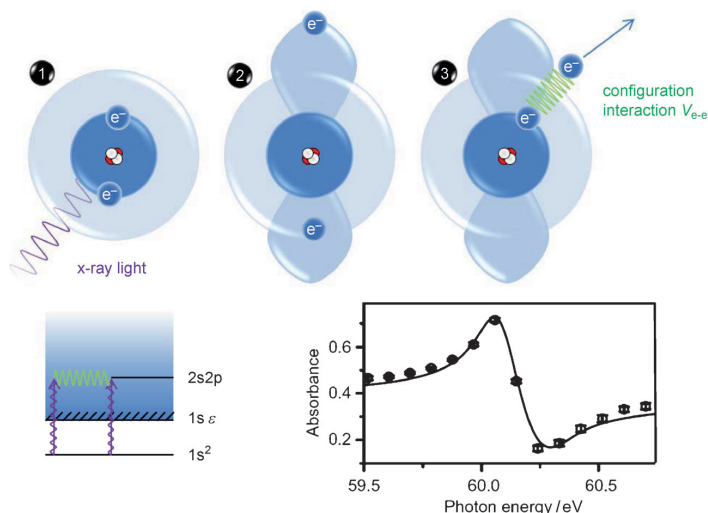


Figure 4. Illustration of the origin of Fano resonance line profiles for the example of autoionization in a He atom. Upper panels: excitation (1), evolution in the autoionized state (2), and relaxation (3) by emitting an electron while the second electron recombines to the inner shell. Lower left: Energy-level diagram: X-ray excitation directly to the continuum ($1s\varepsilon$) and via the autoionizing $2s2p$ configuration state creates interference between these two pathways that gives rise to a characteristic line shape of the ionization cross section at the corresponding energy of ≈ 60.1 eV as seen in the lower right graph (adapted from ref. [28], copyright (2008) with permission from Elsevier; ionization cross section measured via spectrally resolved absorption of light produced by high-order harmonic generation.)

enough sample, and in photoemission spectroscopy, which measures the kinetic energy of ionized electrons. The Fano line shape arises, in other words, because the presence of the two-electron autoionizing excited state at energy E_{exc} results in a modification of the ionization continuum for the continuum states that are energetically close to E_{exc} .

A few years ago, an experiment was theoretically suggested to study the temporal dynamics of electrons ionizing energetically near a Fano resonance^[29] by employing the method of attosecond streaking spectroscopy (described in Section 4.3). Due to the nontrivial

structure of the continuum created by the quasi-bound autoionizing state (as opposed to a structureless continuum as typically the case in such experiments), the expected streak-field traces, that is, photoelectron energy as a function of delay time, exhibited a much richer structure than observed in previous traditional streaking experiments carried out in a flat continuum of free-electron states. The simulation was carried out for autoionization times on the order of a few hundred attoseconds, and thus corresponding to the situation in atomic systems such as the lanthanides, where this decay is much faster than in He or other light (few-electron) systems. It was found that the characteristic signature of the streaking trace corresponding to autoionization was most pronounced when the duration of the attosecond pulse was on the order of the autoionization time, that is, the lifetime of the transient bound configuration state.

Very recently, an experiment was performed to measure the autoionization of He directly in the time domain in the photon energy region around the $1s^2 \rightarrow 2s2p$ Fano resonance (also referred to as $sp,2,0$; for a discussion of different notations see ref. [30]) at 60.1 eV using isolated attosecond pulses. Optical streaking was performed by temporally delaying an attosecond pulse with respect to an intense IR pulse. A characteristic resonance-like feature at a free-electron energy of 35.5 eV was found to vary as a function of time delay, and exhibited a characteristic exponential behavior with a time constant of 17 fs at times where the IR pulse arrived after the exciting attosecond XUV pulse (see Figure 5). This exponential evolution was interpreted as being due to the population of the excited autoionizing $2s2p$ state, the decay time of which was expected to be 17 fs based on previous line width measurements (e.g. ref. [30]). This direct time-resolved measurement was based on the assumption that the intense IR pulse depleted the autoionization state by ionizing at least one of the two electrons in the $2s2p$ configuration, thus decreasing the contribution of this quasi-bound state to the continuum-electron emission

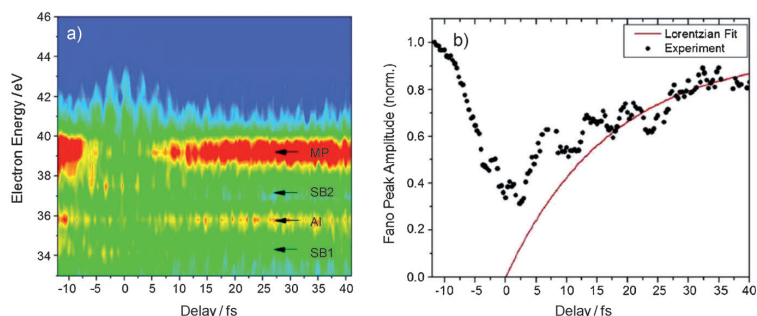


Figure 5. Time-resolved measurement of autoionization in He around the Fano resonance (from ref. [32]).

a) Streak-field trace: photoelectron spectra in dependence on the delay time between attosecond and intense 800 nm IR laser pulse, where negative time delays refer to the situation of the IR pulse preceding the attosecond pulse. AI: electron signal corresponding to the autoionization resonance; SB1/2: sidebands generated as a consequence of streaking the evolving autoionization process over multiple optical periods; MP: center energy of the attosecond pulses used. b) Time-dependent photoelectron signal on top of the Fano resonance near 35.5 eV. The red line corresponds to an assumed lifetime of 17 fs. Reprinted with permission from ref. [32]. Copyright (2010) by the American Physical Society.

around 35.5 eV. Characteristic sidebands spaced by one photon energy from this original resonance energy were also observed, in agreement with an earlier theoretical study.^[31]

In an even earlier experiment employing femtosecond XUV pulses in He, it was shown that different autoionizing states can be efficiently coupled by a strong near-infrared (NIR) laser field to modify and control the spectral shape of the Fano resonance profile.^[28] The experiment was carried out in transmission geometry, that is, not the free electrons' kinetic energy but the spectrally resolved light of the attosecond pulses transmitted through (and absorbed by) the sample was used as the experimental signal, measured again as a function of time delay between an intense 40 fs NIR laser and a shorter weak XUV probe pulse produced by HHG.^[34] The results were theoretically explained by including the coupling between the $2s2p$ and $2p^2$ autoionizing states by the laser, however only if the laser-induced ionization of the excited states was also included. It could be shown that by this laser-induced coupling an electromagnetically induced transparency (EIT), such as switching of the strong $2s2p$ absorption line to almost fully transparent, could be facilitated by the controlling NIR laser field.

These time-resolved experiments and corresponding theory and simulations illustrate the large potential of attosecond pulses in combination with strong laser fields to study, understand, and control multielectron processes. A recent theoretical study examined the control of an ionization branching ratio in He, which leaves behind either an excited $2s$ or $2p$ ionic state by using the temporal dynamics of autoionization that proceed in bursts if several autoionizing states are coherently populated by an attosecond pulse.^[35] In combination with further experiments and theoretical insight, these first basic steps on the study of two-electron correlated dynamics can lead to novel physical concepts, pictures, and descriptions of multielectron dynamics with a rich prospect of applications in physics (creating exotic dynamical states of matter), chemistry (controlling molecular bonds), and life sciences, by employing such

knowledge and techniques for the study and possibly control of macromolecular processes.

3.2. Interatomic Coulombic Decay

Electron correlation plays a fundamental role in the relaxation mechanisms not only in atoms but also in excited molecules and clusters. Among others the process of interatomic (or intermolecular) Coulombic decay (ICD) has attracted considerable attention over the last 10 years because of its potential implications in chemistry and biology. Recently, the ICD process was investigated in water clusters^[36] and water dimers,^[37] showing that this mechanism is responsible for the production of low-energy electrons that play a fundamental role in several phenomena taking place in biomolecules surrounded by an aqueous environment. In the ICD process, the initially excited system gets rid of its excess energy by an ultrafast energy transfer to a neighboring species, which uses this energy to emit a low-energy electron from its outer-valence shell.

The process of ICD was predicted for the first time in 1997^[38] and it was first observed in neon clusters^[39] and neon dimers.^[40] Since its discovery the ICD process has been intensively studied, both theoretically^[41–47] and experimentally^[39,40,48–52] (for recent review articles see refs. [53,54]). It has been shown that this is a very general relaxation mechanism that takes place in various kinds of weakly bound systems, ranging from van der Waals clusters^[41,43,55,56] and hydrogen-bonded complexes^[36–38,57–59] to endohedral fullerenes.^[44] Moreover, ICD appeared to be extremely efficient compared to the other possible relaxation modes of the initially excited system (e.g. photon emission or relaxation via nuclear dynamics). The typical ICD lifetimes are in the order of a few^[44] to a few tens^[45,60,61] of femtoseconds, depending on the chemical environment surrounding the initially excited atom or molecule.

The ICD can be illustrated by considering the dynamics taking place in neon dimers after ionization of an inner-valence 2s electron, shown schematically in Figure 6. For an isolated neon ion, an Auger-like relaxation mechanism (in which a 2p electron fills the inner valence-shell hole and a 2p electron is emitted) is energetically forbidden as the energy difference between the 2s and 2p shells is not enough to overcome the Coulomb barrier of the doubly charged ion Ne^{2+} . The situation changes drastically in the case of neon dimers, as the presence of a second neon atom allows the energy required to doubly ionize the composite system to be lowered because the two charges can be shared between the two atoms. In the case of a dimer, therefore, the excess energy of the Ne^{+*} is transferred to the neutral neon that is ionized emitting an ICD electron. Theoretical computations showed that in the case of neon dimer the ICD lifetime is about 80 fs,^[60,61] which decreases strongly in larger clusters (about 3 fs in Ne_{13} ^[60,61]) due to the higher number of open ICD channels.

So far, a time-resolved study on the ICD process has been done only theoretically^[45] using a multielectron wave-packet propagation technique,^[14] without taking into account the primary ionization field (see the discussion in Section 2). In this study, the time evolution of the ICD process in the NeAr cluster

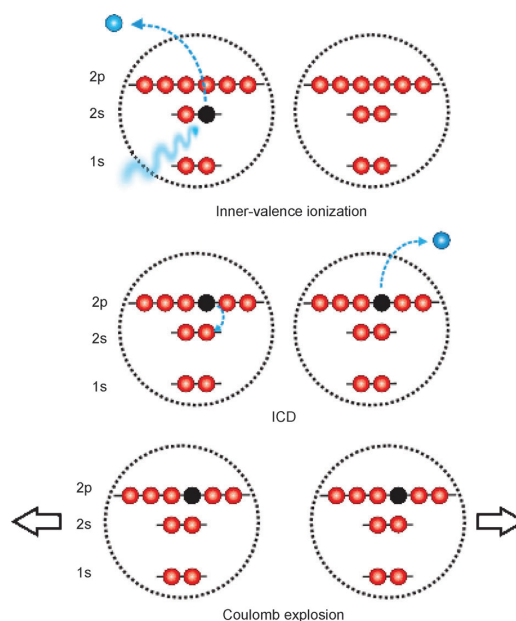


Figure 6. Schematic view of the ICD process in neon dimer. A 2s electron is emitted after absorption of an XUV photon (upper panel). A 2p electron fills the hole and the excess energy is transferred to the second neon atom leading to the emission of an ICD electron from the 2p level of the neighboring neon (central panel). Due to the repulsion between the two ions produced by ICD, the dimer fragments by Coulomb explosion (lower panel).

triggered by $\text{Ne}(2s)$ ionization was traced in time and space. Experimentally, the ICD has been investigated until now only using XUV radiation generated by synchrotron facilities. The availability of femtosecond XUV radiation generated either by high-order harmonic generation (HHG) or by free electron lasers (FELs) opens the way for the time-resolved investigation of the relaxation mechanism using a pump–probe approach.

In the case of HHG, due to the low photon flux usually associated with the harmonic pulses, an XUV pump–IR probe approach can be envisaged. In this case the XUV pulse will create the inner vacancy in the system and the ICD electron will be subsequently emitted in the presence of a variably-delayed IR pulse. Due to the presence of the IR pulse, the ICD electrons can absorb or emit an additional IR photon leading to the formation of sidebands. As the sidebands can be formed only if the ICD electron is emitted in the presence of the IR field, the timescale of the decay mechanism can be inferred by the sideband signal as a function of the relative delay between the XUV and IR pulses.

A different approach to investigate ICD is to focus the attention on a slightly different mechanism characterized by the simultaneous emission of an inner valence electron and excitation of a second electron (shake-up process). The energy of this state is then transferred to the neighboring neon atom and a 2p electron is emitted. The IR pulse can ionize the shake-up state due to the lower ionization potential and can therefore affect the characteristics of the emitted ICD elec-

trons. In this case, by measuring the characteristics of the ICD electrons as a function of the relative delay, it should be possible to infer information about the relaxation dynamics.

The higher photon flux achievable by FELs allows the investigation of ICD using an XUV pump–XUV probe approach. In this case, after the initial ionization event, the characteristics of the dynamics of the system can be modified by further ionizing the system (e.g. a dimer) and therefore affecting the nuclear and electronic dynamics of the cluster. The variation of the signal as a function of the relative delay should offer information about the timescale of the nuclear motion and of the electronic decay.

The investigation of the ICD mechanism has greatly benefited from the possibility to distinguish the signal emitted by the dimers and clusters from that of the monomers that usually represents a large background in the molecular gas jet used in the experiments. The distinction can be performed by means of coincidence measurement of electron and ions and exploiting momentum conservation of the system resulting from the Coulomb explosion of the doubly charged ions [a technique known as cold-target recoil-ion-momentum spectroscopy (COLTRIMS)^[62] or by reaction microscope (REMI)^[63]]. Even though the coincidence measurement of electrons and ions allows one to disentangle the contributions of the different channels and also to identify shake-up satellites, it limits the number of events to less than one per laser shot and thus requires a long acquisition time to collect a statistically meaningful number of counts. This issue represents the key problem that has to be overcome to apply the experimental approach outlined before.

3.3. Charge Migration in Biomolecules

Charge transport and charge transfer in large molecules and in interfaces have attracted great interest for their potential implications in the understanding of biological processes and in the development of more efficient light-based devices. Even though these processes involve a complex interplay between nuclear and electronic structure and therefore evolve on rather slow timescales, recent experimental and theoretical studies have evidenced a new ultrafast mechanism based on the electronic response that could influence the subsequent dynamics taking place in the molecule. In 1996–97 Weinkauff and co-workers showed^[64,65] that localized ionization of a chromophore in peptide chains results in the bond breaking in a different position of the system. In these first works the energy flow from the ionization site to the broken bond was not resolved in time. A few years later, a theoretical work showed^[66] that a pure electronic charge rearrangement could be responsible for such ultrafast energy transfer. The hole created at a specific site of the system can migrate on a timescale of a few femtoseconds or even attoseconds over the entire molecule due to electron correlation^[14,66–68] (see also refs. [69,70]).

An example of this charge-migration phenomenon is shown in Figure 7. As seen, the positive charge created upon ionization out of the inner-valence orbital 28a' of the molecule Gly-Gly-NH-CH₃ migrates from one end of the system to the other

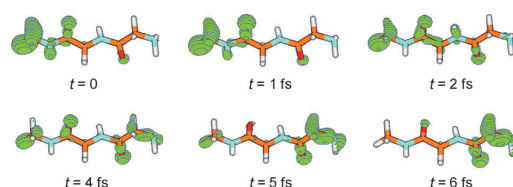


Figure 7. Snapshots of the evolution of the density of the positive charge created upon ionization out of the inner-valence orbital 28a' of the system Gly-Gly-NH-CH₃. The charge migrates from one side of the molecule to the other in only 6 fs solely due to the electron correlation and relaxation effects.

in about 6 fs. Due to the ultrafast timescale of this motion, nuclear dynamics can be neglected and the positions of the nuclei can be regarded as frozen even though at later times the nuclear motion has to be considered to understand how the initial energy redistributes among the different degrees of freedom of the system. A complete theoretical description of such processes will, therefore, require the development of models beyond the Born–Oppenheimer approximation. First steps in this direction have already been undertaken.^[71]

The physical origin of the ultrafast charge migration relies on the fact that ionization out of a particular molecular orbital (MO) does not leave the ion in a stationary state. Indeed, the removal of an electron from the *i*-th MO creates a state that can be described by $|\Phi_i\rangle = \hat{a}_i|\Phi_0\rangle$ while the exact cationic states $|I\rangle$ are given by (in analogy with expansion (3)) [Eq. (16)]:

$$|I\rangle = \sum_j c_j^{(I)} \hat{a}_j |\Phi_0\rangle + \sum_{a,k < l} c_{akl}^{(I)} \hat{a}_a^\dagger \hat{a}_k \hat{a}_l |\Phi_0\rangle + \dots \quad (16)$$

where $c^{(I)}$ are expansion coefficients, \hat{a}_p^\dagger and \hat{a}_q are creation and annihilation operators, respectively, and the standard notation where indices *ij,k,l...* denote occupied orbitals (holes) while *a,b,c...* denote unoccupied orbitals (particles) is used. The terms $\hat{a}_j|\Phi_0\rangle$ are called one-hole (1h) configurations, since one electron has been removed from the corresponding occupied orbital, and the terms $\hat{a}_a^\dagger \hat{a}_k \hat{a}_l |\Phi_0\rangle$ are referred to as two hole–one particle (2h1p) configurations, thereby indicating that in addition to the removal of one electron another one is excited to a virtual orbital, and so forth. It is seen from Equation (16) that the removal of an electron from a particular MO may contribute to several, even many, ionic states. The initially prepared state is thus a superposition of several or many stationary ionic states. This coupling of ionic states is responsible for the charge-migration phenomenon. If the electrons were not correlated the ionic states would be represented by single 1h configurations (HF picture, see Section 2) [Eq. (17)]:

$$|I\rangle = \hat{a}_i |\Phi_0\rangle \quad (17)$$

and hence no coupling and no electron dynamics will appear. The charge-migration phenomenon is, therefore, solely due to the electron correlation and relaxation effects.

Depending on the structure of the coupled ionic states, three basic mechanisms of charge migration have been identi-

fied:^[67] the hole mixing case, the dominant satellite case, and the breakdown of the MO picture case. In what follows we will briefly describe them.

1) Hole mixing case. For simplicity, we will consider two-hole mixing, that is, the situation when two ionic states are coupled each of them being a linear combination of two 1h configurations $\hat{a}_i|\Phi_0\rangle$ and $\hat{a}_k|\Phi_0\rangle$. Note that the mixing of these two HF holes is due to many-body effects, that is, to their mutual coupling to 2h1p and higher configurations. In this idealized case, if we create the initial hole in one of the orbitals, say φ_p , this hole will oscillate between the two orbitals φ_j and φ_k with a frequency determined by the energy difference between the two ionic states. If the two orbitals are localized on two different sites of the system, the hole-mixing mechanism will lead to an oscillation of the initially created positive charge between these two sites. The hole-mixing mechanism was identified as the driving force of the ultrafast charge migration following outer- and inner-valence ionization in many different molecular systems (see, for example, refs. [14, 68, 72, 73]).

2) Dominant satellite case. Let us consider the situation when we have two ionic states, a main state and a satellite, both having overlap with the original 1h configuration. In CI language these states can be written as:

$$|I_m\rangle = c_1 \hat{a}_i |\Phi_0\rangle + c_2 \hat{a}_o^\dagger \hat{a}_k \hat{a}_i |\Phi_0\rangle$$

$$|I_s\rangle = c_2 \hat{a}_i |\Phi_0\rangle - c_1 \hat{a}_o^\dagger \hat{a}_k \hat{a}_i |\Phi_0\rangle$$

where the two coefficients c_1 and c_2 satisfy the equation $c_1^2 + c_2^2 = 1$. In this idealized case, and assuming that all involved orbitals φ_i , φ_k , φ_j , and φ_o are different, that is, the case of a correlation satellite, we will observe the following electron dynamics succeeding the ionization out of orbital φ_i . The hole initially localized on orbital φ_i will migrate to the orbital φ_k (or φ_j) accompanied by an excitation from orbital φ_i (or φ_k) to the virtual orbital φ_o . Again the dynamics will be oscillatory with a period determined by the energy difference between the states $|I_m\rangle$ and $|I_s\rangle$. This type of mechanism was identified to be responsible for the ultrafast electron dynamics taking place after inner-valence ionization in several systems.^[14, 74, 75] There is also a dominant relaxation satellite mechanism, when i is equal to k or l , which is discussed in ref. [76].

3) Breakdown of the MO picture case. In the inner-valence region, where the electron correlation is stronger, the removal of an electron from a particular orbital will typically couple a large number of states. In such cases the initially ionized orbital will "lose" its positive charge quasi-exponentially with time. If the states are below the double ionization threshold, the charge will be typically transferred to many other orbitals and at the end of the process will be spread more or less uniformly over the whole cation. Therefore, if the initial charge is localized, an ultrafast delocalization will take place. This situation was studied in refs. [67, 75].

As we saw, when only a few states are coupled by the initial ionization the charge migration consists in an oscillation of the positive charge. It has been recently shown that these oscilla-

tory electron dynamics should generate IR radiation,^[77] which can be used as an experimental proof of the charge-migration phenomenon.

Experimental investigations performed so far have been focused on the localized excitation of the system and on the observation of the fragmentation products after irradiation with an intense pulse (see, e.g. ref. [78] and references therein). The pump-probe studies performed^[79] did not allow resolution in time of the ultrafast charge migration that, however, could be accessible using attosecond and few-femtosecond pulses extending from the XUV down (in photon energy) to the visible region. Many experimental challenges should be solved to resolve in time such a motion.

1) Sample preparation. The characteristics of the charge migration, such as the oscillation period, can depend on the molecular structure, as shown for the different conformers of the glycine amino acid.^[74] Selection of a single conformer was recently demonstrated by exploiting the spatial separation of the different rotational levels of a molecule induced by a static electric field.^[80] Such a technique could be implemented to perform experiments on a well-defined molecular conformer.

Many molecules of biological interests cannot be heated to the gas phase without inducing relevant modifications or fragmentation. Alternative techniques should be used to prepare a molecular beam for use in the experiment. Recently, laser desorption in combination with expansion with a buffer gas has demonstrated the possibility to achieve stable operation for extended time periods.^[81]

2) Charge-migration excitation. The most straightforward method to excite a charge-migration process is to use an ultrashort UV-XUV pulse to realize the sudden removal of a valence or inner-valence electron. The use of a broadband XUV pulse will result in ionization from a manifold of energy levels and, therefore, several processes will be initiated at the same time. To limit the effect of simultaneous excitation of several states, a compromise between spectral bandwidth and time resolution should be reached. Recently, it has been shown that time-compensated XUV monochromators can select a single harmonic generated by HHG, thereby preserving the original femtosecond (or even attosecond) pulse duration with high throughput efficiency.^[82]

3) Probing of the charge migration. Different schemes could be implemented to probe the dynamics of charge migration. As suggested by Remacle and Levine,^[83] a UV pump-XUV probe approach could be used to initiate and probe this mechanism in oligopeptides. As discussed above, after the removal of the electron by the UV pulse the cation may be brought to a state that is a coherent superposition of, let us say, two eigenstates of the cation built up from 1h configurations localized at the two opposite ends of the molecule. A charge migration over the entire molecule will then appear via the hole-mixing mechanism. An XUV pulse could be used to eject a second electron, the energy distribution of which contains information about the charge migration.

A different approach could be used for molecules presenting an aromatic ring characterized by an absorption band in the UV region ($\lambda \approx 200$ nm). The imaging of the charge migration

could be accomplished by illuminating the excited molecules with an ultrashort UV pulse, because the presence (or the absence) of the charge in proximity of the aromatic ring could modify the absorption of the UV probe leading to variations of the transmitted light as a function of the delay between the pump and probe pulses. For both strategies, it would be important to use ultrashort femtosecond or sub-femtosecond UV pulses that have been demonstrated by nonlinear conversion in dense gas jets using single-cycle IR driving pulses.^[84,85]

4. Attosecond Spectroscopy

Attosecond dynamics are straightforwardly excited in an atom or a molecule interacting with an IR pulse with intensity on the order (or larger than) 10^{14} – 10^{15} W cm⁻². As the IR electric field is comparable to (or larger than) the Coulomb field, the potential experienced by an electron in the valence shell is distorted leading to the formation of an energy barrier through which the electron can tunnel (see Figure 8a). The process can be described by using the Keldysh parameter given by the relation [Eq. (18)]:

$$\gamma = \sqrt{\frac{I_p}{2U_p}} \quad (18)$$

where I_p is the ionization potential and $U_p = E^2/4\omega_L^2$ (atomic units) is the ponderomotive potential of the IR pulse with electric field amplitude E and frequency ω_L . For $\gamma < 1$, ionization can be described in terms of a tunneling process and is temporally confined to short time intervals, around the peaks of the electric field, which last only a small fraction of the optical cycle oscillation T_0 . This condition leads to the creation of an attosecond electron wave packet every half cycle of the laser field (see Figure 8a). Such wave packets are then accelerated by the external electric field (see Figure 8b) and, depending on the ionization instant, can be driven back towards the parent ion when the electric field changes sign (see Figure 8c). After about $T_0/2$, they revisit the initial position and can recombine with the ground state releasing a photon with energy typically in the X-ray/XUV range (see Figure 8d). As the recombination can take place in a time window lasting a few hundreds of attoseconds, the light is emitted in the form of an attosecond pulse.

The motion of the electron in the field of the ionic core and of the external laser field can be described in the framework of the strong-field approximation,^[86] which neglects the influence of the external laser field on the dynamics of the bound electron, and the role of the Coulomb potential during the motion of the electron in the continuum. Under this assumption it is possible to derive a simple set of equations, referred to as saddle-point equations, that govern the motion of the electron [Eq. (19a–c)].^[87,88]

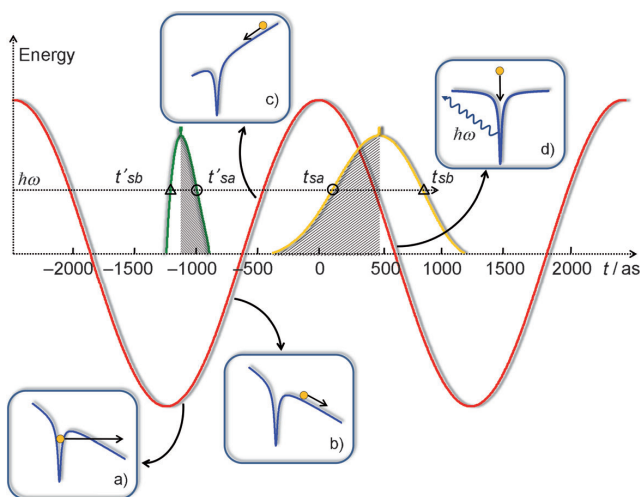


Figure 8. Attosecond electron dynamics during the interaction of an atom/molecule with an intense IR field. Real part of the ionization (green curve) and recombination (yellow curve) times, t'_s and t_s , respectively, obtained as solutions of Equations (19) for a half cycle of an intense IR field (red curve). The attosecond electron wave packet is ionized close to the peak of the electric field (a) and is then accelerated (b). When the electric field changes sign, the electron moves back (c) and finally revisits the parent ion, recombining with the ground state and emitting an XUV photon (d). The ionization (t'_s) and recombination (t_s) times for the short (a) and long (b) paths for a photon of energy $h\omega$ are indicated by circles and triangles, respectively. The dashed region indicates the contribution of the short path, which is selected by the phase-matching condition.

$$\mathbf{p}_s = \frac{1}{t - t'} \int_{t'}^t \mathbf{A}(t'') dt'' \quad (19a)$$

$$\frac{[\mathbf{p}_s - \mathbf{A}(t'_s)]^2}{2} + I_p = 0 \quad (19b)$$

$$\frac{[\mathbf{p}_s - \mathbf{A}(t_s)]^2}{2} + I_p = \omega_{XUV} \quad (19c)$$

where \mathbf{p}_s is the canonical momentum of the electron emitted at time t'_s and recombining with the parent ion at time t_s , $\mathbf{A}(t)$ is the vector potential of the IR field, and ω_{XUV} is the XUV photon energy. The physical interpretation of these equations allows one to obtain a simple physical picture for the harmonic generation process. Equation (19a) implies that $\mathbf{r}(t) = \mathbf{r}(t')$ (\mathbf{r} indicates the position of the electron) meaning that the recombination takes place when the electron occupies again the release position, that is, when the electron revisits the parent ion. Equation (19b) determines the ionization instant t'_s and cannot be satisfied for real times due to the ionization potential I_p (positive). The introduction of a complex time t'_s is due to the fact that the initial process of tunneling ionization cannot be interpreted in the framework of classical mechanics. Finally, Equation (19c) states that at the recombination instant t_s , the total energy of the electron wave packet is released as a photon with energy ω_{XUV} .

The real part of the solutions t_s (yellow curve) and t'_s (green curve) of the saddle-point Equations (19) are shown for a half optical cycle in Figure 8 with the IR electric field (red curve).

The maximum photon energy (cutoff energy $\hbar\omega_{\text{co}}$) that can be achieved is related to the ponderomotive potential U_p by the relation [Eq. (20)]:

$$\hbar\omega_{\text{co}} = I_p + 3.17 U_p \quad (20)$$

For an energy $\hbar\omega < \hbar\omega_{\text{co}}$ (dashed line in Figure 8) two different solutions for the ionization t'_s and recombination t_s instants exist for every half optical cycle. The electron can be released at an instant t'_{sar} , accelerated by the electric field between t'_{sa} and t_{sa} (marked with circles in Figure 8) when it can recombine with the parent ion. Alternatively, the electron can be released at an instant t'_{sb} and then accelerated by the field and brought to the parent ion at time t_{sb} (marked with triangles in Figure 8). The subscripts a and b indicate the two different trajectories that lead to the same final photon energy and that are usually referred to as the short and long path, respectively, depending on the time spent by the electron in the continuum. During the propagation of the IR field in the gas jet, the phase-matching condition usually enhances the contribution of the short path with respect to that of the long path, thus leading to the generation of sub-femtosecond pulses.^[89] As the ionization, acceleration, and recombination processes are repeated every half cycle of the electric field, multicycle driving pulses lead to the generation of a train of attosecond pulses. Different techniques for the generation of an isolated attosecond pulse have been experimentally demonstrated.^[90–95] The process of HHG, therefore, leads to the generation of attosecond bursts of light (train or isolated) that can be used to initiate and probe attosecond dynamics.

It is important to point out that when the accelerated electronic wave packet recollides with the parent ion other processes, such as elastic scattering with emission of very high energy electrons (up to $10 U_p$), inelastic scattering with excitation of the ionic core, or ionization of a second electron (non-sequential double ionization), can occur. Due to the attosecond duration of the recolliding wave packet, such processes carry information on the subcycle dynamics taking place in the parent ion after ionization and have been used for imaging electronic and nuclear molecular dynamics with sub-femtosecond resolution.^[96,97]

In the next sections some of the spectroscopy techniques that have been used so far to study attosecond dynamics will be discussed. In particular, the capability of such techniques to characterize correlated electron dynamics will be highlighted.

4.1. Nonlinear Attosecond Spectroscopy

The extreme time resolution offered by attosecond pulses still comes at the expense of a limited photon flux; the energies of isolated attosecond pulses are currently limited to the picojoule or at most nanojoule levels^[98] and only a few experiments have demonstrated nonlinear effects in the XUV region using sub-femtosecond pulses.^[99] The low achievable intensities and the low nonlinear cross sections in the XUV region make experiments such as the TPDI of helium (discussed in Section 3.1.1) challenging.

Nonlinear effects in the XUV spectral range have been used to characterize the pulse duration of an attosecond pulse train $E(t)$ ^[100] composed of the odd harmonics of the fundamental field [Eq. (21)]:

$$E(t) = \sum_{n_1}^{n_2} A_{2n+1}(t) \exp[-i(\omega_{2n+1}t + \phi_{2n+1})] \quad (21)$$

where n_1 and n_2 are the minimum and maximum harmonic orders, and $A_{2n+1}(t)$, ω_{2n+1} , and ϕ_{2n+1} are the amplitude, frequency, and initial phase of the $2n+1$ harmonic, respectively.

Nabekawa et al.^[101] used a low-repetition-rate (10 Hz), multi-millijoule driving laser system to generate high-energy attosecond pulse trains. The driving pulses were loosely focused in a gas cell with a length of few centimeters. The loose focusing geometry allows one to achieve large focal volumes and favorable phase-matching conditions, thus leading to a conversion efficiency on the order of 10^{-3} – 10^{-4} and XUV energy of a few microjoules. In their work the authors exploited the Coulomb explosion of N_2 molecules after absorption of two XUV photons, to record an interferometric autocorrelation trace of the attosecond pulse train $E(t)$ (see Figure 9a). Two replicas of the attosecond pulse train with a variable delay δ were generated by using a grazing incidence split mirror.^[102]

Nonlinear attosecond XUV spectroscopy methods might be very efficient for characterizing coupled electronic–nuclear dynamics proceeding in molecules.^[103] First experiments were performed in D_2 and CO_2 molecules using trains of intense attosecond pulses generated by multicycle driving IR pulses. The technique is based on the measurement of the ion signal $I(\tau)$ as a function of the delay between two replicas of the attosecond electric field $E(t)$. The signal can be expressed as [Eq. (22)]:

$$I(\tau) = \sum_{p,q} I_{p,q}(\tau) \quad (22)$$

where $I_{p,q}$ indicates the signal generated by the absorption of one photon of the $2q+1$ and one of the $2p+1$ harmonic. Performing a Fourier analysis, it is possible to isolate the different Fourier components and to retrieve the order of the harmonic fields involved in the photoabsorption process. Using this analysis, named nonlinear Fourier transform spectroscopy (NFTS), three different reaction pathways have been identified in the two-photon absorption process of an intense attosecond pulse train by a CO_2 molecule, leading to the formation of CO_2^{2+} , C^+ , and O^+-CO^+ ions.^[104] NFTS was also applied by Furukawa et al.^[105] to retrieve information about the photodissociation of D_2 molecules; they acquired the angular distribution of D^+ ions generated by irradiation of D_2 molecules with an attosecond pulse train containing harmonics from $n_1=1$ up to $n_2=19$.

The application of nonlinear spectroscopy on the attosecond timescale is currently pushing the development of new driving sources characterized by short pulse duration (few-cycle pulses) and high energy^[106] or high repetition rate.^[107] In combination with HHG from solid surfaces,^[108] these sources might

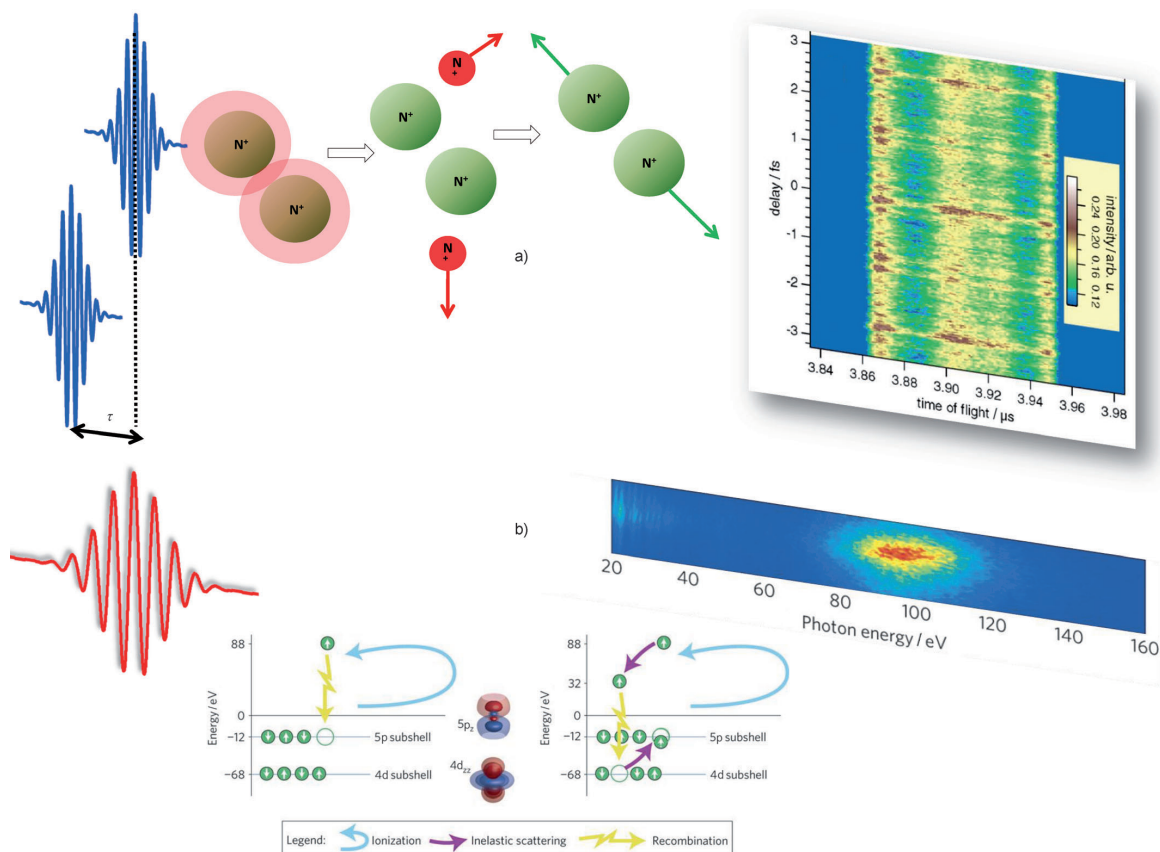


Figure 9. a) *Nonlinear attosecond spectroscopy.* An N_2 molecule is doubly ionized by the combination of two attosecond waveforms with a variable delay τ . The Coulomb explosion of the N_2^{2+} ion leads to the formation of N^+ ions whose yield, as a function of τ , represents an interferometric autocorrelation of the attosecond pulses (adapted from ref. [101]. Reprinted with permission from ref. [101]. Copyright (2006) by the American Physical Society). b) *Attosecond recollision spectroscopy.* High-order harmonic spectra generated by a long-wavelength driving laser in xenon. The harmonic yield enhancement at 100 eV is due to the interference between two quantum paths leading to the same XUV photon energy. In the first one, a 5d electron tunnels out and, upon revisiting the parent ion, recombines with the hole left in the ionization process. In the second one, the 5d electron, through correlation effects, promotes a 4d electron in the 5p shell forming an excited ionic state. Upon revisiting the parent ion, the accelerated electron recombines with the 4d hole (adapted from ref. [109]. Reprinted with permission from Macmillan Publishers Ltd.: *Nat. Phys.* **2011**, *7*, 464–467, copyright (2011)).

deliver in the near future intense, short attosecond pulses at hundreds of kilohertz, opening the way to the investigation of nonlinear processes such as TPD (see Section 3.1.1).

4.2. Attosecond Recollision Spectroscopy

As shown in Figure 8, the electronic wave packet returns to the parent ion after a few hundreds of attoseconds. Therefore, the outcomes of the interaction between the parent ion and the recolliding electron allow one to probe with attosecond time resolution the dynamics proceeding in the ion after the ionization process. In molecules, the ionization step induces a nuclear motion in the ion, that is, the outgoing electronic wave packet launches a perfectly synchronized vibrational wave packet. In 2003 Niikura et al.^[97] imaged, with a resolution of about 200 as, the nuclear motion induced by the strong

field ionization of D_2 molecules in the molecular ion D_2^+ . They measured for different wavelengths of the driving pulse the energy of the fragments D^+ created by inelastic scattering of the returning electron that can excite or doubly ionize the D_2^+ molecular ion. The energy of the fragments depends on the recollision time (about $T_0/2$ after ionization, as shown in Figure 8) and reflects the nuclear distance at that instant. Changing the wavelength of the driving laser is equivalent to varying the delay between the ionization and recollision instants, thus allowing one to visualize the nuclear motion in time.

In a similar way, the characteristics (spectral intensity and phase distributions, polarization state, etc.) of the high-order harmonics, generated by the recombination of the returning electron with the parent ion, encode information about the multielectron dynamics initiated by the photoionization pro-

cess as recently demonstrated by Smirnova et al.^[96] The authors used the high-order harmonics generated in an aligned sample of CO₂ molecules to take snapshots of the hole motion created in the ionized molecule CO₂⁺ by the tunneling process. The charge motion is the result of a coherent superposition of the fundamental (corresponding to a hole in the HOMO level) and of the first excited state (corresponding to a hole in the HOMO-1 level) of the ion.

The role played by electron correlation in the multielectron dynamics can be visualized by studying the high harmonic properties, as evidenced by Shiner and co-workers.^[109] They used a long-wavelength driving pulse to generate harmonic radiation in xenon atoms, and observed a strong emission peak around 100 eV assigned by previous photoionization studies to an enhancement of the cross section of the 4d subshell. This interaction influences the HHG process determining two pathways along which emission of harmonics around 100 eV can be realized, as shown in Figure 9b. In the first one, tunneling ionization releases a 5p electron that is accelerated and then recombines with the parent ion, without interacting with the 4d subshell electron. In the second one, the 5p electron, during the ionization process, inelastically scatters on the 4d subshell promoting it to the vacancy left in the 5p shell. After acceleration, the emitted electron recombines with the hole in the 4d shell leading to the same final photon energy. The interference between these two pathways leads to the enhancement of the signal around 100 eV as shown in Figure 9b.

4.3. Attosecond Streaking Spectroscopy

Several attosecond investigations performed so far have been based on the use of an attosecond XUV pulse and a synchronized IR pulse (usually a replica of the IR field used in the HHG). Due to their large photon energy, attosecond pulses can easily ionize atoms and molecules leading to electron wave packets emitted directly (through direct photoionization) or as a consequence of intermediate processes (such as Auger decay, ICD, autoionization, etc.). When the electron is emitted in the field of an intense IR pulse, it is modified and acquires an asymptotic value \mathbf{p} given by (atomic units) [Eq. (23)]:

$$\mathbf{p} = \mathbf{v}(t_0) + \mathbf{A}(t_0) \quad (23)$$

where $\mathbf{v}(t_0)$ and $\mathbf{A}(t_0)$ are the electron velocity and the IR vector potential at the ionization instant t_0 , respectively.^[110–112] Changing the delay between the attosecond and the IR pulses induces a modulation in the momentum of the emitted electrons that follows the vector potential $\mathbf{A}(t)$. Thus the ionization instant t_0 is encoded in the final momentum \mathbf{p} . This technique was termed attosecond streak camera and was used to characterize the temporal waveform of attosecond pulses, under the assumption that the released electron wave packet is a replica of the XUV spectrum.^[91, 113]

In the case of a photoionization event shorter than the IR cycle (T_0), the action of the IR field on the outgoing wave packet is mainly a shift of the overall momentum distribution, as schematically shown in Figure 10a. This is the situation real-

ized for photoionization of valence electrons of noble gases by a short attosecond pulse.^[114] On the other hand, for ionization processes lasting more than the optical cycle, as in the case of decay processes with lifetimes $\tau > T_0$, the IR determines the formation of sidebands of the main photoelectron peak.^[115] The intensity of the sidebands as a function of the delay between the attosecond and IR pulses allows one to determine the lifetime of the decay process. This approach was used to resolve in time the Auger decay induced in krypton by photoionization from a 5d shell.^[115] A similar approach could be used to determine the timescale of the ICD process in van der Waals or hydrogen-bonded clusters (discussed in Section 3.2).

Recently, the possibility to extend the attosecond streak-camera principle to the study of electron correlations was investigated by Emmanouilidou and co-workers.^[116] The authors analyzed the single-photon double ionization process of helium prepared in a (1s2s) state. Such a system represents a prototype for the single-photon breakup of multielectron systems. It is well known that for small and intermediate excess energies, that is, the energy difference between the XUV photon and the double ionization potential, the process can be described as a knockout mechanism: the first electron absorbs an XUV photon at $t=0$ and on its way out of the atom knocks out the second electron at a time $t=t_{\text{col}}$. The angle θ_{12} between the final momenta \mathbf{p}_1 and \mathbf{p}_2 of the first and the second electron peaks is around a well-defined value characteristic of the XUV photon energy.

Emmanouilidou et al. proposed to use a synchronized IR field to determine the collision instant t_{col} by measuring the inter-electron angle θ_{12} as a function of the relative delay between the attosecond and IR pulses. According to Equation (23), the vector potential determines a momentum shift given by $\mathbf{A}(t_0)$. This additional momentum adds to the initial momenta of the two electrons leading to a decrease or an increase of the angle θ_{12} depending on whether the component along the IR field of the initial momentum of the first electron is directed along or opposite to the vector potential. This condition determines a splitting of the observed angles θ_{12} that turns out to be maximal when the maximum of the vector potential coincides with $t=t_{\text{col}}$. By measuring the time difference between the maximum splitting of θ_{12} and the maximum of the vector potential (which can be obtained by a single-electron streak camera process) the collision time can be derived.

4.4. Attosecond Tunneling Spectroscopy

Core electron dynamics are characterized by a large variety of processes that involve many electrons and thus electron correlations. Such dynamics evolve on a short timescale and can give rise to short-lived transient excited electronic states that rapidly decay through either radiative or nonradiative mechanisms such as Auger decay or ICD. Whereas attosecond streaking allows characterization of the dynamics of states that are linked to the emission of an electron in the continuum, relaxation processes of an excited multielectron state do not necessarily imply the emission of an electron and require a different spectroscopic approach to probe the internal dynamics. For ex-

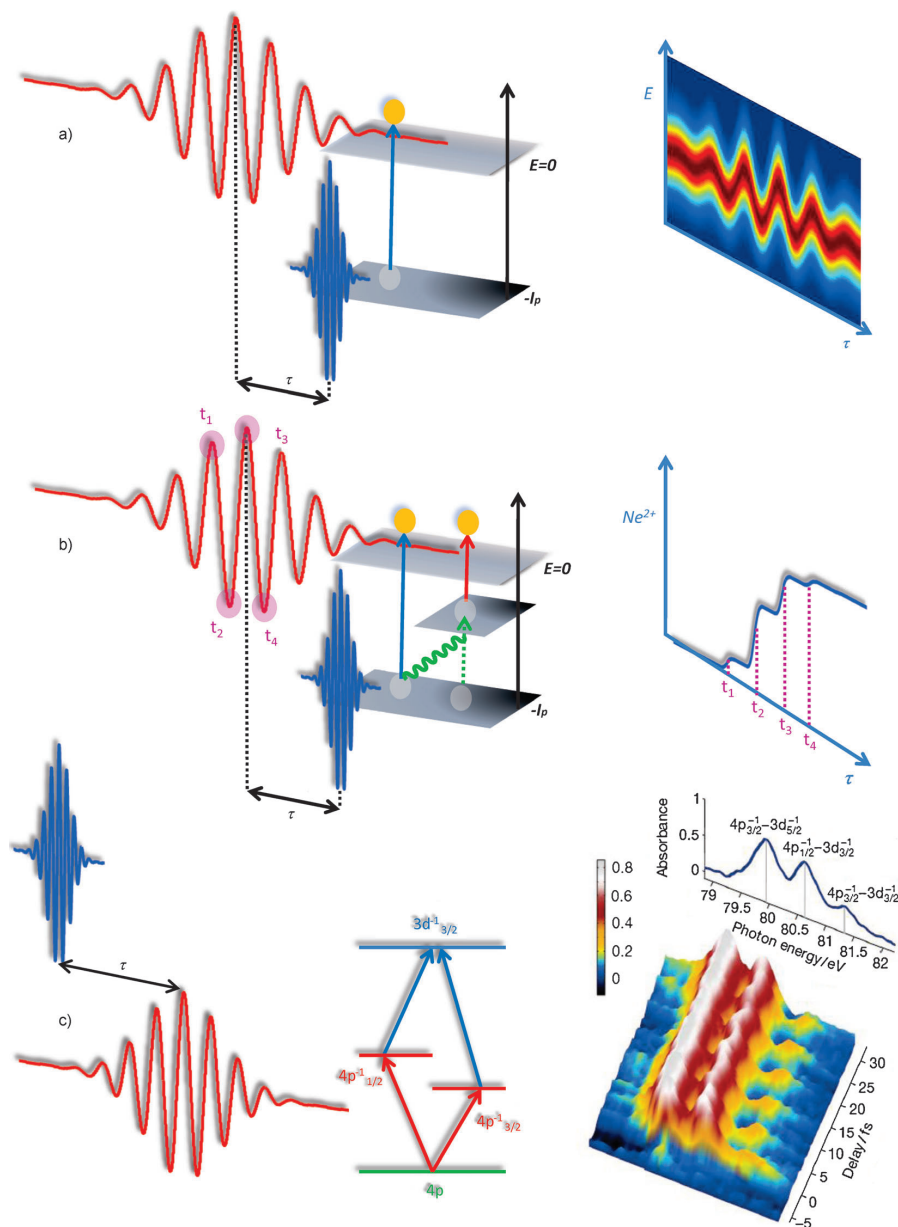


Figure 10. a) *Attosecond streaking spectroscopy.* An attosecond pulse ionizes an electron in the presence of an intense IR field. The oscillation of the electric IR field accelerates the electron wave packet, which acquires an additional momentum given by the value of the vector potential at the electron's release instant. Upon changing the delay between the IR and XUV pulses, the energy distribution of the electron wave packet oscillates according to the vector potential $A(\tau)$. b) *Attosecond tunneling spectroscopy.* Absorption of an XUV photon can lead to photoionization and simultaneous excitation of a shake-up state through electron correlation. The dynamics of the relaxation processes of the shake-up state can be probed by strong field ionization using a synchronized IR field and measuring the doubly charged ion yield. In the case of tunneling ionization ($\gamma < 1$), the ionization from shake-up states is confined around the peaks of the electric field. The ion yield exhibits sharp steps at those time instants corresponding to the time overlap between the peaks of the electric field and the attosecond pulse occurring at delay t_1, t_2, t_3 , etc. c) *Attosecond transient absorption spectroscopy.* A few-cycle IR pulse ionizes a valence electron in krypton launching a hole oscillation corresponding to the coherent superposition of two manifolds of states ($4p_{3/2}^{-1}$ and $4p_{1/2}^{-1}$). The period of the hole oscillation is measured by shining in an attosecond pulse and measuring the transmitted XUV spectrum. The XUV pulse promotes the coherent superposition to the excited ionic state $3d_{5/2}^{-1}$ leading to a quantum interference between the two paths that determines a modulation of the absorption of the XUV radiation with the period of the hole oscillation.

ample, ionization of a core electron is often accompanied by excitation to an unoccupied state of a second electron through electron correlation, thus leaving the multielectron system in an excited state referred to as a shake-up state. The population of this state can be probed by measuring the ionization probability using an intense IR pulse, as first demonstrated in ref. [117].

The proof-of-principle experiment was realized in neon, by monitoring the population of shake-up states populated in the inner-valence ionization of 2s electrons by an attosecond pulse centered at 91 eV. The time-dependent population of such states can be inferred by using IR pulses of different intensities and measuring the Ne^{2+} yield as a function of the delay between the XUV pulse and the IR pulse, as schematically shown in Figure 10b. For loosely bound states the ionization process is expected to be in the multiphoton regime (Keldysh parameter $\gamma > 1$) and to follow the envelope of the IR pulse. In contrast, ionization from shake-up states with higher binding energy is expected to be in the tunneling regime ($\gamma < 1$) and to be characterized by rapid steps in the ionization probability, as shown in Figure 10b. In this last case, as the tunneling ionization is confined around the peak of the IR field (see Figure 10b), the rapid variation of the Ne^{2+} ion signal corresponds to those time instants t_i (with $i = 1, 2, 3, 4$, etc.) when the XUV pulse and the maximum of the IR electric field overlap (see Figure 10b). This approach was used to characterize cascaded Auger processes taking place in xenon and krypton.^[117,118] It is important to point out that attosecond tunneling spectroscopy allows one to follow in time the dynamics of excited multielectron states and to order in time the relaxation processes initiated by the initial absorption of an XUV photon; such information cannot be obtained by time-integrated spectral measurements.

4.5. Attosecond Transient Absorption Spectroscopy

The properties of the interaction of an atom or a molecule with an external electromagnetic pulse can be strongly influenced by the evolving electronic dynamics involving valence and core levels. In particular, the absorption and the dispersion properties of a medium can be modulated on a timescale reflecting the dynamics taking place in the system. Transient absorption spectroscopy is a well-established technique in the visible region (corresponding to dynamics in the femtosecond domain) and first experiments in the XUV using trains of attosecond pulses were demonstrated in atoms and molecules in 2007^[119] and 2008,^[120] respectively. The advantage of this spectroscopic method resides in the measurement of photons rather than charged particles (electrons and ions), thus allowing superior signal-to-noise ratio and reduced acquisition times. Moreover, due to the excellent spectral resolution achieved by XUV spectrometers,^[121] fine structures of the energy levels involved in the electronic wave packet can in principle be resolved.

Recently, attosecond transient absorption spectroscopy was used to visualize the few-femtosecond motion of a hole created in krypton by ionization using a single-cycle IR pulse.

Strong-field ionization populates not only the ground-state manifold ($4p_{3/2}^{-1}$) but also an excited-state manifold ($4p_{1/2}^{-1}$) of the ion Kr^+ (see Figure 10c), thereby determining a wave packet in the valence shell. According to the spin-orbit energy splitting of these two manifolds $\Delta E_{so} = 0.67$ eV, the hole oscillates in time with a period of $T_{so} = 6.2$ fs. The motion of the hole density was imaged by measuring the absorption of an attosecond pulse through the sample. Indeed, absorption of an XUV photon can promote the ($4p_{3/2}^{-1}$) and ($4p_{1/2}^{-1}$) manifolds to the ($3d_{3/2}^{-1}$) manifold creating a core vacancy in the Kr^+ . The population transferred to the excited level and therefore the absorption will be modulated in time depending on the relative phase $\Delta\Phi$ between the two paths according to the relation [Eq. (24)]:

$$\Delta\Phi = \frac{\Delta E_{so}}{\hbar} t \quad (24)$$

Attosecond transient absorption spectroscopy was also used to directly time resolve the evolution of autoionizing states in argon atoms.^[33] Several absorption lines corresponding to the excitation from the ground $3s^2 3p^6$ configuration state to the autoionizing $3s 3p^6 n p$ manifold of states were observed in the absence of the intense NIR pulse. When the NIR pulse was temporally far away from the autoionizing pulse, the same field-free spectral absorption profile was observed as expected for the case of autoionizing states that only have a limited lifetime. When the time delay between NIR and attosecond pulses was reduced, a characteristic broadening, splitting, shifting, and weakening of the absorption lines became apparent, which indicated a modification of the ionization dynamics by the presence of the NIR pulse. The experimental findings were again theoretically explained^[28] by considering the NIR-induced coupling among different autoionization states as well as taking into account the additional ionization channel created by the laser. While coupling among the quasi-discrete autoionization states (also including the $3s 3p^6 n d$ manifold) leads to Rabi oscillations and thus explains the state splitting (see also Autler-Townes splitting^[122]), the additional coupling to the continuum by NIR-induced ionization of the autoionizing states effectively reduces their lifetime, thus explaining the broadening and weakening of the absorption lines.

5. Conclusions

Correlated multielectron dynamics can play a fundamental role in the processes triggered by absorption of XUV photons. Phenomena such as autoionization, excitation of shake-up states, ICD, and Auger decay are just a few examples of mechanisms that are linked to the interaction of an atom or a molecule with an XUV field. Such mechanisms have been extensively studied in the energy (frequency) domain exploiting the availability of tunable, monochromatic XUV radiation offered by synchrotron sources. Complementary information in the time domain has been so far out of reach because of the ultrafast (few femtosecond and attosecond) timescale typical of such processes. Nowadays, the availability of intense ultrashort IR

fields offers experimentalists the possibility to create attosecond electron wave packets leading to the generation of attosecond pulses that encode information about the electron and nuclear dynamics initiated by the photoionization process. The application of trains and isolated attosecond pulses in pump-probe experiments using different spectroscopic techniques has allowed the tracing in time of valence and core electron dynamics with unprecedented temporal resolution. Future developments, such as the generation of intense attosecond sources, will pave the way for the investigation of nonlinear processes in the XUV domain and will offer new methods for the investigation of ultrafast electron correlation.

Acknowledgements

G.S. and K.S. acknowledge financial support from the Ateneo italo-tesesco (Programma-Vigoni 2007–2009). G.S. acknowledges financial support from the Alexander von Humboldt Foundation (Project "Tirinto") and from the Italian Ministry of Research (FIRB RBID08CRXK). T.P. gratefully acknowledges support by an MPRG grant of the Max-Planck Gesellschaft. A.I.K. thanks J. Schirmer for valuable discussions and gratefully acknowledges funding from the DFG.

Keywords: electron correlation · electronic structure · lasers · nonlinear optics · X-ray absorption spectroscopy

- [1] E. Goulielmakis, M. Schultze, M. Hofstetter, V. S. Yakovlev, J. Gagnon, M. Uiberacker, A. L. Aquila, E. M. Gullikson, D. T. Attwood, R. Kienberger, F. Krausz, U. Kleineberg, *Science* **2008**, *320*, 1614–1617.
- [2] H. Mashiko, A. Suda, K. Midorikawa, *Opt. Lett.* **2004**, *29*, 1927–1929.
- [3] J. Breidbach, L. S. Cederbaum, *Phys. Rev. Lett.* **2005**, *94*, 033901.
- [4] A. Szabó, N. S. Ostlund, *Modern Quantum Chemistry: Introduction to Advanced Electronic Structure Theory*, Dover, New York, **1996**.
- [5] R. McWeeny, *Methods of Molecular Quantum Mechanics*, Academic Press, London, **1989**.
- [6] T. Helgaker, P. Jørgensen, J. Olsen, *Molecular Electronic-Structure Theory*, Wiley, New York, **2000**.
- [7] P. Hohenberg, W. Kohn, *Phys. Rev.* **1964**, *136*, B864–B871.
- [8] R. J. Bartlett, M. Musiał, *Rev. Mod. Phys.* **2007**, *79*, 291–352.
- [9] D. Cremer in *Encyclopedia of Computational Chemistry* (Ed.: P. v. R. Schleyer), Wiley, New York, **1998**.
- [10] J. Linderberg, Y. Öhrn, *Propagators in Quantum Chemistry*, Wiley-Interscience, New York, **2004**.
- [11] J. Schirmer, L. S. Cederbaum, O. Walter, *Phys. Rev. A* **1983**, *28*, 1237–1259.
- [12] L. S. Cederbaum in *Encyclopedia of Computational Chemistry* (Ed.: P. v. R. Schleyer), Wiley, New York, **1998**.
- [13] J. Schirmer, *Phys. Rev. A* **1991**, *43*, 4647–4659.
- [14] A. Kuleff, J. Breidbach, L. Cederbaum, *J. Chem. Phys.* **2005**, *123*, 044111.
- [15] A. D. Dutoi, L. S. Cederbaum, M. Wormit, J. H. Starcke, A. Dreuw, *J. Chem. Phys.* **2010**, *132*, 144302.
- [16] M. Awasthi, Y. Vanne, A. Saenz, *J. Phys. B* **2005**, *38*, 3973–3985.
- [17] O. Koch, W. Kreuzer, A. Scrinzi, *Appl. Math. Comput.* **2006**, *173*, 960–976.
- [18] M. Nest, T. Klamroth, P. Saalfrank, *J. Chem. Phys.* **2005**, *122*, 124102.
- [19] E. Runge, E. K. U. Gross, *Phys. Rev. Lett.* **1984**, *52*, 997–1000.
- [20] J. Schirmer, A. Dreuw, *Phys. Rev. A* **2007**, *75*, 022513.
- [21] K. Ishikawa, K. Midorikawa, *Phys. Rev. A* **2005**, *72*, 013407.
- [22] I. Barna, J. Wang, J. Burgdorfer, *Phys. Rev. A* **2006**, *73*, 023402.
- [23] J. Parker, L. Moore, K. Meharg, D. Dundas, K. Taylor, *J. Phys. B* **2001**, *34*, L69–L78.
- [24] J. Feist, S. Nagele, R. Pazourek, E. Persson, B. I. Schneider, L. A. Collins, J. Burgdorfer, *Phys. Rev. Lett.* **2009**, *103*, 063002.
- [25] U. Fano, *Phys. Rev.* **1961**, *124*, 1866–1878.
- [26] H. Beutler, *Z. Phys.* **1935**, *93*, 177–196.
- [27] A. E. Miroshnichenko, S. Flach, Y. S. Kivshar, *Rev. Mod. Phys.* **2010**, *82*, 2257–2298.
- [28] Z.-H. Loh, C. H. Greene, S. R. Leone, *Chem. Phys.* **2008**, *350*, 7–13.
- [29] M. Wickenhauser, J. Burgdorfer, F. Krausz, M. Drescher, *Phys. Rev. Lett.* **2005**, *94*, 023002.
- [30] M. Domke, K. Schulz, G. Remmers, G. Kaindl, D. Wintgen, *Phys. Rev. A* **1996**, *53*, 1424–1438.
- [31] Z. Zhao, C. Lin, *Phys. Rev. A* **2005**, *71*, 060702.
- [32] S. Gilbertson, M. Chini, X. Feng, S. Khan, Y. Wu, Z. Chang, *Phys. Rev. Lett.* **2010**, *105*, 263003.
- [33] H. Wang, M. Chini, S. Chen, C.-H. Zhang, F. He, Y. Cheng, Y. Wu, U. Thumm, Z. Chang, *Phys. Rev. Lett.* **2010**, *105*, 143002.
- [34] Z.-H. Loh, M. Khalil, R. E. Correa, S. R. Leone, *Rev. Sci. Instrum.* **2008**, *79*, 073101.
- [35] L. Argenti, E. Lindroth, *Phys. Rev. Lett.* **2010**, *105*, 053002.
- [36] M. Mucke, M. Braune, S. Barth, M. Förstel, T. Lischke, V. Ulrich, T. Arion, U. Becker, A. Bradshaw, U. Hergenhahn, *Nat. Phys.* **2010**, *6*, 143–146.
- [37] T. Jahnke, H. Sann, T. Havermeier, K. Kreidi, C. Stuck, M. Meckel, M. Schöffler, N. Neumann, R. Wallauer, S. Voss, A. Czasch, O. Jagutzki, A. Malakzadeh, F. Afaneh, Th. Weber, H. Schmidt-Böcking, R. Dörner, *Nat. Phys.* **2010**, *6*, 139–142.
- [38] L. Cederbaum, J. Zobeley, F. Tarantelli, *Phys. Rev. Lett.* **1997**, *79*, 4778–4781.
- [39] S. Marburger, O. Kugeler, U. Hergenhahn, T. Möller, *Phys. Rev. Lett.* **2003**, *90*, 203401.
- [40] T. Jahnke, A. Czasch, M. Schöffler, S. Schössler, A. Knapp, M. Käsz, J. Titze, C. Wimmer, K. Kreidi, R. Grisenti, A. Staudte, O. Jagutzki, U. Hergenhahn, H. Schmidt-Böcking, R. Dörner, *Phys. Rev. Lett.* **2004**, *93*, 163401.
- [41] R. Santra, J. Zobeley, L. Cederbaum, N. Moiseyev, *Phys. Rev. Lett.* **2000**, *85*, 4490–4493.
- [42] R. Santra, L. Cederbaum, *Phys. Rev. Lett.* **2003**, *90*, 153401.
- [43] V. Averbukh, I. B. Müller, L. Cederbaum, *Phys. Rev. Lett.* **2004**, *93*, 263002.
- [44] V. Averbukh, L. Cederbaum, *Phys. Rev. Lett.* **2006**, *96*, 053401.
- [45] A. I. Kuleff, L. S. Cederbaum, *Phys. Rev. Lett.* **2007**, *98*, 083201.
- [46] A. I. Kuleff, K. Gokhberg, S. Kopelke, L. S. Cederbaum, *Phys. Rev. Lett.* **2010**, *105*, 043004.
- [47] N. Sissourat, N. V. Kryzhevoi, P. Kolorenč, S. Scheit, T. Jahnke, L. S. Cederbaum, *Nat. Phys.* **2010**, *6*, 508–511.
- [48] G. Öhrwall, M. Tchapyguine, M. Lundwall, R. Feifel, H. Bergersen, T. Rander, A. Lindblad, J. Schulz, S. Peredkov, S. Barth, S. Marburger, U. Hergenhahn, S. Svensson, O. Björneholm, *Phys. Rev. Lett.* **2004**, *93*, 173401.
- [49] Y. Morishita, X. J. Liu, N. Saito, T. Lischke, M. Kato, G. Prümper, M. Oura, H. Yamaoka, Y. Tamenori, I. H. Suzuki, K. Ueda, *Phys. Rev. Lett.* **2006**, *96*, 243402.
- [50] T. Jahnke, A. Czasch, M. Schöffler, S. Schössler, M. Käsz, J. Titze, K. Kreidi, R. E. Grisenti, A. Staudte, O. Jagutzki, L. P. H. Schmidt, T. Weber, H. Schmidt-Böcking, K. Ueda, R. Dörner, *Phys. Rev. Lett.* **2007**, *99*, 153401.
- [51] T. Aoto, K. Ito, Y. Hikosaka, E. Shigemasa, F. Penent, P. Lablanquie, *Phys. Rev. Lett.* **2006**, *97*, 243401.
- [52] T. Havermeier, T. Jahnke, K. Kreidi, R. Wallauer, S. Voss, M. Schöffler, S. Schössler, L. Foucar, N. Neumann, J. Titze, H. Sann, M. Kühnel, J. Voigtsberger, A. Malakzadeh, N. Sissourat, W. Schöllkopf, H. Schmidt-Böcking, R. E. Grisenti, R. Dörner, *Phys. Rev. Lett.* **2010**, *104*, 153401.
- [53] V. Averbukh, Ph. V. Demekhin, P. Kolorenč, S. Scheit, S. D. Stoychev, A. I. Kuleff, Y.-C. Chiang, K. Gokhberg, S. Kopelke, N. Sissourat, L. S. Cederbaum, *J. Electron Spectrosc. Relat. Phenom.* **2011**, *183*, 36–47.
- [54] U. Hergenhahn, *J. Electron Spectrosc. Relat. Phenom.* **2011**, *184*, 78–90.
- [55] S. Scheit, V. Averbukh, H.-D. Meyer, J. Zobeley, L. Cederbaum, *J. Chem. Phys.* **2006**, *124*, 154306.
- [56] Ph. V. Demekhin, Y.-C. Chiang, S. D. Stoychev, P. Kolorenč, S. Scheit, A. I. Kuleff, F. Tarantelli, L. S. Cederbaum, *J. Chem. Phys.* **2009**, *131*, 104303.
- [57] J. Zobeley, L. Cederbaum, F. Tarantelli, *J. Chem. Phys.* **1998**, *108*, 9737–9750.

- [58] I. B. Müller, L. S. Cederbaum, *J. Chem. Phys.* **2006**, *125*, 204305.
- [59] S. D. Stoychev, A. I. Kuleff, L. S. Cederbaum, *J. Chem. Phys.* **2010**, *133*, 154307.
- [60] R. Santra, J. Zobeley, L. Cederbaum, *Phys. Rev. B* **2001**, *64*, 245104.
- [61] R. Santra, L. Cederbaum, *Phys. Rep.* **2002**, *368*, 1–117.
- [62] R. Dörner, V. Mergel, O. Jagutzki, L. Spielberger, J. Ullrich, R. Moshhammer, H. Schmidt-Böcking, *Phys. Rep.* **2000**, *330*, 95–192.
- [63] J. Ullrich, R. Moshhammer, A. Dorn, R. Dörner, L.-P.-H. Schmidt, H. Schmidt-Böcking, *Rep. Prog. Phys.* **2003**, *66*, 1463–1545.
- [64] R. Weinkauff, P. Schanen, A. Metsala, E. Schlag, M. Burgle, H. Kessler, *J. Phys. Chem.* **1996**, *100*, 18567–18585.
- [65] R. Weinkauff, E. Schlag, T. Martinez, R. Levine, *J. Phys. Chem. A* **1997**, *101*, 7702–7710.
- [66] L. Cederbaum, J. Zobeley, *Chem. Phys. Lett.* **1999**, *307*, 205–210.
- [67] J. Breidbach, L. Cederbaum, *J. Chem. Phys.* **2003**, *118*, 3983–3996.
- [68] H. Hennig, J. Breidbach, L. Cederbaum, *J. Phys. Chem. A* **2005**, *109*, 409–414.
- [69] F. Remacle, R. Levine, M. Ratner, *Chem. Phys. Lett.* **1998**, *285*, 25–33.
- [70] G. Periyasamy, R. D. Levine, F. Remacle, *Chem. Phys.* **2009**, *366*, 129–138.
- [71] L. S. Cederbaum, *J. Chem. Phys.* **2008**, *128*, 124101.
- [72] S. Lünemann, A. I. Kuleff, L. S. Cederbaum, *Chem. Phys. Lett.* **2008**, *450*, 232–235.
- [73] S. Lünemann, A. I. Kuleff, L. S. Cederbaum, *J. Chem. Phys.* **2008**, *129*, 104305.
- [74] A. I. Kuleff, L. S. Cederbaum, *Chem. Phys.* **2007**, *338*, 320–328.
- [75] H. Hennig, J. Breidbach, L. Cederbaum, *J. Chem. Phys.* **2005**, *122*, 249901.
- [76] S. Lünemann, A. I. Kuleff, L. S. Cederbaum, *J. Chem. Phys.* **2009**, *130*, 154305.
- [77] A. I. Kuleff, L. S. Cederbaum, *Phys. Rev. Lett.* **2011**, *106*, 053001.
- [78] E. W. Schlag, S.-Y. Sheu, D.-Y. Yang, H. L. Selzle, S. H. Lin, *Angew. Chem.* **2007**, *119*, 3258–3273; *Angew. Chem. Int. Ed.* **2007**, *46*, 3196–3210.
- [79] L. Lehr, T. Horneff, R. Weinkauff, E. Schlag, *J. Phys. Chem. A* **2005**, *109*, 8074–8080.
- [80] F. Filsinger, U. Erlekam, G. von Helden, J. Küpper, G. Meijer, *Phys. Rev. Lett.* **2008**, *100*, 133003.
- [81] M. Taherkhani, M. Riese, M. BenYezzer, K. Müller-Dethlefs, *Rev. Sci. Instrum.* **2010**, *81*, 063101.
- [82] L. Poletto, P. Villorosi, E. Benedetti, F. Ferrari, S. Stagira, G. Sansone, M. Nisoli, *Opt. Lett.* **2007**, *32*, 2897–2899.
- [83] F. Remacle, R. D. Levine, *Z. Phys. Chem.* **2007**, *221*, 647–661.
- [84] F. Reiter, U. Graf, M. Schultze, W. Schweinberger, H. Schröder, N. Karpowicz, A. M. Azzeer, R. Kienberger, F. Krausz, E. Goulielmakis, *Opt. Lett.* **2010**, *35*, 2248–2250.
- [85] F. Reiter, U. Graf, E. E. Serebryannikov, W. Schweinberger, M. Fiess, M. Schultze, A. M. Azzeer, R. Kienberger, F. Krausz, A. M. Zheltikov, E. Goulielmakis, *Phys. Rev. Lett.* **2010**, *105*, 243902.
- [86] P. Corkum, *Phys. Rev. Lett.* **1993**, *71*, 1994–1997.
- [87] M. Lewenstein, P. Balcou, M. Ivanov, A. L'Huillier, P. Corkum, *Phys. Rev. A* **1994**, *49*, 2117–2132.
- [88] G. Sansone, C. Vozzi, S. Stagira, M. Nisoli, *Phys. Rev. A* **2004**, *70*, 013411.
- [89] M. B. Gaarde, J. L. Tate, K. J. Schafer, *J. Phys. B* **2008**, *41*, 132001.
- [90] M. Hentschel, R. Kienberger, C. Spielmann, G. Reider, N. Milosevic, T. Brabec, P. Corkum, U. Heinzmann, M. Drescher, F. Krausz, *Nature* **2001**, *414*, 509–513.
- [91] G. Sansone, E. Benedetti, F. Calegari, C. Vozzi, L. Avaldi, R. Flammini, L. Poletto, P. Villorosi, C. Altucci, R. Velotta, S. Stagira, S. De Silvestri, M. Nisoli, *Science* **2006**, *314*, 443–446.
- [92] H. Mashiko, S. Gilbertson, C. Li, S. D. Khan, M. M. Shakya, E. Moon, Z. Chang, *Phys. Rev. Lett.* **2008**, *100*, 103906.
- [93] X. Feng, S. Gilbertson, H. Mashiko, H. Wang, S. D. Khan, M. Chini, Y. Wu, K. Zhao, Z. Chang, *Phys. Rev. Lett.* **2009**, *103*, 183901.
- [94] M. J. Abel, T. Pfeifer, P. M. Nagel, W. Boutu, M. J. Bell, C. P. Steiner, D. M. Neumark, S. R. Leone, *Chem. Phys.* **2009**, *366*, 9–14.
- [95] F. Ferrari, F. Calegari, M. Lucchini, C. Vozzi, S. Stagira, G. Sansone, M. Nisoli, *Nat. Photonics* **2010**, *4*, 875–879.
- [96] O. Smirnova, Y. Mairesse, S. Patchkovskii, N. Dudovich, D. Villeneuve, P. Corkum, M. Y. Ivanov, *Nature* **2009**, *460*, 972–977.
- [97] H. Niikura, F. Légaré, R. Hasbani, M. Ivanov, D. Villeneuve, P. Corkum, *Nature* **2003**, *421*, 826–829.
- [98] G. Sansone, L. Poletto, M. Nisoli, *Nat. Photonics*, **2011**, *5*, 655–663.
- [99] T. Sekikawa, A. Kosuge, T. Kanai, S. Watanabe, *Nature* **2004**, *432*, 605–608.
- [100] P. Tzallas, D. Charalambidis, N. Papadogiannis, K. Witte, G. Tsakiris, *Nature* **2003**, *426*, 267–271.
- [101] Y. Nabekawa, T. Shimizu, T. Okino, K. Furusawa, H. Hasegawa, K. Yamanoouchi, K. Midorikawa, *Phys. Rev. Lett.* **2006**, *97*, 153904.
- [102] T. Shimizu, T. Okino, K. Furusawa, H. Hasegawa, Y. Nabekawa, K. Yamanoouchi, K. Midorikawa, *Phys. Rev. A* **2007**, *75*, 033817.
- [103] K. Midorikawa, Y. Nabekawa, A. Suda, *Prog. Quantum Electron.* **2008**, *32*, 43–88.
- [104] T. Okino, K. Yamanoouchi, T. Shimizu, R. Ma, Y. Nabekawa, K. Midorikawa, *J. Chem. Phys.* **2008**, *129*, 161103.
- [105] Y. Furukawa, Y. Nabekawa, T. Okino, S. Saugout, K. Yamanoouchi, K. Midorikawa, *Phys. Rev. A* **2010**, *82*, 013421.
- [106] F. Tavella, Y. Nomura, L. Veisz, V. Pervak, A. Marcinkevicius, F. Krausz, *Opt. Lett.* **2007**, *32*, 2227–2229.
- [107] F. Tavella, A. Willner, J. Rothhardt, S. Haedrich, E. Seise, S. Düsterer, T. Tschentscher, H. Schlarb, J. Feldhaus, J. Limpert, A. Tünnermann, J. Rossbach, *Opt. Express* **2010**, *18*, 4689–4694.
- [108] G. Tsakiris, K. Eidmann, J. Meyer-ter-Vehn, F. Krausz, *New J. Phys.* **2006**, *8*, 19.
- [109] A. D. Shiner, B. E. Schmidt, C. Trallero-Herrero, H. J. Wörner, S. Patchkovskii, P. B. Corkum, J.-C. Kieffer, F. Légaré, D. M. Villeneuve, *Nat. Phys.* **2011**, *7*, 464–467.
- [110] J. Itatani, F. Quéré, G. Yudin, M. Ivanov, F. Krausz, P. Corkum, *Phys. Rev. Lett.* **2002**, *88*, 173903.
- [111] M. Kitzler, N. Milosevic, A. Scrinzi, F. Krausz, T. Brabec, *Phys. Rev. Lett.* **2002**, *88*, 173904.
- [112] G. Sansone, *ChemPhysChem* **2010**, *11*, 3581–3583.
- [113] Y. Mairesse, F. Quéré, *Phys. Rev. A* **2005**, *71*, 011401.
- [114] R. Kienberger, E. Goulielmakis, M. Uiberacker, A. Baltuška, V. Yakovlev, F. Bammer, A. Scrinzi, T. Westerwalbesloh, U. Kleineberg, U. Heinzmann, M. Drescher, F. Krausz, *Nature* **2004**, *427*, 817–821.
- [115] M. Drescher, M. Hentschel, R. Kienberger, M. Uiberacker, V. Yakovlev, A. Scrinzi, T. Westerwalbesloh, U. Kleineberg, U. Heinzmann, F. Krausz, *Nature* **2002**, *419*, 803–807.
- [116] A. Emmanouilidou, A. Staudte, P. B. Corkum, *New J. Phys.* **2010**, *12*, 103024.
- [117] M. Uiberacker, Th. Uphues, M. Schultze, A. J. Verhoef, V. Yakovlev, M. F. Kling, J. Rauschenberger, N. M. Kabachnik, H. Schröder, M. Lezius, K. L. Kompa, H. G. Müller, M. J. Vrakking, S. Hendel, U. Kleineberg, U. Heinzmann, M. Drescher, F. Krausz, *Nature* **2007**, *446*, 627–632.
- [118] T. Uphues, M. Schultze, M. F. Kling, M. Uiberacker, S. Hendel, U. Heinzmann, N. M. Kabachnik, M. Drescher, *New J. Phys.* **2008**, *10*, 025009.
- [119] Z.-H. Loh, M. Khalil, R. E. Correa, R. Santra, C. Buth, S. R. Leone, *Phys. Rev. Lett.* **2007**, *98*, 143601.
- [120] Z.-H. Loh, S. R. Leone, *J. Chem. Phys.* **2008**, *128*, 204302.
- [121] L. Poletto, S. Bonora, M. Pascolini, P. Villorosi, *Rev. Sci. Instrum.* **2004**, *75*, 4413–4418.
- [122] S. H. Autler, C. H. Townes, *Phys. Rev.* **1955**, *100*, 703–722.

Received: July 9, 2011

Published online on December 8, 2011



Contents lists available at SciVerse ScienceDirect

Chemical Physics

journal homepage: www.elsevier.com/locate/chemphys

Electron-correlation-driven charge migration in oligopeptides

Alexander I. Kuleff*, Siegfried Lünemann, Lorenz S. Cederbaum

Theoretische Chemie, PCI, Universität Heidelberg, Im Neuenheimer Feld 229, 69120 Heidelberg, Germany

ARTICLE INFO

Article history:
Available online xxx

Keywords:
C-terminally methylamidated dipeptide
Ionization spectra
Ultrafast electron dynamics
Charge migration

ABSTRACT

Due to many-body effects an ultrafast removal of an electron from a molecule can trigger electron dynamics in which the created hole charge migrates throughout the system on a few-femtoseconds time scale. Here we report *ab initio* calculations of the positive-charge migration following inner-valence ionization of the C-terminally methylamidated dipeptide Gly–Gly–NH–CH₃. To investigate the influence of the molecular symmetry on the process, two different conformations of the system are studied. Our results show that in both conformers the charge initially localized on the methylamine end of the system migrates to the remote glycine in only 5–6 fs jumping thereby over an entire amino acid. Our computations also show that the symmetry of the system facilitates the process – a larger fraction of the charge migrates over a larger distance if the molecule is symmetric. Ionization spectra of both studied conformers are also reported.

© 2012 Elsevier B.V. All rights reserved.

1. Introduction

During the last decade tremendous development of laser pump–probe and ultrashort-pulse generation techniques (see, e.g., the review articles [1,2]) made possible a direct observation in real time of different kinds of ultrafast processes taking place in many-electron systems with sub-femtosecond resolution. With pulses as short as few tens of attoseconds available nowadays [3,4] one is able to initiate and probe processes that take place before the nuclear dynamics come into play, i.e. to study electron dynamics on their natural time scale. In particular, the possibility to characterize electronic processes determined by electron correlations, i.e. caused by the interaction between electrons, is attracting a great interest (for a recent review see Ref. [5]).

Among the processes that fall into this category is the phenomenon known as charge migration following ultrafast ionization of a many-electron system. More than 10 years ago it was shown [6] that after ionizing a molecular system the electronic many-body effects *alone* can beget rich ultrafast electron dynamics. The positive charge created after the ionization can migrate throughout the system on a time scale of only few femtoseconds *solely* driven by the electron correlation and electron relaxation [6,7]. This ultrafast redistribution of the electronic cloud can, of course, influence the nuclear dynamics which will come into play at later times, since, at least within the Born–Oppenheimer approximation, the electronic motion governs the effective potential seen by the nuclei. To draw conclusions on the reorganization of the molecular

structure and, from there, on the reactivity of the cationic system, it is thus of high importance to study this initial step of electron dynamics that follows the ionization.

This becomes especially important in the light of the series of pioneering experiments by Schlag, Weinkauff, and co-workers (see, e.g. [8–10] and references therein) showing site-selective reactivity of the electronically excited ionic states in oligopeptides. It was observed in these experiments that after a localized ionization on a specific site of a peptide chain, a bond breaking on a remote site of the chain occurs. The authors proposed that a fast electronic transfer mechanism is responsible for transporting the positive charge to the latter site of the molecule. Therefore, it is important to know to what extent the purely electronic mechanism of charge migration plays a role in bringing the charge to the remote end of the system.

Until now the efforts in studying the charge migration were concentrated in establishing the general mechanisms of the phenomenon and naturally only relatively small compounds (single amino acids or systems containing a single peptide bond) were studied. It was shown that the charge migration triggered by ionization is a general phenomenon taking place both after inner- [7,11–14] and outer-valence [15–18] ionization of molecules.

In order to connect between the charge migration and the site-selective reactivity in peptide chains observed by Schlag, Weinkauff, and co-workers, it is important to see whether the purely electronic charge migration mechanism is also operative in longer chain molecules and can bring an initially prepared localized charge to a remote side of the system, jumping over entire amino acid sites. As we will see the answer to this question is yes and in order to exemplify this we will present in this work results for

* Corresponding author.
E-mail address: alexander.kuleff@pci.uni-heidelberg.de (A.I. Kuleff).

the C-terminally methylamidated dipeptide Gly–Gly–NH–CH₃. The system consists of two glycine amino acids (Gly) and a NH–CH₃ terminus (see the sketch in Fig. 1).

It is also interesting, of course, to see whether the symmetry of the molecule plays a role in the charge migration process. That is why, in addition to the ground-state conformer of Gly–Gly–NH–CH₃, which does not possess any symmetry, we performed calculations on the symmetric conformer of the same oligopeptide. Our results show that the symmetry of the molecule does indeed play a role and facilitates the process. The charge can migrate over larger distances if the molecule possesses a symmetry.

2. Theoretical background

In this section we briefly describe the methodologies used in obtaining the results presented in this paper.

The structures of the ground-state and the symmetric conformers of the studied oligopeptide were optimized at MP2/TZVP level. All the remaining calculations were run using these geometry structures and standard Dunning DZ basis sets [19]. The ionization spectra of the Gly–Gly–NH–CH₃ were obtained using Green's function based method, namely the non-Dyson version of the algebraic diagrammatic construction (ADC) scheme correct up to third order of perturbation theory – ADC(3) [20].

A convenient quantity for tracing in time and space the migration of the positive charge created upon ionization is the so-called *hole density*. The hole density is defined as the difference between the electronic density of the neutral and that of the cation:

$$Q(\vec{r}, t) := \langle \Psi_0 | \hat{\rho}(\vec{r}, t) | \Psi_0 \rangle - \langle \Phi_i | \hat{\rho}(\vec{r}, t) | \Phi_i \rangle = \rho_0(\vec{r}) - \rho_i(\vec{r}, t), \quad (1)$$

where $\hat{\rho}$ is the density operator, $|\Psi_0\rangle$ is the ground state of the neutral, and $|\Phi_i\rangle$ is the initially prepared cationic state. The second term in Eq. (1), ρ_i , is time-dependent, since $|\Phi_i\rangle$ is not an eigenstate of the cation. The quantity $Q(\vec{r}, t)$ describes the density of the hole at position \vec{r} and time t and by construction is normalized at all times t . For calculating the hole density we use *ab initio* methods only. The cationic Hamiltonian, represented in an effective many-body basis via the Green's function method mentioned above, is used for directly propagating in the electronic space an initial state via the Lanczos technique [21,11]. The electronic wavepacket thus obtained is then utilized to construct the hole density at each time point via Eq. (1). Theoretical and technical details concerning construction and analysis of the hole density are given in Refs. [7,11–13].

Before presenting our results we would like to comment on the choice of the initial state $|\Phi_i\rangle$. In the numerical calculations to be discussed in this paper the initial state is prepared through a sudden removal of an electron from a particular Hartree–Fock (HF) orbital. The assumption made is that the ionized electron is removed from the system on a shorter time scale than that of the charge migration and that the interaction between the ionized electron and the remaining core can be neglected – sudden approximation (see, e.g., Refs. [22,23]). Such a situation can be realized when the ionization is performed, for example, by a high-energy photon (well above the corresponding ionization threshold) such that the removed electron has a high kinetic energy and thus

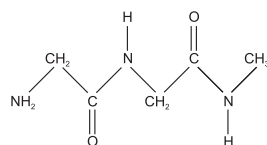


Fig. 1. Sketch of the chemical structure of the studied C-terminally methylamidated dipeptide consisting of two glycine amino acids (Gly) and a NH–CH₃ terminus (Gly–Gly–NH–CH₃).

leaves rapidly the interaction volume. In the weak-field regime, the pulse length will not play a role in the preparation of the state, as long as the intensity is weak enough such that the probability for multiphoton absorption is low. In strong-field regime, where multiphoton processes become important, in addition to the photon energy the pulse length becomes important. To minimize the probability of multiphoton absorption, the pulse should be extremely short, e.g., with a sub-femtosecond duration. In both cases, however, in order to observe field-free charge dynamics, it is preferable that the ionizing pulse is as short as possible.

Irrespective of the particular way of ionization, in the sudden ionization limit the remaining electrons will not have time to relax and therefore one may assume that the electron is removed from a single molecular orbital, being a result of an independent-particle model. The Hartree–Fock approximation provides the best independent-particle theory to describe the ionization since the many-body corrections to the ionization energies begin to contribute at a higher order of perturbation theory than with other choices of approximations [24]. That is why, we may assume that the initial hole created upon sudden ionization is described favorably by a HF-orbital. We have to note that the time needed for the other electrons to respond to a sudden creation of a hole is about 50 asec [25] (see also Ref. [26]). It was shown [25] that this time is universal, i.e. it does not depend on the particular system, and as such appears as the time scale of the electron correlation. Thus, in practice, sudden ionization is equivalent to ionization performed faster than the electron correlation. Although so short laser pulses are still not available (as we mentioned above the shortest pulse reported in the literature is ~80 asec [4]), we believe that in the not-so-distant future one will be able to approach this limit experimentally.

3. Results

In the first part of this section we report the ionization spectra of the ground-state and the symmetric conformers of the studied oligopeptide Gly–Gly–NH–CH₃, computed using the ADC(3) methodology mentioned above. In the second part, we study the charge migration process triggered by a sudden ionization out of an inner-valence orbital localized on the methylamine end of both conformers.

We would like to note that the calculations presented are done within a full active space. Only the core orbitals were frozen, resulting in 112 active orbitals (29 occupied). Thus, the electron dynamics computations, reported in the second part of this section, represent the response of 57 correlated electrons to the inner-valence ionization of Gly–Gly–NH–CH₃.

3.1. Ionization spectra

Let us first discuss the ground-state conformer of Gly–Gly–NH–CH₃. For the ease of interpretation of the results presented below, it is useful to formally represent the exact cationic state $|I\rangle$ as an expansion in a series of electronic configurations, as this is traditionally done in configuration interaction (CI) calculations (see, e.g. Ref. [24]):

$$|I\rangle = \sum_j c_j^{(I)} \hat{a}_j |\Psi_0\rangle + \sum_{a,k<l} c_{akl}^{(I)} \hat{a}_a^\dagger \hat{a}_k \hat{a}_l |\Psi_0\rangle + \dots \quad (2)$$

In Eq. (2) $|\Psi_0\rangle$ is the exact ground state of the neutral system and $c^{(I)}$'s are the expansion coefficients. The indices a, b, \dots refer to unoccupied (virtual) orbitals (or particles), whereas the indices i, j, \dots indicate occupied orbitals (or holes). The operators \hat{a}_a^\dagger (\hat{a}_i) are creation (annihilation) operators that create (annihilate) an electron on (from) the corresponding molecular orbital φ_a (φ_j).

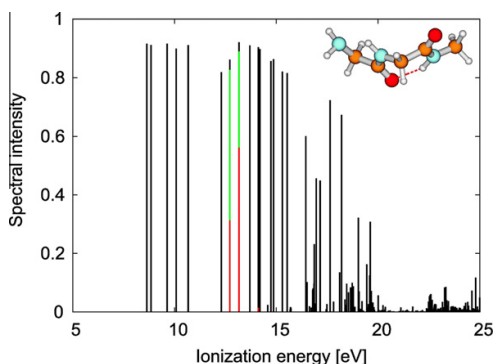


Fig. 2. Ionization spectrum of the ground-state conformer of Gly-Gly-NH-CH₃ (shown in the inset) computed using the *ab initio* many-body Green's function method ADC(3). Each vertical line shown is related to a final cationic state and is located at the corresponding ionization energy. The colors are related to different 1 h-configurations resulting from the removal of an electron out of a specific HF-orbital. The contributions of the 1 h configuration (33a)⁻¹ to the cationic states are given in red, while the contributions of the (32a)⁻¹ configuration in green. (For interpretation of the references to colour in this figure legend, the reader is referred to the web version of this article.)

Accordingly, the terms $\hat{a}_i|\Psi_0\rangle$ are called one-hole (1h) configurations, since one electron has been removed from the corresponding occupied orbital, the terms $\hat{a}_i^\dagger\hat{a}_k\hat{a}_i|\Psi_0\rangle$ are referred to as two-hole-one-particle (2h1p) configurations, indicating that in addition to the removal of one electron another one is excited to a virtual orbital, and so forth. Note that in the ADC approach used, which accounts also for the ground-state correlations, in Eq. (2) the expansion is applied on the exact ground state $|\Psi_0\rangle$, rather than on the uncorrelated Hartree-Fock one $|\Phi_0\rangle$ as in usual CI calculations.

The analysis in terms of configurations that the representation (2) of the cationic state allows is very useful for the proper understanding of the electron dynamics that follow the ionization of the system under study.

The ionization spectrum of the molecule obtained via non-Dyson ADC(3) approach is shown in Fig. 2 and the states up to 15 eV are listed in Table 1. Each line in the calculated spectrum represents a cationic eigenstate $|I\rangle$ (see Eq. (2)). The position of the line is given by the ionization energy, and its height – by the absolute square of the transition amplitude $\langle\Psi_i|I\rangle$. The latter is called pole strength, or spectral intensity, and is related to the ionization cross section (see Ref. [27]). As $|\Psi_i\rangle$ is obtained by removing an electron from a particular HF orbital ($|\Psi_i\rangle = \hat{a}_i|\Psi_0\rangle$), it is clear that only 1h configurations contribute to the spectral intensity.

Let us now take a closer look at the two cationic states located at 12.7 eV and 13.2 eV, respectively (see also Table 1). The analysis of these states shows that they are built mainly from two 1h configurations – one that corresponds to the removal of an electron from orbital 33a and one that corresponds to the removal of an electron from orbital 32a. In Fig. 2 the contributions of these 1h configurations are depicted in red and green, respectively. Thus, we encounter the situation known as *hole mixing* [28] where two (or more) lines in the spectrum are linear combinations of two (or more) 1h configurations. Note that the mixing of these 1h configurations is due to the many-body effects, i.e. to their mutual coupling to 2h1p and higher configurations (see expansion (2)). Therefore, if we prepare an initial state by taking out an electron from orbital 33a, we will create a state which can be represented as a linear combination of the two states at 12.7 eV and 13.2 eV, with a bigger overlap with the state at 13.2 eV. This coupling of ionic states introduced by a removal of the electron from a particular molecular orbital (MO) is responsible for the charge-migration

Table 1
Ionization potentials (in eV) of the two studied conformers of Gly-Gly-NH-CH₃ up to 15 eV obtained via non-Dyson ADC (3) method using Dunning DZ basis sets [19]. The spectral intensities (SI) are given in columns 2 and 5. The assignments of the states made by the leading 1h contribution (given in brackets) are listed in columns 3 and 6. The states discussed in the text and given in colors in Figs. 2 and 3 are denoted by '*'.

GS conformer		Assignment	C _s conformer		Assignment
IP	SI		IP	SI	
8.64	0.92	39a (0.90)	9.07	0.93	31a' (0.92)
8.84	0.91	38a (0.90)	9.19	0.92	8a' (0.90)
9.64	0.92	37a (0.88)	9.80	0.92	7a' (0.90)
10.08	0.90	36a (0.86)	9.98	0.90	30a' (0.88)
10.67	0.91	35a (0.88)	10.45	0.90	29a' (0.88)
12.30	0.82	34a (0.79)	12.28	0.88	6a' (0.86)
12.72*	0.86	32a (0.52)	13.07	0.86	5a' (0.83)
13.17*	0.92	33a (0.56)	13.90*	0.91	27a' (0.49)
13.71	0.91	31a (0.83)	14.19	0.87	4a' (0.81)
14.12	0.90	30a (0.77)	14.28*	0.92	28a' (0.38)
14.20	0.90	29a (0.83)	14.53*	0.92	26a' (0.40)
14.58	0.02	25a (0.01)	14.67*	0.92	25a' (0.52)
14.74	0.86	28a (0.69)			
14.87	0.86	27a (0.74)			

phenomenon that we will discuss in the following subsection. If the electrons were not correlated the ionic states would be represented by single 1h configurations (independent-particle model) and hence no coupling, respectively no electron dynamics will appear. The charge migration phenomenon is, therefore, solely due to the electron correlation and relaxation effects.

Before discussing the results for the symmetric conformer of Gly-Gly-NH-CH₃, we would like to note that the analysis of our results show that all the states lying energetically below the two states discussed above are 1h states (see Table 1), i.e. they are almost entirely built from single 1h configurations and therefore an ionization out of the corresponding orbitals does not introduce a coupling between ionic states and hence will not trigger electron dynamics.

Now let us see how the ionization spectrum changes when the molecule is in C_s symmetry. The ionization spectrum of the symmetric molecule obtained via non-Dyson ADC(3) approach is shown in Fig. 3 and the states up to 15 eV are listed in Table 1. The states belonging to the different irreducible representations of the C_s symmetry group are depicted in black (a') and grey (a''). Apart from the small absolute and relative shifts of the states up to about 15 eV, the overall shape of the outer-valence part of the spectrum is very similar. One clearly distinguishes two groups of states – the first group of 5 states around 10 eV separated by about 2 eV from the second group of states between 12 and 15 eV. Above about 15 eV when the correlation effects become stronger the spectra start to differ substantially.

Despite of the overall similarity, however, the character of some of the states between 12 and 15 eV is different for the two molecular geometries of the studied molecule. There are four close lying states between 13.7 and 14.6 eV that are strongly coupled via the mixing of four 1h configurations (see also Table 1). The contributions of these 1h configurations to these four states are depicted in different colors in Fig. 3 – (28a')⁻¹ is given in red, (27a')⁻¹ in green, (26a')⁻¹ in pink, and (25a')⁻¹ in blue. Therefore, the ionization out of the orbital 28a', which, as the orbital 33a of the ground-state conformer, is localized mainly on the methylamine end of the molecule, will populate coherently four states. Already at this point one can expect that creating an initial state corresponding to a hole localized on the methylamine end of the molecule will trigger different electron dynamics in the two conformers.

We would like to note that also in the symmetric conformer all the states lying energetically below the just discussed four ionic states are 1h states (see Table 1) and therefore not coupled to each other.

4

A.I. Kuleff et al. / Chemical Physics xxx (2012) xxx–xxx

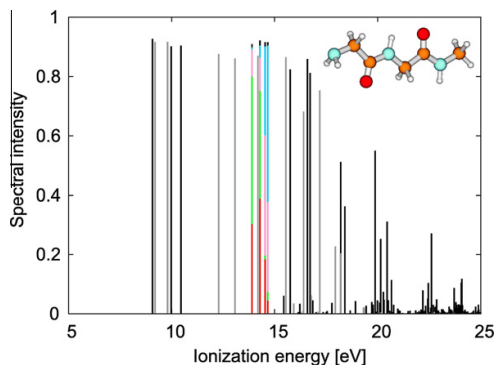


Fig. 3. Ionization spectrum of the C_s symmetric conformer of Gly-Gly-NH-CH₃ (shown in the inset) computed using the *ab initio* many-body Green's function method ADC (3). Each vertical line shown is related to a final cationic state and is located at the corresponding ionization energy. The states belonging to the a' irrep are plotted in black and those belonging to a'' irrep in gray. All other colors are related to different 1h configurations resulting from the removal of an electron out of a specific HF-orbital. The contributions of the 1h configuration $(28a')^{-1}$ to the cationic states are given in red, those of the $(27a')^{-1}$ configuration in green, those of $(26a')^{-1}$ in pink, and those of $(26a'')^{-1}$ in blue. (For interpretation of the references to colour in this figure legend, the reader is referred to the web version of this article.)

3.2. Electron dynamics after valence ionization

We analyze first the ground-state conformer of the molecule Gly-Gly-NH-CH₃. As it was discussed in the previous subsection, the ionization out of the orbital $33a$ populates mainly 2 cationic states lying at 12.7 eV and 13.2 eV, respectively. Thus, the removal of an electron from this orbital creates a wavepacket which is a coherent superposition mainly of these 2 states. Of course, the $(33a)^{-1}$ configuration participates in, and thus couples, many other states, but their influence on the correlated dynamics is much weaker due to the small contribution of this 1h configuration to those states. The situation when the ionization creates a coupling between two states via hole mixing was studied in details in Ref. [7]. In this case oscillatory dynamics are expected with a period of the oscillations determined by the energy difference between the coupled states.

Snapshots of the hole density $Q(\vec{r}, t)$ following sudden ionization out of the orbital $33a$ are shown in Fig. 4 for the first 5 fs. As seen, the hole is initially localized mainly on the methylamine end of the molecule. As time proceeds, the charge starts to migrate to the "left" glycine and after only 5 fs a large fraction of it is localized mainly on the left carbonyl group. As expected from the

two-hole mixing mechanism, after that time the process continues in a reversed order and after about 9 fs the charge returns back on the methylamine side. The energy difference between the two coupled states is 0.45 eV corresponding to an oscillating period of about 9.3 fs.

This charge oscillation will be strongly perturbed at later times by the nuclear dynamics. At the same time, the way the nuclei will start to move will be, of course, influenced by this fast charge reorganization, as it will predetermine the effective potential seen by the nuclei. We would like also to mention that the reorganization of the electronic cloud will also introduce ultrafast changes of the electric dipole moment of the system. It was recently shown that these fluctuations of the dipole moment in a few-femtosecond time scale generate a characteristic radiation in the infrared spectrum [18].

Let us now see how the symmetry of the molecule can influence the electron dynamics following an ultrafast ionization. For this purpose we trace the evolution of the electronic cloud after a sudden removal of an electron from an orbital the orbital $28a'$ of the C_s symmetric conformer. This orbital is very similar to the orbital $33a$ of the ground-state conformer and is also localized mainly on the methylamine end of the molecule. However, as we saw in the preceding subsection, the ionization out of the orbital $28a'$ strongly couples four ionic states. We encounter, therefore, the situation of four-hole mixing. In this case, the dynamics are more involved and although again oscillatory a beating pattern, coming from the different oscillation periods involved, is expected. It is seen from Fig. 3 that the strongest coupling is between the states located at 13.9 and 14.3 eV and, therefore, the leading oscillation period is about 5.5 fs.

Snapshots of the hole density $Q(\vec{r}, t)$ following sudden ionization out of the orbital $28a'$ are shown in Fig. 5 for the first 6 fs. We see that starting from the methylamine site the charge almost completely migrates to the other side of the molecule in about 6 fs. The process then continues in a reverse order bringing the charge back to the methylamine site. However, these oscillations are not purely repetitive and exhibit a beating pattern due to the other states involved.

Comparing the first few femtoseconds of electron dynamics in the two studied conformers of Gly-Gly-NH-CH₃ (see Figs. 4 and 5) we see that when the molecule is symmetric nearly the whole charge migrates to the remote end of the system, while in the non-symmetric case only a fraction of the charge migrates and, in addition, it never reaches the other end of the molecule. One may tend to conclude that the bent structure of the non-symmetric ground-state conformer "impedes" the flow of the charge and that is why it cannot reach the other end of the molecule being trapped at the carbonyl group. Although attractive, such an interpretation does not reflect the quantum nature of the charge migration

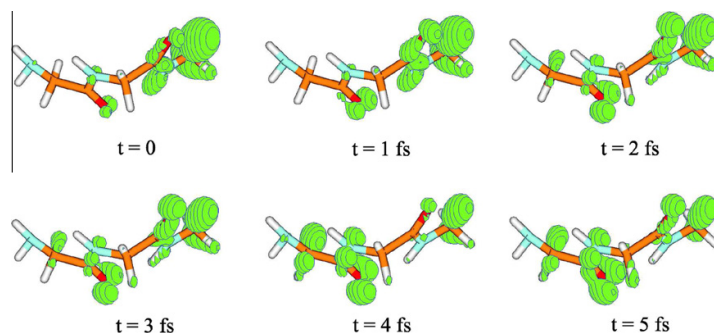


Fig. 4. Snapshots of the evolution of the hole density $Q(\vec{r}, t)$ after ionization out of orbital $33a$ of the ground-state conformer of Gly-Gly-NH-CH₃.

A.I. Kuleff et al./Chemical Physics xxx (2012) xxx–xxx

5

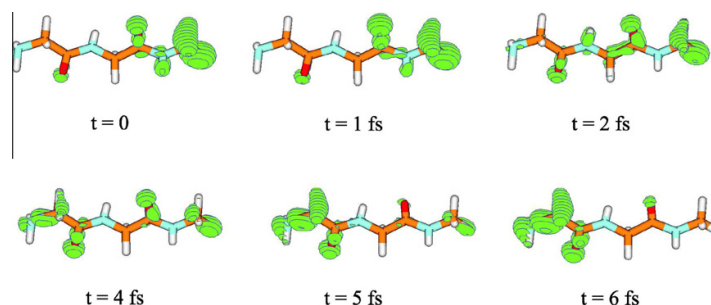


Fig. 5. Snapshots of the evolution of the hole density $Q(\vec{r}, t)$ after ionization out of orbital $28a'$ of the C_s symmetric conformer of Gly-Gly-NH-CH₃.

phenomenon. The charge actually does not flow from one side of the system to another along the molecular backbone. As can be seen from Figs. 4 the hole charge which disappears from its initial position appears on its final one without showing up in between. This behavior is a typical signature of the many-body character of the underlying charge migration mechanism. The charge movement is actually mediated by the large number of $2h1p$ configurations to which the corresponding $1h$ configurations are coupled. The symmetry of the system, however, does play a role by facilitating these couplings. It seems that in the symmetric case the $2h1p$ configurations are more extended in space and, therefore, two remote orbitals can indirectly couple to each other via their direct interaction to these excitations.

At the end we would like to briefly comment on the preparation of the initial state and its practical realizability. In reality, a short pulse that is able to remove an electron from the orbital $33a$ or $28a'$ and therefore to coherently populate the corresponding number of ionic states around 13–14 eV, will have enough energy to populate all the states lying lower in energy. The probability to populate those states will be proportional to the square of the corresponding transition matrix elements. As we noted in the previous subsection, all the states lying below the group around 13–14 eV are $1h$ states. Thus, in reality, an ultrashort pulse will create an initial state being some linear combination of the $1h$ configurations corresponding to ionization out of the molecular orbitals contributing to the group of states around 13–14 eV and all the states lying below. The dynamical evolution of such an initial state will be, therefore, a superposition of the dynamics that one would expect if we were able to address each individual orbital separately, weighted by the corresponding probabilities. A sudden ionization out of the MOs contributing to the states lying below the group around 13–14 eV will not trigger electron dynamics – the created hole will be stationary, since ionization out of these orbitals does not couple different ionic states. We might, therefore, conclude that the electron dynamics triggered by the preparation of such more involved and realistic state will be predominantly governed by the dynamics triggered by $(33a)^{-1}$ and $(28a')^{-1}$ alone which are discussed above.

4. Conclusion

We have performed an *ab initio* study of the ultrafast migration of the positive charge created upon inner-valence ionization of the C-terminally methylamidated dipeptide, Gly-Gly-NH-CH₃. In order to study the influence of the molecular symmetry on the process we have performed calculations on two of the conformers of the system – the ground-state non-symmetric conformer and a conformation in which the system belongs to the C_s symmetry. Our results show that in both conformations after creating a hole localized on the methylamine end of the system the charge

migrates to the remote glycine in about 5–6 fs. If the nuclei would stay fixed, the charge would oscillate between the methylamine and the remote glycine. The nuclear dynamics, however, will come into play at later times and will perturb these oscillations, since the charge migration is very sensitive to the momentary configuration of the nuclear skeleton [14,17]. The movement of the nuclei may eventually trap the charge on the remote site and thus achieve irreversibility of the process, i.e. an effective transfer of the charge from one moiety of the system to another.

Final comments are in order. Several models for explaining the site-selective reactivity observed in peptide chains have been proposed in the literature [29–31]. All those models rely on some hopping mechanism in which the charge is supposed to hop from one amino acid to the next one along the peptide chain. Although not in contradiction and not excluding such plausible mechanisms, our results show that due to the electron correlation the charge can jump over entire amino acids and not necessarily flow along the molecular backbone site by site. We would like to mention that similar charge migration behavior following ionization in oligopeptides was reported also by Remacle and Levine [32]. We note, however, that the theoretical method used by Remacle and Levine is not fully adequate to the problem and the reported dynamics could be an artifact of the methodology used (see, Ref. [33]).

The effect of the molecular symmetry found by us may also be related to the “rest and fire” mechanism of charge transfer suggested by Schlag et al. [30,31]. In this bifunctional mechanism the charge is supposed to reside on the corresponding site (amino acid) until the Ramachandran rotations [34] bring the adjacent amino acids to a particular orientation with respect to each other, opening the “door” for the charge to move to the next amino acid. This “firing state” appeared to be the symmetric configuration of the carbonyls of the two adjacent sites as in the case of our symmetric conformation (see in the inset of Fig. 3). Our results confirm that for some molecular geometries the charge migration is indeed strongly enhanced. However, in this case the charge migrates over longer distances jumping over entire amino acids.

Clearly, in the site-selective reactivity in peptide chains a complicated interplay between electron and nuclear dynamics takes place and more thorough and systematic studies are needed for a proper understanding of the underlying mechanism. We hope that our work will stimulate such studies.

Acknowledgments

Financial support by the DFG is gratefully acknowledged.

References

- [1] F. Krausz, M. Ivanov, Rev. Mod. Phys. 81 (2009) 163.
- [2] M. Nisoli, G. Sansone, Prog. Quant. Electron. 33 (2009) 17.

ARTICLE IN PRESS

- 6 *A.I. Kuleff et al./Chemical Physics xxx (2012) xxx–xxx*
- [3] G. Sansone, E. Benedetti, F. Calegari, C. Vozzi, L. Avaldi, R. Flammini, L. Poletto, P. Villoresi, C. Altucci, R. Velotta, S. Stagira, S. De Silvestri, M. Nisoli, *Science* 314 (2006) 443.
- [4] E. Goulielmakis, M. Schultze, M. Hofstetter, V.S. Yakovlev, J. Gagnon, M. Uiberacker, A.L. Aquila, E.M. Gullikson, D.T. Attwood, R. Kienberger, F. Krausz, U. Kleineberg, *Science* 320 (2008) 1614.
- [5] G. Sansone, T. Pfeifer, K. Simeonidis, A.I. Kuleff, *ChemPhysChem* 13 (2012) 661.
- [6] L.S. Cederbaum, J. Zobeley, *Chem. Phys. Lett.* 307 (1999) 205.
- [7] J. Breidbach, L.S. Cederbaum, *J. Chem. Phys.* 118 (2003) 3983.
- [8] R. Weinkauf, P. Aicher, G. Wesley, J. Grote Meyer, E.W. Schlag, *J. Phys. Chem.* 98 (1994) 8381.
- [9] R. Weinkauf, E.W. Schlag, T.J. Martinez, R.D. Levine, *J. Phys. Chem. A* 101 (1997) 7702.
- [10] E.W. Schalg, S.-Y. Sheu, D.-Y. Yang, H.L. Selzle, S.H. Lin, *Angew. Chem. Int. Ed.* 46 (2007) 3196.
- [11] A.I. Kuleff, J. Breidbach, L.S. Cederbaum, *J. Chem. Phys.* 123 (2005) 044111.
- [12] H. Hennig, J. Breidbach, L.S. Cederbaum, *J. Phys. Chem. A* 109 (2005) 409.
- [13] J. Breidbach, L.S. Cederbaum, *J. Chem. Phys.* 126 (2007) 034101.
- [14] A.I. Kuleff, L.S. Cederbaum, *Chem. Phys.* 338 (2007) 320.
- [15] S. Lünemann, A.I. Kuleff, L.S. Cederbaum, *Chem. Phys. Lett.* 450 (2008) 232.
- [16] S. Lünemann, A.I. Kuleff, L.S. Cederbaum, *J. Chem. Phys.* 130 (2009) 154305.
- [17] S. Lünemann, A.I. Kuleff, L.S. Cederbaum, *J. Chem. Phys.* 129 (2008) 104305.
- [18] A.I. Kuleff, L.S. Cederbaum, *Phys. Rev. Lett.* 106 (2011) 053001.
- [19] T.H. Dunning Jr., *J. Chem. Phys.* 53 (1970) 2823.
- [20] J. Schirmer, A.B. Trofimov, G. Stelter, *J. Chem. Phys.* 109 (1998) 4734.
- [21] C. Leforestier, R.H. Bisseling, C. Cerjan, M.D. Feit, R. Friesner, A. Gulberg, A. Hammerich, G. Jolicard, W. Karrlein, H.-D. Meyer, N. Lipkin, O. Roncero, R. Kosloff, *J. Comput. Phys.* 94 (1991) 59.
- [22] H.W. Meldner, J.D. Perez, *Phys. Rev. A* 4 (1971) 1388.
- [23] B.T. Pickup, *Chem. Phys.* 19 (1977) 193.
- [24] A. Szabo, N.S. Ostlund, *Modern Quantum Chemistry*, McGraw-Hill, New York, 1989.
- [25] J. Breidbach, L.S. Cederbaum, *Phys. Rev. Lett.* 94 (2005) 033901.
- [26] A.I. Kuleff, L.S. Cederbaum, *Phys. Rev. Lett.* 98 (2007) 083201.
- [27] L.S. Cederbaum, W. Domcke, *Adv. Chem. Phys.* 36 (1977) 205.
- [28] W. von Niessen, G. Bieri, J. Schirmer, L.S. Cederbaum, *Chem. Phys.* 65 (1982) 157.
- [29] F. Remacle, R.D. Levine, M.A. Ratner, *Chem. Phys. Lett.* 285 (1998) 25.
- [30] E.W. Schlag, S.-Y. Sheu, D.-Y. Yang, H.L. Selzle, S.H. Lin, *Proc. Natl. Acad. Sci. USA* 97 (2000) 1068.
- [31] E.W. Schlag, S.-Y. Sheu, D.-Y. Yang, H.L. Selzle, S.H. Lin, *J. Phys. Chem. B* 104 (2000) 7790.
- [32] F. Remacle, R.D. Levine, *Proc. Natl. Acad. Sci. USA* 103 (2006) 6793.
- [33] A.I. Kuleff, A. Dreuw, *J. Chem. Phys.* 130 (2009) 034102.
- [34] G.N. Ramachandran, C. Ramakrishnan, V. Sasisekharan, *J. Mol. Biol.* 7 (1963) 95.

Appendix A

Full list of publications

1. R. L. Pavlov, J. Maruani, Ya. I. Delchev et A. I. Kuleff, *Theorie de la fonctionnelle de la densité avec spin. VIII. Equation d'Euler-Lagrange pour $f(r)$* , C. R. Acad. Sci. Paris, **325**, série II b, 719 (1997).
2. Ya. I. Delchev, A. I. Kuleff, J. Maruani, and R. L. Pavlov, *A consistent calculation of atomic energy shell corrections Strutinsky's method in the Hartree-Fock-Roothaan scheme*, Adv. Quantum Chem. **31**, 53 (1998).
3. J. Maruani, S. Drenska, A. Kuleff, P. Raychev, and P. Terziev, *Supershell quantization of staggering patterns in the rotational bands of the iodine molecule*, Phys. Rev. A **62**, 022511 (2000).
4. R. L. Pavlov, A. I. Kuleff, P. Tz. Yotov, and J. Maruani, *Reduced density-matrix treatment of spin-spin interaction terms in many-electron systems*, Adv. Quantum Chem. **39**, 295 (2001).
5. J. Maruani, A. Khoudir, A. Kuleff, M. Tronc, G. Giorgi, and C. Bonnelle, *A method of combined treatment for evaluation of core excitation energies in molecules involving heavy atoms: application to CrF_6 , MoF_6 , and WF_6* , Adv. Quantum Chem. **39**, 307 (2001).
6. A. I. Kuleff, J. Maruani, and P. P. Raychev, *Reproduction of the metal-cluster magic numbers using a q -deformed, 3-dimensional, harmonic oscillator model*, Adv. Quantum Chem. **40**, 279 (2001).
7. Ya. I. Delchev, A. I. Kuleff, P. Tz. Yotov, J. Maruani, and R. L. Pavlov, *Orbital local-scaling transformation approach: fermionic systems in the ground states*, Progr. Theor. Chem. & Phys. B **6**, 45 (2001).
8. R. L. Pavlov, A. I. Kuleff, P. Tz. Yotov, J. Maruani, and Ya. I. Delchev, *Reduced density-matrix treatment of spin-orbit interaction terms in many-electron systems*, Progr. Theor. Chem. & Phys. B **6**, 63 (2001).
9. A. I. Kuleff, Ya. I. Delchev, P. Tz. Yotov, Tz. Mineva, and J. Maruani, *Formulation of Strutinsky's method for atomic systems in the extended Kohn-Sham scheme*, Int. J. Quantum Chem. **89**, 217 (2002).
10. D. Bonatsos, A. I. Kuleff, J. Maruani, P. P. Raychev, and P. A. Terziev, *Derivation of shell effects and magic numbers in metal clusters by the application of Strutinsky's method to the Clemenger-Nilsson and q -deformed 3-D harmonic oscillator models*, Int. J. Quantum Chem. **89**, 377 (2002).

11. J. Maruani, A. I. Kuleff, Ya. I. Delchev, and C. Bonnelle, *Shell effects in the relaxation energy of 1s-core ionization of atoms from He through Xe*, in E. S. Kryachko and E. J. Brändas (eds), *Fundamental Aspects in Quantum Chemistry: A tribute volume to the memory of Per-Olov Löwdin*, vol. 1, p. 639 (Kluwer, Dordrecht, 2003)
12. A. I. Kuleff, J. Maruani, and P. P. Raychev, *Search for isotope effects in $\Delta J = 1$ staggering patterns of diatomic molecules*, *Progr. Theor. Chem. & Phys. B* **12**, 361 (2003).
13. Ya. I. Delchev, A. I. Kuleff, Tz. Mineva, F. Zahariev, and J. Maruani, *Strutinsky's shell-correction method in the extended Kohn-Sham scheme for the investigation of binding energies of atoms and cations in the ground state*, *Int. J. Quantum Chem.* **99**, 265 (2004).
14. J. Maruani, A. I. Kuleff, Ya. I. Delchev, and C. Bonnelle, *Shell effects in the relaxation energy of 2s-core ionization of atoms from B through Xe*, *Israel J. Chem.* **44**, 71 (2004).
15. J. Maruani, A. I. Kuleff, D. P. Chong, and C. Bonnelle, *Ansatz for the evaluation of the relativistic contributions to core ionization energies in complex molecules involving heavy atoms*, *Int. J. Quantum Chem.* **104**, 397 (2005).
- * 16. A. I. Kuleff, J. Breidbach, and L. S. Cederbaum, *Multielectron wave-packet propagation: General theory and application*, *J. Chem. Phys.* **123**, 044111 (2005).
17. Ya. I. Delchev, A. I. Kuleff, J. Maruani, Tz. Mineva, and F. Zahariev, *Strutinsky's shell-correction method in the extended Kohn-Sham scheme: application to the ionization potential, electron affinity, electronegativity and chemical hardness of atoms*, *Prog. Theor. Chem. & Phys. B* **15**, 159 (2006).
18. X.-J. Liu, N. Saito, H. Fukuzawa, Y. Morishita, S. Stoychev, A. Kuleff, I. H. Suzuki, Y. Tamenori, R. Richter, G. Prümper, and K. Ueda, *Evidence of sequential interatomic decay in argon trimers obtained by electron-triple-ion coincidence spectroscopy*, *J. Phys. B* **40**, F1 (2007).
- * 19. A. I. Kuleff and L. S. Cederbaum, *Tracing ultrafast interatomic electronic decay processes in real time and space*, *Phys. Rev. Lett.* **98**, 083201 (2007).
20. N. Saito, Y. Morishita, I. H. Suzuki, S. D. Stoychev, A. I. Kuleff, L. S. Cederbaum, X.-J. Liu, H. Fukuzawa, G. Prümper, and K. Ueda, *Evidence of radiative charge transfer in argon dimers*, *Chem. Phys. Lett.* **441**, 16 (2007).
- * 21. A. I. Kuleff and L. S. Cederbaum, *Charge migration in different conformers of glycine: The role of nuclear geometry*, *Chem. Phys.* **338**, 320 (2007).
22. S. D. Stoychev, A. I. Kuleff, F. Tarantelli, and L. S. Cederbaum, *On the doubly ionized states of Ar_2 and their intra- and interatomic decay to Ar_2^{3+}* , *J. Chem. Phys.* **128**, 014307 (2008).
- * 23. S. Lünemann, A. I. Kuleff, and L. S. Cederbaum, *Ultrafast charge migration in 2-Phenylethyl-N,N-dimethylamine*, *Chem. Phys. Lett.* **450**, 232 (2008).
24. S. D. Stoychev, A. I. Kuleff, F. Tarantelli, and L. S. Cederbaum, *On the interatomic electronic processes following Auger decay in neon dimer*, *J. Chem. Phys.* **129**, 074307 (2008).
- * 25. S. Lünemann, A. I. Kuleff, and L. S. Cederbaum, *Charge migration following ionization in systems with chromophore-donor and amine-acceptor sites*, *J. Chem. Phys.* **129**, 104305 (2008).
- * 26. A. I. Kuleff and A. Dreuw, *Theoretical description of charge migration with a single Slater-determinant and beyond*, *J. Chem. Phys.* **130**, 034102 (2009).

- * 27. S. Lünemann, A. I. Kuleff, and L. S. Cederbaum, *Ultrafast electron dynamics following outer-valence ionization: The impact of low-lying relaxation satellite states*, J. Chem. Phys. **130**, 154305 (2009).
- * 28. A. I. Kuleff, S. Lünemann, and L. S. Cederbaum, *Ultrafast charge migration following ionization in oligopeptides* in *Ultrafast Phenomena XVI*, edited by P. Corkum, S. De Silvestri, K. Nelson, E. Riedle, and R. W. Schoenlein (Springer Series in Chemical Physics, 2009), p. 586.
- 29. Ph. V. Demekhin, Y.-C. Chiang, S. D. Stoychev, P. Kolorenč, S. Scheit, A. I. Kuleff, F. Tarantelli, and L. S. Cederbaum, *Interatomic Coulombic decay in NeAr following K-LL Auger transition in the Ne atom*, J. Chem. Phys. **131**, 104303 (2009).
- 30. Y.-C. Chiang, P. V. Demekhin, A. I. Kuleff, S. Scheit, and L. S. Cederbaum, *Linewidth and lifetime of atomic levels and the time evolution of spectra and coincidence spectra*, Phys. Rev. A **81**, 032511 (2010).
- * 31. A. I. Kuleff, S. Lünemann, and L. S. Cederbaum, *Ultrafast charge migration following valence ionization of 4-methylphenol: jumping over the aromatic ring*, J. Phys. Chem. A **114**, 8676 (2010).
- 32. A. I. Kuleff, K. Gokhberg, S. Kopelke, and L. S. Cederbaum, *Ultrafast interatomic electronic decay in multiply excited clusters*, Phys. Rev. Lett. **105**, 043004 (2010).
- 33. S. D. Stoychev, A. I. Kuleff, and L. S. Cederbaum, *On the intermolecular Coulombic decay of singly and doubly ionized states of water dimer*, J. Chem. Phys. **133**, 154307 (2010).
- 34. K. Sakai, S. Stoychev, T. Ouchi, I. Higuchi, M. Schöffler, T. Mazza, H. Fukuzawa, K. Nagaya, M. Yao, Y. Tamenori, A. I. Kuleff, N. Saito, and K. Ueda, *Electron-transfer-mediated decay and interatomic Coulombic decay from the triply ionized states in argon dimers*, Phys. Rev. Lett. **106**, 033401 (2011).
- * 35. A. I. Kuleff and L. S. Cederbaum, *Radiation generated by the ultrafast migration of a positive charge following the ionization of a molecular system*, Phys. Rev. Lett. **106**, 053001 (2011).
- 36. V. Averbukh, Ph. V. Demekhin, P. Kolorenč, S. Scheit, S. D. Stoychev, A. I. Kuleff, Y. Chiang, K. Gokhberg, S. Kopelke, N. Sisourat, and L. S. Cederbaum, *Interatomic Coulombic decay processes in singly and multiply ionized clusters*, J. Electr. Spectr. Rel. Phen. **183**, 36 (2011).
- 37. M. Pernpointner, A. I. Kuleff, and L. S. Cederbaum, *Tracing ultrafast electron dynamics by modern propagator approaches*, in *Modeling of Molecular Properties*, edited by P. Comba (Wiley-VCH, Weinheim, 2011), p. 65.
- 38. T. Ouchi, K. Sakai, H. Fukuzawa, X.-J. Liu, I. Higuchi, Y. Tamenori, K. Nagaya, H. Iwayama, M. Yao, D. Zhang, D. Ding, A. I. Kuleff, S. D. Stoychev, Ph. V. Demekhin, N. Saito, and K. Ueda, *Three-electron interatomic Coulombic decay from the inner-valence double-vacancy states in NeAr*, Phys. Rev. Lett. **107**, 053401 (2011).
- 39. S. D. Stoychev, A. I. Kuleff, and L. S. Cederbaum, *Intermolecular Coulombic decay in small biochemically relevant hydrogen bonded systems*, J. Am. Chem. Soc. **133**, 6817 (2011).
- 40. T. Ouchi, K. Sakai, H. Fukuzawa, I. Higuchi, Ph. V. Demekhin, Y.-C. Chiang, S. D. Stoychev, A. I. Kuleff, T. Mazza, M. Schöffler, K. Nagaya, M. Yao, Y. Tamenori, N. Saito, and K. Ueda, *Interatomic Coulombic decay following Ne 1s Auger decay in NeAr*, Phys. Rev. A **83**, 053415 (2011).

- * 41. A. I. Kuleff, S. Lünemann, and L. S. Cederbaum, *Ultrafast reorganization of the hole charge created upon outer-valence ionization of porphyrins*, Chem. Phys. (in press)
DOI:10.1016/j.chemphys.2011.10.015.
- 42. Ph. V. Demekhin, S. D. Stoychev, A. I. Kuleff, and L. S. Cederbaum, *Exploring interatomic Coulombic decay by free electron lasers*, Phys. Rev. Lett. **107**, 273002 (2011).
- * 43. G. Sansone, T. Pfeifer, K. Simeonidis, and A. I. Kuleff, *Electron correlation in real time*, ChemPhysChem **13**, 661 (2012).
- * 44. A. I. Kuleff, S. Lünemann, and L. S. Cederbaum, *Electron-correlation-driven charge migration in oligopeptides*, Chem. Phys. (in press) DOI:10.1016/j.chemphys.2012.02.019.

Publications denoted by * are included in the present Habilitation thesis.